University of Illinois
at
Urbana-Champaign
Aeronautical and Astronautical Engineering

AAE 241
Aerospace Vehicle Design, Sapcecraft Section
Final Project Reports

Volume I
Aircraft Section Groups 1 through 4

May 1988

75 PAGES
JH

ROMULUS AIRCRAFT

Final Design Report
AAE 241
Spring 1988

Group One
Ron Dunn ---------- Structures
Sam Huber ----------Weights and Balance
Dan Jensen ---------- Aerodynamics
Martin Kim ----------Surface Operations
Norman Knapp ------ Power and Propulsion
Greg Maloney ------- Stability and Control
Ken Markuson -------Performance

Romulus - Martian Aircraft

Overview

Despite the advances in technology that man has accomplished, a manned martian aircraft that can be used for scientific research of the Mars surface has yet to be accomplished.

NOT THE BEST SENTENCE ↑

Initially, Group #1 set out to design a Martian aircraft which would be used to collect samples from the ground for scientific experiments to transport men and material to distant sites. However, in trying to develop a martian aircraft that could land on areas of Mars other than the home base, many obstacles were encountered which could not be overcome. Getting the plane off the ground under its own power was the biggest problem Group #1 faced and it forced the group to change the mission of Romulus.

Therefore, it is the objective of Group #1 to create a manned Martian aircraft which can perform: scientific surveys of particular sites distant from the base; a deployment of scientific instrument packages by air drop that land rovers cannot accomplish; and rescue operations. All of these missions require that Romulus fly back to its home base after the mission is completed.

Since the aircraft will be operating in a Martian atmosphere, there will be some changes in the aircraft design as compared to a conventional Earth airplane. The Mars atmosphere has a very low density which will reduce the dynamic pressure read by the aircraft. Therefore, the aircraft will be operating in very low Reynolds numbers (Re) - approximately 100,000 as compared to values 10 times that on Earth. Because of this large reduction in Re and the requirement for more lift , a wingspan of 44.01 meters will be necessary to produce enough lift for flight.

Designing the airfoil requires a wing which can operate within the low Re apparent on Mars. The final airfoil, NASA NLF (1) - 1015 was chosen over the intial airfoil because of its lower drag characteristics.

As shown on the 3-D view, the design of the aircraft is comparable to a P-38 military airplane. Attached to the fuselage pod is a high wing device and the two booms extend from the high wing back to the horizontal stabilizer.

In powering the aircraft, the initial design of using a combination of fuel cells and solar cells has been rejected. The plane now has only fuel cells to power the two propellers.

Although enough power has been generated for cruise flight, Romulus cannot takeoff solely with the power from its two engines. Therefore, a rocket-assisted takeoff analogous to a glider takeoff is necessary to enable Romulus to liftoff. The rocket still acts as a pulling force, but this limits Romulus to landing and taking off only at the home base.

Because more fuel cells were required to provide enough power for Romulus to fly, the initial design goal of 4250 Newton-Mars was not met. The weights division then set a new design goal of 5000 Newton-Mars that was met in the final configurations (In the following reports, all weights and forces will be assumed to be on Mars).

Structurally, Romulus has encountered no major problems, and in fact, the use of wood on some parts of the plane has greatly reduced the cost of the aircraft.

Based upon the results of Group #1 work, there appears to be no serious technical difficulty involved in operating Romulus on Mars. Although the design and creation of Romulus would be an expensive adventure, such a vehicle could be most useful in evaluating the Mars surface and in creating a habitat for mankind.

AAE 241
Spring 1988
INITIAL SIZING DATA SUMMARY

Gross Weight: 4250 N

Wing Loading: 20.9 N/m^2

Fuel Weight: 471.8 N

Useful Load Fraction: 0

Maximum Take-off Power

Power Loading:

Fuel Fraction:

Geometry

Ref. Wing Area = 203.2 m^2

AR = 10

Propulsion

Engine/Motor Type: Samarium-Cobalt motor

No. of Engines/Motors = 2

$P_{o_{max}}$ /engine = 13.0 kw

c_p at cruise = 0.0484

Aerodynamics

Cruise; C_{D_o} = .0252

e_o = .8

C_L = .6

$(\frac{L}{D})_{max}$ = 15.3

Take-off; C_L =

$C_{L_{max}}$ = 1.6

Landing; C_L =

$C_{l_{max}}$ = 1.6

Cruise Performance

h = 1.5 km

V = 70 m/s

AAE 241
Spring 1988
DESIGN DATA SUMMARY

Gross Weight: 5000 N-Mars
Wing Loading: 25.8 N/m^2
Maximum Fuel Weight: 472 N
Useful Load Fraction: 0.24

Maximum Take-off Power 26 kw
Power Loading:
Fuel Fraction: .0944

Geometry

Ref. Wing Area = 193.81 m^2
AR = 10
Λ_{LE} = 0°
λ = .67
t/c = .15

Propulsion

Engine Description: Samarium-Cobalt motor
Number of Engines = 2
$P_{O_{max}}$ /Engine = 13.0 kw
Weight/Engine = 56.4 N
c_p at Cruise = .0484
Prop. Diam. = 7.5 m
No. of Blades = 2
Blade Cruise R_e = 84,700@ tip

Performance

Cruise R_e = 500,000
Cruise h = 1.5 km
Cruise M = .31
Cruise V = 70 m/s
Take-off Field Length = 892 m
Take-off Speed = 53.5 m/s
Landing Field Length = 676.6 m
Landing Speed = 49.6 m/s
Maximum Landing Weight = 5000 N
OEI Climb Gradient (%): = -3.09 %
2nd Segment = N/A
Missed Approach = Can't be done
Sea Level $(R/C)_{max}$ = 1.16 m/s

Aerodynamics

Airfoil: NASA NLF(1)-1015
High Lift System: plain flaps

Cruise; C_{D_o} = .0282
e_o = .8
C_L = .6
(L/D_{max}) = 14.3
Take-off; C_L = .6
$C_{L_{max}}$ = 1.4
Landing; C_L = 1.78
$C_{L_{max}}$ = 1.78

Stability and Control

Static Margin Range = .1 (m) to .617 m
Acceptable C.G. Range = .3925 forward of a.c.; .1245 aft of a.c.
Actual C.G. Range = .2850 forward of a.c.; .0005 aft of a.c.

All dimensions in meters
Scale: 1:200

FOLDOUT FRAME

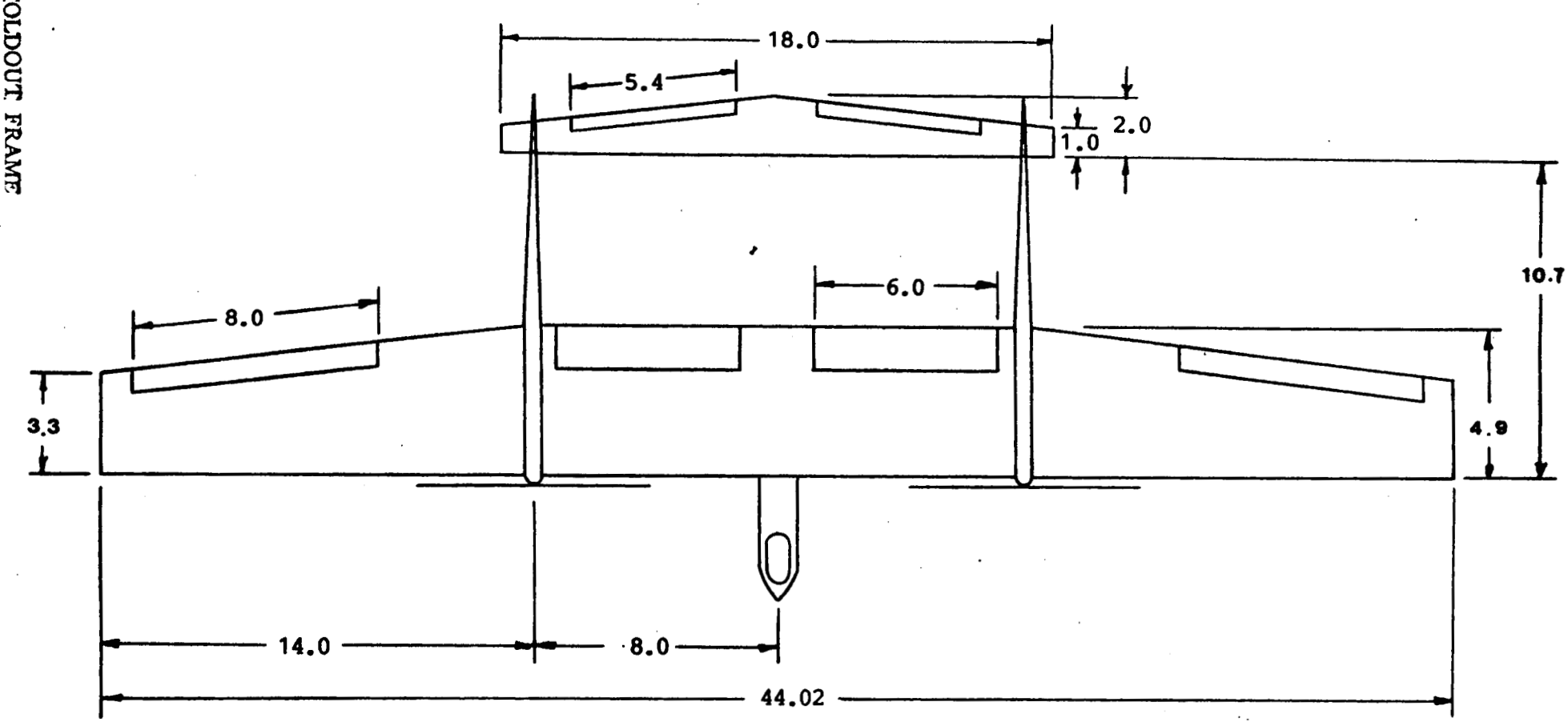

Scale: 1:200

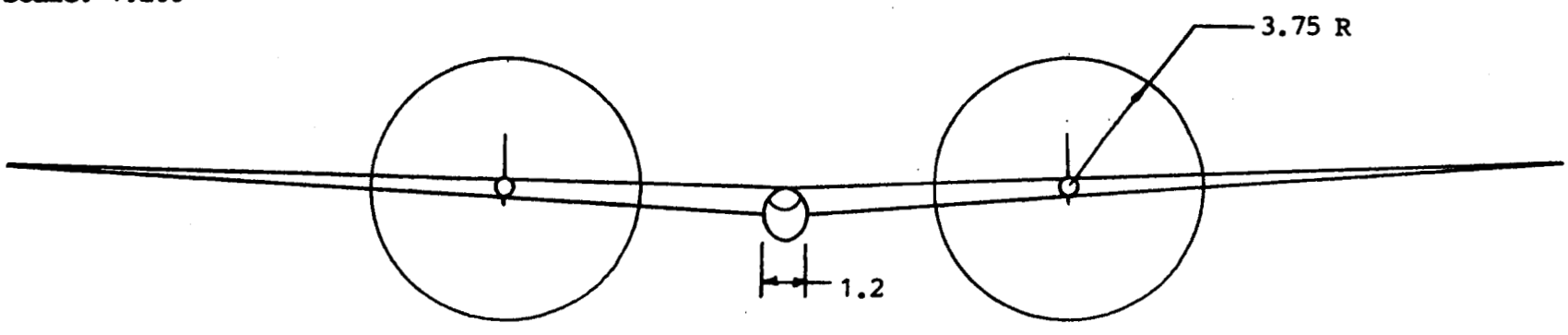

Scale: 1:100

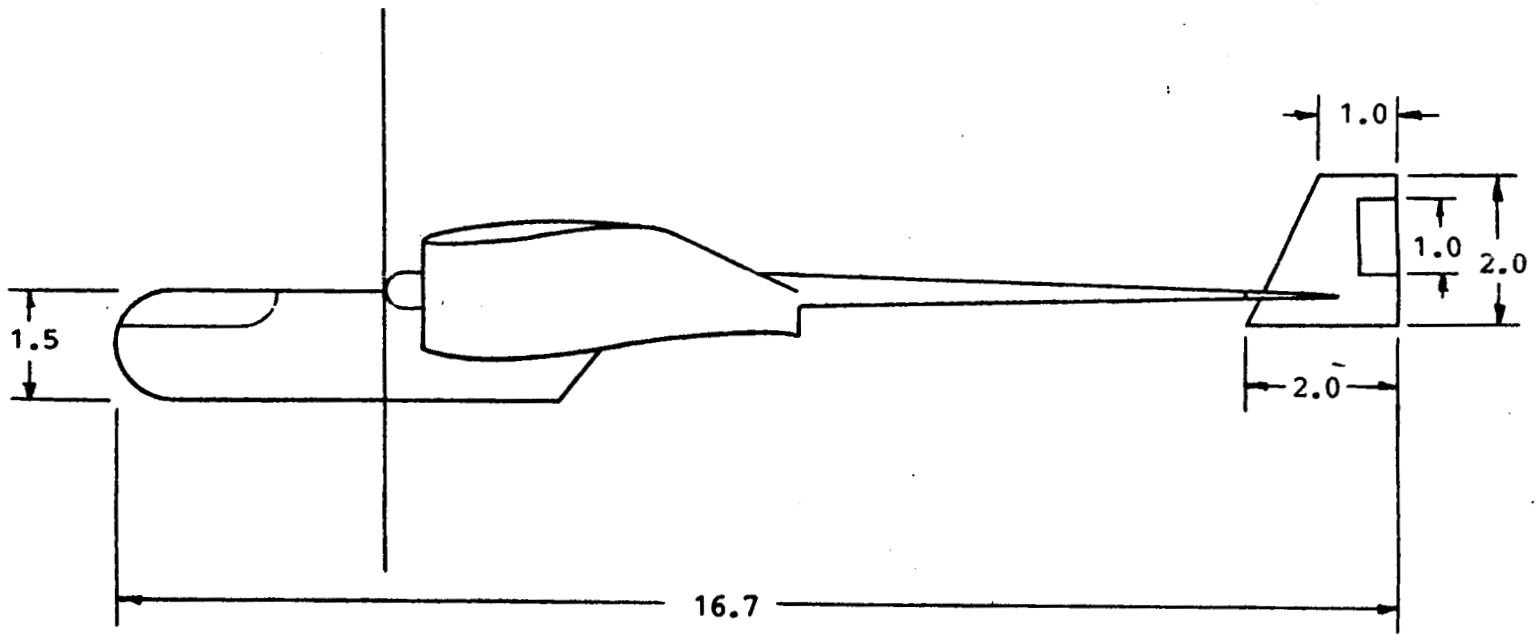

FOLDOUT FRAME 2

THREE-VIEW DRAWING OF THE ROMULUS AIRPLANE

Drawing by
Martin Kim

AERODYNAMICS

Daniel T. Jensen

As with other aspects of this mission, the aerodynamic requirements of the proposed Mars airplane are quite challenging. Of primary importance is the unusually low Reynolds number (for this plane, R_e = 500,000) at which the aircraft will operate. On Earth, applications for airfoils optimized for this Reynolds number are quite limited; Reynolds numbers in this range are usually found only with birds and model aircraft. Research into this flight regime has been understandably sparse.

With today's level of technology, it is normal to size and configure the aircraft prior to selecting an airfoil. Additionally, airfoils are usually created and optimized for the particular design. Design studies with similar mission profiles have taken this approach.[1]

For this aircraft, since design of an optimized airfoil was beyond the scope of the project, airfoil selection was done early in the design process. Airfoils optimized for flight at very low Reynolds numbers were compared; the NASA NLF(1)-1015 was selected. While other airfoils had similar maximum lift coefficients and drag characteristics, the NASA airfoil is unique in that it has been designed to maximize natural laminar flow over the chord at design Reynolds numbers. For this airfoil, upper-surface separation is controlled through the use of a "separation ramp". The ramp limits flow separation to a small area near the trailing edge. This is especially helpful with the large chord present on this design. Sectional data for the airfoil are presented in Figure 2-1. Because elliptical loading has been assumed, the sectional lift coefficient can be assumed to be equal to the lift coefficient for the wing. Lift curves for take-off, cruise and landing are presented in Figure 2-2. The aircraft takes off conventionally without flaps. The lift curve is thus identical for take-off and cruise.

The ruling factor in the configuration was simplicity of design. For the mission description used, it was felt that the simplest and most conventional design would probably also be the most reliable and best. Because of the large wing area required, a high-wing

design was chosen. This allows the top of the planform to interact freely with the incident freestream and facilitates placement of control surfaces and high-lift devices. Lastly, the wing itself must be relatively high off the ground to allow for propeller clearance. This configuration therefore makes cabin access much easier. The conventional aft tail is connected by two booms. Because interior cabin space is minimal, the cabin itself fits entirely under the wing. The booms are used to allow a conventional tail with minimal drag and weight penalties.

Wing design was certainly challenging. Initially a sizing exercise was done using Lift = 1/2x(density)x(velocity squared)x(surface area)x(lift coefficient). Target gross weight was used as the required lift at cruise and cruise lift coefficient was set at 0.6. This was done to compare required wing area versus cruise speed. After selection of the cruise speed, the next step was providing the requisite wing area most efficiently. In the wing design process, minimization of span was given high priority. Because the plane must fit into a small spacecraft compartment for transport to Mars, span had to be kept as low as possible. For this reason, an aspect ratio of 10 was selected. At the chosen cruise speed of 70 meters per second, the required wing area is 193.81 square meters. This converts to a span of 44.02 meters and a chord length of 4.93 meters. Between the booms, the wing section has a rectangular planform. Outboard of the booms, the wing tapers to 67% of chord. This makes the lift distribution much more elliptical and causes the stall onset to move outboard. Because tip stall is not desirable, a 3 degree washout twist is incorporated. The wing has 3 degrees of dihedral and is mounted at an angle of -2 degrees to provide level flight at cruise.

Selection of cruise speed was a compromise between conflicting inputs. For the mission profile, a moderate flying speed is mandated by the rate at which data can be collected and transmitted by the equipment aboard.[2] Additionally, speeds past 70 meters per second must take compressibility effects into account and require added power.

However, faster speeds decrease required wing area, which is certainly desirable. The design velocity was thus set at 70 meters per second as best satisfying the inputs.

A drag decomposition on the design has been completed. Its results are presented in tabular form in Table 2-1. As expected, drag of the wing is dominant, followed by drag of the fuselage. Complete polars are presented for take-off, cruise and landing in Table 2-2 amd Figure 2-3.

Aerodynamically, further refinements are both possible and desirable. These would best be done with a scale model in a wind tunnel. It would not be economically sound to send anything but an optimum aircraft the millions of miles to Mars.

[1] Mark D. Maughmer and Dan M. Somers, "Design and Experimental Results for an Airfoil for a High-Altitude, Long-Endurance, Remotely Piloted Vehicle," The Pennsylvania State University, University Park, PA.

[2] Developmental Sciences, Inc., "A Concept Study of a Remotely Piloted Vehicle for Mars Exploration," City of Industry, CA, 1978.

Table 2-1

CRUISE DRAG COEFFICIENT BREAKDOWN

Component	C_{d_o}	Percent
Wing	.0150	53.20
Fuselage	.0069	24.50
Twin Booms	.0034	12.10
Tail	.0011	3.80
Trim Requirements	.0009	3.20
Interference and Gap	.0005	1.80
Miscellaneous	.0004	1.40
	.0282	100.00

Table 2-2

FOR CRUISE (CLEAN) CONFIGURATION,

$$C_D = .0398C_L^2 - .0008C_L + .0282$$

FOR TAKE-OFF CONFIGURATION,

$$C_D = .0398C_L^2 - .0008C_L + .0390$$

FOR LANDING CONFIGURATION

$$C_D = .0398C_L^2 - .0008C_L + .1514$$

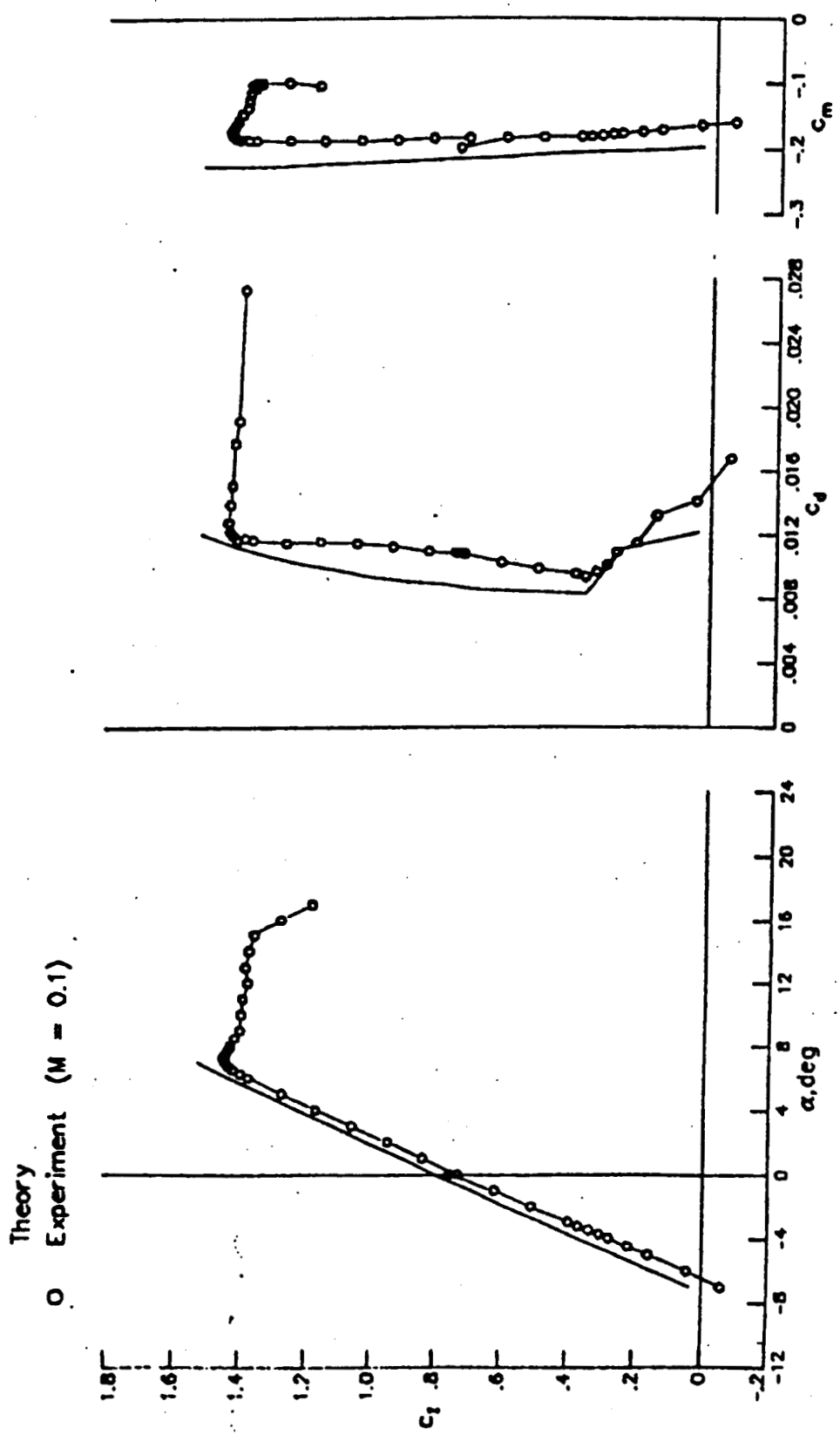

FIGURE 2-1
COMPARISON OF THEORY AND EXPERIMENT
NLF(1)-1015 R=500,000

FIGURE 2-2

C_L VERSUS α

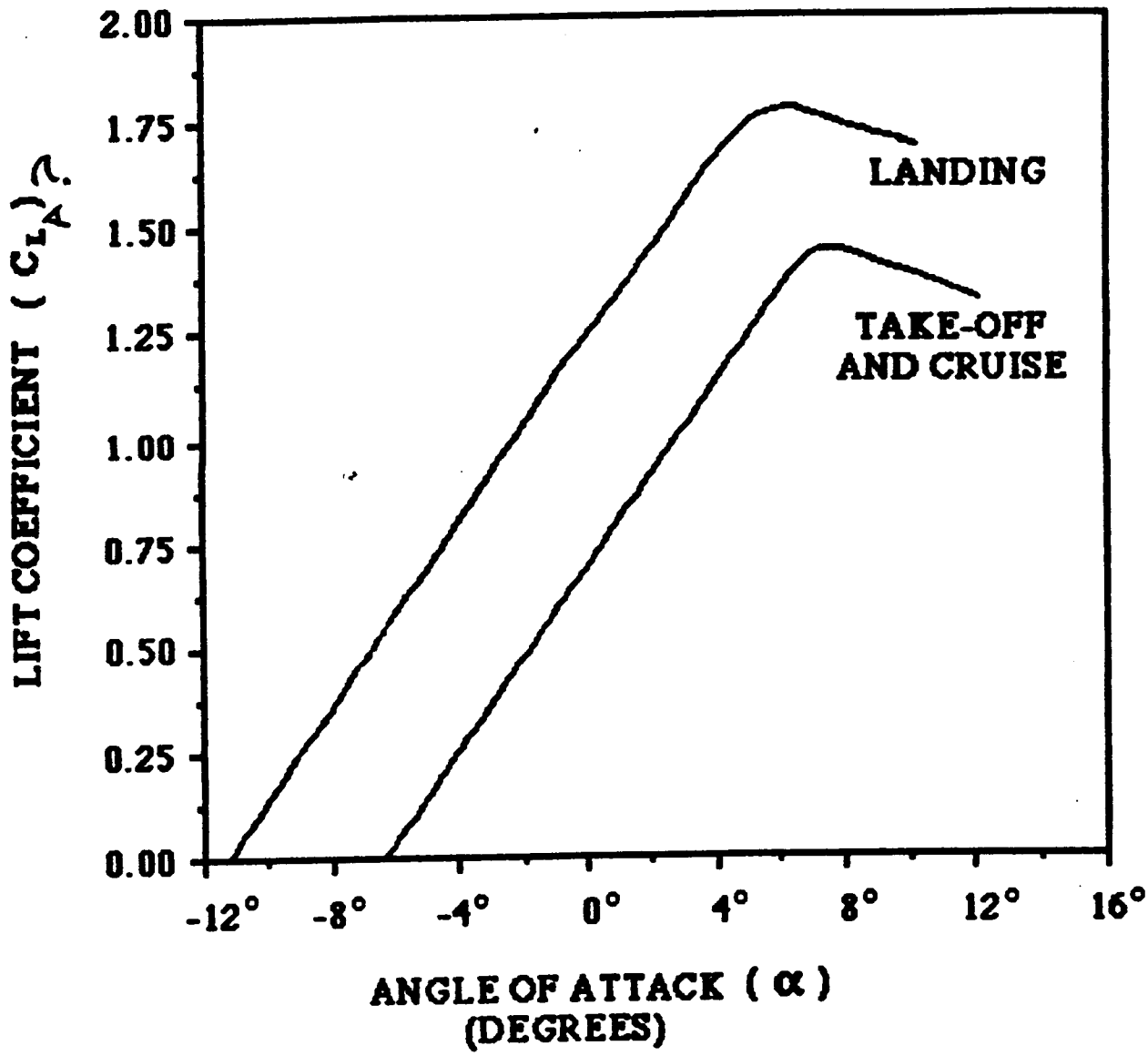

FIGURE 2-3

DRAG POLARS

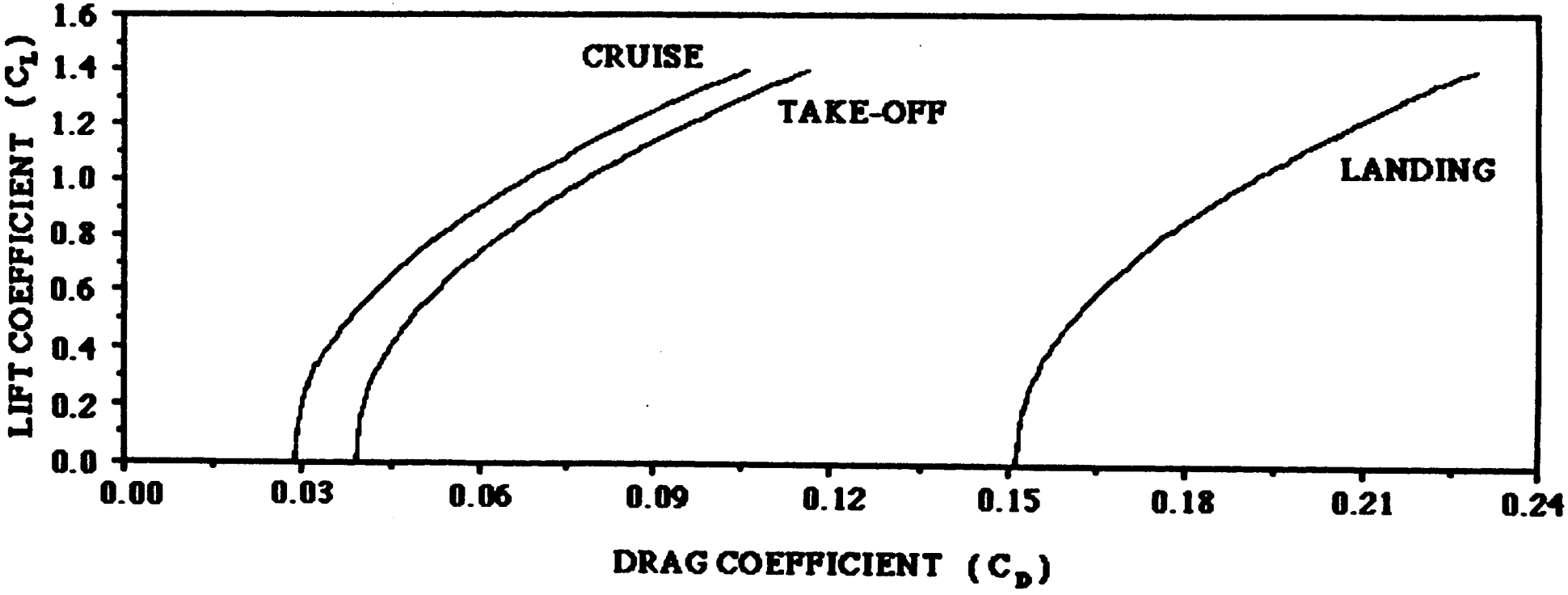

PERFORMANCE:

Ken Markuson

Data Used:

Weight of Aircraft =	5000 (Newtons)
Oswald's Efficiency Factor =	.8
Wing Area =	193.81 (Meters Squared)
Aspect Ratio =	10
Maximum Lift Coefficient =	1.4
Parasitic Drag Coefficient =	.0282
Change in Parasite Drag Coefficient Due to Stall =	.008

The performance results have changed appreciably since the preliminary design report. The self-powered take-off has been abandoned for a rocket assisted take-off. This type of take-off decreased the need for large amounts of excess power. A rocket assisted take-off was used because of the weight problems associated with the large amounts of fuel cells needed for take-off and the increase in the weight of the structure. The rate of climb for this final report would therefore be about one quarter that of the preliminary design report. This lack of excess power lead to a critical condition with one engine inoperative.

This aircraft would be unable to complete a missed approach and it would also be unable to hold any altitude with one engine inoperative. The aircraft would descend with one engine inoperative, but at a very slow rate. It would take approximately 36 minutes to descend to sea level from 1500 meters and would cover approximately 115.5 kilometers.

This would give the pilot plenty of time to get back to base or to find a suitable landing spot.

The new airfoil that was chosen by the aerodynamics section gave a lower power required at each altitude and flight condition. But the overall power required was higher because of the increase in the weight of the aircraft. Figure 3-1 presents the power required and power available at sea level. Power available was obtained from the propulsion section. It also presents the stall speed and the increase of power required needed close to the stall speed due to the increased drag at stall. The one engine inoperative power available curve was not shown because it fell below the scope of the graph. Figure 3-2 gives the same data but at the cruise altitude of 1.5 kilometers. All these calculations were obtained by using an electric engine with all products retained so that there was no change in weight throughout the flight.

Figure 3-3 shows the level flight performance envelope. The left side of the figure depicts the stall velocity at several different altitudes. The middle line presents the maximum excess power at the same altitudes. The airspeed corresponding to the maximum rate of climb occurs at about 55 meters per second. The right line depicts the maximum velocity possible at each altitude due to the propulsion limitations. Where these graphs intersect would give the maximum ceiling of the aircraft. This maximum altitude occurs at approximately at 2800 meters. Figure 3-4 gave the same results using a different method. Plotting the maximum rate of climb versus the altitude also gave a maximum altitude of about 2800 meters.

These graphs were used to determine the complete mission profile characteristics. The maximum rate of climb at sea level was 1.16 meters per second. The time to climb to cruise altitude was calculated at approximately 36 minutes. Down field range during climb was calculated at approximately 122 kilometers. The rate of descent was determined to be approximately 2 meters per second at cruise altitude with power off. The time to descend from cruise altitude to sea level was calculated at 12.63 minutes with power off. Down field range was calculated at approximately 42 kilometers for descent. A power off

descent was chosen to save battery charge and because a long, smooth, controllable descent was achieved without power. This leaves a total maximum cruise time of approximately 7 hours. This time includes approximately 10 minutes for take-off and landing including taxiing time. This maximum cruise time of 7 hours would give a maximum total cruise range of 1769 kilometers. This gave a maximum total range of 1933 kilometers. All these results were based on a maximum pilot endurance of 8 hours.

These results show a slight decrease in the performance calculations from the preliminary design report. For example the range was decreased by about 100 kilometers. If the weight of the aircraft could have been decreased and if more fuel cells could have been used then this aircraft would have been able to take-off under its own power. It would have then been able to climb out at a much faster rate because of the increase in excess power. This aircraft still has relatively good performance characteristics with this low excess power. Only 13 percent of the total flight time was used for climb and descent, this would leave ample time to perform the scientific studies.

Fig. 3-1

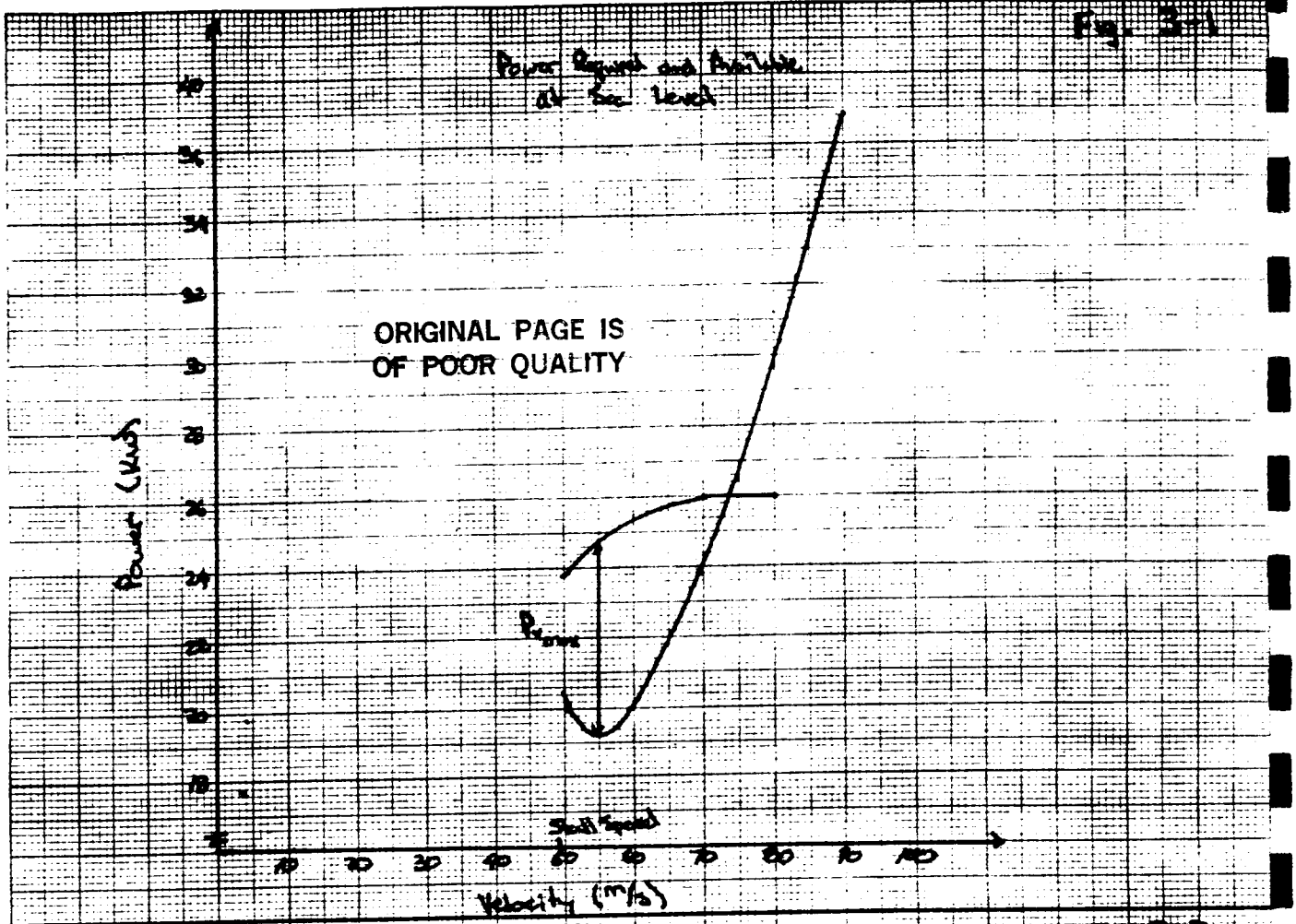

Fig. 3-2

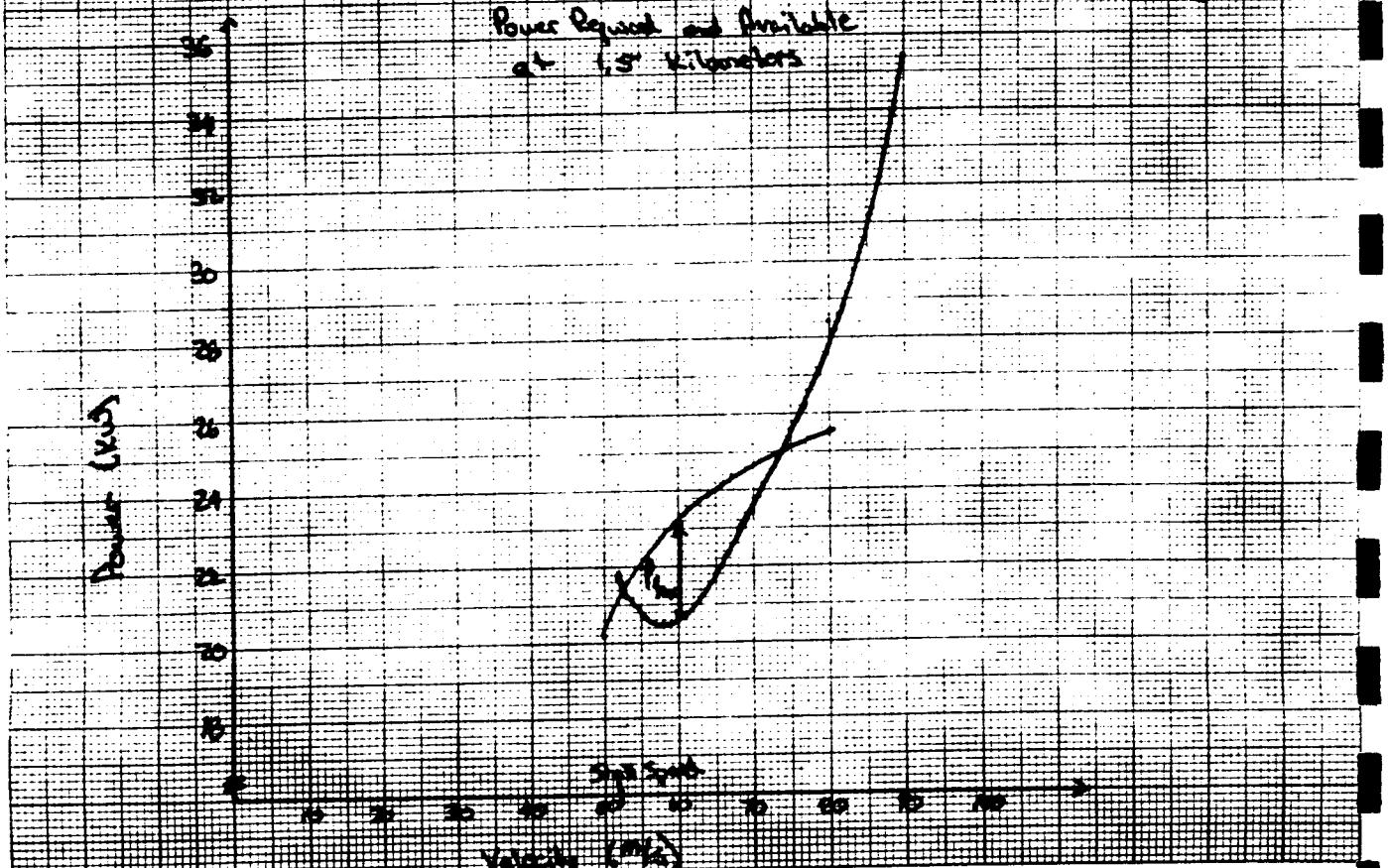

Level Flight Performance Envelope

Fig 3-3

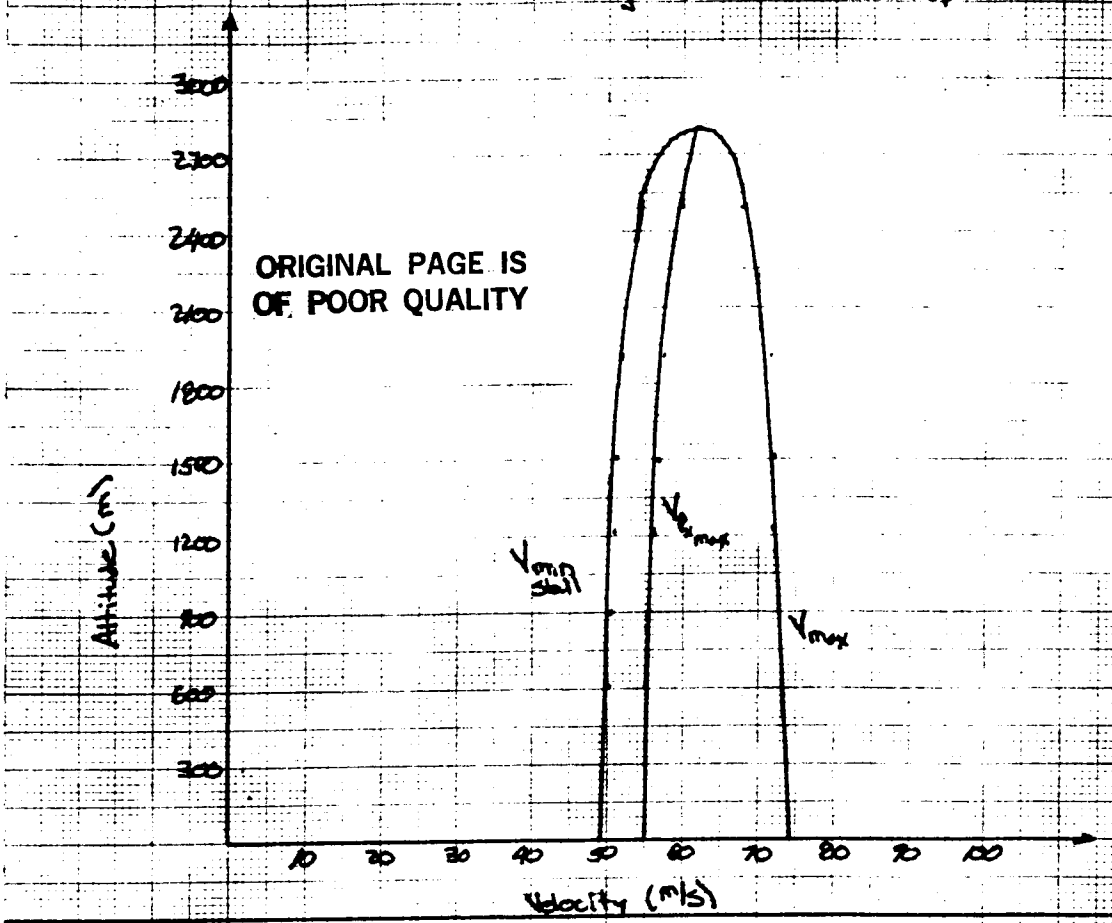

Fig 3-4

Maximum Rate of Climb at Various Altitudes

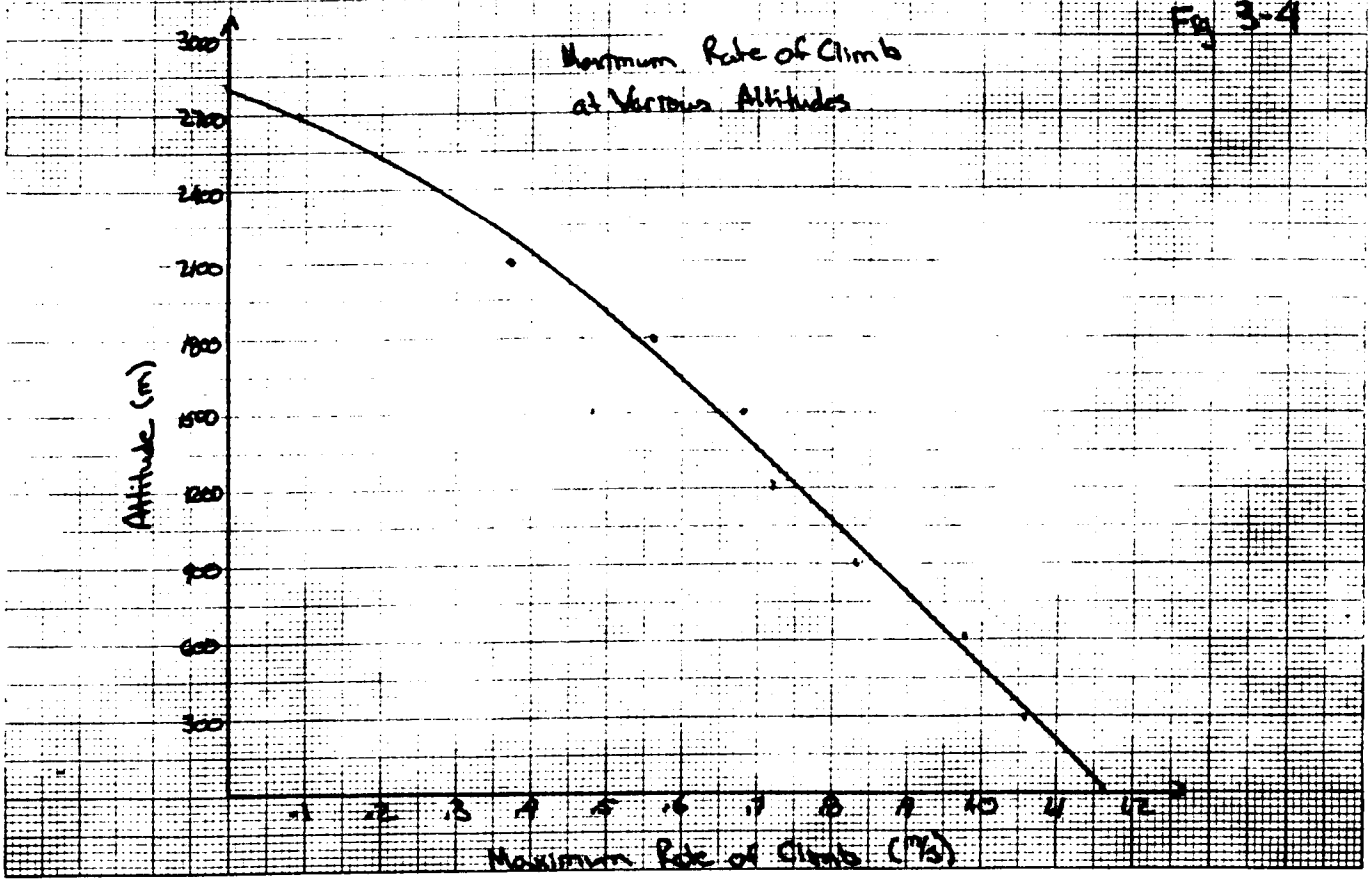

POWER & PROPULSION

Norman Knapp

The conditions on Mars present unique problems for the propulsion system of a Mars Airplane. Due to the low percentage of oxygen in the Martian atmosphere, either a monopropellant fuel must be used or the fuel oxidizer must be carried within the aircraft. However, combustible fuels may be neglected altogether in favor of sources of electrical power. Early in the design process, electric propulsion was considered advantageous in that the problems and costs involved with procuring expendable propellants for each flight were overcome. An aircraft powered by solar cells or fuel cells could be ready for use every other Martian day. The following design was originally based on an aircraft powered by a combination of solar cells and fuel cells. However, a comparison of the two types of power systems indicated that fuel cells had a greater energy-to-mass ratio. Thus, the final design is powered exclusively by fuel cells. An overview of the power and propulsion systems is given in Table 4.1.

Power System: Hydrogen and Oxygen Fuel Cells

Hydrogen and oxygen fuel cells were chosen as the sole power source for the Romulus Aircraft because they are characterized by the relatively high energy-to-mass ratio of 3.69 kW-hr/kg. A realistic cell efficiency of 80 percent reduces the ratio to 2.95 kW-hr/kg [1]. The energy-to-mass ratio of solar cells depends in part on the cell efficiency and the area covered by the cells. The Romulus has a total wing and horizontal tail area of 226 m^2 with control surfaces covering 17 percent of this surface. Assuming that the remaining 188 m^2 of the wing could be covered with solar cells having an 18 percent efficiency and that the mean solar flux at the Martian surface is 590 W/m^2 [2], solar cells could provide the aircraft motor or engine with approximately 20 kW. Using silicon solar cells with a surface

density of 0.414 kg/m^2 and a total mass of 78 kg, an eight hour flight would place the energy-to-mass ratio of the cells at 2.05 kW-hr/kg, well below the ratio for fuel cells.

There are two additional drawbacks to the use of solar power arrays. First, the available area on the wings and horizontal tail is not sufficient enough to carry solar cells to provide the total power necessary to operate the aircraft. An additional source of power would be required. Second, the solar flux of 590 W/m^2 represents a maximum. The actual solar power incident on the solar arrays would be less and would vary from hour to hour.

The combined weight of the fuel cell reactants is 472 N. This value is set by power requirements and system efficiencies which are discussed below. The hydrogen is stored in gaseous phase under elevated pressures and weighs 52.8 N. The oxygen is also gaseous and weighs 419 N. The reactants are stored in tanks underneath and behind the cockpit. Once they are combined in the actual fuel cells, the water that is produced is stored in a tank in the fuselage area. When the aircraft has returned to its home base, the water will be separated by means of electrolysis into hydrogen and oxygen for use on future flights. Power for the electrolysis process will be supplied with ground based solar arrays.

In addition to the weight of the reactants, the weight of the fuel tanks and fuel cell accessories must also be considered. Using Table 13 from reference [1] and assuming a reduction in weight due to future advances in lightweight materials, fuel cell accessories and tanks will have a weight of 205 N. The volume of each of the holding tanks are as follows: hydrogen, 0.90 m^3; oxygen, 2.00 m^3; water, 0.13 m^3. It is important to note that considering the additional weight of fuel cell accessories and tanks, the energy-to-mass ratio for fuel cells is 2.05 kW-hr/kg, a value equal to the ratio for solar cells. Fuel cells are still favored, however, due to the drawbacks for solar cells listed above.

Power Available and Required

Power available data for varying speed and altitude conditions is listed in Table 4.2. This data was obtained using the physical characteristics of the propeller and Figures 4.1

and 4.2. Power required data for the same conditions is listed in the performance section. The maximum power available for the propulsion system is set at 26 kW and corresponds to 80 m/s flight at an altitude of 1200 m. This sets the fuel cell maximum fuel flow rates at 1.75 kg/hr for hydrogen and 13.9 kg/hr for oxygen. However, the aircraft will usually be operating with lower power availability and lower fuel flow rates For the cruise condition of 70 m/s at 1500 m altitude, the power available for the propulsion system is 24.88 kW, and the fuel flow rates are 1.66 kg/hr for hydrogen and 13.2 kg/hr for oxygen. For the climb condition of 55 m/s at ground level, the power available is approximately 25 kW and the fuel flow rates will be similar to the cruise condition.

With a maximum power available of 26 kW for the propulsion system and a minimum electrical system power available of 0.50 kW, system efficiencies (gearbox, propeller, and motor) require that the fuel cells provide a maximum of 46.25 kW. The electrical system power is used to operate two sets of systems: scientific instrumentation located in the cargo area and aircraft avionics. These systems will each require approximately 0.10 kW.

When the aircraft is in take-off mode, it will be propelled by external means and will not be using its own propulsion system until it lifts off the ground. Shortly after take-off, the power available will correspond to the climb condition. As for the landing procedure, the aircraft's propulsion system will be shut down at cruise altitude and the plane will glide down to the runway. The purpose of the glide is twofold. First, the time for descent is decreased as opposed to powered flight. Second, a savings in power is achieved. At any point during the glide the propulsion system could be reactivated in order to effect maneuvers.

Motor, Gearbox, and Controller

The Romulus Aircraft design incorporates two propeller/motor propulsion systems located on the wings. Each propeller is linked through a gearbox to a samarium-cobalt magnet rotor motor which is a derivative of a design listed in reference [3]. Each of these

powertrains is monitored by an electronic controller which is able to analyze conditions and set the propeller rpm in order to maximize efficiency. The total weight of each propulsion system including propeller, motor, gearbox, and controller is 271 N.

The rare-earth motor was chosen due to its high reliability and relatively low mass. Each motor weighs 56.4 N and has an average efficiency of 87 percent [3]. Each gearbox is of the planetary type and weighs 47.0 N. The average efficiency of the gearbox is 95 percent. Each controller weighs only 18.8 N. The controller is located alongside the motor while the gearbox is located between the motor and the propeller hub [4].

Propeller

The system propeller is based on the 5868-9 propeller with a Clark-Y section and consists of two blades. Figures 4.1 and 4.2 refer to this propeller and plot speed, power, and torque coefficients versus various physical properties of the blade such as blade pitch, efficiency, and advance ratio. The propeller design for the cruise condition was based on a advance ratio, J, of one. This value allowed for a reasonable blade pitch and high efficiency while maintaining a propeller tip Mach number of less than one.

The blade pitch of the propeller at the three-quarter radius point is 25 degrees. Each propeller has a diameter of 7.5 m, an efficiency of 86 percent, and a weight of 150.4 N. When the aircraft is at cruise conditions, the propeller operates at 556 rpm which allows for a tip Mach number of 0.95 and a tip Reynold's number of 84,700. The propellers rotate in opposite directions in order to avoid instabilities. A final characteristic of interest is the ability of the system to lock the propellers in a horizontal position during take-off and landing procedures. This is accomplished with the use of a locking mechanism located in the gearbox.

REFERENCES

1. Hall, David W., Fortenbach, Charles D., Dimiceli, Emanual V., and Parks, Robert W., A Preliminary Study of Solar Powered Aircraft and Associated Power Trains, NASA Contractor Report 3699.

2. Augenstein, B. W., "The Mars Airplane Revived - Global Mars Surface Surveys", pp. 1 - 11.

3. Clarke, Victor C., Kerem, Abraham, and Lewis, Richard, "A Mars Airplane?", Astronautics & Aeronautics, January 1979, pp. 42 - 54.

4. Bent, Ralph D. and McKinley, James L., Aircraft Powerplants, New York, McGraw - Hill, 1985.

5. Smith, Robert E. and West, George S., Compilers, "Space and Planetary Environment Criteria Guidelines for Use in Space Vehicle Development, 1982 Revision, Section 6: Mars", NASA Technical Memorandum 82478.

TABLE 4.1: POWER & PROPULSION PARAMETERS

I.	**POWER SYSTEM: HYDROGEN AND OXYGEN FUEL CELLS**	
	Energy Density	3.69 kw-hr/kg
	Efficiency	80.00 %
	Maximum Stored Power	46.25 kw
	Maximum Propulsive Power	26.00 kw
	Minimum Electrical System Power	0.30 kw
	Weight of Components	676.80 N
	Hydrogen	52.80 N
	Oxygen	419.00 N
	Accessories	205.00 N
	Volume of Fuel and Water Tanks	
	Hydrogen	0.90 m^3
	Oxygen	2.00 m^3
	Water	0.13 m^3
II.	**POWER TRAIN**	
	Samarium-Cobalt Motor (2)	
	Weight	56.40 N
	Efficiency	87.00 %
	Maximum Rated Power	16.00 kW
	Planetary Gearbox (2)	
	Weight	47.00 N
	Efficiency	95.00 %
	Electronic Controller (2)	
	Weight	18.80 N
	5868-9 Clark-Y Section Propeller (2)	
	Weight	150.40 N
	Diameter	7.50 m
	RPM at Cruise Conditions	556.00 rpm
	Blade Pitch Angle (0.75 R)	25.00 degrees
	Efficiency	86.00 %
	Number of Blades	2

Cricket Graph Data

TABLE 4.2 POWER AVAILABLE (KW)

Wed, Apr 27, 1988 12:27 AM

	VELOCITY	HEIGHT = 0	H = 300 (M)	H = 600 (M)	H = 900 (M)	H = 1200 (M)	H = 1500 (M)	H = 2000 (M)	H = 2500 (M)
1									
2	30	14.19	13.97	13.65	13.33	13.10	12.96	12.03	11.76
3									
4	40	18.53	18.24	17.82	17.41	16.34	16.17	15.90	15.55
5									
6	50	23.84	23.47	22.94	21.56	20.40	20.20	19.12	18.71
7									
8	60	25.99	25.59	25.01	23.65	23.25	23.02	22.64	22.15
9									
10	70	26.00	26.00	26.00	25.56	25.13	24.88	23.81	22.66
11									
12	80	26.00	26.00	26.00	26.00	26.00	25.42	24.42	23.91
13									
14									
15									
16									
17	Density	0.0152	0.0149	.0145	0.0141	0.0138	0.0136	0.0132	0.0128
18	(kg/m3)								

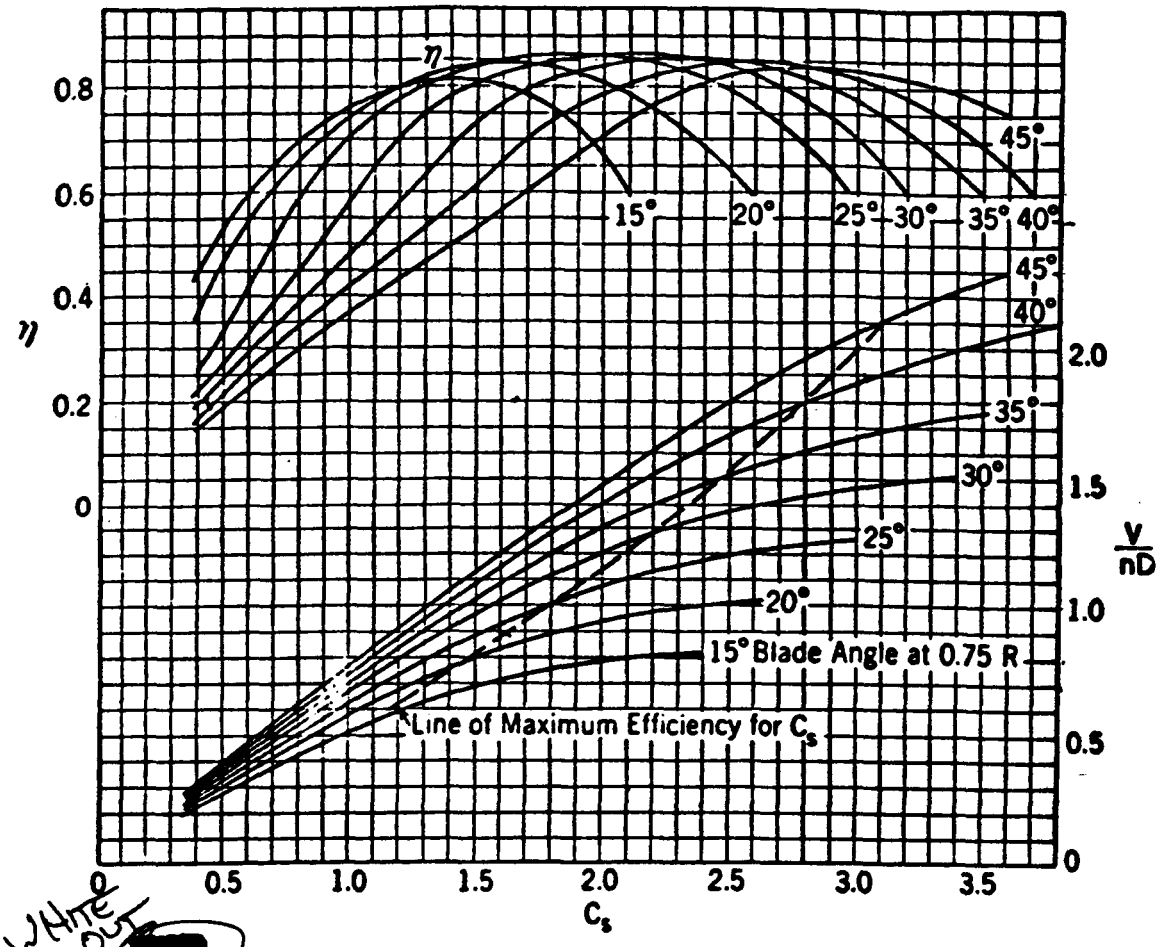

WHITE OUT

FIG. [redacted] 4. Design chart for propeller 5868-9, Clark-Y section, two blades. (*NACA Tech. Rept. 640.*)

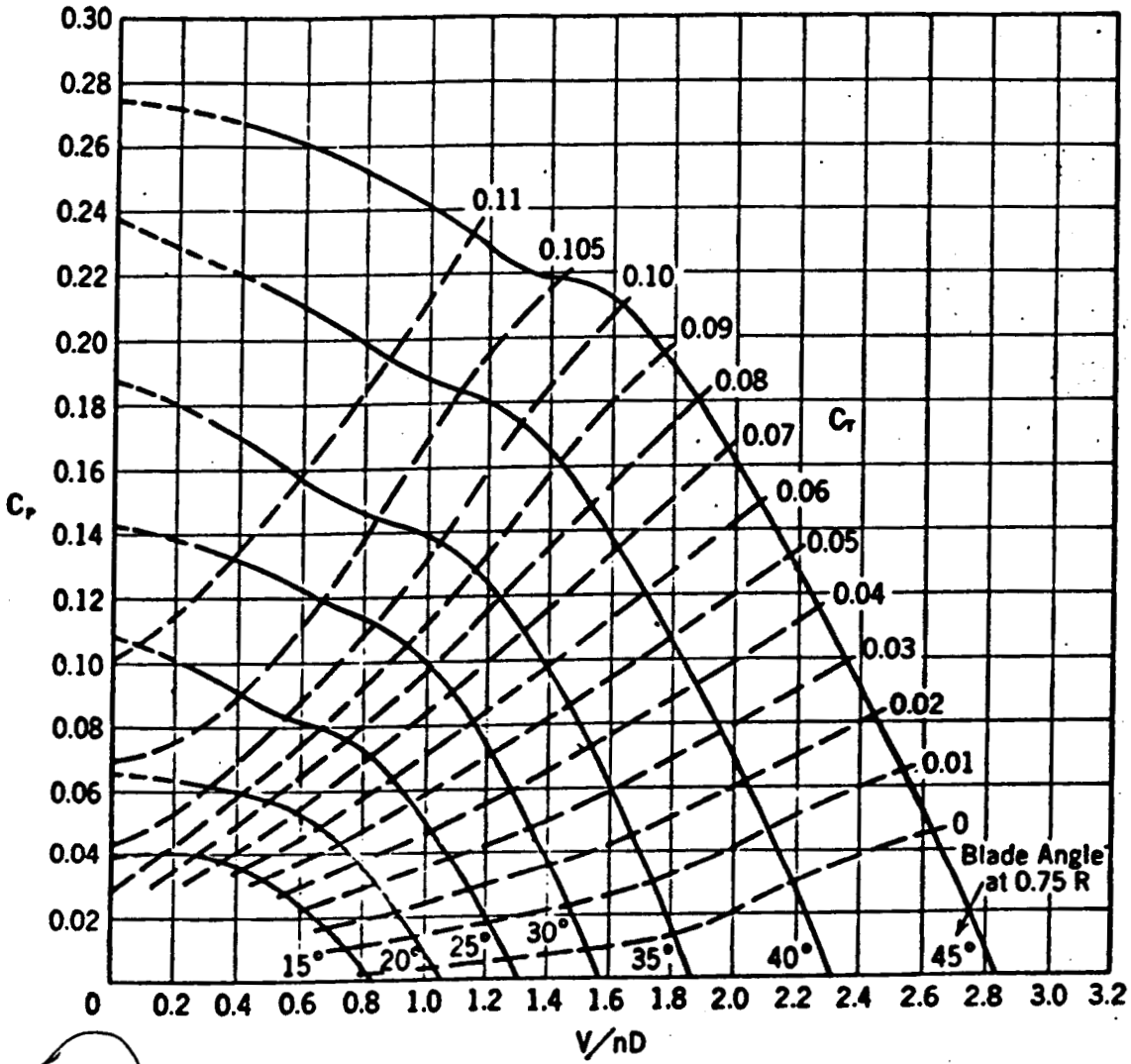

FIG. 4.2 Power coefficient curves for propeller 5868-9, Clark-Y section, two blades. (*NACA Tech. Rept. 640.*)

STABILITY AND CONTROL

GREG MALONEY

GROUP #1

Although the Romulus aircraft may be aerodynamically sound and be able to produce enough power for flight, it must meet several stability requirements to be safely controllable and maneuverable during climb, level flight, and landing. In order to achieve this Romulus must be longitudinally, directionally, and laterally stable.

According to Professor Sivier, a reasonable value for the ratio of the horizontal tail area to wing area is .20. Due to the large chord and wing span associated with Romulus, a cooresspondingly large tail span is also evident - 18 meters. Initially, a larger rectangular horizontal tailspan was chosen, but the weight of the tail was so big that it caused the plane to be tail heavy. Therefore, the tail has been tapered and its span was reduced to lower the weight of the plane. Also, the horizontal tail section was changed from a Wortmann FX 63-137, to a NASA-NLF(1)-1015 in order to give the plane better drag characteristics (Reference 1).

A negative tail incidence angle was chosen for Romulus to ensure that a down force is applied on the tail and thus to allow Romulus a more effective lift. Fortunately, the wing incidence angle is less negative than the tail incidence angle so that the wing will have a higher effective lift.

Despite a stabilizing effect from the dihedral angle for the rolling moment due to sideslip, the horizontal tail was not inclined because it provided more beneficial effects for longitudinal stability at zero dihedral angle.

The verical tails were also selected according to Professor Sivier's recommendations. The two tails were designed to have a total area equal to .15 of the horizontal tial area. Once again, the veritical tails were tapered so as to reduce weight and to create a more nose heavy plane.(An excellent picture of what the tails look like is shown in the 3-D view). In early design configurations, an error was made in choosing the vertical tail sections to be identical to the wing

section. Vertical tail sections should have a symmetrical design so that no negative angle of attack will be produced. Unfortunately, the airfoils used for the wing are cambered and give this unwanted result. Therefore, the NACA 0009 airfoil was chosen to prevent this occurance (Reference 2). See Figure 5-1 to get a better idea of what is occuring at the vertical tails. The Aspect Ratio for the vertical tails are operating at a much lower value than for the wings because of the small areas involved.

In order to determine an acceptable center of gravity (c.g.) range to satisfy longitudinal stability and trim requirements in ground effect (IGE), the neutral point location must be calculated. With IGE, the c.g. will decrease and this results in a larger Static Margin range (S.M.). S.M. is the dimensionless distance between the c.g. and the neutral point (See Figure 5-2). See Figure 5-3 to understand how IGE affects the plane. By increasing the S.M., Romulus will become a more stable plane. The c.g. most forward limit is located .3925 meters in front of the aerodynamic center of the wing (a.c.). The most aft c.g. limit is located .1245 meters in back of the a.c. of the wing. The result is a plane which has positive static stability (See Figure 5-4).

After the horizontal and vertical tail sizings have been completed, the stability and control requirements at takeoff, cruise, and landing can be calculated. In determining the longitudinal and directional stability, the horizontal and vertical tail sections were designed to be big enough so that the control surfaces could be placed onto these sections. The elevator and the rudder are the control surfaces which provide the necessary longitudinal and directional stability respectively. Ailerons provide the necessary deflection for rolling the plane and are involved with the lateral stability of the plane. The sizes of the control surfaces are described in Figure 5-5b. Although Professor Sivier did not suggest any reasonable values for the sizings, Reference 5 gave some fairly common sizes and they were tailored to the plane's design. The 3-D view shows the control surfaces and how they are dimensioned according to the plane. Figure 5-6 shows an excellent description of how the control surfaces work and what they produce.

* Tabulated results for the following are found under the Addendum *

For takeoff rotation, sufficient longitudinal control power is needed to lift the nosewheel at .9 of the takeoff speed with the c.g. at the forward limit. An elevator deflection of 6° is needed because the plane itself has a restoring moment that wants to keep the plane at equilibrium. By applying the elevator deflection, the plane can lift off with the help of the pitching moment (Figure 5-5 shows a

typical deflection). Romulus has enough elevator control to lift-off. Even though Romulus is not using a conventional takeoff, the rocket-assisted takeoff still acts in the same way by pulling the aircraft - analogous to a glider takeoff.

Another problem which may cause problems for Romulus is if one of its two engines shuts down during the takeoff. After the rocket has successfully given the plane enough power to lift, the propellers will immediately start to rotate. Although the performance section has shown that the plane cannot hold altitude with one engine out (OEI), the plane can still be held in a straight path with sufficient directional control. The rudder supplies directional control and produces a yawing moment around the z-axis that will counteract the drag produced by the inoperative engine. Since Romulus has two tails, the rudder deflection must total 14° (7° on each) to account for the drag with OEI at .9 of the takeoff speed - well below the rudder maximum deflection of 30°. See Figure 5-7. Romulus must also meet the more difficult requirement of maintaining straight flight with no more than .75 of the available directional control power and no more than 5° of bank with the engine failed at 1.10 times the takeoff speed. The rudder deflection produced by Romulus is 9.3° on each vertical tail - below the maximum rudder deflection again. With the rudder deflected to balance the yawing moment of the engine, a side force is produced that must be counteracted by rolling the plane less than or equal to 5°. This rolling gives a component of weight along the y-axis that can then counteract the rudder sideforce.

In a coordinated turn, the ailerons and the rudders need to be deflected. Because the higher wing has more drag when a plane is rolled, it causes an adverse yaw which needs to be corrected by deflecting the rudder. Romulus met the requirement of sustaining a 30° banked and coordinated turn at cruise speed and altitude because the sectional wing lift coefficient of .470 is much less than the maximum sectional lift coefficient of the wing. In other words, the lift required to generate the turn is less than the maximum lift of the wing.

The next step for Romulus was to develop a bank angle of 30° in two seconds after the controls are applied. During this maneuver, the ailerons are applied to determine the roll response. Romulus was able to meet the specifications, and in fact, Romulus was able to perform the maneuver in 1 second.

Although Romulus will be flying with power off during the landing approach, the aircraft will still be able to stall just before landing. In effect, Romulus will be gliding into the base with wings

level ; the plane itself will be losing altitude. With the c.g. at the forward limit, Romulus only needs an elevator deflection of -2.0° on each elevator. The elevator deflection is so small because the tail incidence angle is already negative. Since the tail angle is negative, a down load on the tail is produced, and thus an effective lift on the wing is produced.

In the event that Romulus encounters a crosswind landing, it must be able to produce a sufficient directional control so that a steady sideslip angle of 10° is developed. A sideslip angle creates a yawing moment. Fortunately, the rudder deflection is 11° on each rudder so that this requirement is met (8° below the maximum rudder deflection).

Using no more than .75 of the lateral control power (ailerons), Romulus is still able to maintain wings level flight in a full-rudder sideslip.

In covering the stability and control requirements, Romulus managed to pass all of the specifications. However, this does not mean that the initial values were used throughout the design. The stability of the plane depended heavily on the aerodynamics and weight of the plane. Changes were constantly being made to accomodate the c.g. locations given by the weights division. In the final design, the horizontal and vertical tails were reduced to accomodate the structures and weights divisions.

References

1) Mark D. Maughmer and Dan M. Somers, "Design and Experimental Results for an Airfoil for a High-Altitude, Long-Endurance, Remotely Piloted Vehicle," The Pennsylvania State University, University Park, PA.

2) Abbott, Ira H. "Theory of Wing Sections," 1949, Dover Publications Inc., New York, NY.

3) McCormick,"Aerodynamics, Aeronautics, and Flight Mechanics," 1979, John Wiley and Sons, Inc., New York, NY.

4) Roskam,Jan , "Methods For Estimating Stability And Control Derivatives of Conventional Subsonic Airplanes," University of Kansas, Lawrence, Kansas

5) Jones, Bradley, M.S. , "Elements of Practical Aerodynamics," 1939, John Wiley and Sons, Inc., New York, NY

FIGURE 5-1 - CAMBERED VERTICAL TAIL

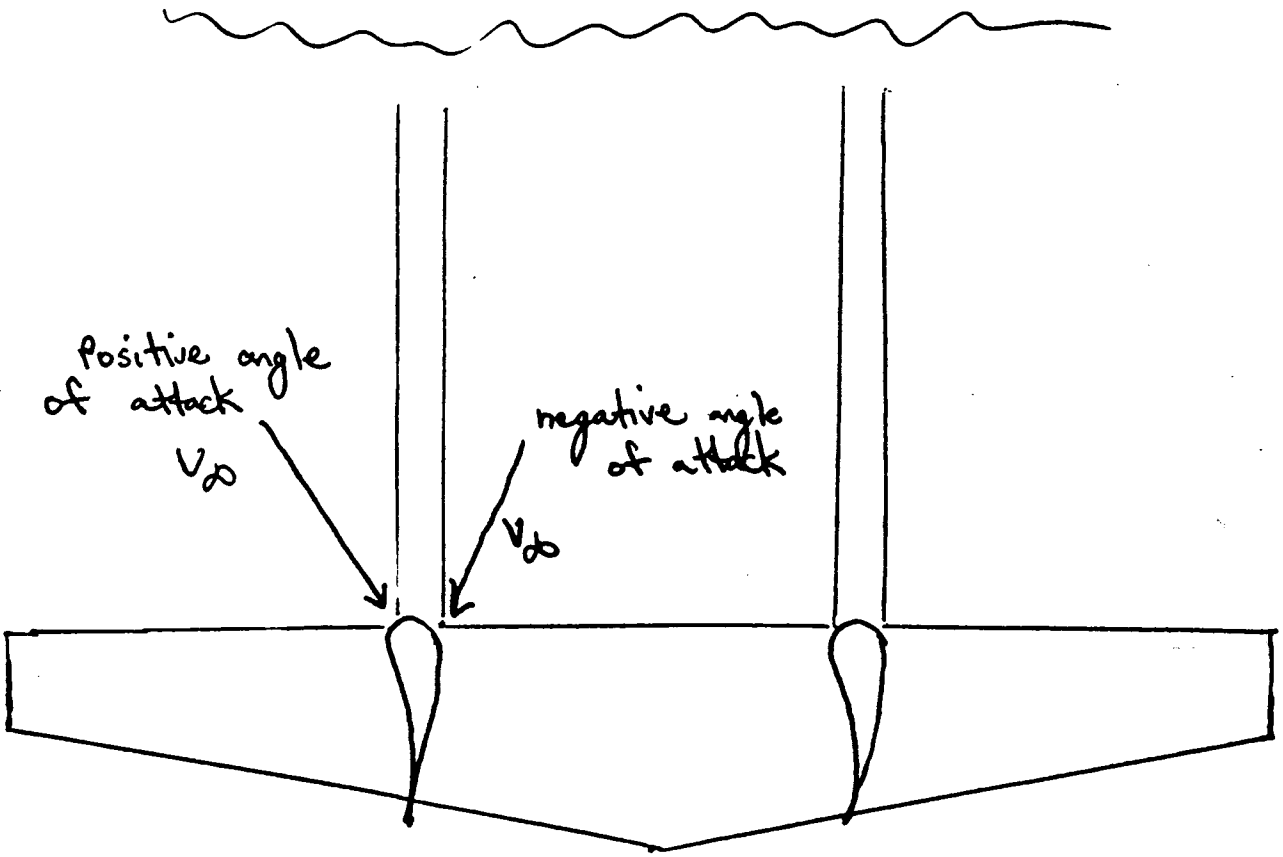

Negative angle of attack is unwanted.

FIGURE 5-2 - DESCRIPTION OF S.M.

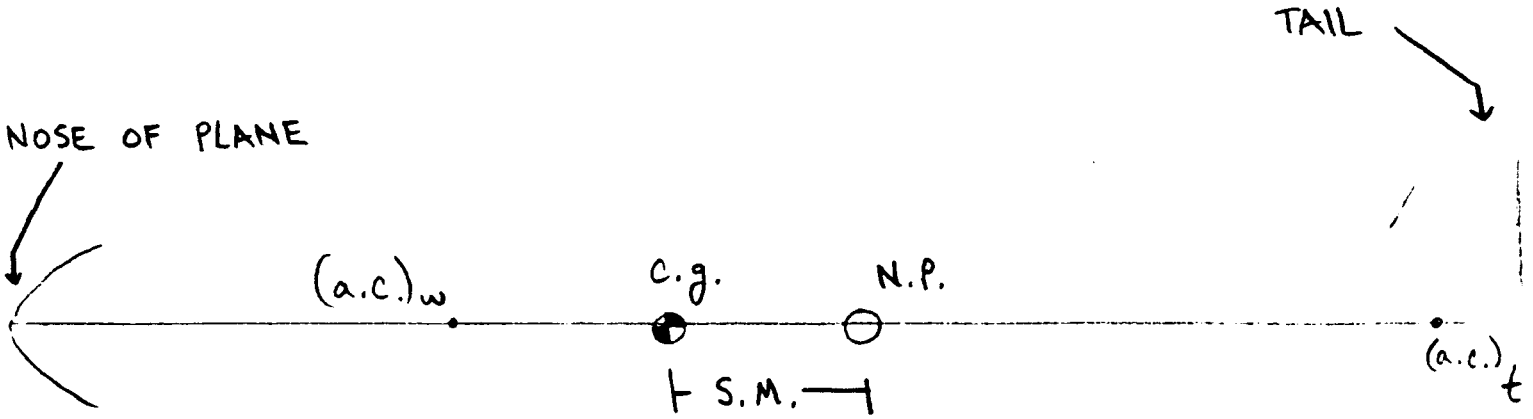

FIGURE 5-3 - IGE EFFECTS

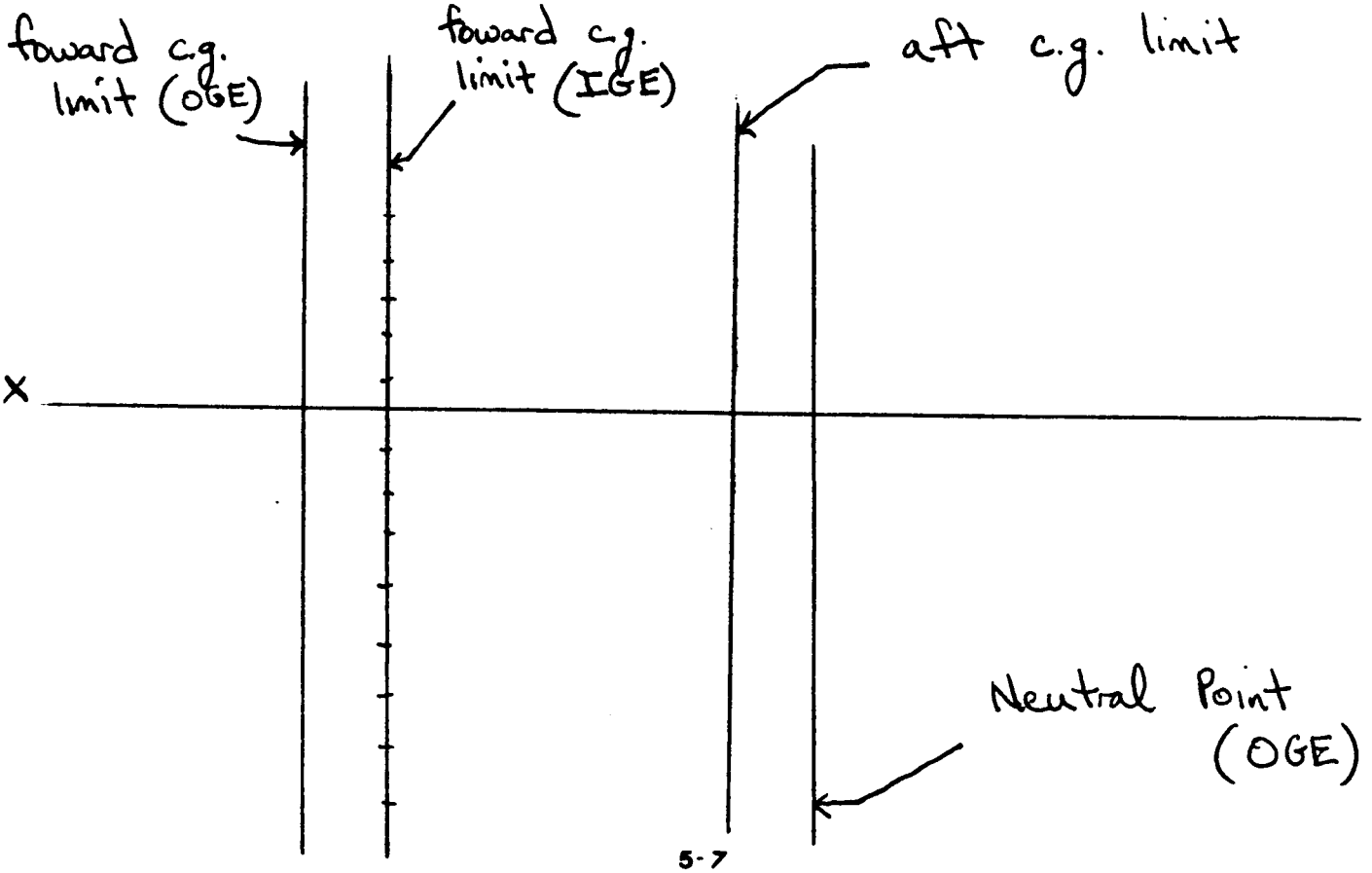

FIGURE 5-4 - C.G. RANGE

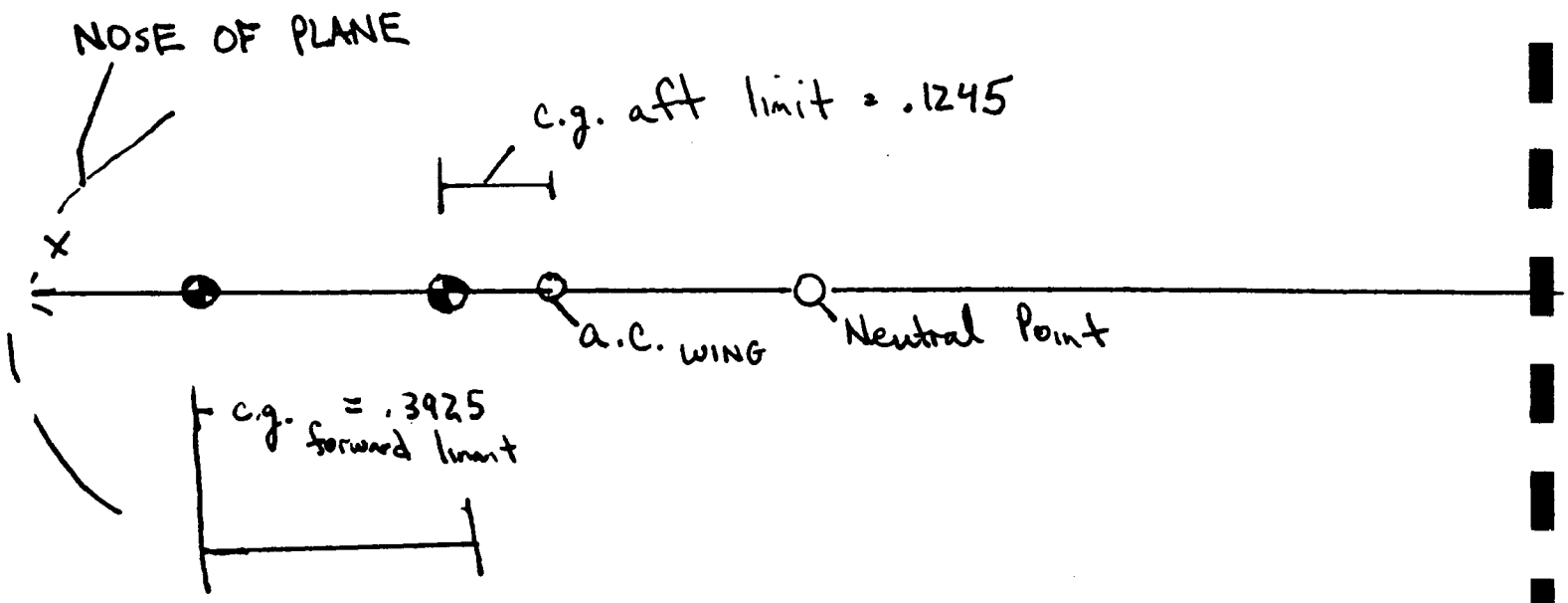

FIGURE 5-5 – C_M VS. C_L

$C_{m_{STABILITY}} = -C_{m_{RESTORING\ MOMENT}}$

$C_{m_{\delta_e}} \Rightarrow \delta_{e_0}$; Trimmed value of elevator deflection

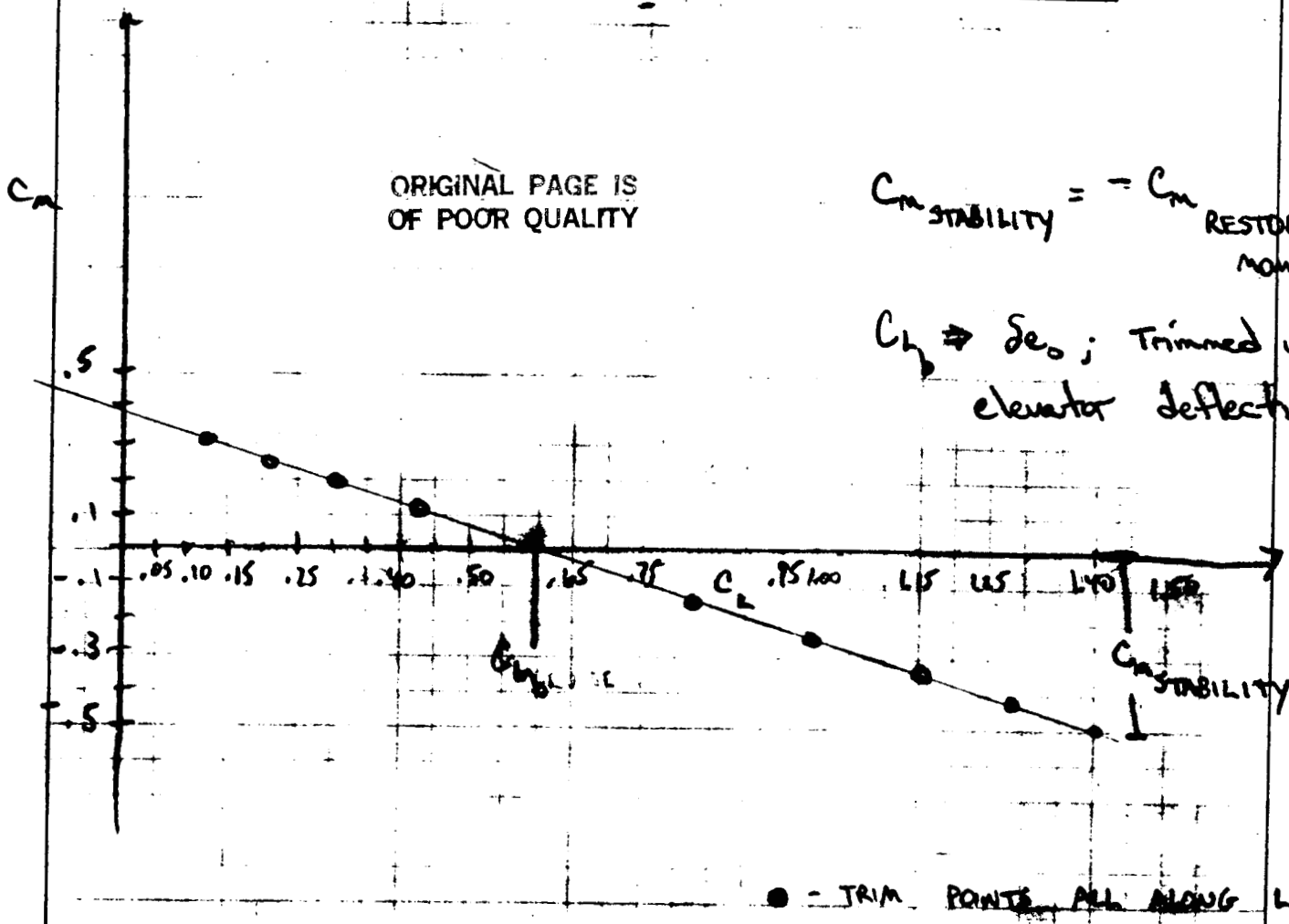

● - TRIM POINTS ALL ALONG LINE

PITCHING MOMENT DUE TO ELEVATOR DEFLECTION

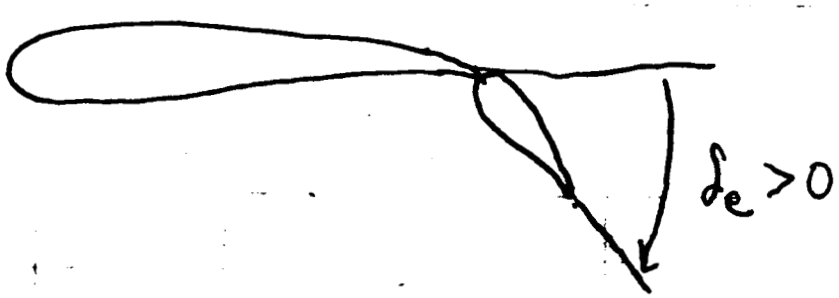

FIGURE 5-5b

TABLE OF SIGNIFICANT DATA

HORIZONTAL TAIL DESIGN

SECTION AR = 12.83 $\quad b = 18.00$ m

$\lambda = C_R/C_T = 2$

$\Lambda = 0^\circ$

$i_t = -3.63^\circ$

$\Gamma = 0^\circ$

VERTICAL TAIL DESIGN

SECTION AR = 1.14

$\lambda = C_R/C_T = 2$

$\Lambda = 0^\circ$

ELEVATOR DESIGN

$b = 5.4$ meters (each one) $\quad \bar{c} = .5$ meters

$\frac{S_e}{S_H} = .17$

RUDDER DESIGN

$b = 1.0$ meter (each tail) $\quad \bar{c} = .5$ meters

$\frac{S_e}{S_W} = .14$

AILERON DESIGN

$b = 8.0$ meters (each one) $\quad \bar{c} = .5$ meters

$\frac{S_a}{S_W} = .20$

FIGURE 5-6A - AXES

I'm NOT A DIE FAN OF PENCIL

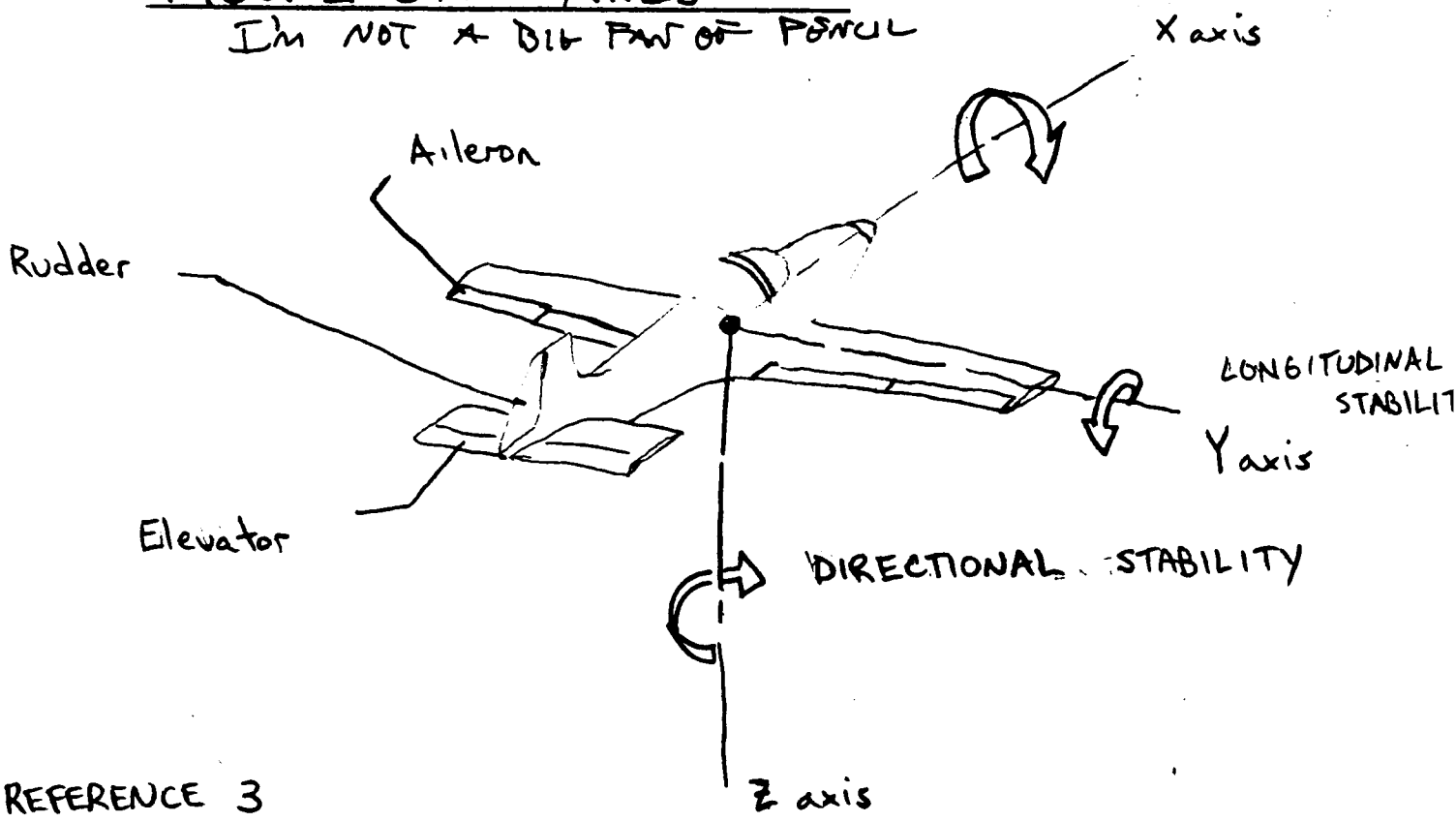

REFERENCE 3

FIGURE 5-6B - CONTROL DESCRIPTION

LONGITUDINAL CONTROL

Elevators provide pitching moment about Y axis

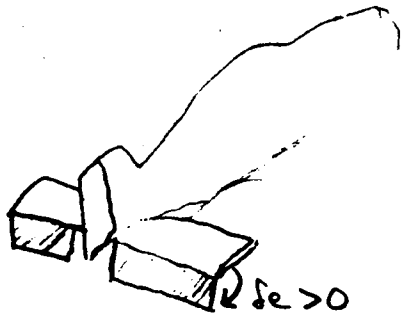

DIRECTIONAL AND LATERAL CONTROL

Ailerons provide rolling moment about X-axis

Rudders provide direction stability about Z-axis

Y = side force; positive t... righ...

L' = rolling moment; positive right wing dow...

N = Yawing moment; posit... nose right

ORIGINAL PAGE IS
OF POOR QUALITY

ADDENDUM (*)

STABILITY AND CONTROL REQUIREMENTS

CONDITION	REQUIREMENT	PERFORMANCE
1) TAKEOFF ROTATION	$V = .9V_{TO}$ $\Sigma C_{m_{c.g.}} = 0$ c.g. at forward limit	$\delta_e = 6°$
) ONE ENGINE OUT	$V = .9V_{TO}$ zero sideslip full rudder	$\delta_r = .47\delta_{r_{MAX}}$
) ONE ENGINE OUT	$V = 1.1V_{TO}$ at $.75\delta_{r_{MAX}}$ $\phi_{TRIM} \leq 5°$	$\delta_r = .62\delta_{r_{MAX}}$
4) CRUISE - BANKED TURN	$\phi = 30°$ $C_{L_{CRUISE}} = .6$	$C_L = .470$
5) CRUISE - ROLL RESPONSE	30° IN 2 seconds with δ_a = maximum	30° IN 1.0 SECOND WITH $\delta_{a_{MAX}} = 30°$
6) LANDING STALL	Center of gravity = .3925 forward limit $C_{m_{NET}} = 0$ at $\alpha = 7°$	$C_{m_{stability}} = -.494$ $\delta_e = -2.0°$
) LANDING - ROLL RESPONSE	SAME AS CRUISE	
8) CROSSWIND LANDING	$\beta = 10°$	$\delta_r = 21°$ $\delta_r = .70\delta_{r_{MAXIMUM}}$
) LANDING - FULL RUDDER SIDESLIP	$.75\delta_{a_{MAXIMUM}}$	$(C_l)_{.75\delta_{a_{MAXIMUM}}} = .1602 \geq$

R. Seeman 4

FIGURE 5-7 - ONE ENGINE OUT

NO BANK ANGLE

Y_e = Distance to operating engine from c.g.

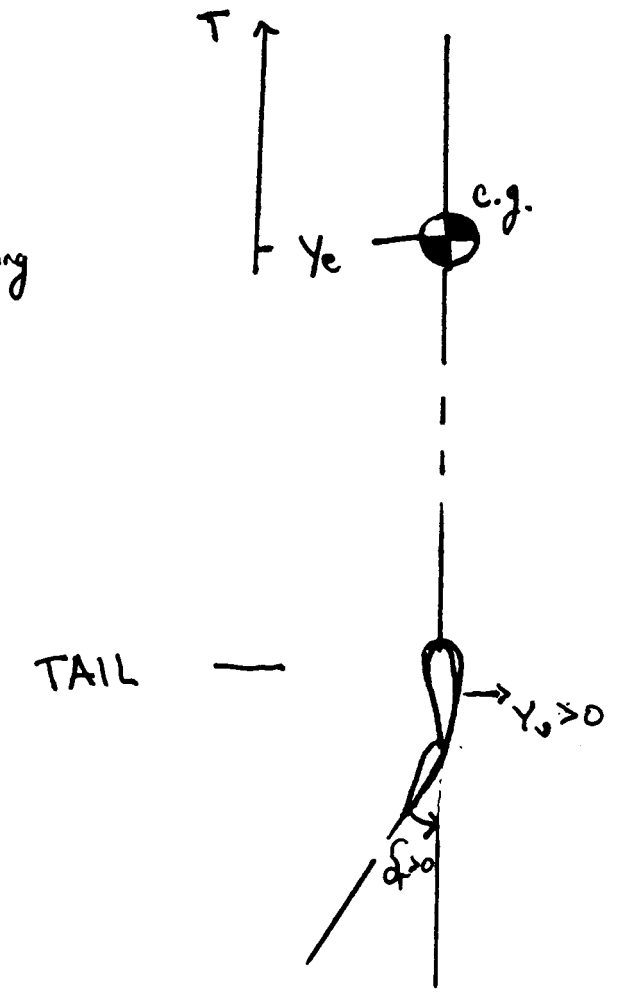

STRUCTURES

Ron Dunn

Structures Overview

The Romulus structures group tasks for developing a Martian based aircraft were five-fold. The first task was to determine the wing loading, shear, torsional moment (about the elastic axis), and the bending moment diagrams for the flight condition which is design determining. Second, a wing loading, shear, and bending moment diagram for the maximum gross weight on the ramp. Third, a discussion of the various materials used and how the Weights and Balance group influenced the decisions. Fourth, a discussion of the methods used to size the Romulus wing. Finally, the airframe structural layout including specialized take-off and landing components developed by the structures group.

Structural Analysis of In-flight Conditions

Romulus will have level flight wing loading of 25.8 N/m^2. This corresponds to a maximum wing loading of 129.1 N/m^2 under the maximum allowable load of 5g's. The aircraft will experience a maximum 5g torsional moment at the root of 15,595 N*m and a maximum 5g bending moment of 5422 N*m also at the root. Figures 6-1a, 6-1b, and 6-1c illustrate how the wing loading, shear, and bending moment behaves along the span in level flight. Figures 6-2a, 6-2b, and 6-2c will be explained in the ramp section. Torsion as a function of span is depicted in figure 6-3.

Obviously, it is the 5g values which yield the most critical information. With a safety factor of 1.5 built in, it was necessary to find materials which could easily withstand the inflated values of shear and moment which a high-g manuver induces. The Romulus structures group have accomplished these goals and the details will be discussed shortly.

Structural Analysis of Ramp Conditions at Maximum Gross Weight

A similiar analysis to the previous section was performed for ramp conditions. The only differences considered were the lack of torsion and the addition of the effects of the extended landing gear. Figures 6-2a, 6-2b, and 6-2c illustrate wing loading, shear, and bending moment as a function of span. Naturally, the maximum values of shear and moment had to be analyzed so that some type of failure, such as creep, would not occur while being stored on the ramp. Since this type of failure is beyond the scope of this group and the magnitude of values did not intuitively seem excessive, it is assumed that ramp conditions are not inherently dangerous. However, in the interest of safety, a stress relieving storage system will be deployed during long term storage. The details of this system can be found in the Maintenance section of this report.

Materials Selection

The key selection parameter in the choice of materials was weight. Table 6-1 shows the density of the materials selected for Romulus.

Material	Density (N/m^3)	Yield Strength (KSI)
GR(HMS)EP (0/45/90) (Ref. 1)	5569.9	240
Al (2219-T857) (Ref. 1)	9313.5	57
Al 7178 (Ref. 2)	9313.5	88
Spruce (Ref. 3)	1369.7	61
Birch plywood (Ref. 3)	2556.6	64
Kevlar-49	79.3	180 (Ref. 4)

Table 6-1. Densities of Romulus materials.

With the advent of composite materials it is not surprising to see such materials as graphite/epoxy and aluminum alloys as primary materials. Since high strength and stiffness is required for spars, graphite/epoxy with its $4.8X10^{11}$ N/m^2 modulus will be the material of choice for the spar. Romulus will have tubular spars manufactured by wrapping preimpregnated carbon/epoxy strings in helical layers on a varying cross-section aluminum tube. The composite will then be cured followed by chemically etching out the aluminum.

While very few materials can match the structural integrity of graphite/epoxy and aluminum, wood also has significant structural benefits. Spruce, a major material in Romulus' ribs, exceeds many

of the mechanical properties of aluminum (except for stiffness) and weighs only 15% as much. (Ref. 4) Similiar characteristics are exhibited by birch. Therefore, combining these two woods results in a significant weight savings. Figure 6-4 illustrates a typical rib cross section constructed of the above materials. Additionally, since NASA has used these types of wood for high altitude earth flight where the climate is similiar to Romulus' Martian climate, spruce and birch are further justified for structural materials.

Finally, a decision on the skin for Romulus was chosen. The materials are kevlar, mylar,and dacron. The choice of kevlar as the primary skin, especially in the wing, was due to kevlar's higher resistance to crack propogation.

The advantages of these materials are apparent in the final weight breakdown. The results for the major components, in terms of weight, are listed in the Weights and Balance section of this report.

Wing Structure Sizing

A variety of criteria were used in the sizing of the wing with failure criteria being the most critical. A prime candidate for failure, especially in high load situations, is the relatively long spars in Romulus. A qualitative approach to reduce the risk of buckling is to effectively make the spar "shorter". This is naturally achieved since the aircraft must be broken down for transport. The effect of the segmented spar is to increasing the load needed for critical buckling according to the Euler theory. Additionally, styrofoam biscuits will be placed inside the hollow spars at the rate of 2/meter. The

biscuits will reduce the chance of local warpage thus further increasing the load needed for buckling. Biscuits will also be used extensively in the area of the engine in order to act as vibrational dampers.

The spars will also have additional strength by virtue of being connected to many ribs. Figure 6-4 depicts the method of attachment of the spar to the ribs. However, the analysis of this coupling was beyond the analytical capabilities of this group. Therefore the primary area in which failure analysis was performed occured by utilizing the torsional analysis of thin-walled cylinders theory. A preliminary value indicated that a spar of at least 0.5mm would be sufficient to prevent buckling. Although this number is valid for a section, it is assumed that an entire spar with this thickness would not be applicable. Therefore, a final 5% thick spar (upper limit of thin wall torsion theory) with a radius of .13m at the root and linearly tapering to 0.09m at the tip was analyzed. This resulted in a $4.64X10^7 N/m^2$ stress which is tolerable by the spar material. A similiar analysis was performed on the secondary spar. This spar is also 5% thick and tapers from 0.08m to 0.07m and exhibits a $1.98X10^9 N/m^2$ stress under load. Each analysis assumed a 1.5 safety factor and assumed each spar carried the full amount of torsion in the wing. Although the above method seems ultraconservative, it should yield a failure free spar.

? .26 m .026m .013m IT WOULD BE NICE TO SEE IT!

Airframe Structural Layout

The details of the airframe structural layout are illustrated in Appendix 6-A.

Conclusion

It should be noted that the above discussiions are the resutls of detailed analysis. However many assumptions were made and consequently many areas were just briefly mentioned. The foremost topic was skin allocation. Since this group was unable to trully analyze skin properties, the design was primarily borrowed from current designs that high-altitude earth aircraft employ and assumed applicable to Romulus.

Plates and bulkheads analysis were also essentially ignored. They are simply mentioned in an attempt to emphasize the need for extra reinforcement. Only the braces are shown in Appendix 6-A so that a mass of solid areas does not distract from viewing the drawings.

Finally, the mechanics of Romulus are also assumed. Althought many items are accounted for in terms of weight (i.e. actuators, plumbing, etc.) they are not depicted in any of the views. The primary assumption was that since Romulus' wing is nearly thirty inches thick, more than sufficient room is available for mechanical devices.

References

1) Armstrong, H. H.: Organic and Metal Matrix Composites for Spacecraft Applications. SAMPE Quarterly, January 1978, p. 18.

2) Materials Selector: Materials Engineering. December 1986, p. 73.

3) Hall, David W.: Structural Sizing of a Solar Powered Aircraft.

4) Clarke, Victor C.: A Mars Airplane? AAE 241 notes, copyright 1988.

FOLDOUT FRAME

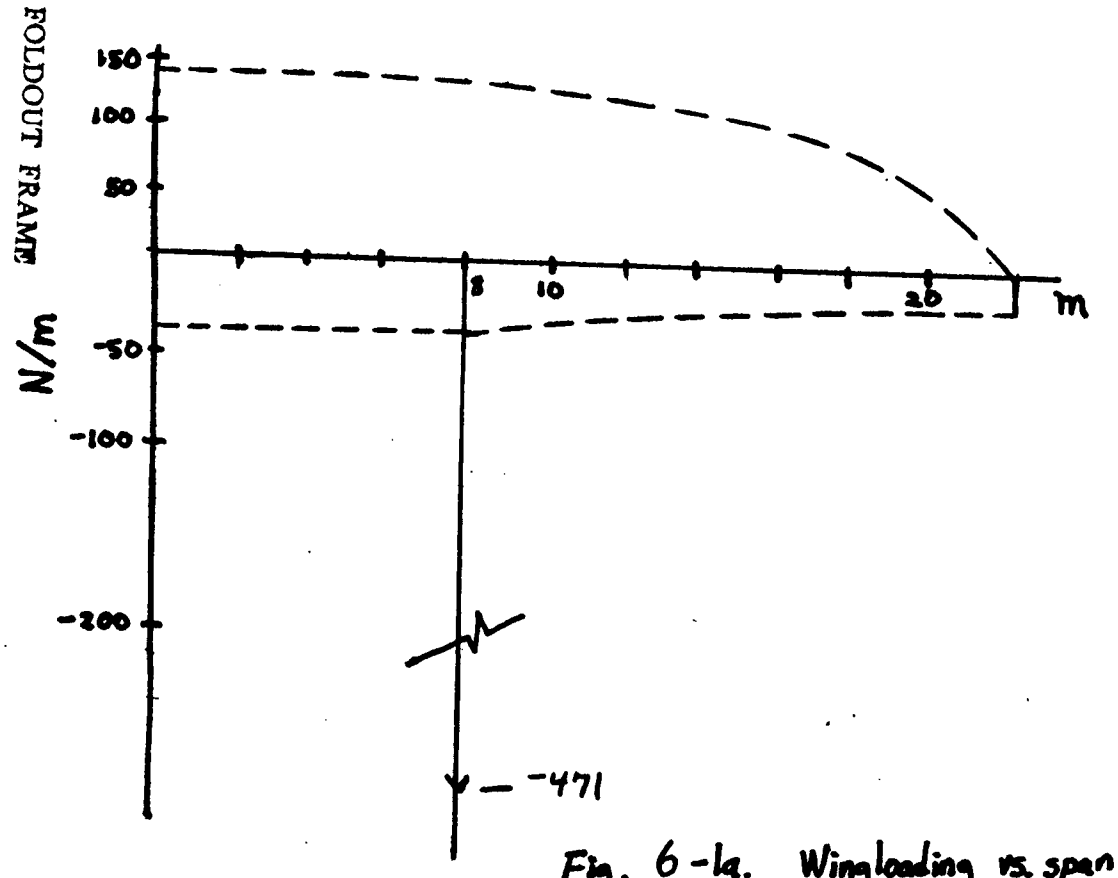

Fig. 6-1a. Wingloading vs. span for level flight.

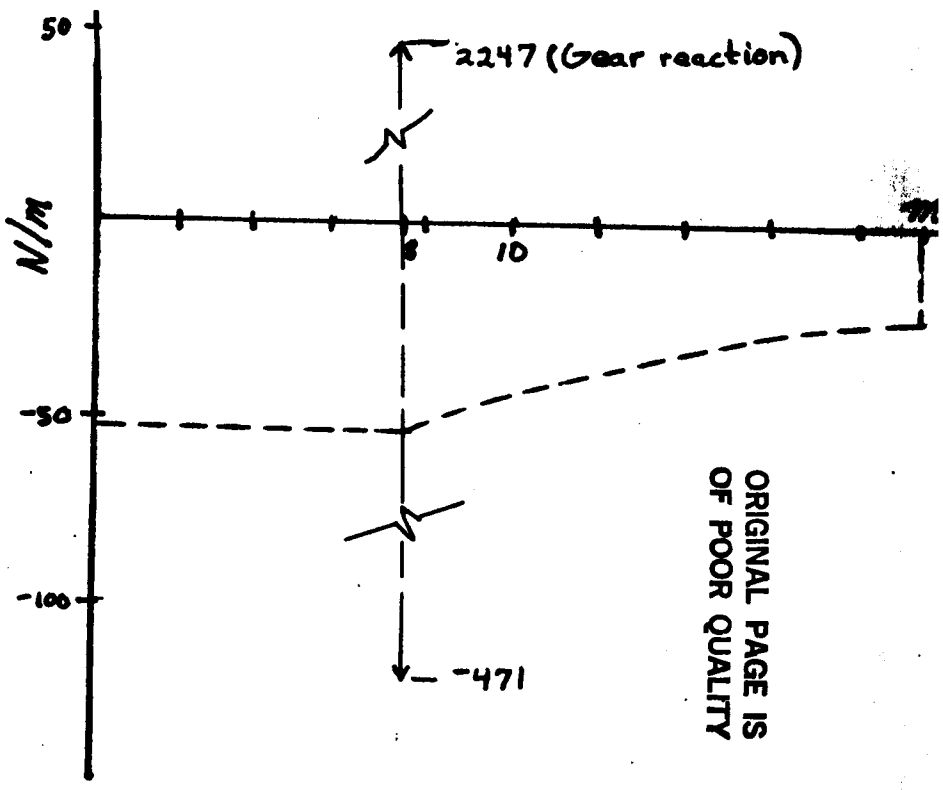

Fig. 6-2a. Maximum gross weight loading on the ramp.

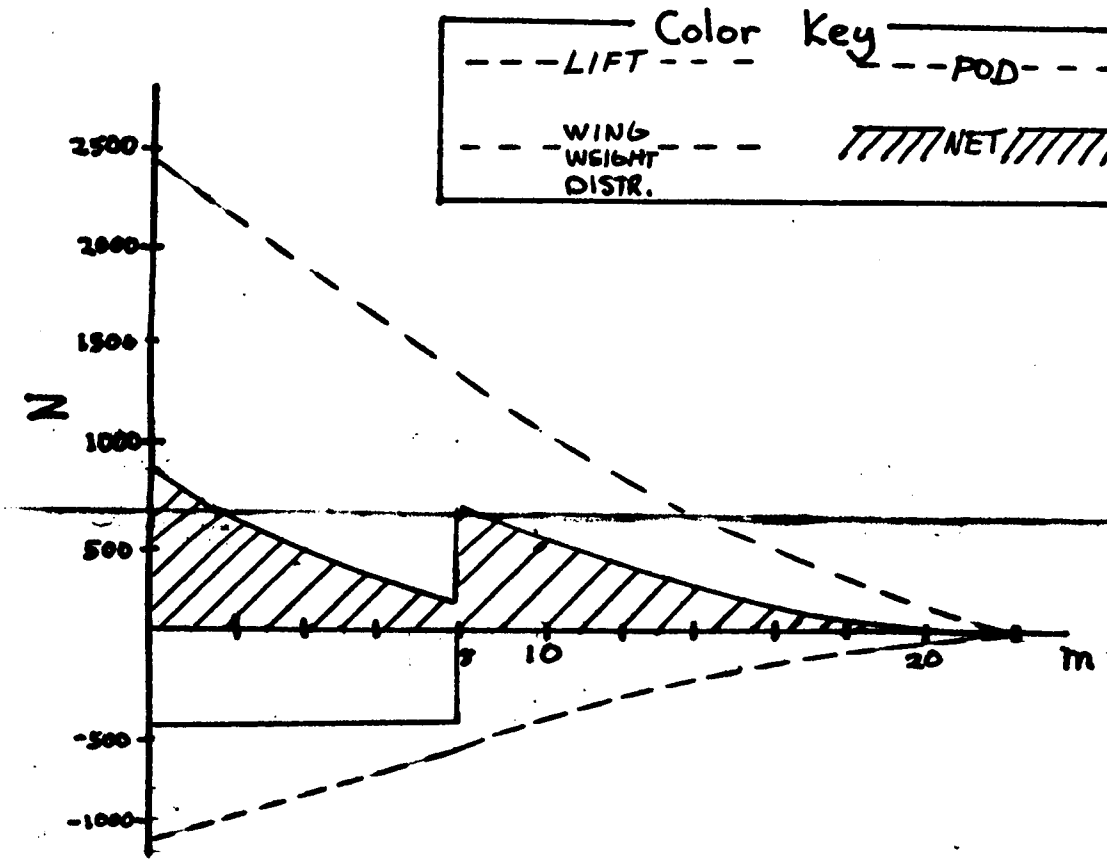

Fig. 6-1b. Shear vs. span for level Flight.

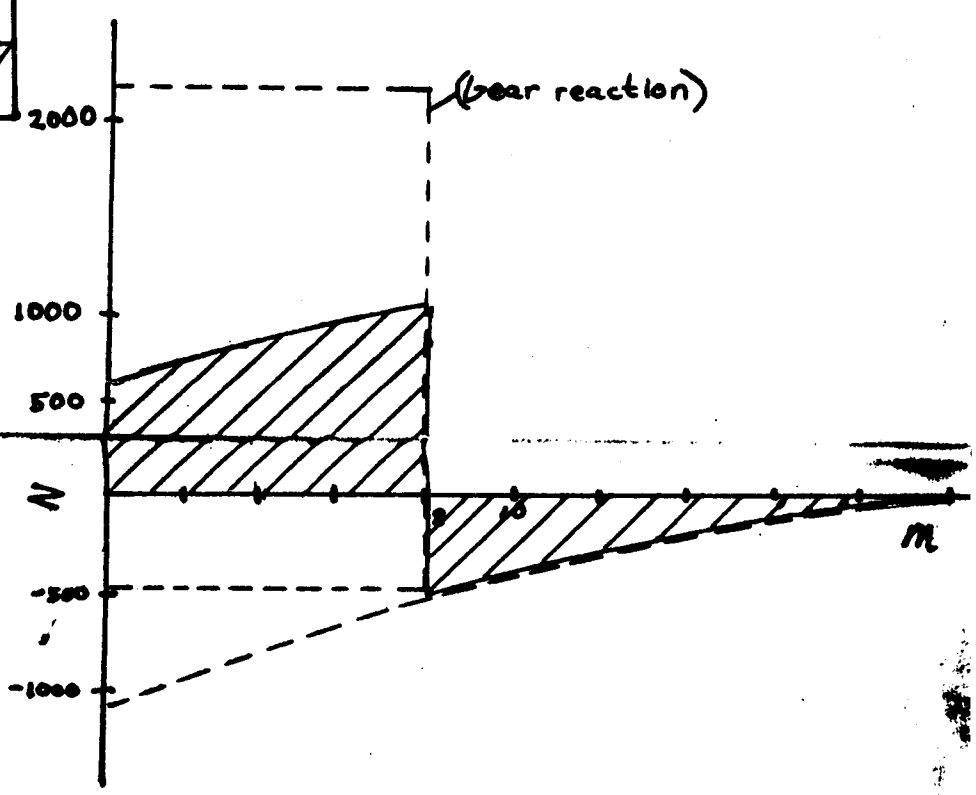

Fig. 6-2b. Maximum gross weight shear on the ramp.

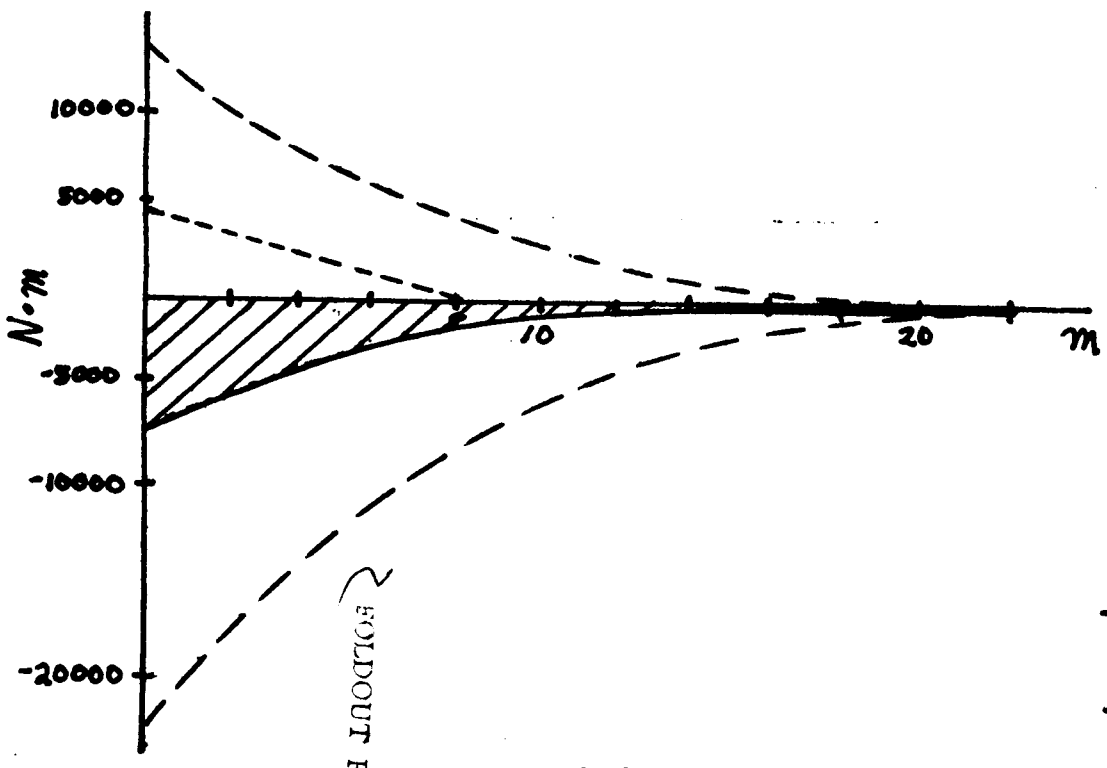

FOLDOUT FRAME

Fig. 6-1c. Moment vs. span for level Flight.

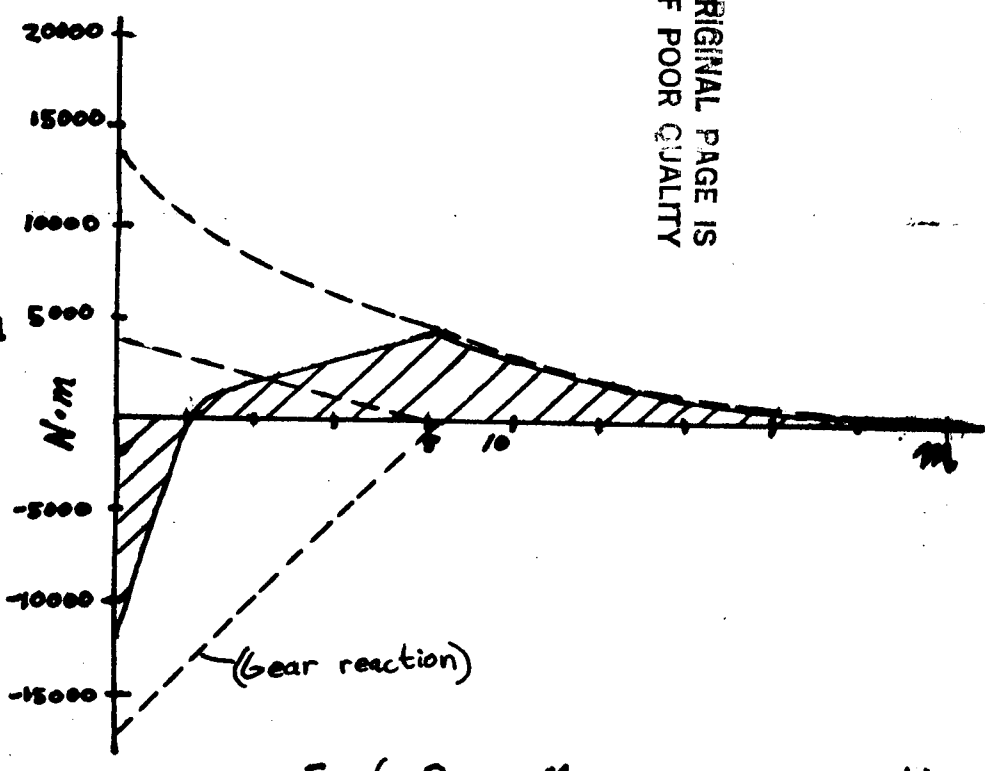

Fig. 6-2c. Maximum gross weight moment on the ramp.

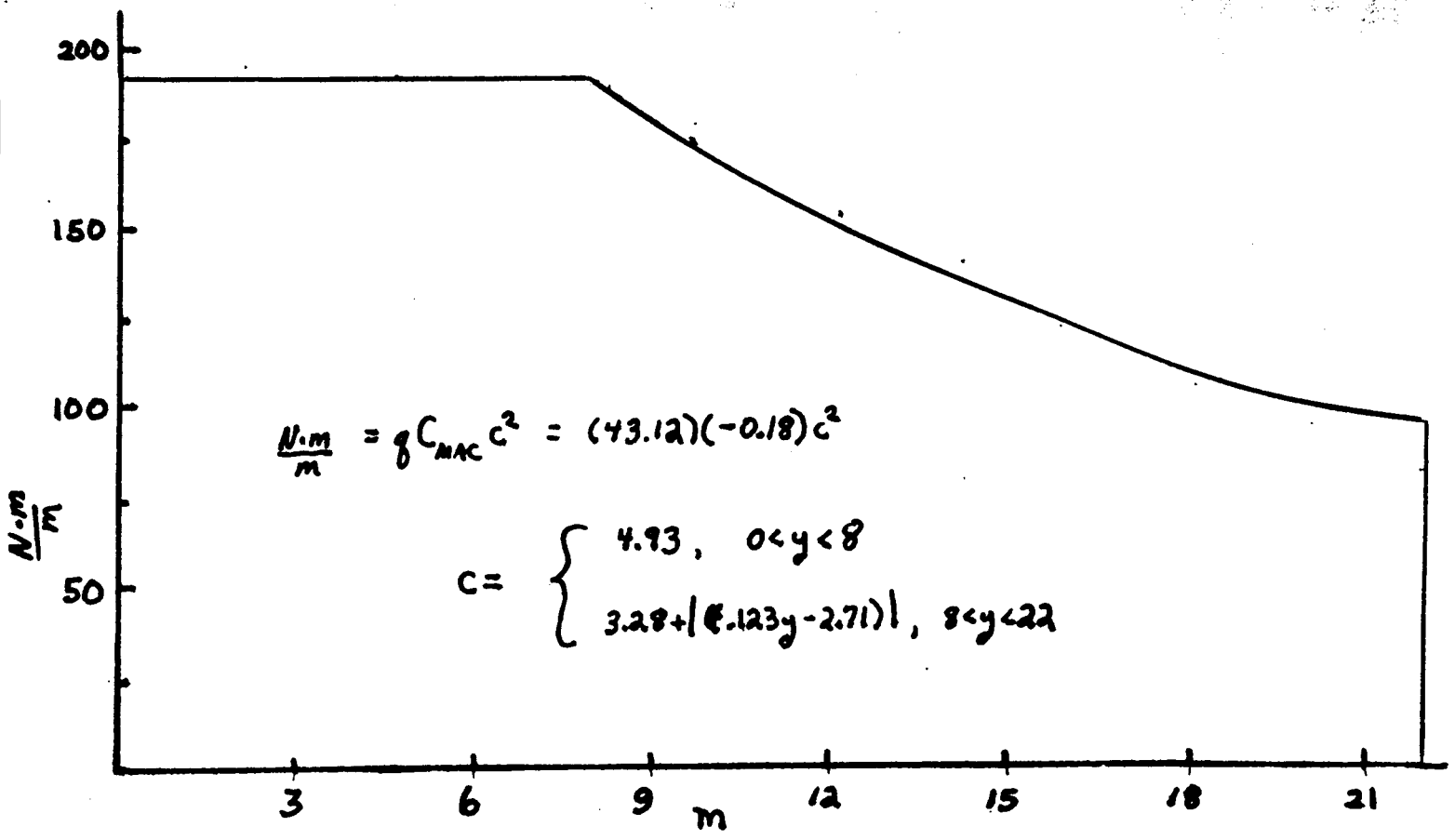

Figure 6-3. Torsional moment about the elastic axis.

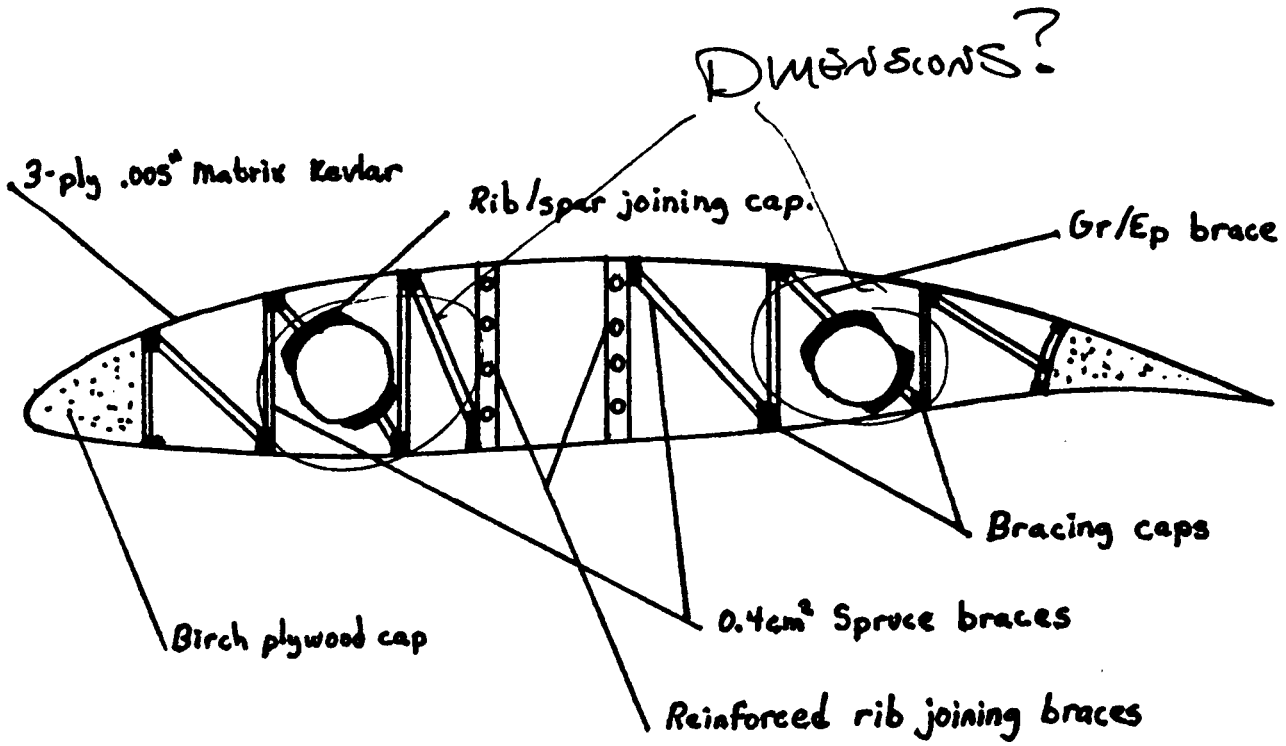

Figure 6-4. Rib construction detail.

Appendix 6-A

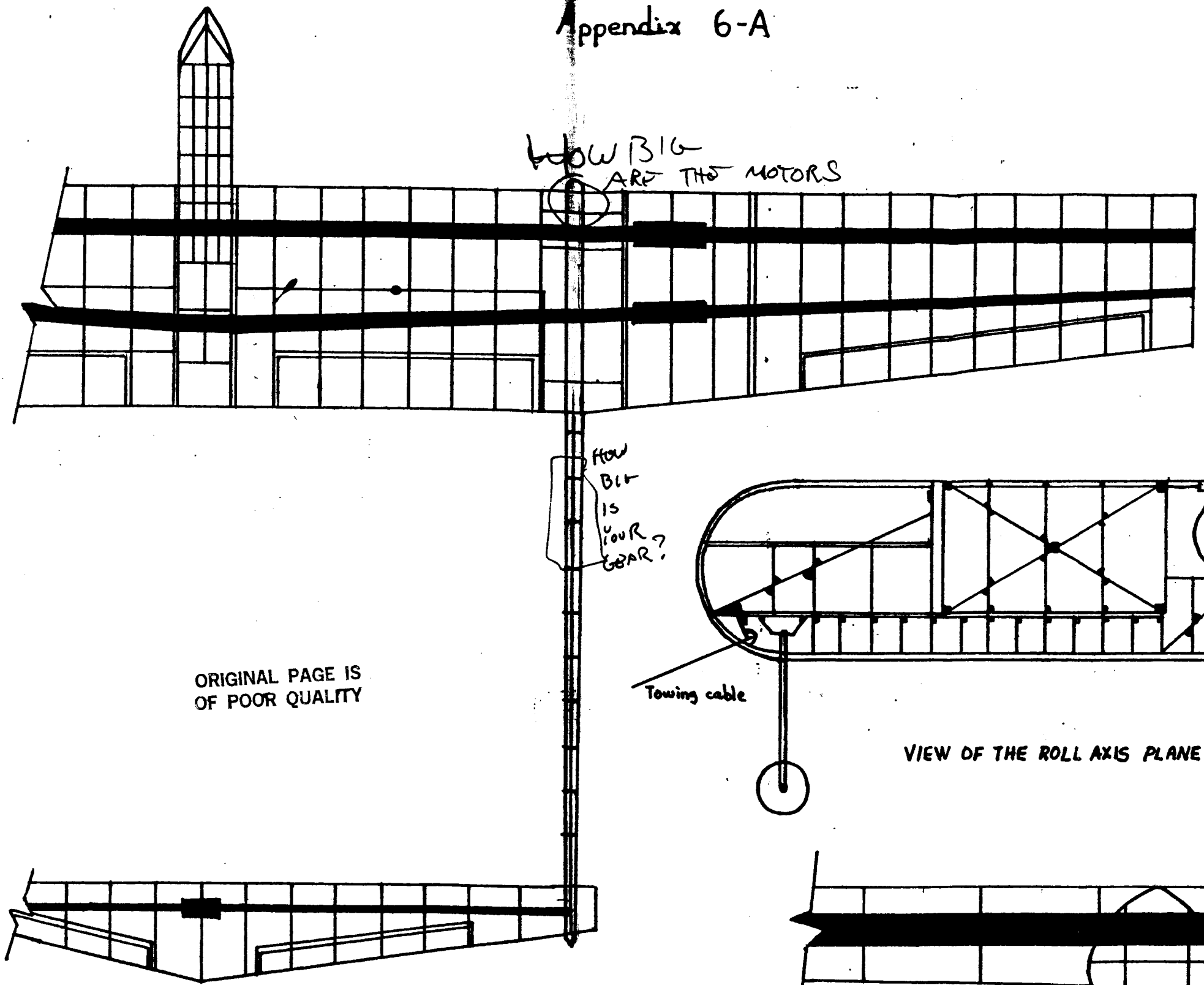

FOLDOUT FRAME

VIEW OF THE ROLL AXIS PLANE W/OUT WING

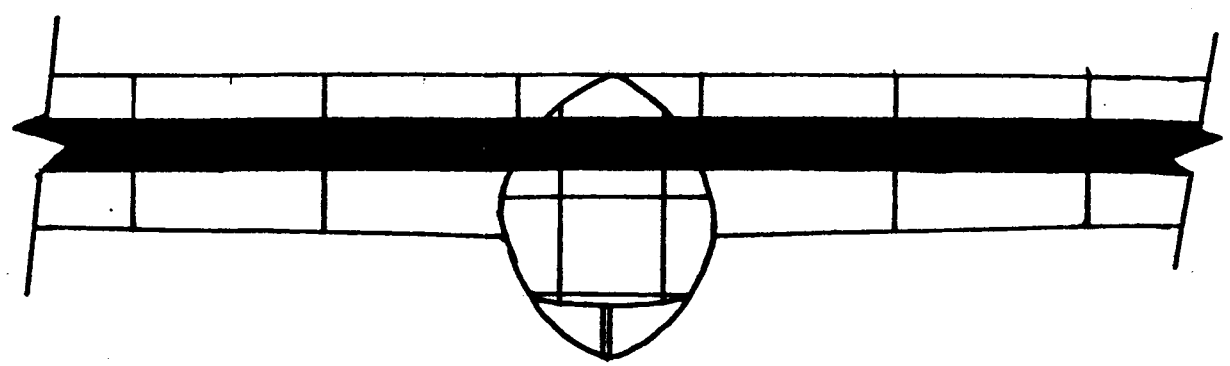

FOLDOUT FRAME

Surface Operations

Martin Kim

Many previous problems associated with the take-off and landing, TOL, performance were finally handled and worked out. A feasible high-lift device was designed and incorporated into the airfoil. Finally, the sizing of the landing gears and their placements were calculated. Also, other minor areas of interest were dealt with.

Initially, a conventional TOL with flap deflection was carefully investigated. Attempting to take-off conventionally with flaps within the required one kilometers of runway was found to be impossible. The best minimal distance possible was 2200 meters. Therefore, other alternatives were investigated for taking off. The obvious solution was a vertical take-off scenario. Unfortunately, it was found that the weight such a system added was infeasible for the Romulus airplane design goal. An assisted take-off was needed without adding any weight to the airplane. A simple solution was found when the take-off scenario of a glider was investigated. Gliders are usually towed into the air by airplanes or by ground vehicles. Hence, tow the Romulus down the runway with rockets, see Fig. 7-1. Rockets were chosen because they provided the needed thrust to take-off in Martian atmosphere. It was calculated that a thrust of 5000 Newtons (N) will be enough for take-off. Viking rockets were chosen for its performance and availability. One rocket produces 2500 N of thrust and it was not too large or heavy. A towing vehicle was designed, Fig. 7-2, using two rockets producing the needed thrust. It has a 50 meter cable that keeps the airplane far behind the heat produced by the rockets. The towing vehicle is radio controlled. Once the Romulus is prepared for take-off, the rockets are turned on and the vehicle begins to tow. During the transition stage of the take-off, the propellers will be turned on as soon as it clears the ground. It was estimated that 6 seconds are needed for the propellers to reach maximum power after being turned on. Therefore, it was found that a total of 10 seconds were needed before the cable can be unhooked from the plane in the

transition to climb stage. Upon release of the cable, the plane will have enough power to climb to the desired altitude and clear the 15 meter obstacle. At the same time, the rockets on the vehicle will be turned off and the vehicle will be caught in a net at the end of the runway. The vehicle is then serviced and prepared for the next take-off.

The G-force experienced by Romulus during the towing was found to be 2.7-G's. The structures group found that the plane can handle at least 5-G's of force during cruise. Therefore, no structural damage will be caused by the towing of the plane. With all this in mind, the total take-off distance with a 15 meter obstacle was calculated to be 892 meters with a climb angle of 4 degrees. The stall speed was 48.6 m/s and the lift-off velocity was 53.5 m/s.

High-lift systems were extensively analyzed for use during the landing. Plain flaps were chosen for its simplicity in design and lightness in weight. In the initial sizing, a flap chord to wing chord ratio, c_f/c, of 0.20 was used. This did not produce the necessary drag for landing within the 1000 meter limit. It was found that a c_f/c ratio of 0.30 will be suitable. The span of the flaps were 6 meters long. The ratio of flap area to wing area was 0.3049. A flap deflection of 45 degrees was used. Table 7-1 lists the change in coefficients of lift, maximum lift, and drag due to flap deflections. The stall speed produced was 43.1 m/s, the approach speed was 56 m/s, and the touch down speed was 49.6 m/s^2. The drag was 4516.17 N and the lift was 3659.47 N which produced a deceleration of 3.83 m/s . The total landing distance was 676.6 meters. A conventional landing with flaps can be achieved without the need for external assist.

The next area of interest covers the TOL gear design. The locations of the gear placements are shown in figure 7-3. The method of calculations were found in reference 1. The main gears are located 6.1 meters from the tip of the nose and 8 meters out from the center of the fuselage. The nose gear is at 0.5 meters from the tip of nose. All the gears are 2.2 meters long from the vertical center of the plane to the center of a 15 inch diameter wheels. This distance mainly depended on a 12 to 15 degree allowance for the clearance of

the tail. The clearance for the propellers was not a concern since the propellers will be locked horizontally during taxing and TOL. The main gears will retract into the underside of the booms. The nose gear will retract under the cockpit into the fuselage. The weight of the whole system is less than 150 N. The maximum static loads on each main gears are 2187.5 N. The maximum and minimum static loads on the nose gear is 1092.85 N and 625 N respectively.

Finally, the plane will be taxied by a towing vehicle from the hanger to the runway and back since the plane was not designed to taxi on its own. Once the plane is ready on the runway, a step ladder will be placed for the pilot to get in and out of the plane. All servicing of the plane will be handled by the maintenance and servicing department in the hanger. A detailed report on this is found in the auxiliary section.

In conclusion, it was a challenging task for the surface operations group as it was for all other groups. Many problems were encountered and interesting and creative solutions were found. The major design philosophy was on basics and simplicity. A summary of results is listed in Table 7-2. All the requirements were able to be met and everything was able to be integrated with the plane as a whole.

References

1. N. S. Curry, Landing Gear Design Handbook, Lockheed-Georgia Company, Marietta, Georgia, 1982

2. DATACOM Material on High Lift Wing Systems

Table 7-1. Change in Coefficients of Lift, Maximum Lift, and Drag Due to Flap Deflections.

$\delta°$	ΔC_L	$\Delta C_{L_{max}}$	ΔC_{D_i}
15	0.5034	0.1944	0.0326
20	0.5424	0.2399	0.0415
25	0.5678	0.2812	0.0521
30	0.6203	0.3143	0.0677
35	0.6762	0.3412	0.0846
40	0.7322	0.3639	0.1044
45	0.7932	0.3805	0.1250

Table 7-2. Summary of Results

Take-off	Landing
5000 N of thrust No flap deflection V_{stall} = 48.6m/s	Power off Flap deflection = 45° V_{stall} = 43.1 m/s
V_{lo} = 53.5 m/s	$V_{approach}$ = 56 m/s V_{td} = 49.6 m/s
Climb angle = 4° S_{tot} = 892 m	Flare angle = 4.8° S_{tot} = 676.6 m
D = 81.79 N L = 1084.86 N	D = 4516.17 N L = 3659.47 N $\bar{a}$ = 3.83 m/s^2
W_g = 5000 N	

Max. static load on each main gear = 2187.5 N
Max. static load on nose gear = 1092.85 N
Min. static load on nose gear = 625.0 N
Estimated weight of gear system = 150 N

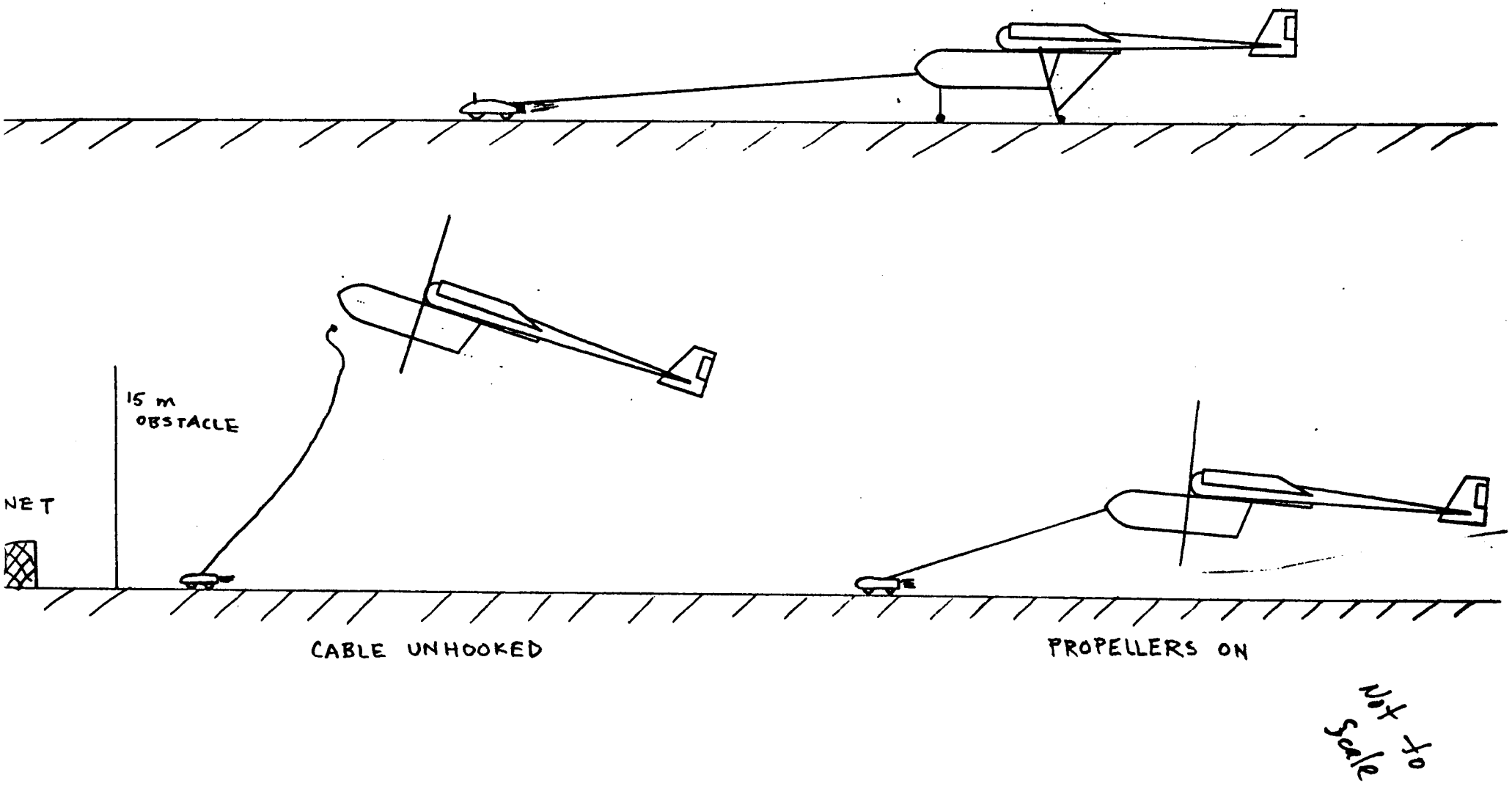

Figure 7-1. Take-off Scenario

Figure 7-2. The Romulus Towing Vehicle

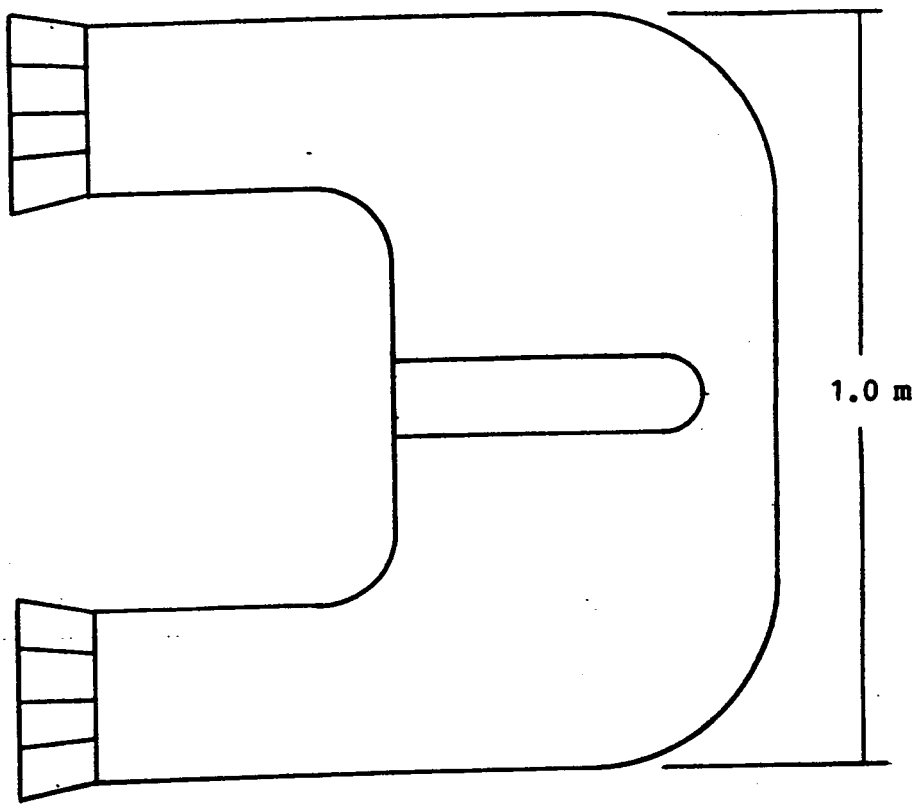

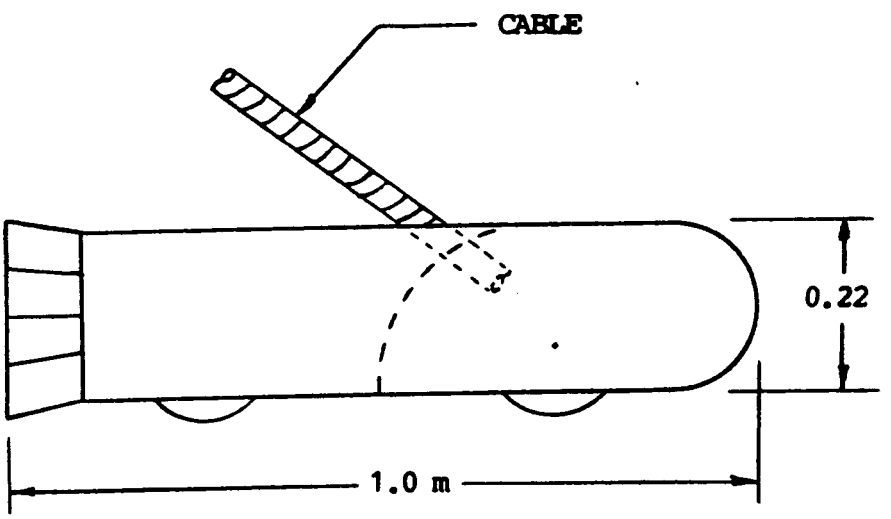

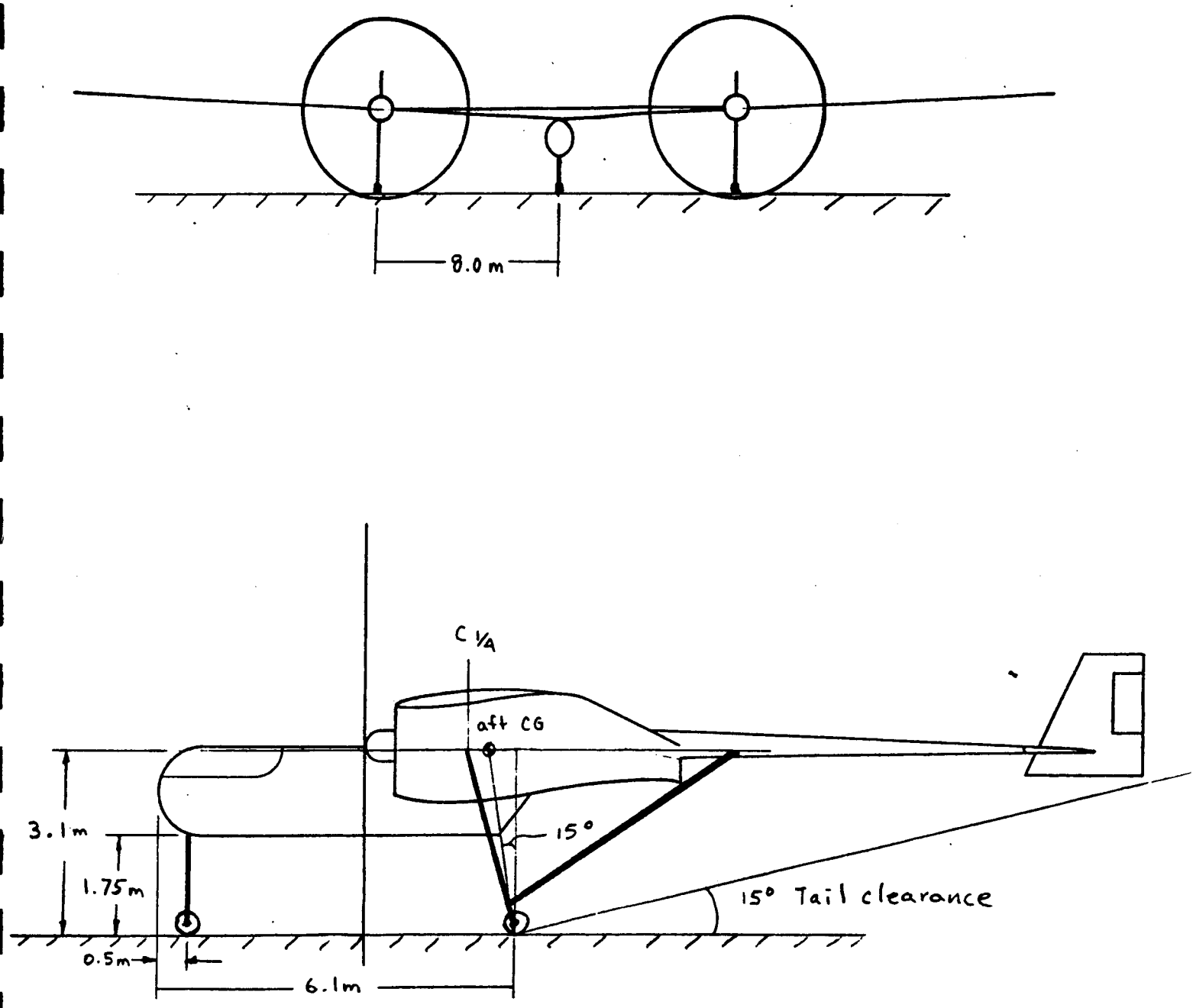

Figure 7-3. Gear placement

WEIGHTS AND BALANCES

SAMUEL HUBER

The Romulus aircraft has mission objectives of flying a 1200 N-Mars payload for eight hours at an altitude of 1500 m. In designing this aircraft, the main consideration was to keep the aircraft as light as possible. The design process led from a crude estimation of total weight to a detailed calculation of all components of the aircraft and center of gravity calculations for all possible configurations.

Various methods can be used to estimate the gross take-off weight of the aircraft. For a first estimation of weight, Lofton's method for estimating gross take-off weight as presented in Professor Sivier's AAE 241 notes was used.(ref. 1) Using 1200N-Mars as the payload weight, useful load fraction of .525, and a fuel fraction of .15, Lofton's method resulted in an estimated gross take-off weight of 3200 N-Mars.

A second estimate of gross take-off weight was made using Roskam's Airplane Design, Part V : Component Weight Estimation . (ref. 2) This method consists of a series of weight formulas that calculate the weights of the various components of an aircraft by an iterative process. After gathering required information from the other group members, Roskam's method was utilized. This method calculated a gross take-off weight of 4250 N-Mars. This weight was used as the target weight.

After actual component weights were found, the actual weight of the aircraft exceeded the target weight by 1200 N-Mars. An increase in composite usage to the maximum extent possible reduced the weight to 4800 N-Mars, but this weight still exceeded the target weight by a significant and unacceptable amount. Examination of the weight breakdown showed that propulsion system

and structural weights were not accurately predicted by Roskam's method. The reason for the failure of Roskam's method is that the method predicts the weight for earth-based general aviation aircraft. The Martian enviroment and operating objectives of the Romulus aircraft are significantly different than those assumed in the formulas used by Roskam. After a group discussion, a decision was made to increase the target weight to 5000 N-Mars.

This target has been met. The gross take-off weight of the Romulus aircraft with full payload is 5000 N-Mars (see table 8-1). The weights of various components were arrived at in various ways. The weight of the wing, fuselage, and nacelle are actual weights calculated from the amount of material used in construction. The weight of the tail was found by the USAF formula as presented in Roskam. (ref. 2) The weight of the tailbooms and landing gear were calculated from methods used in NASA Contractor Report 172313. (ref. 3) The weight of the propulsion system was provided by the propulsion system designer. Avionics and other fixed equipment weights were calculated from methods used in Roskam. (ref.2) The combined weight of all fixed equipment was reduced by 30 percent to account for advanced design and extensive use of lightweight materials. The gross take-off weight of the aircraft with full payload was 4953 N-Mars. An air supply of 47 N-Mars was placed in the cargo area to provide an emergency resevoir in case the plane went down away from the base. This brought the gross take-off weight to 5000 N-Mars.

A note should be made about the extensive use of wood in the Romulus aircraft. The structural properties of wood are comparable to aluminum and carbon-based composite materials in all respects except for stiffness. Stiffness is not a critical property for wing ribs and tailbooms, and the resultant weight savings are significant. The weight of spruce, the material used in the Romulus aircraft, is only 15 percent of the weight of the thinnest aluminum alloy, and 25 percent of the weight of carbon graphite epoxy.

Maximum take-off weight,operating empty weight, maximum landing weight, useful load fraction, and maximum fuel fraction are presented in table 8-2. Maximum take-off and landing weight are the same since the combustion product (water) is kept for reuse.

Center of gravity calculations were made using the weight breakdown of the aircraft and

stability limits as set by the stability and control designer. The center of gravity of the various aircraft components was calculated from information presented in tables 8.1,8.2,and 8.3 of Roskam's Airplane Design, Part V : Component Weight Estimation (ref.2) As can be seen in table 8-3, the center of gravity for all flight conditions is within stability limits. The main landing gear is located 6.1 meters behind the nose. This is .32 meters behind the extreme center of gravity location. The center of gravity in the z-direction shifts down 0.033 meters during a flight with a full payload.

References :

1) Sivier K. R. Aeronautical & Astronautical Engineering 241 Notes
University of Illinois, 1988

2) Roskam, Jan Airplane Design, Part V : Component Weight Estimation
Roskam Aviation and Engineering Corp. , 1985

3) Hall, D.W. and Hall, S.A. Structural Sizing of a Solar Powered Aircraft
NASA Contractor Report 172313 ; NASA Langley Research Center,
Hampton, VA

TABLE 8-1
COMPONENT WEIGHTS AND CENTER
OF GRAVITY LOCATION

COMPONENT	WEIGHT (N-MARS)	%	DISTANCE FROM NOSE (M)	MOMENT (NM)
AIRFRAME STRUCTURE	(2435)	(48.70)		
WING	1300	26.00	5.960	7748
TAIL	300	6.00	15.225	4567
TAILBOOMS	150	3.00	9.130	1369
FUSELAGE	515	10.30	2.800	1442
LANDING GEAR	150	3.00	4.483	672
NACELLE	20	0.40	3.700	74
PROPULSION GROUP	(1210)	(24.20)		
MOTOR	113	2.26	4.500	509
GEARBOX	94	1.88	4.200	395
HYDROGEN	53	1.06	5.019	266
OXYGEN	419	8.38	3.000	1257
FUEL CELLS (ACCESORIES)	205	4.10	3.135	643
(WATER)	(472)	(9.44)	4.545	(2145)
ENGINE CONTROLS	25	0.50	4.500	113
PROPELLERS	301	6.02	3.500	1054
AIRFRAME SERVICES AND EQUIPMENT	(155)	(3.10)		
AVIONICS	38	0.76	0.600	23
ELECTRICAL SYSTEM	20	0.40	3.500	70
FLIGHT CONTROLS	25	0.50	7.430	186
FURNISHINGS	20	0.40	1.750	35
EMERGENGY AIR	47	0.94	5.600	263
BASIC EMPTY WEIGHT	3800	76.00	5.443	20686
PILOT	600	12.00	1.750	1050
PLANE + 1 PILOT	4400	88.00	4.940	21736
CARGO(PASSENGER)	600	12.00	6.300	3780
PLANE + FULL PAYLOAD	5000	100.00	5.103	25516

TABLE 8-2

AIRCRAFT WEIGHTS

MAXIMUM TAKE-OFF WEIGHT	5000 N-MARS
OPERATING EMPTY WEIGHT	3800 N-MARS
MAXIMUM LANDING WEIGHT	5000 N-MARS
USEFUL LOAD FRACTION	.24
MAXIMUM FUEL FRACTION	.0944

TABLE 8-3

CENTER OF GRAVITY RANGES

	WEIGHT (N)	MOMENT (NM)	CENTER OF GRAVITY (METERS FROM NOSE)
EMPTY-WITH FUEL -ON RAMP	3800	20686	5.443
PILOT-ON RAMP	4400	21808	4.940
PILOT & CARGO -ON RAMP	5000	25516	5.103
PILOT-WITH FUEL EXPENDED	4400	22322	5.073
PILOT & CARGO -WITH FUEL EXPENDED	5000	26102	5.220
EMPTY-WITH FUEL EXPENDED	3800	21272	5.598
EMPTY-WITH NO FUEL	3504	19228	5.778

FORWARD STABILITY LIMIT 4.838 METERS FROM NOSE

AFT STABILITY LIMIT 5.349 METERS FROM NOSE

ALL CENTERS OF GRAVITY ARE CALCULATED WITH GEAR IN THE DOWN POSITION. WITH GEAR IN THE RETRACTED POSITION, THE CENTER OF GRAVITY FOR ALL CASES MOVES 0.01 METER REARWARD.

FIGURE 6-1

CENTER OF GRAVITY TRAVEL DIAGRAM

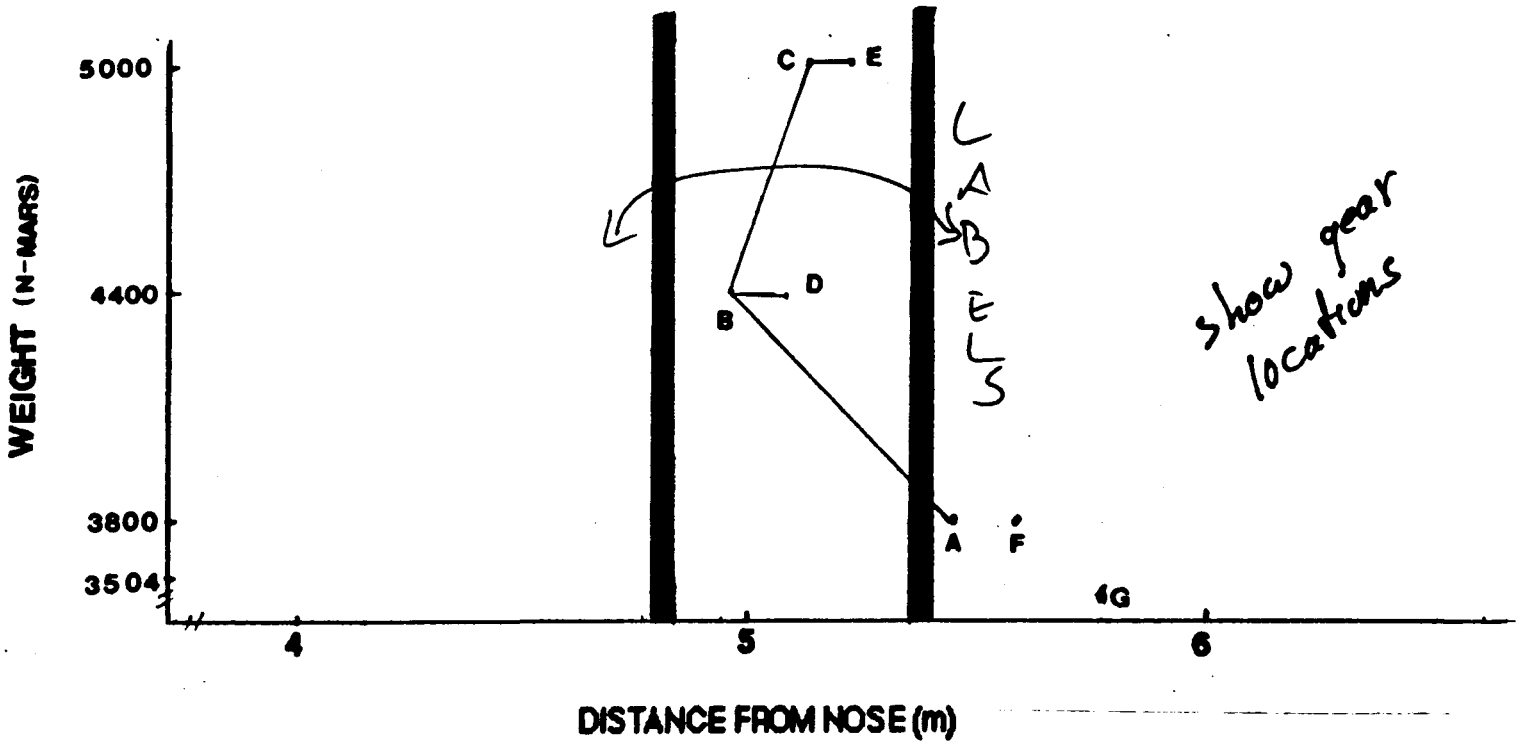

FORWARD STABILITY LIMIT - 4.838 M FROM NOSE
AFT STABILITY LIMIT - 5.349 M FROM NOSE

	CENTER OF GRAVITY (m FROM NOSE)
A - EMPTY WITH FUEL - ON RAMP	5.443
B - 1 PILOT - ON RAMP	4.940
C - PILOT & CARGO - ON RAMP	5.103
D - PILOT - WITH FUEL EXPENDED	5.073
E - PILOT & CARGO - WITH FUEL EXPENDED	5.220
F - EMPTY WITH FUEL EXPENDED	5.598
G - EMPTY - WITH NO FUEL	5.778

MAINTENANCE AND SERVICING ON MARS

Norman Knapp

Between flights the Romulus Aircraft will be towed to a special hanger area for protection and necessary maintenance and servicing. The Romulus will not feature folding wings or a folding tail section, so the hanger will have minimum dimensions which correspond to the aircraft's 44 m wingspan and 20 m tail-to-nose distance. The hanger will be constructed in order to withstand the Martian weather extremes, but it will not be able to contain a pressurized environment. Instead, the pressure and composition of the atmosphere inside the hanger will correspond to conditions outside the hanger. Thus, personnel providing maintenance services for the Romulus will be required to wear protective gear.

Once the aircraft is parked within the hanger, stress relieving supports will be placed underneath the wings in order to keep them from sagging. The water from the fuel cells will be extracted from its holding tank and separated into hydrogen and oxygen by means of electrolysis. The hydrogen and oxygen will then be reused on future flights. Power for the electrolysis process will be obtained from ground based solar arrays. If necessary, scientific instruments will be removed from the cargo area and repaired or replaced. In addition, maintenance will be conducted on major systems such as powertrains, control surfaces, and structures. Necessary replacement parts will be kept on inventory at the hanger. It is important to note that since the mid-point of the aircraft is located 2.5 m off the ground, ladders and scaffolding equipment will be required to conduct much of the servicing.

COST ANALYSIS OF THE ROMULUS AIRCRAFT

SAMUEL HUBER

The cost of development and production of the Romulus aircraft was estimated by the LOTUS spreadsheet program "Planetary Program Cost Model" developed by Science Applications International Corporation. The estimate is somewhat inaccurate because of the inherent differences between aircraft and spacecraft. However, there are several similiarities between spacecraft and aircraft in developing a cost estimate; specifically, the structural and propulsion components are very similiar in terms of cost.

The spreadsheet was utilized by placing the components of the aircraft in the categories shown on the spreadsheet. The Romulus aircraft used four of the seven categories; structures, attitude control and determination, communications and data handling, and propulsion.

The estimate of total costs for development and production of the Romulus aircraft is 223.5 million dollars. This figure is broken down into two main components; 194 million dollars for development design, testing, and engineering, and 29.5 million dollars for production management and support. A detailed breakdown of costs is shown on table 10-1.

Several parameters on the spreadsheet could be varied. These parameters included budget constraints, technical complexity, ability of the design team, and inheritance factors. Various combinations of these factors yielded costs between 205 and 283 million dollars. The 223.5 million dollar figure is based on the common set of parameters used by all design groups.

Raw materials for the Romulus aircraft before fabrication cost approximately one million dollars.

TABLE 10-1

COST CHART FOR THE ROMULUS AIRCRAFT

CATEGORY	DESIGN, DEVELOPMENT, TESTING,& ENGINEERING	PRODUCTION & SUPPORT	TOTAL
STRUCTURES	43.8	12.8	56.6
ATTITUDE & CONTROL	14.6	3.3	17.9
COMM. & DATA HANDLING	5.7	0.8	6.6
PROPULSION	0.5	0.0	0.5
SUBTOTAL	64.6	16.9	81.5
SYSTEMS TEST HARDWARE	26.7	0.0	26.7
SYSTEM TEST OPERATIONS	16.3	0.0	16.3
GSE	13.4	0.0	13.4
SE&I	14.2	3.6	17.8
PROGRAM MANAGEMENT	8.8	1.5	10.3
SUBTOTAL	144.1	21.9	166.0
CONTINGENCY	28.8	4.4	33.2
FEE	17.3	2.6	19.9
PROGRAM SUPPORT	3.8	0.6	4.4
TOTAL	194.0	29.5	223.5

ALL FIGURES ARE IN $(MILLIONS)

Internal Configuration

Samuel Huber

The internal configuration of the Romulus aircraft was designed to maximize cockpit space and cargo space. The cockpit has a length of 2 meters, a width of 1.15 meters, and a height of 1 meter. The seat is similar to a car seat in dimentions and provides a comfortable position from which to operate the aircraft for an extended period of time. The aircraft instruments are placed just below eye level in front of the pilot. A cathode ray tube display adjacent to the instruments can show additional information about the aircraft, flying conditions, or the status of any instruments or experiments in the cargo bay.

The configuration of fuel tanks and cells was designed to minimize total volume and center of gravity shifts in both the x and z directions. The total volume of the fuel tanks and cells is 4.225 cubic meters. The center of gravity of the aircraft with a full payload shifts 0.280 meters in the x-direction and 0.033 meters in the z-direction.

The cargo area, located in the back of the fuselage, has 0.863 cubic meters of volume for cargo or a passenger. A passenger would be seated on the bottom of the fuselage with his back against the rear of the fuselage.

Figure 11.1 shows the internal configuration of the Romulus aircraft, figure 11.2 shows body cross-sections, and figure 11.3 shows the plan view of the aircraft.

FIGURE 11-1

INTERNAL CONFIGURATION

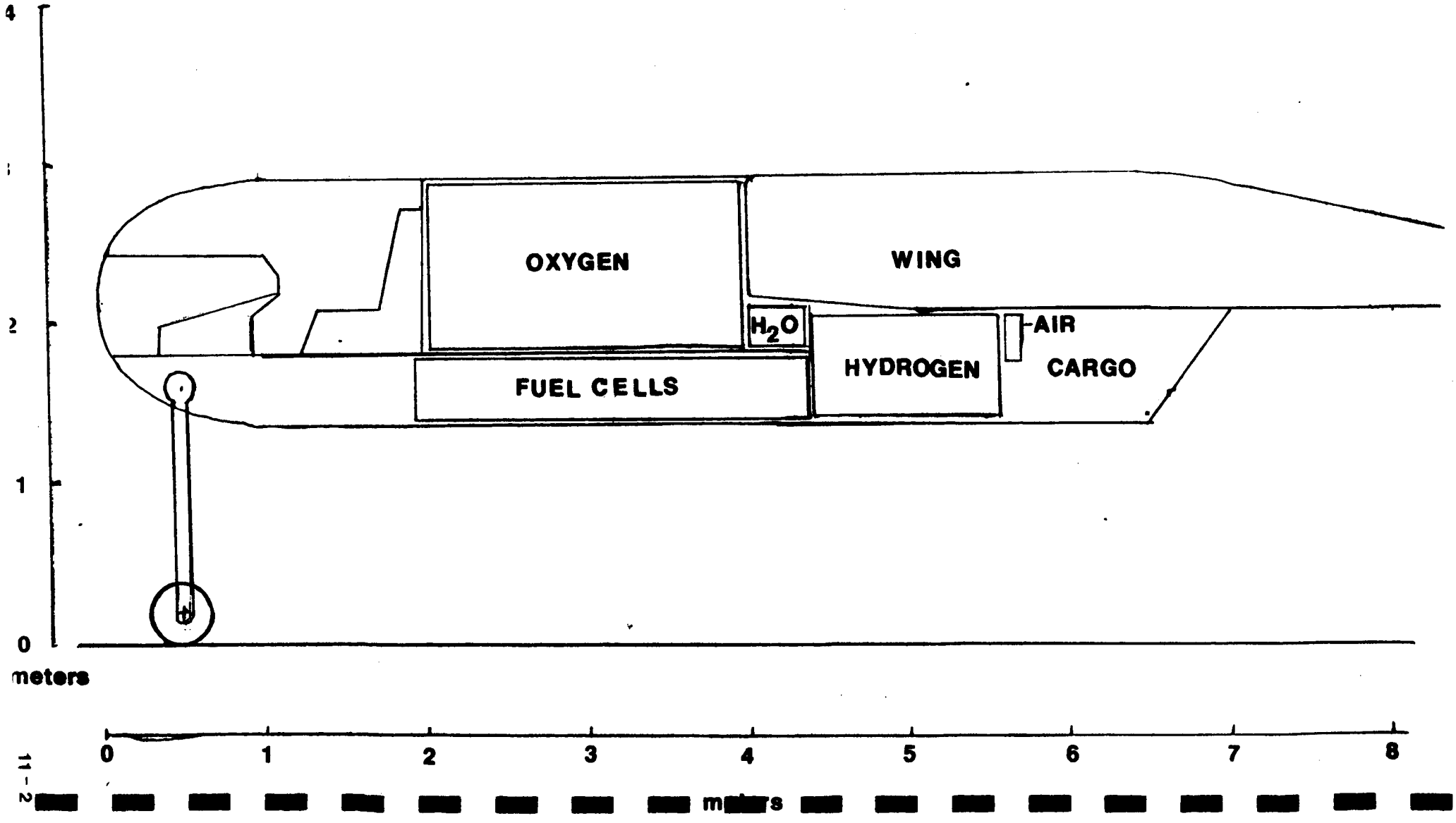

FIGURE 11-2
CROSS SECTIONS

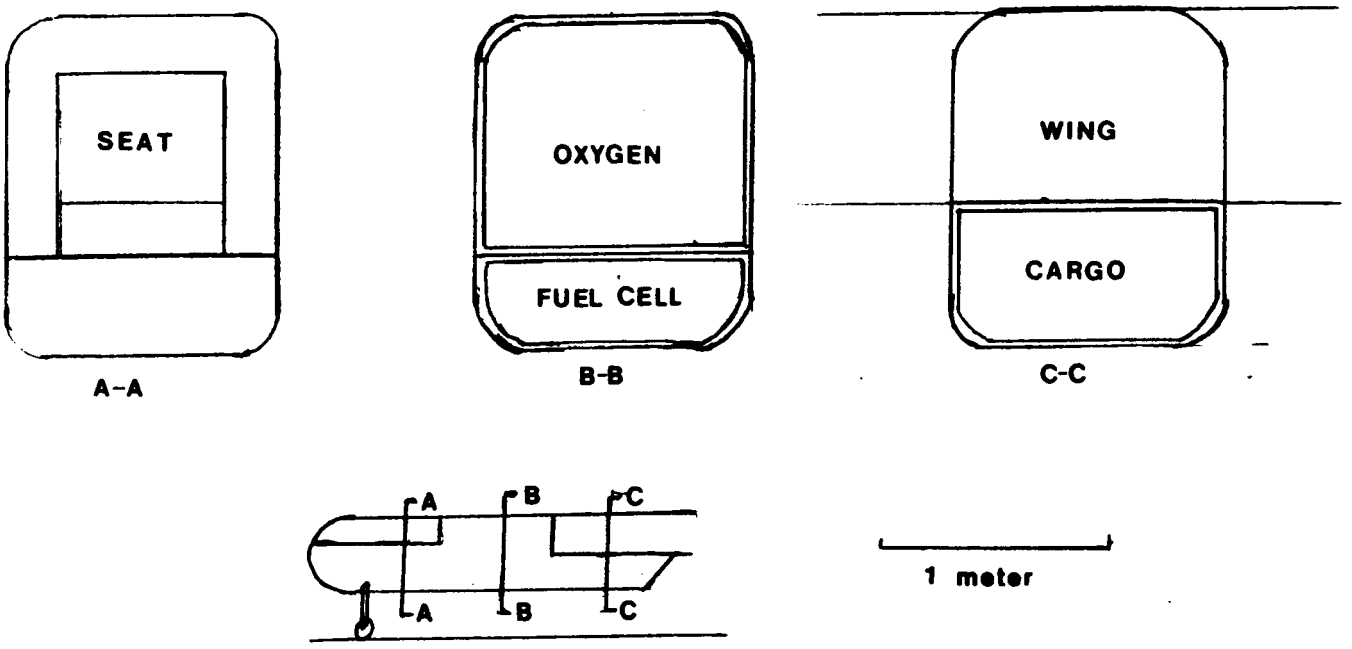

FIGURE 11-3
PLAN VIEW

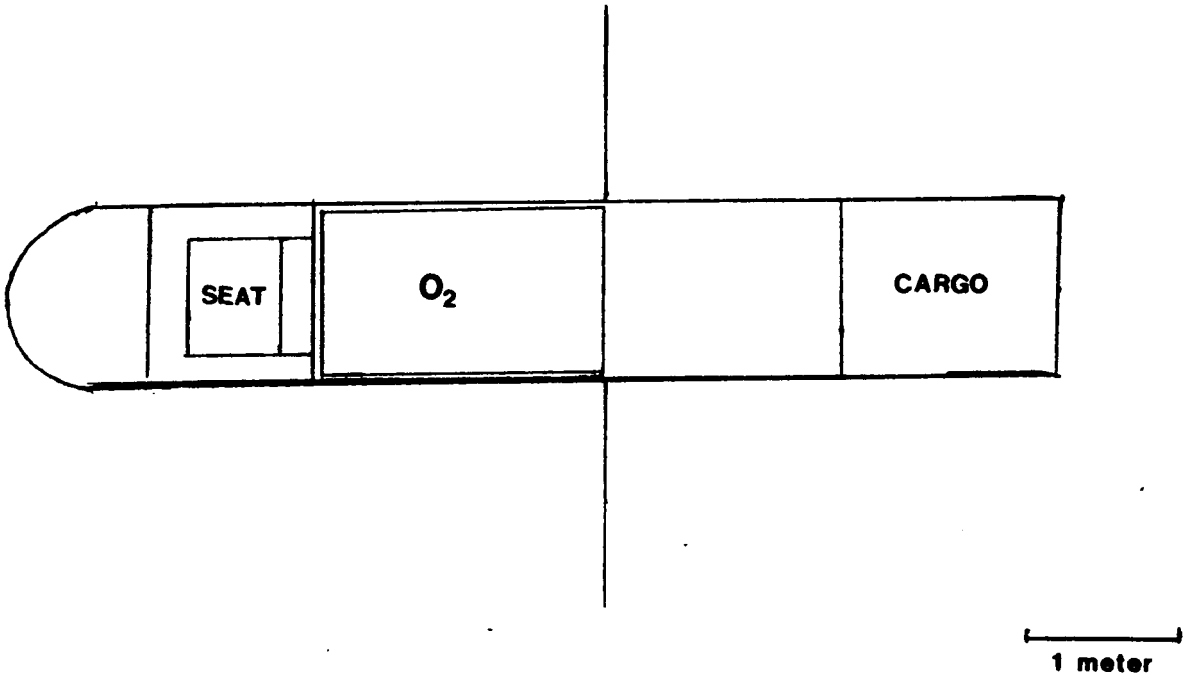

PACKAGING AND ASSEMBLY

Ron Dunn and Greg Maloney

Figure 12.1a illustrates an end view of the storage canister and how the individual pieces of Romulus will be stowed. Figure 12.1b shows the system's five main cargo bays in a profile view. The individual pieces will have to be packed with braces similiar to a scaffold in order to immobilze the individual assemblies during transport.

In assembling Romulus the ribs of the inboard wing section should first be put together as shown in figure 6-4. After completing this operation the outboard 10 meters of the wing section should be bolted at the ribs of the inboard section. Appendix 6-A depicts the location of the reinforced ribs by two parallel lines in close proximity to each other.

With the wing section completed, the one piece tail booms can know be bolted to the upper surface of certain reinforced ribs. Similiarly, the fuselage will then be bolted to the underside of the wing at a bulkhead. This bulkhead consists of a plate which covers the entire area under the wing and encompasses the ceiling of the rear cabin area.

Finally, the horizontal and vertical tail are assembled and attached to the tail booms by inserting the spar of the tail into a opening located within the tailboom. The spar runs along the entire middle 16m of the tail. After, the horizontal tail is assembled, the vertical tails can be bolted to the upper surface of the horizontal tail.

At this point it is beneficial to note that the storage canister can hold the entire aircraft without any modifications needed to the space shuttle cargo bay.

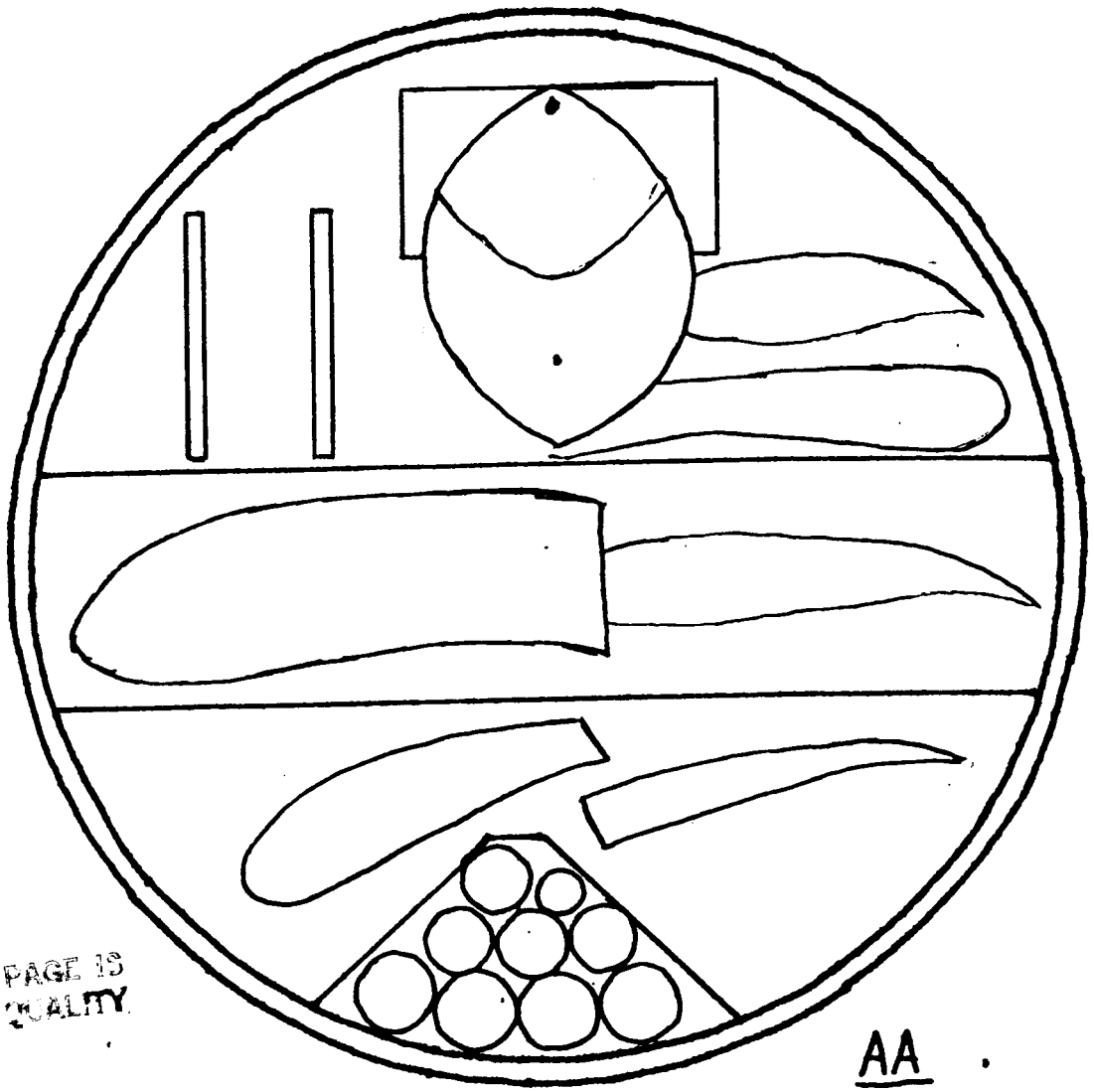

Fig. 12-1a. Storage canister endview.

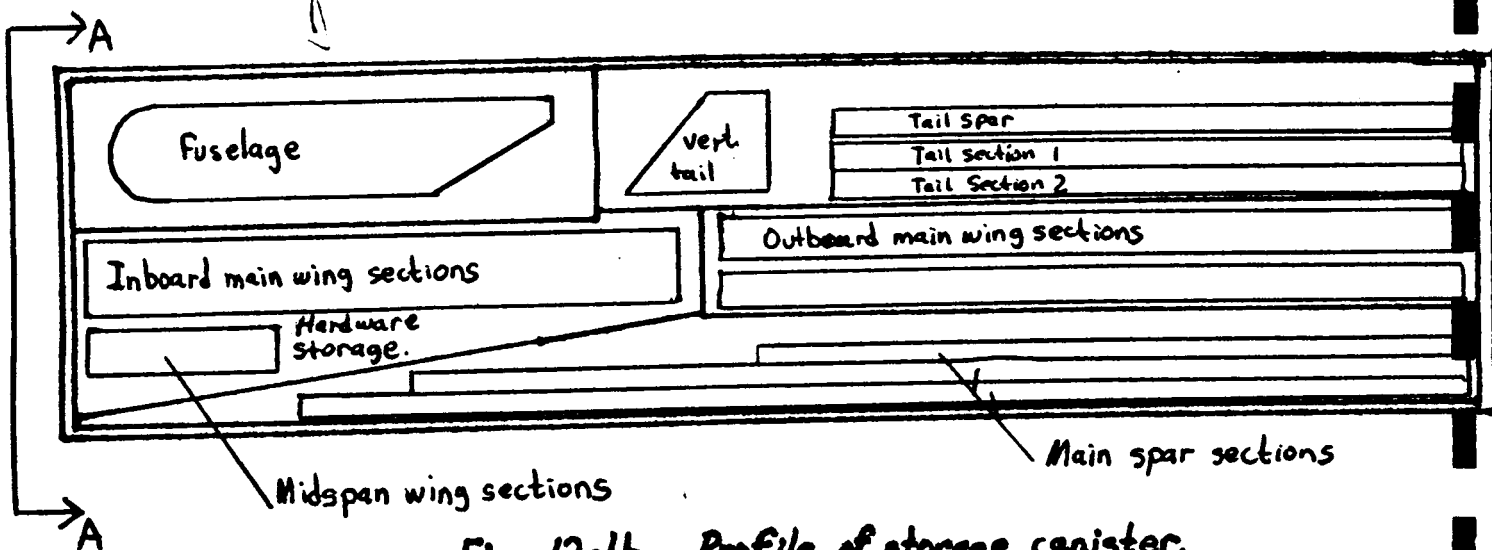

Fig. 12-1b. Profile of storage canister.

RESCUE SCENARIO:

Ken Markuson

The Rescue Scenario has changed from the preliminary design report due to the exclusion of self-powered take-off. Since this aircraft would be unable to take-off under its own power the scenario of landing and picking up the survivor had to be cancelled. In this case the backup scenario would be implemented.

This scenario consists of dropping the survivor a package containing certain equipment needed by the survivor to last 10-12 hours on the Mars surface. The survivor would then have to wait until a ground unit could come and pick him up.

The package would be deployed from the cargo area in the aircraft. The scientific equipment in the cargo area would have to be taken out to accommodate this rescue package. The package would be spring loaded in the cargo area such that when the pilot triggers the spring, the package would be forced out the cargo area. There would be spring loaded doors in the back of the cargo area that would open when pushed by the package and to close automatically when it was gone. The package would be dropped at approximately 300 meters above the ground, terrain permitting, by a parachute of approximately 20 meters in diameter. The package would also be constructed in order to survive a 300 meter drop, because in the Martian atmosphere the parachute will be unable to bring the package down softly.

The package would weigh approximately 68 kilograms. It would contain oxygen, food and water, a battery, a battery operated radio and transponder, medical supplies and a survival tent for moderate protection against the elements, for a duration of 10-12 hours. If

the aircraft survives the crash the survivor could use the extra oxygen that would be on board the aircraft.

Spacecraft Interface Status

Martin Kim

It has been determined by the spacecraft person that the cargo area for the airplane will be 15 feet in diameter and 60 feet long. This is a very limited amount of space, therefore, the airplane will have to be shipped in pieces. The 15 feet diameter translates into 4.2 meters in diameter. This posed a serious problem for the packaging group since the chord of the airfoil is 4.925 meters. This meant that the airfoil had to be cut not only span-wise but chord-wise. With this in mind, the structures group was consulted for the best place to be sectioned off. A feasible place was located and the problem was solved. The final package just fits into the given cargo area and weighs just over 5000 Newtons.

B J JB<

184 PAGES
KS

A A E 241

Aircraft Design

Final Report

April 28, 1988

Manned Martian Aircraft

The HIF II

Group II

Group Member	Assignments
Glen Brown	Structures, Surface Ops, Packaging and Assembly
Dion Buzzard	Power and Propulsion, Cost Analysis
Grant Eaton	Aerodynamics, Coordinator Surface Ops
Art Fletcher	Weights and Balances Internal Config. Surface Ops
Brian Matzel	Performance, Surface Ops, Space Interface
Rich Monke	Stability and Control, Rescue Scenario

DESIGN SUMMARY

The objective of this design project is to design a manned aircraft that will operate from a base on the surface of the planet Mars. The aircraft must satisfy the following requirements:

Payload weight: 318 kg mass, 1200N on Mars
Endurance: eight hours
Cruise altitude: 1500 meters
Landing field length: 1000 meters

The design philosophy followed in this project is dependant on the conditions under which the aircraft must operate.

The atmosphere on Mars is comprised mainly of carbon dioxide and its density is approximately 1% of that on Earth. The low density reduces the dynamic pressure that can be attained in flight so a large wing area is required to produce enough lift for an aircraft to fly in the Martian atmosphere. Also, the low density and corresponding viscosity of the atmosphere produce Reynolds numbers over the wing in the range of 100,000- 300,000. This range of Reynolds numbers requires an airfoil specially designed for low Reynolds number flight.

Considering the above conditions, the design philosophy was to design a lightweight aircraft of simple construction that would satisfy the design requirements. The light weight would keep the wing area and the corresponding wing drag as small as possible. The simple construction would allow easy packaging for transportation to Mars and easy assembly on the planet surface.

Several different design configurations were considered. The configuration finally decided upon is shown in a three view drawing on page 5 and has been named the HIF II. The aircraft consists of a wing of sixty meters span mounted high on a six meter fuselage. The wing is linearly tapered with the root chord equal to 3m and the tip chord equal to 2 meters. Two booms connect the tail assembly to the wing.

The aircraft is powered by an electric motor mounted in the rear of the fuselage. The motor operates with power obtained from batteries and solar cells mounted on the wing. The pusher type propulsion system allows laminar flow over the fuselage which reduces the skin friction drag over the fuselage.

The design point chosen from the initial sizing exercise at a constant cruise velocity of 65 m/s is displayed on page four. During the design process, the values obtained from the initial sizing exercise have changed. A complete list of the current values for the HIF II is presented on page three.

There have been several problems encountered while assembling the final design report for the HIF II. The first problem involves the location of the center of gravity. In order to keep the center of gravity within the

allowable range of the center of gravity, the nose of the aircraft must be heavily weighted. This was accomplished by placing the batteries, instruments, and the pilot as close to the nose as possible; but the result is a cramped pilot compartment and unused space in the rear of the fuselage. These problems could be corrected by lengthening the fuselage in front of the wing. If the length from the nose to the leading edge of the wing was 3 meters instead of the two meters it currently is, the center of gravity would be in the acceptable range and pilot comfort would not be sacrificed.

The second problem involves the power required by the aircraft. An estimated power required at cruise of 13.5kw was given to the propulsion section for engine and propeller sizing. Recent performance analysis of power required at cruise have produced values of approximately 6.5 kw. This value seems very low. Since the propulsion system was sized for a power required of 13.5 kw, the aircraft is over-powered. The low power required is probably due to the small minimum drag coefficient of the drag polar. The minimum drag coefficient is .01753 and occurs at the cruise condition. Calculation of the drag polar should be reexamined.

The last problem is the fact that there is no surface operations member in this design group. Therefore, the surface operations report had to be assembled by several group members. In addition to the fact that these members hadn't been instructed in surface operations, they also had their own reports to work on and didn't have as much time to spend on the surface operations.

The result is an inadequate report based on many estimates, but under the circumstances it will have to suffice.

AAE 241
Spring 1988
DESIGN DATA SUMMARY

Gross Weight: 4616 N
Wing Loading: 30.77 N/m²
Maximum Fuel Weight: 0
Useful Load Fraction:

Maximum Take-off Power 18.5 Kw
Power Loading: .250 N/watt
Fuel Fraction: 0

Geometry

Ref. Wing Area = 150 m²
AR = 24
Λ_{LE} = 0
λ = .667
t/c = .157

Propulsion

Engine Description: Samarium - Cobalt electric motor
Number of Engines = 1
$P_{O_{max}}$ /Engine = 18.5 Kw
Weight/Engine = 22.6 Kg
c_p at Cruise = 0
Prop. Diam. = 8.7m
No. of Blades = 2
Blade Cruise R_e = omitted

Performance

Cruise R_e = 2.33×10^5
Cruise h = 1500 m
Cruise M = .276
Cruise V = 70 m/s
Take-off Field Length = 594m
Take-off Speed = 65 m/s
Landing Field Length = 1134 m
Landing Speed = 58.4 m/s
Maximum Landing Weight = 4616 N
OEI Climb Gradient (%): = N/A
2nd Segment = N/A
Missed Approach = N/A
Sea Level $(R/C)_{max}$ = 3.24 m/s

Aerodynamics

Airfoil: LA 203 A
High Lift System: None

Cruise; $C_{D_{o_{min}}}$ = .01753
C_{D_o} = .027
e_o = .69
C_L = .875
(L/D_{max}) = 54.8
Take-off; C_L = .962
$C_{L_{max}}$ = 1.72
Landing; C_L = 1.16
$C_{L_{max}}$ = 1.72

Stability and Control

Static Margin Range = .6 to .1
Acceptable C.G. Range = 209 m aft of nose to 3.33 m aft of nose
Actual C.G. Range = 3.003m " 3.33 m "

AAE 241
Spring 1988
INITIAL SIZING DATA SUMMARY

Gross Weight: 2400 N

Wing Loading: 15 N/m²

Fuel Weight: 0

Useful Load Fraction: .30

Maximum Take-off Power 24 Kw

Power Loading: .100 N/watt

Fuel Fraction: 0

Geometry

Ref. Wing Area = 180 m²

AR = 20

Propulsion

Engine/Motor Type: electric
Samarium - Cobalt motor

No. of Engines/Motors = 1

$P_{o_{max}}$ /engine = 24 Kw

c_p at cruise = 0

Aerodynamics

Cruise; C_{D_o} = .035

e_o = .75

C_L = .444

$(\frac{L}{D})_{max}$ = 18.35

Cruise Performance

h = 1500 m

V = 65 m/s

Take-off; C_L = 1.4

$C_{L_{max}}$ = 1.7

Landing; C_L = 1.25

$C_{l_{max}}$ = 1.8

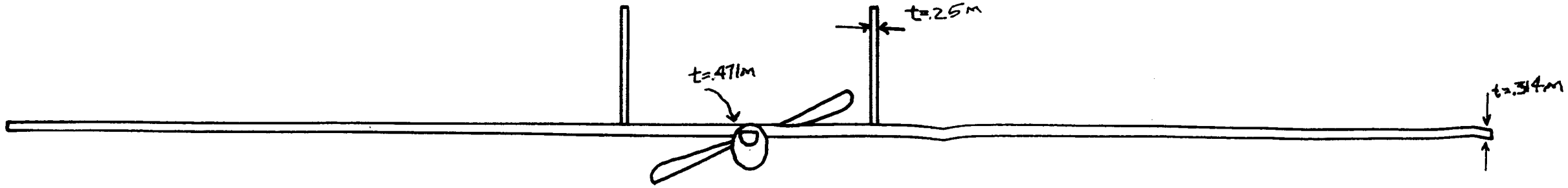

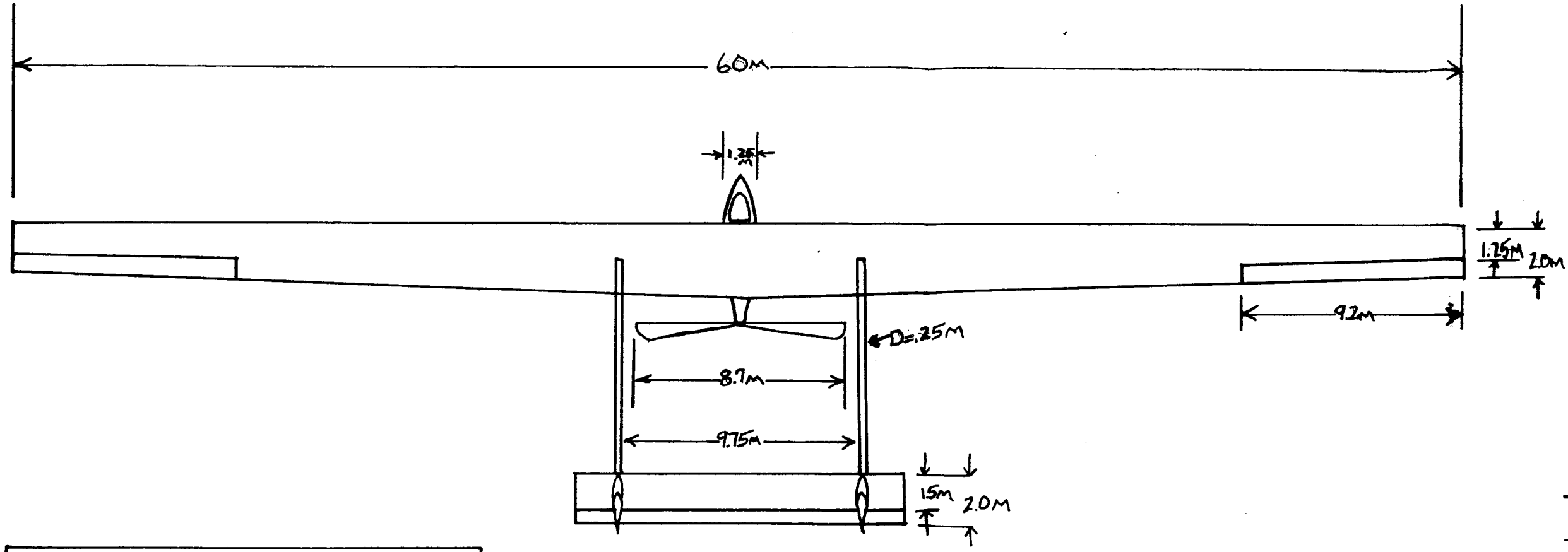

AIRCRAFT DATA	
$W_g = 4616\,N$	$S = 150\,M^2$
$W_g/S = 30.77\,N/M^2$	$b = 60\,M$
$\lambda = .667$	$AR = 24$
$P_{OMAX} = 18.5\,Kw$	$W_g/P_{OMAX} = .250\,N/WATT$

FOLDOUT FRAME

FOLDOUT FRAME

Aerodynamics

Grant Eaton

Several restrictions are placed on the wing design of the HIF II by the conditions under which it must operate. The Martian atmospheric density is very low, approximately 1% of that on Earth. The low atmospheric density and the corresponding viscosity produce Reynolds numbers in the vicinity of 100000. The low Reynolds numbers require an airfoil that is specially designed for this flight condition. Also, the low density of the Martian atmosphere produces low dynamic pressures in flight. This requires a large wing area in order to produce enough lift for the aircraft to remain aloft.

The wing configuration of the HIF II is simple. The wing is a rigid wing with a span of 60 meters. The chord at the root is 3 meters. The wing is linearly tapered to a chord length of 2 meters at the wing tip. The resulting wing area is 150 meters squared.

The Reynolds number for this wing, calculated at the root, is 233000 at cruise conditions. With this condition in mind, the airfoil chosen for the wing is the Liebeck LA 203A airfoil. The two dimensional data for this airfoil was taken from Reference 1 and is presented in Figure 1.1, Figure 1.2, and Figure 1.3 . This airfoil performs well at a Reynolds number very close to the actual Reynolds number of the wing. The minimum drag coefficient of the airfoil is

.0135 . The lift curve slope and the maximum lift coefficient of the airfoil are .101/ degree and 1.7 respectively.

This airfoil is different than the airfoils used for the wing in the preliminary design report. The wing in the preliminary report consisted of a rigid wing for ten meters on either side of the center line. The rigid wing used a Wortmann FX-63-137 airfoil. The remaining twenty meters on either side were a sail wing using a Princeton sail wing airfoil section. Data for these airfoils can we found in References 2 and 3. The rigid wing -sail wing combination was used because it was thought that the weight reduction that would be realized by the use of the sail wing would be beneficial to the design. The rigid wing was needed for the placement of solar cells, control surfaces, and for a place to attach the tail booms.

For several reasons, this preliminary wing configuration was unsatisfactory. First, the ailerons would not provide adequate roll control for the aircraft because they could not be placed far enough out on the wing.

Second, the area available for the placement of solar cells on the rigid wing was only about 50 m^2. Assuming that the solar cells provide more power per unit weight than the batteries, the weight savings that would be attained by using solar cells to replace some of the batteries would increase as the wing area available for the placement of solar cells increased.

The third and strongest reason for the change in wing design is that the parasite drag coefficient of the sail wing is approximately .044 . This is more than three times the minimum drag coefficient for the LA 203A airfoil which is currently being used. The power required for an aircraft increases linearly as the drag coefficient increases; therefore an aircraft using the sail wing requires approximately three times as power as an aircraft using the LA 203A airfoil. After weighing the advantages and disadvantages of the sail wing with the propulsion and structures sections, it was discovered that any weight reduction in the structural weight by the use of the lightweight sail wing was by far outweighed by an increase in the weight of the propulsion system due to the increased power required.

The Wortmann FX-63-137 airfoil used for the rigid wing in the preliminary design also has a minimum drag coefficient greater than that of the LA 203A . The LA 203A also has a larger maximum lift coefficient and lift curve slope than the FX-63-137 . For these reasons, the LA 203A airfoil was selected for the final wing design.

The wing is mounted on top of the fuselage at an incidence angle of 2.75 degrees. The dihedral angle is zero due to the high wing configuration. The high wing configuration is used to eliminate interference from the fuselage on the boundary layer of the upper wing surface which could cause a loss of lift due to flow separation. The

wing is mounted at an incidence angle of 2.75 degrees so the lift coefficient needed for the cruise condition can be reached when the body is at zero angle of attack. This eliminates body drag due the angle of attack.

A list of the geometry is presented in Chart 1 in the Appendix. A high aspect ratio wing was chosen to lower the induce drag. The value for the aspect ratio and for the taper ratio shown in Chart 1 were picked after a trade-off study of the effective aspect ratio versus the taper ratio.

In general, a tapered wing is more efficient than an untapered wing. To show the reason behind this , two equations are needed to explain this more clearly. The first equation is the parabolic drag polar shown below.

$$C_D = C_{Dmin} + C_L^2 / (pi * eo * AR)$$

where

CD = Drag coefficient

CDmin = minimum drag coefficient, CL = lift coefficient, eo = Oswalds efficiency factor, AR = aspect ratio, (pi * eo * AR) = effective aspect ratio

By studying the parabolic drag polar above, it should be obvious that as the effective aspect ratio increases or more specifically, as eo increases, the induced drag decreases. From this point of view, it is therefore beneficial to make

eo as large as possible.

The second equation, found in reference 4 - pg 194, needed to relate effective aspect ratio and the taper ratio is an equation used to calculate eo. The equation is shown below. not a very good symbol

$$eo = 1 / (1 + \& + k * pi * AR)$$

where

k is a constant relating the rate of increase of C_d with C_l^2

& is a factor that increases somewhat with an increase in AR and increases rapidly with increase in the taper ratio (a table of values for & vs AR and taper ratio can be found in Reference 4, pg 191)

The only variable in the above equation is & and as the taper ratio increases it should be obvious that eo and the effective aspect ratio decrease.

A result of wing taper, which must be taken into account when choosing the taper ratio, is the effect of taper on the spanwise sectional lift coefficient distribution. As the taper of the wing increases, the location of the maximum sectional lift coefficient moves toward the tip. This is undesirable because if the location of the maximum sectional lift coefficient is near the ailerons at the onset of stall the flow separation could spread over the ailerons. This

would result in a loss of lateral control. This effect can be controlled by the use of wing twist.

In the process of choosing the taper ratio for the HIF II, two restrictions were placed on the process. First, the wing span would remain a constant 60 m. Therefore as the taper ratio decreases the aspect ratio increases. The second restriction is that the taper ratio will have a value such that no wing twist would be required to control the location of the maximum sectional lift coefficient.

With the above restrictions and conditions in mind, the equations on pages 5 and 6 and values for & interpolated from reference 4, pg 191, were used to select the taper ratio. After comparing the effects of many different taper ratios on the aerodynamic characteristics of the wing, a taper ratio of .667 was chosen. This taper ratio makes the wing root at the wing tip 2 meters and the surface area of the wing equals 150 meters squared. The aspect ratio of this aircraft is 24 and eo is calculated to be .70 . These values work very well in the design.

Figures 1.4 and 1.5 show the sectional lift coefficient and the spanwise lift distribution, respectively, at the cruise condition. These distributions were calculated using the Schrenk Approximation found in Reference 5, pgs 228-229. The maximum sectional lift coefficient is equal to .93 and is located ten meters from the wing root. The sectional lift coefficients decrease more rapidly toward the wing tip than toward the root. If stall starts at the location of the

maximum sectional lift coefficient, the stall will spread to the root of the wing before it reaches the ailerons. This wing requires no twist in order to reduce the sectional lift coefficients near the tip.

The effective aspect ratio of the HIF II wing with a taper ratio of .667 is equal to 16.8 * pi. A rectangular wing under the above mentioned restrictions has an effective aspect ratio of only 13.06 * pi. Therefore, the wing induced drag coefficient of the tapered wing is less than that of the rectangular wing.

The lift curve of the wing is shown in Figure 1.6 . The curve was obtained by correcting the two dimensional lift curve for aspect ratio effects. The lift curve of the trimmed aircraft is presented in Figure 1.7 . Since there are no high lift devices on this aircraft, this curve is valid for the cruise, take-off, and landing configuration.

The drag polar at cruise is presented in Figure 1.8 . The drag polar was calculated by adding the parasite drag, the wing induced drag and the body induced drag. The equation for the drag polar at cruise is presented along with the graph.

The drag polar for the take-off and landing configuration is shown in Figure 1.9 . This value was obtained by adding the parasite drag coefficient increments due to the landing gear and the propeller. The propeller is locked in a horizontal position for take-off and landing. The parasite drag increments and the new drag polar are shown

with Figure 1.9 . The drag increment due to the propeller was supplied by the propulsion section and has a value of .073 . This value seems large, but recalculation yielded similar results. The tabular breakdown of the parasite drag coefficient is shown in Chart 2 in the Appendix. The procedure used to determine these values is shown in Reference 4, pg 196-203 The drag coefficient at zero lift is equal to .02704, but the minimum drag coefficient is .01753 at a lift coefficient of .875 .

The cruise velocity was selected so that the cruise lift coefficient is .875 . This gives a cruise velocity of 70 m/s The cruise condition of velocity = 70 m/s and lift coefficient = .875 correspond to $C_{D_{min}}$ on the drag polar.

The only problem encountered is that the calculated drag polar gives a power required at cruise of 6.5 Kw . This value seems very low. The most likely explanation is that the method used to calculate the parasite drag coefficient is inaccurate. A value of C_{D_o} = .04 seems like a better number, but some recalculations of the parasite drag coefficient should be done.

REFERENCES

Reference 1:

Liebeck, R.H. and Camacho, P.P.
Douglas Aircraft Company
Long Beach, CA

Reference 2:

Bastedo, William G., Jr. and Muller, Thomas
"Performance of Finite Wings at Low Reynolds Numbers"
University of Notre Dame
Notre Dame, Ind 46556

Reference 3:

Maugher, Mark
"A Comparison of the Aerodynamic Characteristeristics of Eight Sailwing Airfoil Sections"
Princeton University

Reference 4:

McCormick, B.W.
Aerodynamics, Aeronautics, and Flight Mechanics
John Wiley & Sons, Inc, 1979
New York

Reference 5:

Sivier, K.
"Classnotes for Applied Aerodynamics"
University of Illinois, 1987

APPENDIX

Chart I

$AR = 24$ $b = 60\,m$ $S = 150\,m^2$

$C_{root} = 3m$ $C_{tip} = 2m$ $\lambda = .667$

$\Lambda = 0$ $\frac{W_g}{S} = 30.77\ N/m^2$ $V_{cruise} = 70\,m/s$

$C_{L\,max} = 1.72$ $\frac{t_{max}}{c} = .157$ $C_{L\,cruise} = .85$

Chart II

Item	Reference AREA	C_{d_o}	$F = C_{d_o} A$	% of total
wing	$150\,m^2$	.0135	2.025	76.85
fuselage	18.4	.00486	.089	.34
tail booms	6.185	.0011	.0065	.25
Horizontal tail	27	.0135	.3645	13.83
Vertical tail	18	.0083	.15	5.7
total			2.635	

Figure 1.1 2-D C_ℓ vs α

Re = 250000

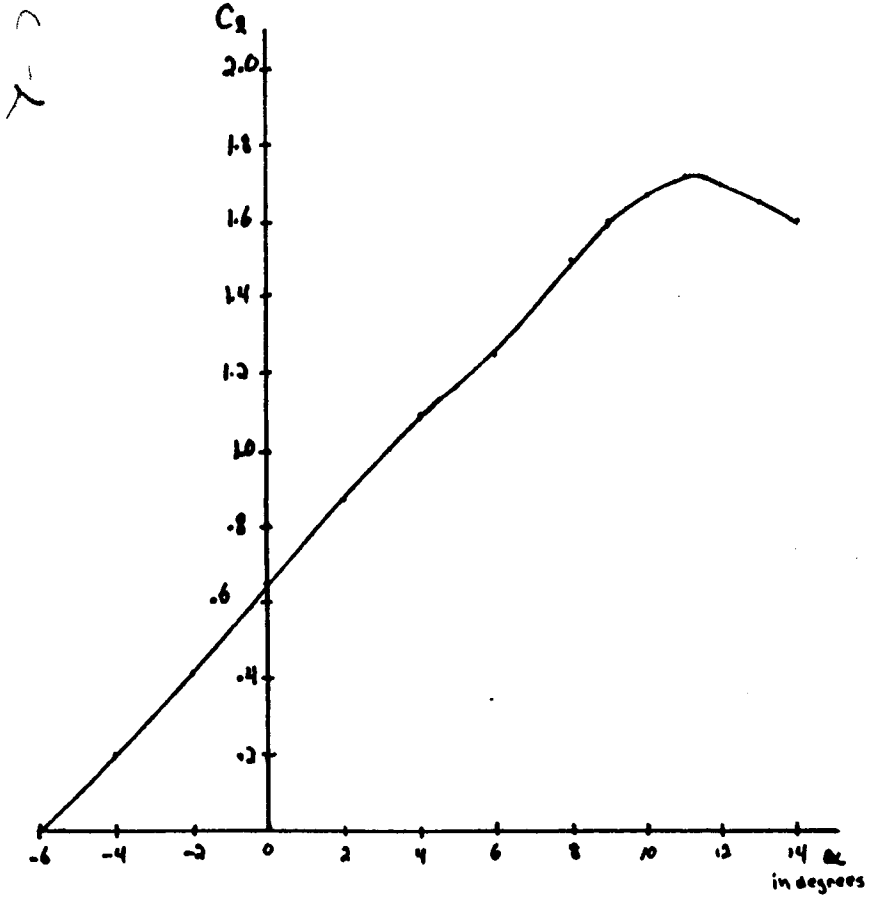

Figure 1.2 C_ℓ vs C_d

Re = 250000

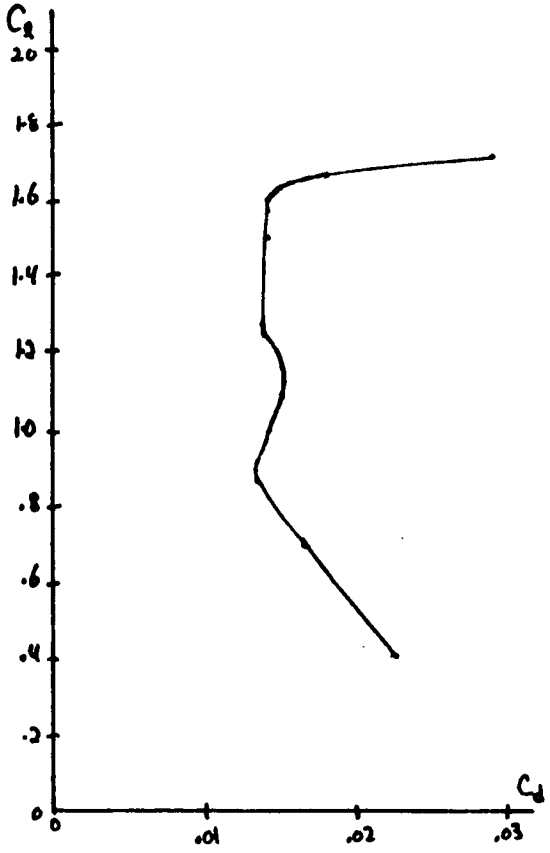

Figure 1.3 C_ℓ vs $C_{m_{c/4}}$

Re = 250000

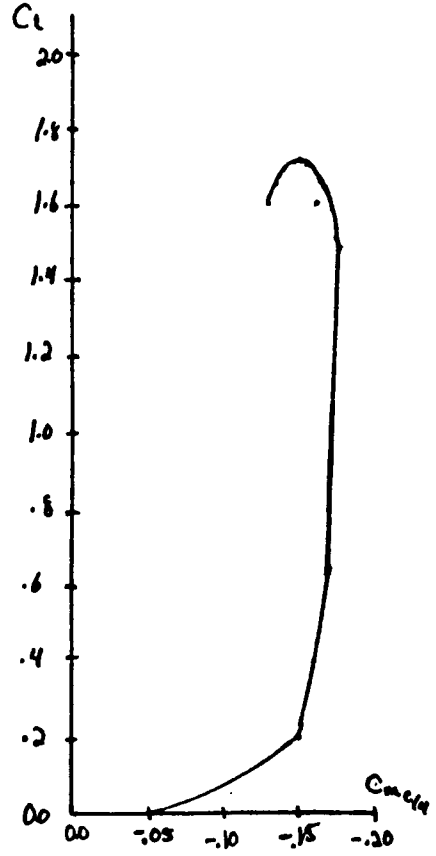

Spanwise C_ℓ Distribution at cruise $C_L = .875 : \lambda = .667$

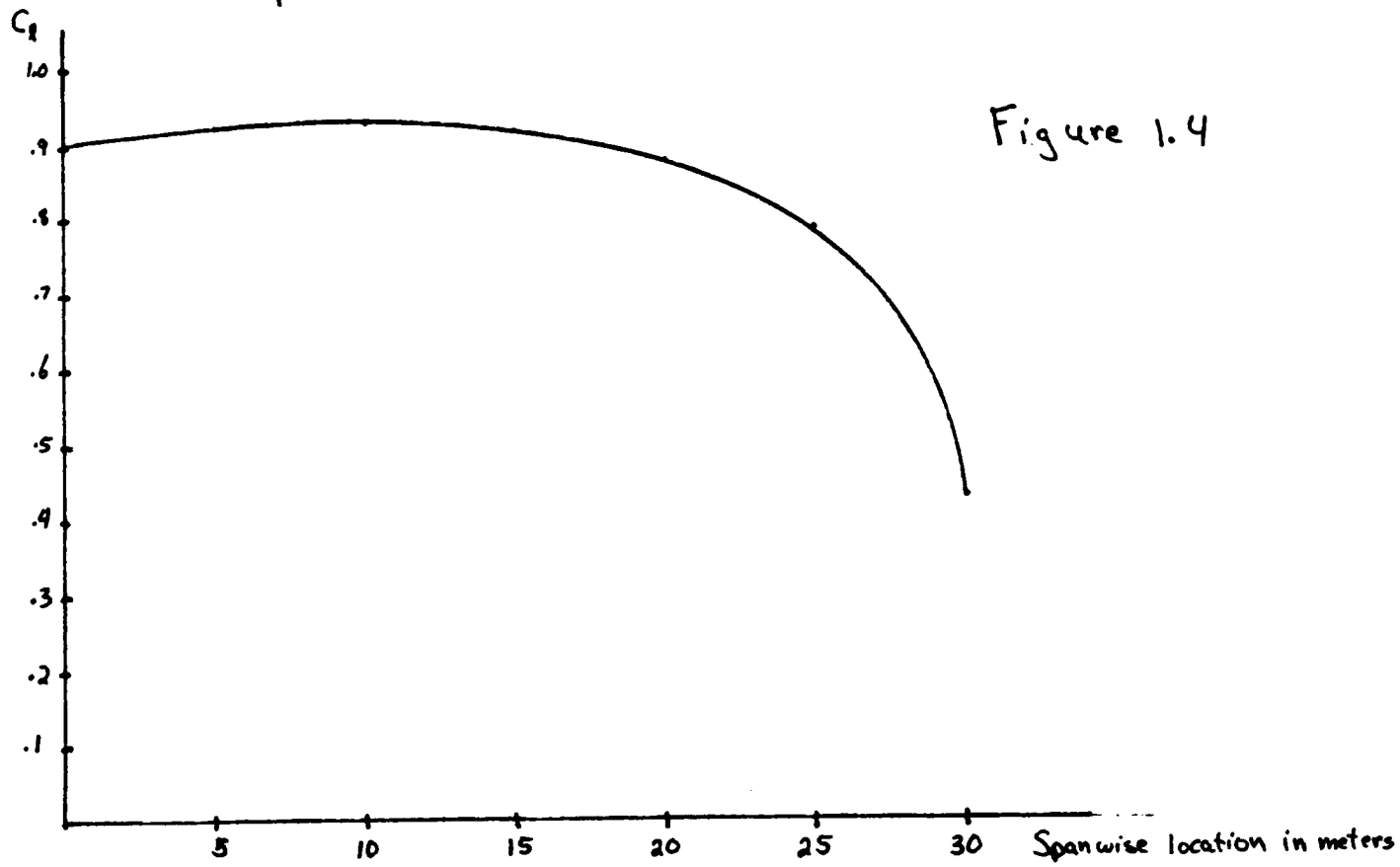

Figure 1.4

Spanwise Lift Distribution at cruise: $\lambda = .667$

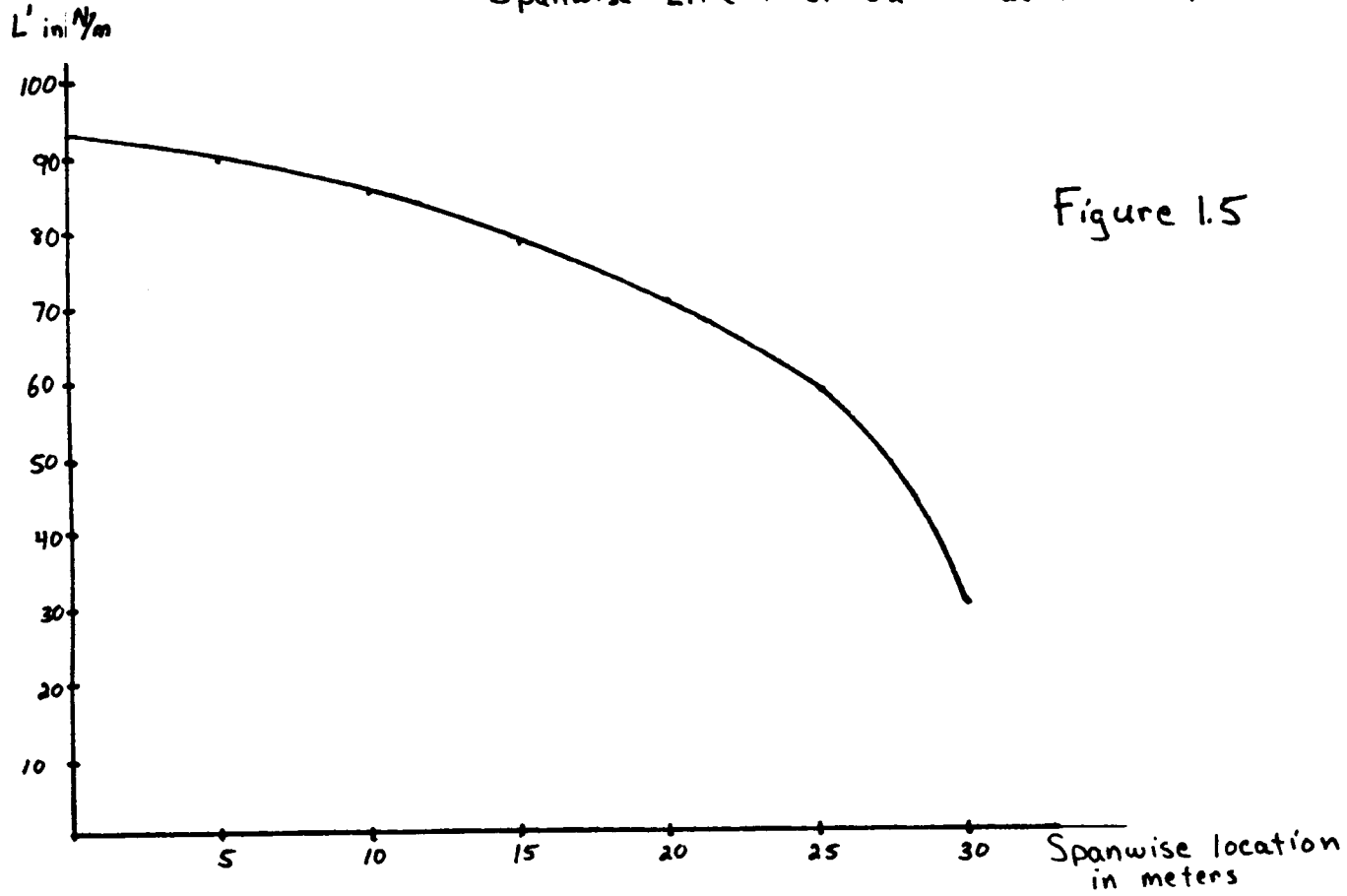

Figure 1.5

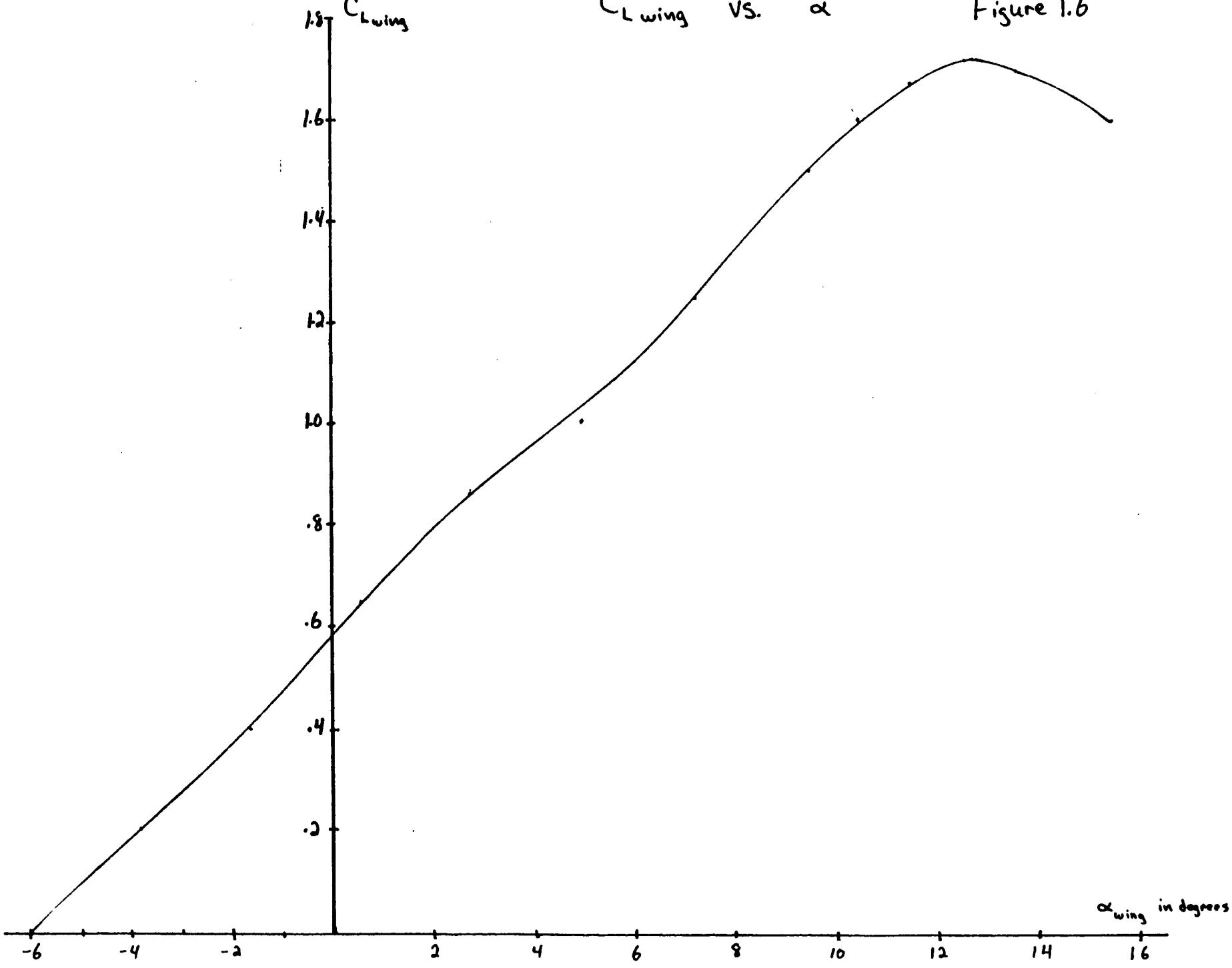
$C_{L\,wing}$ vs. α
Figure 1.6
$C_{L\,wing}$
1.8
1.6
1.4
1.2
1.0
.8
.6
.4
.2
-6
-4
-2
2
4
6
8
10
12
14
16
α_{wing} in degrees

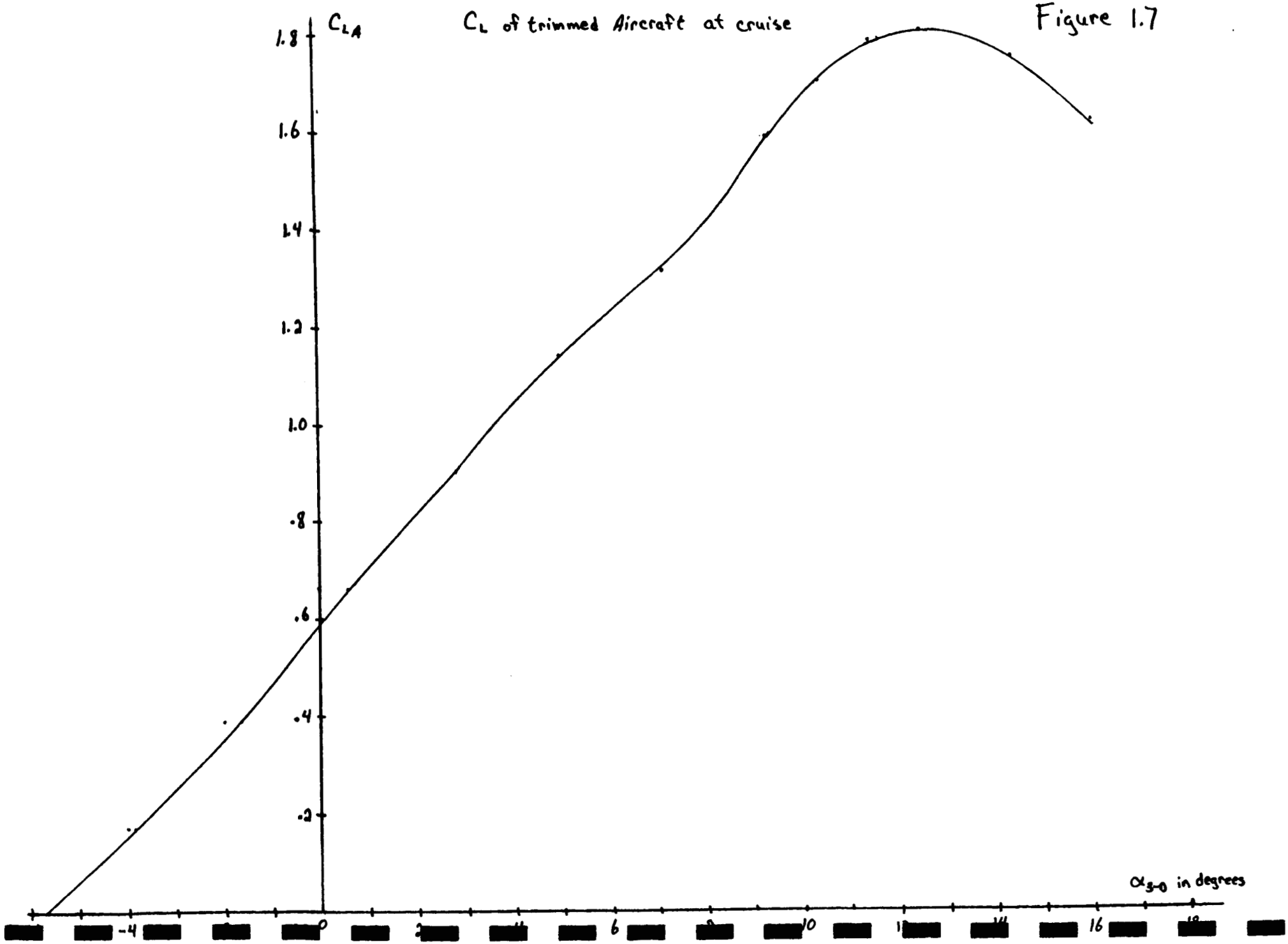

C_L of trimmed Aircraft at cruise

Figure 1.7

Drag Polar at cruise Figure 1.8

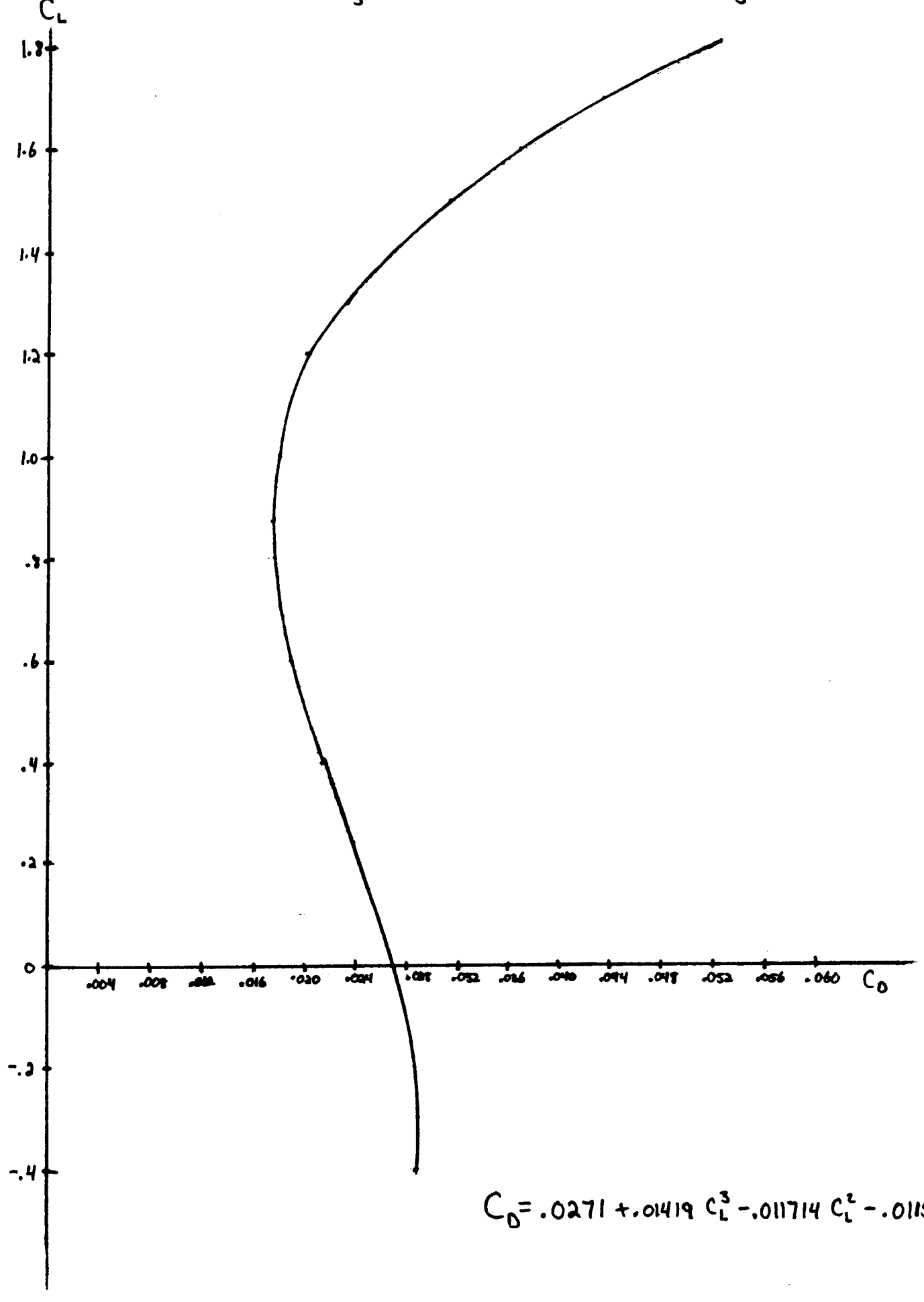

$$C_D = .0271 + .01419\, C_L^3 - .011714\, C_L^2 - .01151 C_L$$

Drag Polar for take-off and landing

Figure 1.9

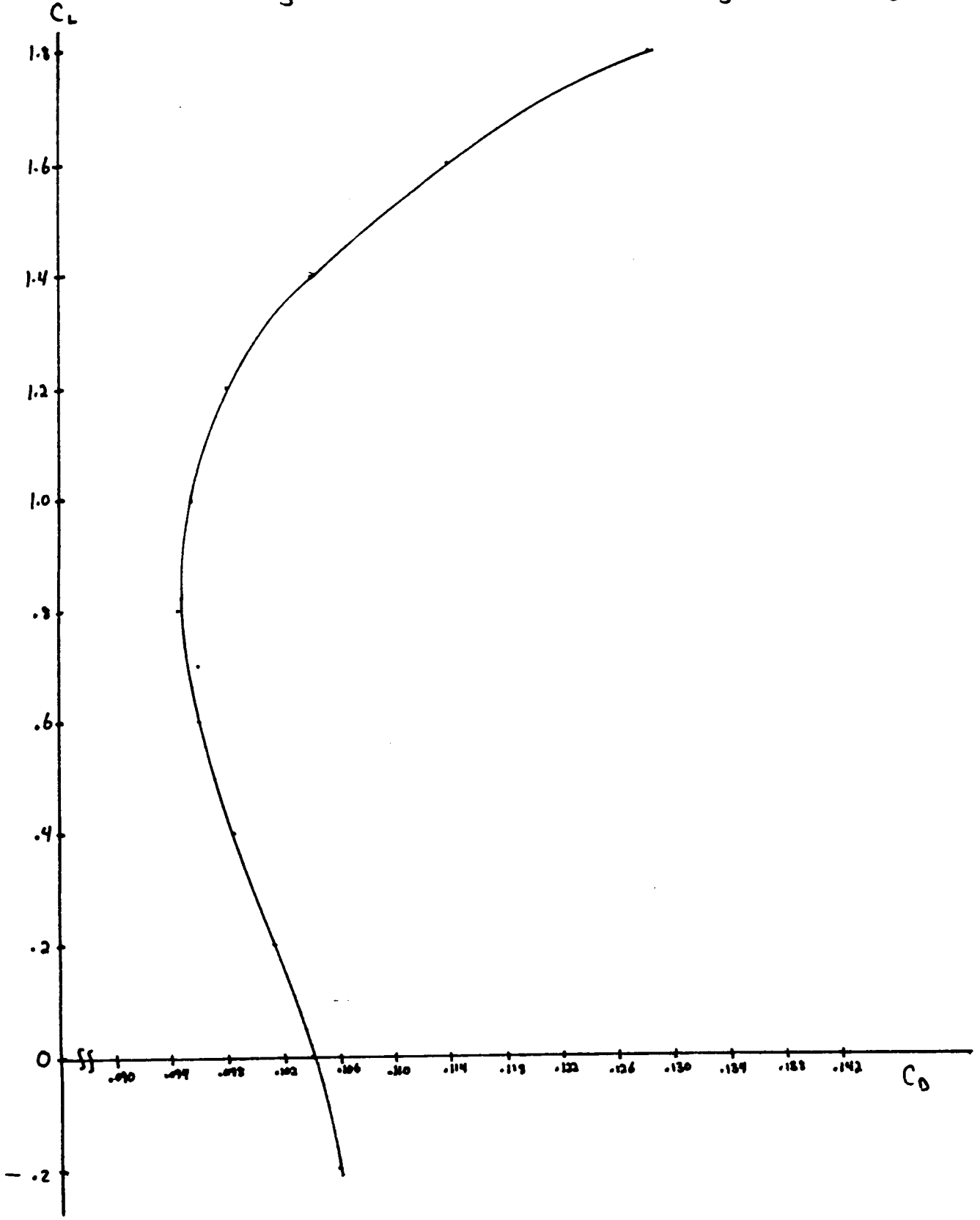

ΔC_{D_0} due to landing gear = .0041

ΔC_{D_0} due to locked propeller = .073

$$C_D = .1042 + .01419\,C_L^3 - .011714\,C_L^2 - .01151\,C_L$$

PERFORMANCE

Bryan Matzl

The performance of the HIF 2 has changed many times during the design process. Every time the weight or drag increased or decreased, it affected the performance of the aircraft. During the final stages of design, it was reasoned that too much power would be better than too little. Assumptions were made for aircraft drag and weight before the final data was obtained. From these assumptions, power needed to climb and cruise was obtained (see Figure 2.1) and the powerplant sized from these results. It will be shown that the aircraft is over-powered and that the powerplant could be down-sized. The final aerodynamic and propulsion data used for calculations are shown in Table 2.1. Portions of the surface operations report have been evaluated and are contained herein. The following is the performance characteristics of the aircraft.

For take-off, two Viking thrusters provide the thrust to get the aircraft off the runway and over the 15 meter obstacle. They will be placed under the wings similiar to air-to-air missles. The propeller will be locked in a horizontal position to keep the propeller tips from hitting the ground. Once the aircraft is safely off the ground, the motor will begin to turn the propeller. The propeller will be up to speed by the time the thrusters are out of fuel, and it will propel

the aircraft for the rest of the flight. The thrusters will then be jetisoned to reduce drag. At maximum thrust of 2500 N for each thruster, minimum take-off distance is accomplished in 594 meters. Take-off velocity is 65 mps. The take-off will take 17.3 seconds. The thrusters will require 21.5 kg of fuel for take-off.

The aircraft was then evaluated for its climb performance. Maximum rate of climb was calculated at intervals of 300 meters from 15 meters to 1500 meters (see Figure 2.2). The maximum rate of climb was 3.2 mps at a velocity of 57 mps. The climb took 7.9 minutes and covered 27.4 km. 9060 KJ were required for this climb. The climb velocity of 57 mps was judged to be too close to the stalling speed of the aircraft. Therefore, climb performance was evaluated again for a constant climb velocity of 65 mps. The average rate of climb at this velocity was 2.9 mps. It took 8.5 minutes to climb and covered 33.0 km. 9693 KJ were required for this climb. When the aircraft reaches its cruise altitude, it levels off and accelerates to its cruise speed. The aircraft will use 690 KJ, take 52 seconds, and cover 3527 meters during its acceleration period.

The aircraft will cruise at a constant velocity and altitude. This can be accomplished because there is no weight loss with its electric powerplant. 70 mps was chosen as the cruise velocity. The specified cruise altitude was 1500 meters. An aircraft endurance of 8 hours was required. From the 8 hour endurance, time to climb and descend were subtracted to give a cruise time of 7.38 hours. During this time the aircraft will cover 1860 km and will use 170195 KJ.

A maximum cruise velocity of 98.8 mps can be attained at a higher altitude (see Figure 2.3). A greater cruise velocity did not seem economically feasible due to the large increase in induced drag above 70 mps.

For the descent phase of flight, the aircraft will glide with engine power off. The propeller will be allowed to spin freely to reduce drag. Descent was evaluated from the final cruise altitude of 1500 meters to the approach altitude of 15 meters. During each descent interval, the velocity of the aircraft was reduced. Descent began from the cruise velocity of 70 mps and was reduced to the approach velocity of 58.4 mps at the end of the descent. The average rate of sink was 1.14 mps. Descent will last 21.4 minutes and will cover 80.5 km.

At the end of the approach, the propeller will be locked in a horizontal position. This will keep the prop tips from hitting the ground during landing. The aircraft will land at 58.4 mps. This is 1.2 times the stall speed of 48.7 mps. Total landing distance required is 1883 meters. This includes an approach distance of 680 meters, a flare distance of 69 meters, and a ground roll distance of 1134 meters. The ground roll requirement of 1000 meters was not achieved by the HIF 2. A small speed brake was used which poped up on top of the canopy. It could be activated by the pilot from inside. Obvoiusly, more deceleration is needed to stop in the required distance. This may be accomplished with the use of wing spoilers, wing flaps, or parachutes. These options need to be further evaluated before application.

The total range of the HIF 2 was calculated at 1979.5 km. The energy used during the 8 hour flight was 182682 KJ supplied from the batteries and solar cells. Also, 21.5 kg of fuel were used for take-off.

The level flight envelope constructed for the aircraft is shown in Figure 2.3. This shows that because the power available varied with altitude only and not with velocity also, the maximum speeds were not reduced until the absolute ceiling was almost reached. Also, the stalling speed governed the minumum speed until very high altitudes. If better power available data was available, the level flight envelope would look more rounded at the top. Also, the maximum speed of the aircraft would occur at a lower velocity. The maximum velocity at cruise is not reached until very near the absolute ceiling of 16.04 km.

TABLE 2.1

PERFORMANCE INPUTS

SYMBOL	VALUE
AR	24
S	150 m^2
$GTOW_{(lo)}$	4756 N
$GTOW_{(cr)}$	4616 N
P_0	19631 W
C_{Do}	0.01753
$C_{Do(lg)}$	0.0041
$C_{Do(boost)}$	0.0020
$C_{Do(f,prop)}$	0.073
C_{Lmax}	1.72
H_{cruise}	1.5 km

FIGURE 2.1

Power vs. Velocity - Sea Level

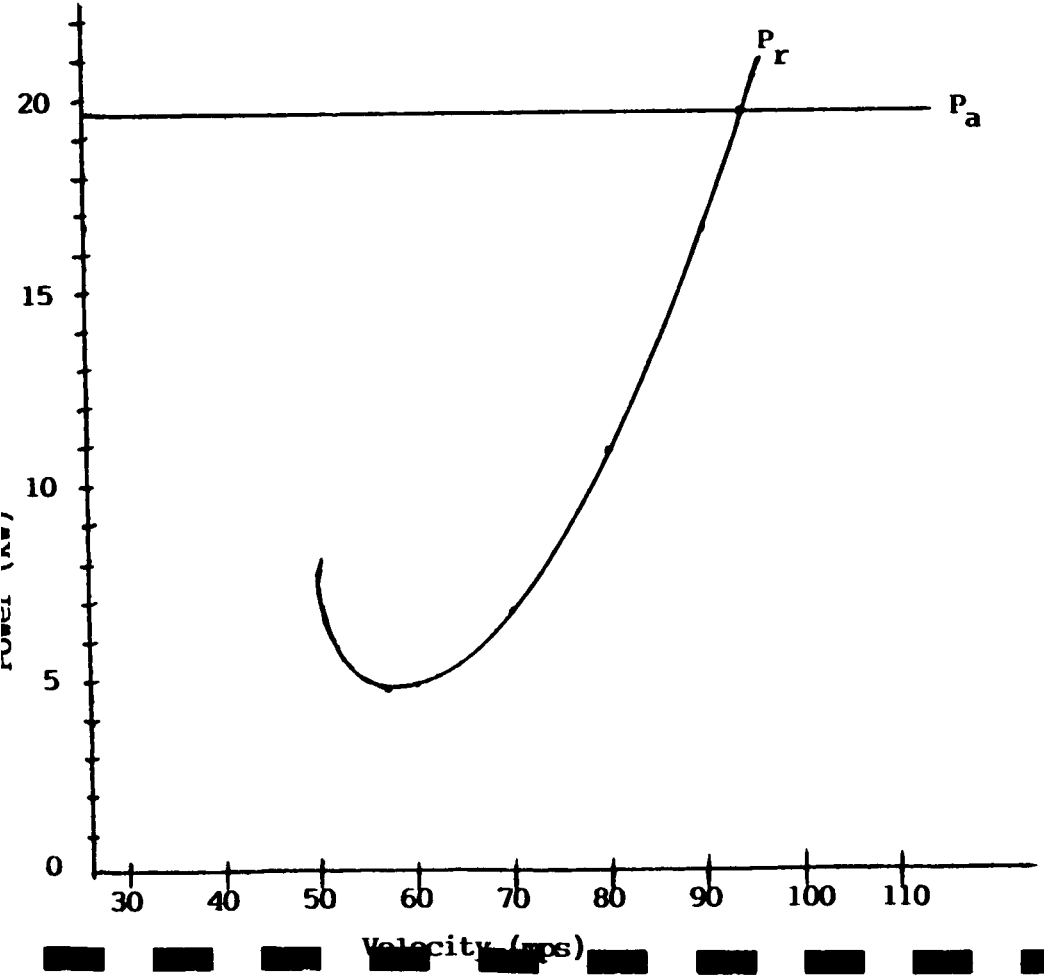

Power vs. Velocity - 1500 m

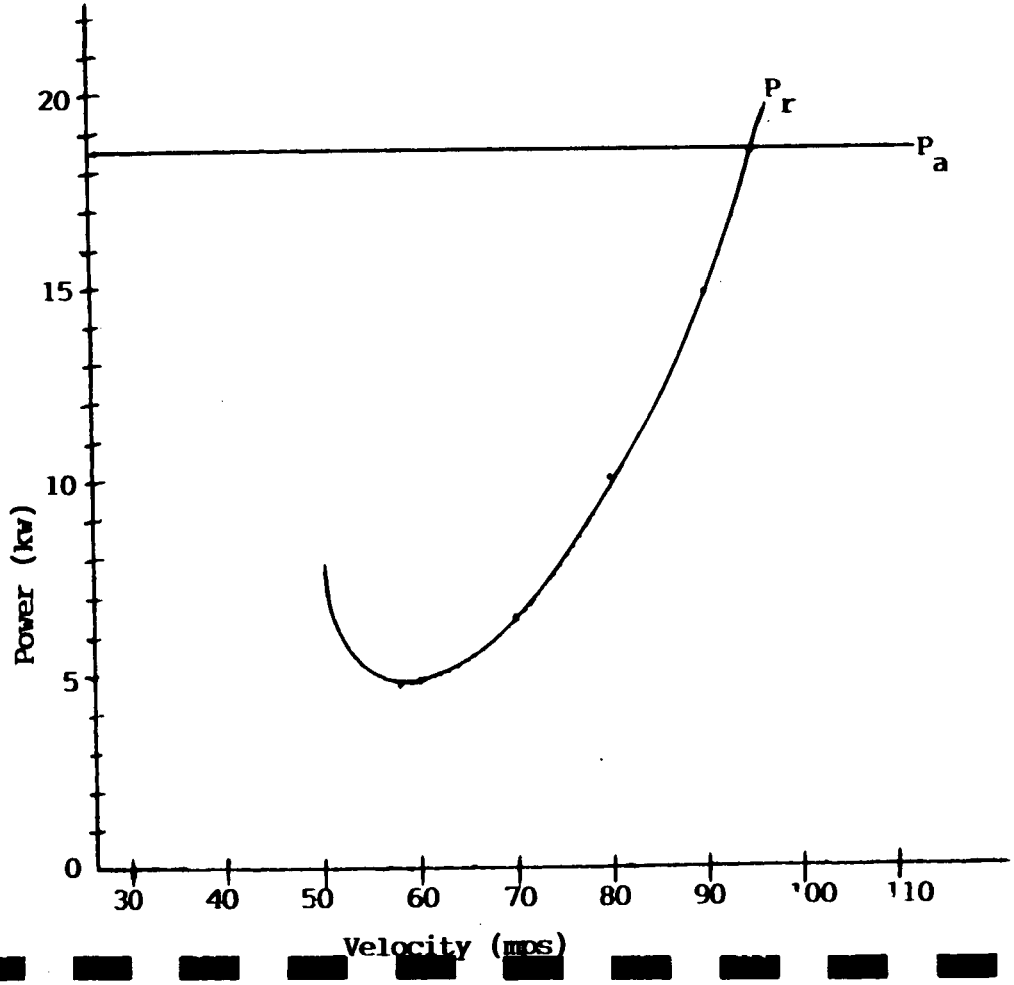

Figure 2.2

R/C vs. Altitude

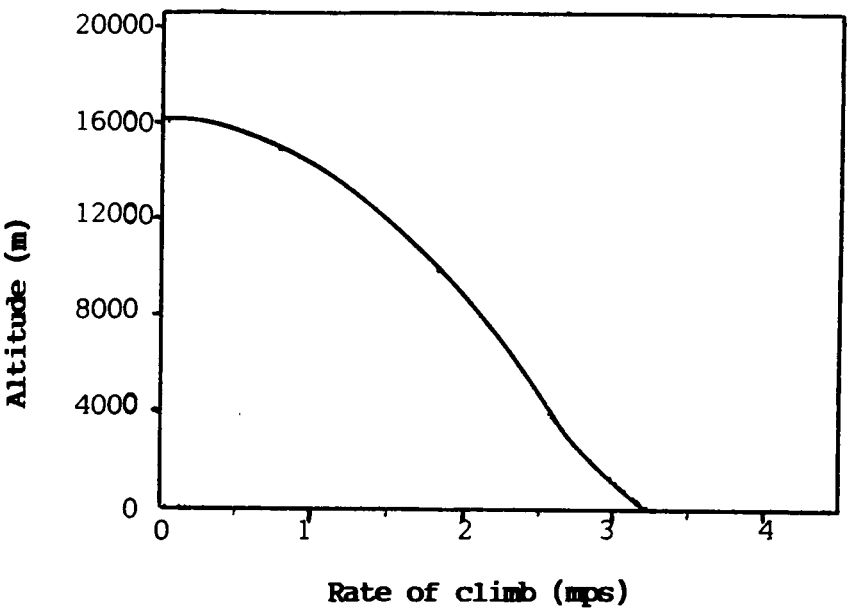

Figure 2.3

Level Flight Envelope

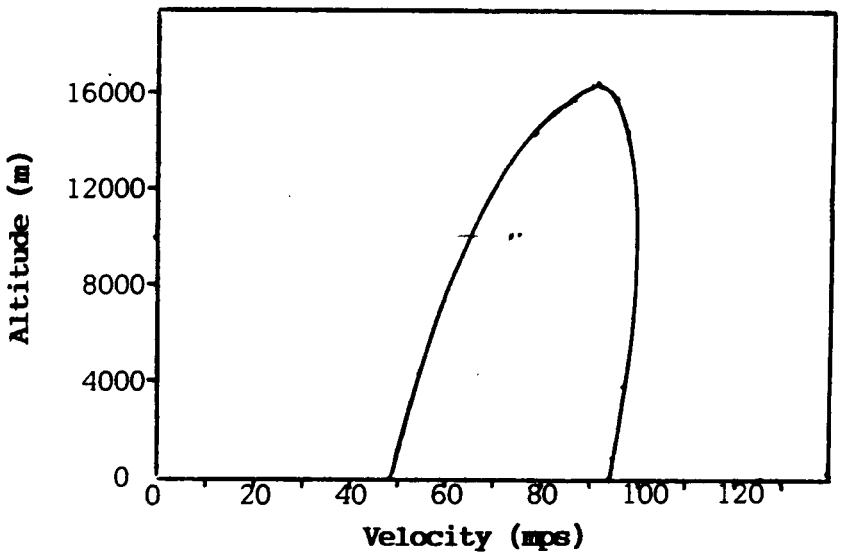

Power and Propulsion

Dion L. Buzzard

The propulsion system is an electric motor which is powered by a solar array and a battery. The electric motor powers a single pusher-type two-bladed propeller which is fixed pitch and variable rpm. The samarium-cobalt motor includes a solid state invertor and planetary gearbox. The power system has a power conditioner which directs power to the motor, avionics, experimental instruments, and back to recharge the battery. The layout of this system can be seen on the flowchart as well as numerical values for efficiencies, power output, and masses. The following will discuss the subsystems chosen.

First, the samarium-cobalt engine has several advantages over other motors. It is an electric motor with an internal permanent magnet rotor, which is very efficient and lightweight. It is also very compact. For example, a ferrite motor which provides the same power would weigh twice as much.[1] The disadvantage of samarium-cobalt is high rotation rates on the order of 20,000 rpm. This will require a large reduction of rpm in the gearbox. Therefore, the gearbox must be very efficient and lightweight. The samarium-cobalt motor, which includes a solid state invertor and planetary gearbox, has an efficiency of 87% and provides 21.5 kw at a mass of 22.6 kg.[1] This is done by

assuming a linear relationship between shaft power and motor weight of the AiResearch motor.[1] The planetary gearbox was chosen because of its simplistic design and high reliability.

The power conditioner is used to maintain maximum efficiency of the solar cells by channeling the power input to the power output. The power conditioner will be able to divert excess power to recharge the battery or obtain more power from the battery at low solar flux densities. This power conditioner is 92% efficient and has a mass of 13.5 kg.[2] This is an important component of the power system due to variations of the solar flux on the solar cells during the eight hours of flight.

The solar array of gallium-arsenide (GaAs) is better because it is more efficient and lighter than the silicon cells (Si).[3] The base efficiencies are 20% and 15% for gallium-arsenide and silicon cells, respectively.[3] It has been assumed an efficiency increase of 5% will occur before production. Thus, the efficiency of gallium-arsenide will be 25% and 20% for silicon. It has been noted that the efficiencies of solar cells are inversely proportional to temperature.[2] There is a larger change in efficiency in silicon cells (.05% / ^{o}K) than gallium-arsenide (.03% / ^{o}K) with temperature.[2] Therefore, a trade study will be made. The atmospheric temperature on Mars at different flight altitudes is essentially constant with an average temperature of 215^{o}K which means that the power available does not vary with altitude for the solar cells.[4] The velocity of the plane is also

independent of the solar power available. The standard operation temperature for the cells is 298°K which is 83°K higher than the actual operating temperatures. This lower temperature results in a total efficiency of 27.6% for gallium-arsenide cells and 24.15% for silicon cells. Gallium-arsenide is still the best choice. The gallium-arsenide has a mass per unit area of 0.026 kg per m^2.[4] The solar array will be placed under a transparent skin inside 87% of the wings, which is 130 square meters. This is done to eliminate drag characteristics and to protect the cells from the elements. The solar flux on Mars has an assumed average value of 0.5 kw per m^2 which varies with latitude and time of day.[3] It would be beneficial to fly at equatorial regions since the solar flux would be greater. The data used will provide a power density of 5.3 kw per kg from the solar array with a total power output of 18 kw.

The other power source will be a rechargeable battery which has an ultra-high energy density. A lithium-type battery has been chosen because of its light weight, long storage life, and high reliability.[5] The problem with lithium batteries is that they tend to be explosive upon recharging. This hazard can be minimized by adding other elements like molybdenum and the careful venting of the toxic gases.[6] In order to maximize the battery energy density, it will be necessary to make one battery. The energy density of this battery will be 515 w-hr/kg from the use of references 6 and 7, which will provide an average of 9.1

kw for eight hours to the power conditioner with a mass of 141.3 kg. The battery has a volume of 0.28 m^3 which assumes the battery is pure lithium with a density of 499.3 kg/m^3.8 The battery will be placed with its center of gravity at 0.75 meters from the nose tip. The battery output will vary inversely with solar flux variations. The battery will be recharged when excess power is provided to the power conditioner, and the battery will discharge at a greater rate when extra power is needed. The power density of the battery is 64 w/kg for eight hours, which compares to the 5300 w/kg power density of the solar cells. This suggests that the use of the solar cells is beneficial. The power available from the batteries is also independent of velocity and altitude like the solar cells. The total average power available from the power source will be 27.1 kw. The use of a fuel cell may be more feasible, but sufficient data were not available.

The HIF2 will require a propeller that can operate in Mars' thin atmosphere. This makes the propeller very large and operational at low shaft speeds. The minimization of shaft power for climb, cruise, and maximum conditions results in a propeller diameter of 8.7 meters, which is shown on the graphs. The maximum power input is minimized because this affects the size of the total power system. The propeller has a constant blade pitch angle which is very reliable. It has a blade pitch angle of 25 degrees which provides the best performance. The propeller

tips operate below the transonic regime for all flight conditions. The shaft rotation rates are 400 rpm for climb, 475 rpm for cruise, and 500 rpm for maximum power. These values were obtained from graphs provided. The data for these graphs were obtained from a propeller design chart 5868-9 of NACA Tech. Report 640. The static performance has been eliminated since a rocket assist will be used for takeoff. Once the HIF2 reaches climb conditions of 55 m/sec, the propeller will take over and maintain flight conditions. Before landing, the propeller will also be locked in horizontal position to avoid the use of large landing gear. The use of a three-bladed propeller has been considered. It has the advantage of reducing blade diameter and vibrations, but it would reduce efficiency and require larger landing gear because it could not be locked in horizontal position.[2] The HIF2 has a propeller with an efficiency range of 84-86%. The propeller has an approximate mass of 37 kg which was obtained from a graph in reference 2. This design produces a maximum power available of 18.5 kw at cruise conditions of 70 m/sec and a density of 0.014 kg/m^3. The power available from the propeller is a function of altitude because of density variations, but it is not a function of velocity. The power available at ground level is greater than at altitude and has a value of 19.63 kw. This corresponds to a power available at cruise of 18.5 kw and 19.1 kw for climb conditions. The inoperative drag estimation at cruise for the propeller has a

value of 375 newtons, which seems very large.

It has been assumed that avionics and experimental devices will require 100 watts of power each. This power is obtained from the power conditioner which obtains an average power of 18 kw from the solar array and an average power of 9.1 kw from the battery. All previous subsystems are independent of altitude and velocity except for the propeller which is dependent on altitude.

Reference Page

1 Secunde, Richard R., Richard M. Schuh, and Raymond F. Beach: Electric Vehicle Propulsion Alternatives. NASA TM-83504.

2 Hall, David W., Charles D. Fortenbach, Emanual V. Dimicele, and Robert W. Parks: A Preliminary Study of Solar Powered Aircraft and Associated Power Trains. NASA Contractor Report 3699, December 1983.

3 Smith, Robert E. and George S. West: Space and Planetary Environment Criteria Guidelines for Use in Space Vehicle Development. NASA Technical Memorandum 82478, 1983.

4 Photovoltaics, Volume 543. Proceedings of SPIE - The International Society of Optical Engineers.

5 Bahniuk, Douglas: A New Look for Lithium Batteries. Machine Design. March 20, 1986.

6 Morrow, G. Editor. Proceedings of the Goddard Space Flight Center Battery Workshop. NASA Conference Publication 2382, 1984.

7 Clarke, Victor C., Abraham Kerem, and Richard Lewis: A Mars Plane ?. American Institute of Aeronautics and Astronautics. 1979.

8 CRC: Handbook of Chemistry and Physics. 68th edition. CRC Press, Inc., Boca Raton, FL. 1987-88.

Significant data:

Engine description:	Samarium cobalt
Number of engines:	1
P_e(max):	18.5 kw
Weight of engine:	86.3 N*
C_p at cruise:	0
Prop. diameter:	8.7 m
Number of blades:	2
P_{avial} (climb):	19.1 kw
P_{avial} (cruise):	18.5 kw
Flight duration:	8 hrs
Blade pitch:	25°
Climb (N):	400 rpm
Cruise (N):	475 rpm
Maximum (n):	500 rpm

* includes invertor and gear box

Nomenclature list:

km - kilometers
kg - mass in kilograms
N - weight on Mars
kw - kilowatts
rpm - revolutions per minute
m - meters
°K - degrees Kelvin
% - percent
km - kilometers
hrs - hours

POWER AND PROPULSION SYSTEM FLOWCHART

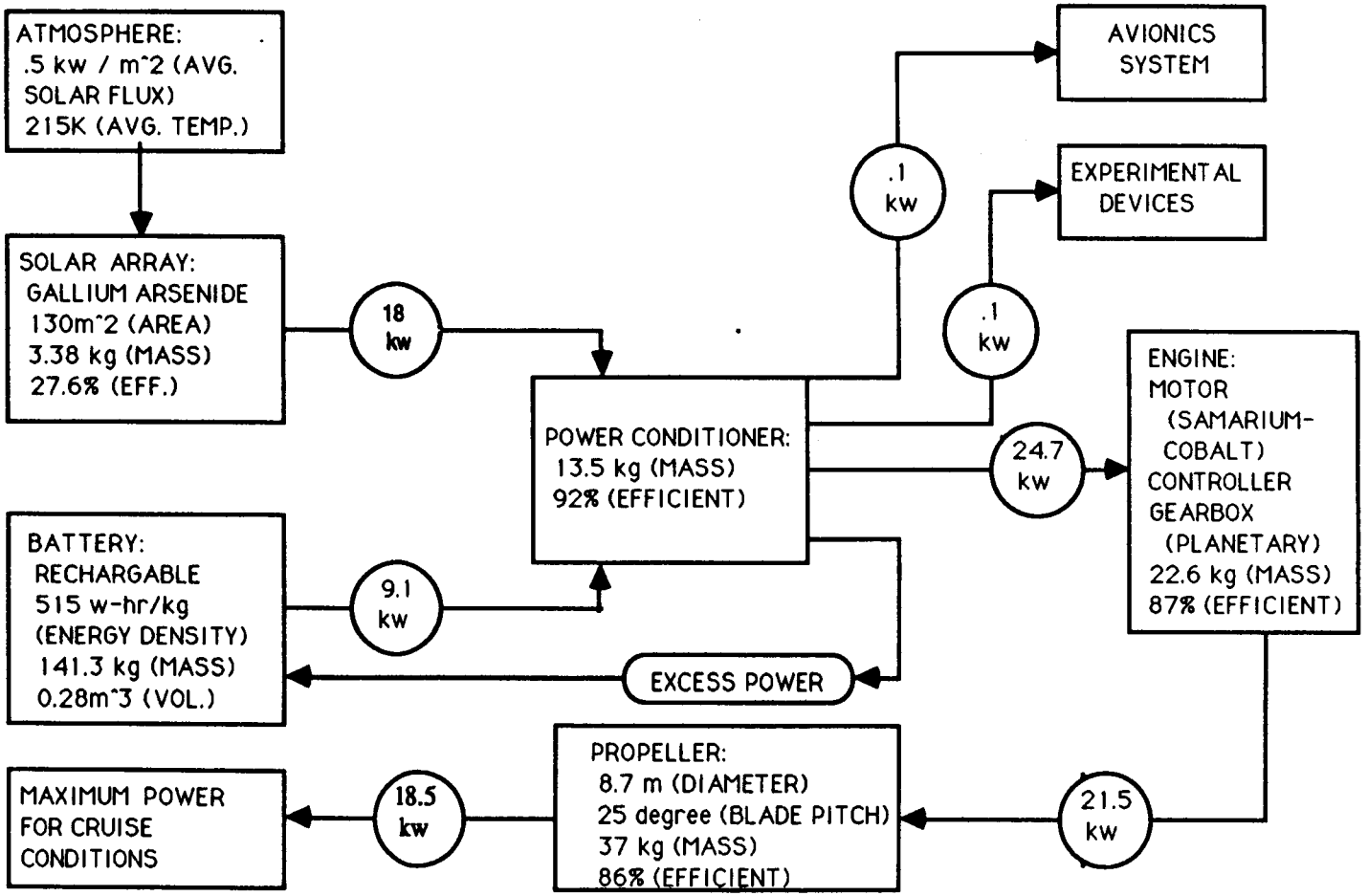

CHART 3-1

POWER IN vs. DIAMETER &RPM
CLIMB CONDITONS

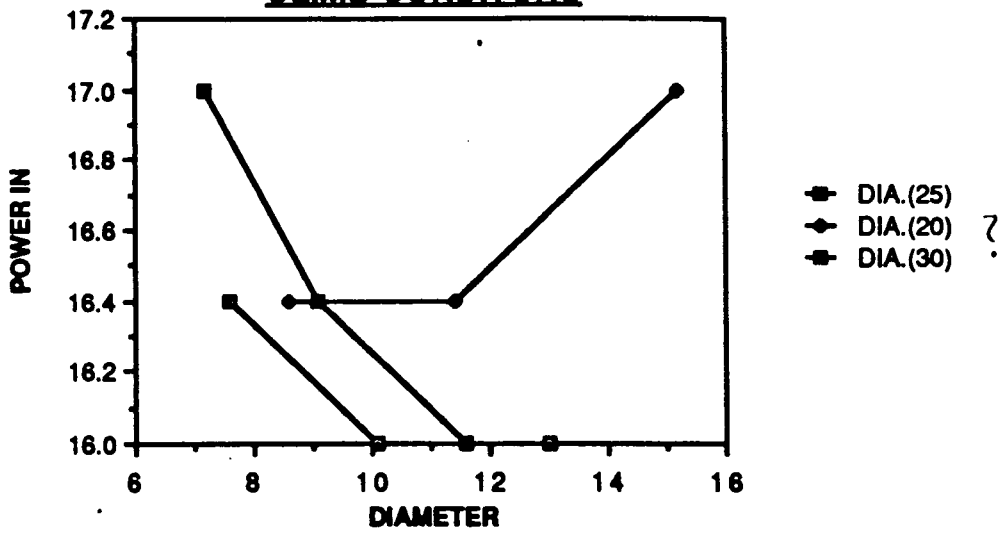

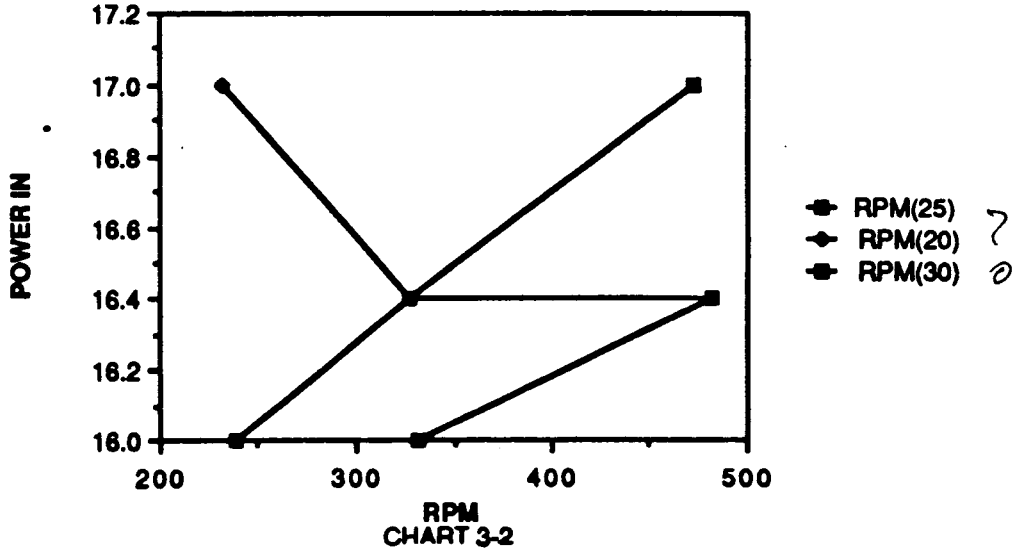

CHART 3-2

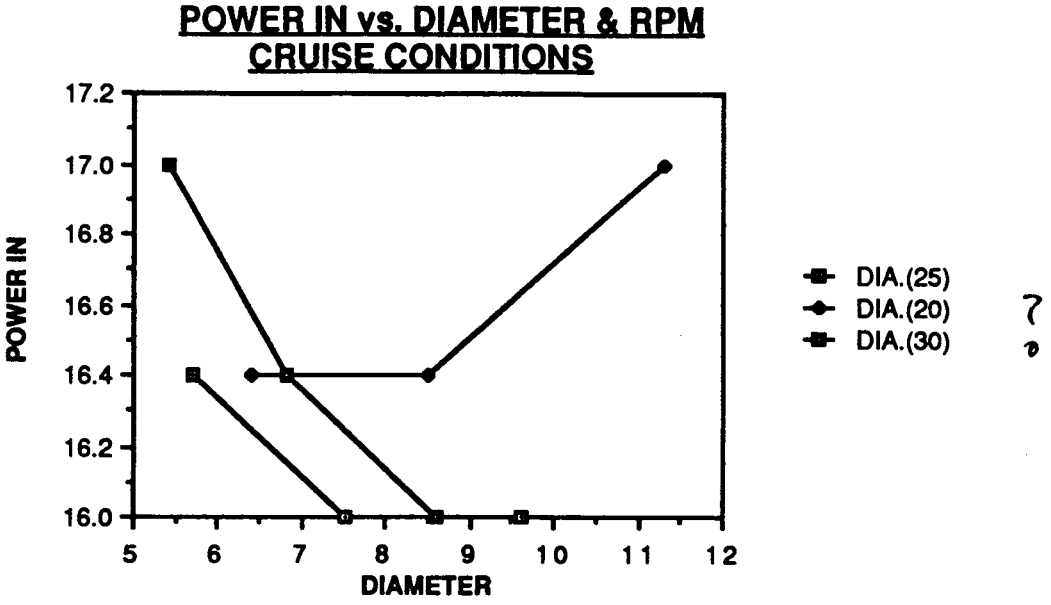
POWER IN vs. DIAMETER & RPM
CRUISE CONDITIONS
17.2
17.0
16.8
16.6
16.4
16.2
16.0
POWER IN
5
6
7
8
9
10
11
12
DIAMETER
DIA.(25)
DIA.(20)
DIA.(30)

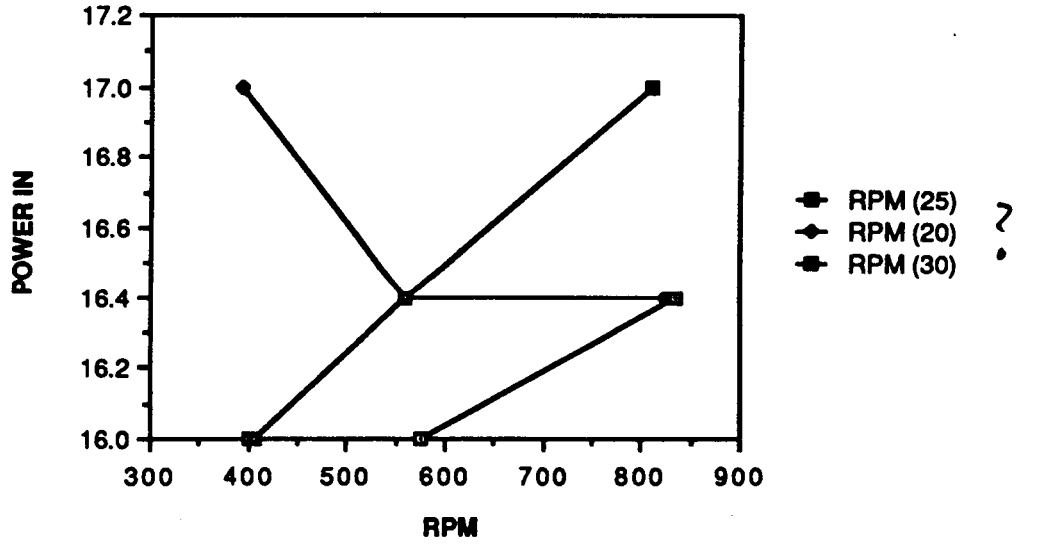
17.2
17.0
16.8
16.6
16.4
16.2
16.0
POWER IN
300
400
500
600
700
800
900
RPM
RPM (25)
RPM (20)
RPM (30)

CHART 3-3

POWER IN vs. DIAMETER & RPM
MAXIMUM CONDITIONS

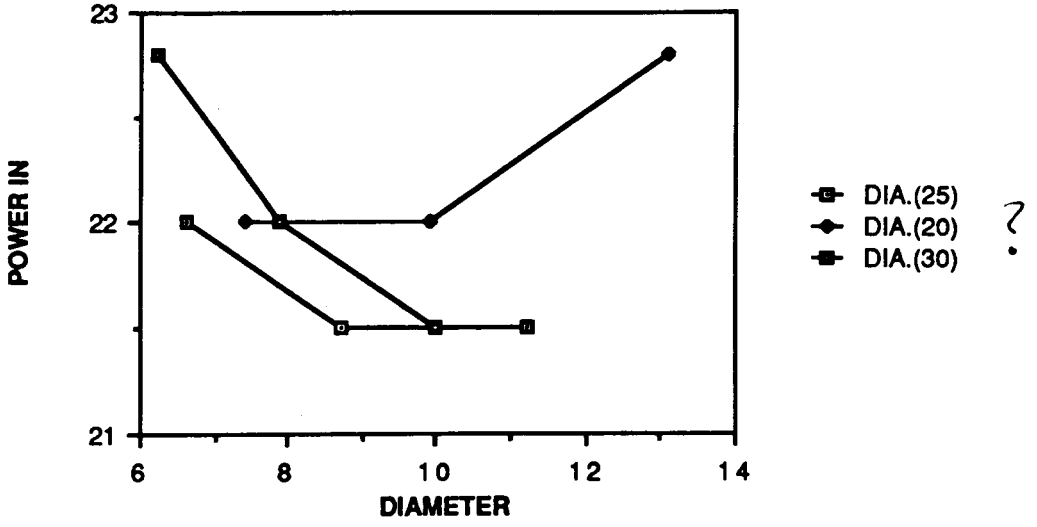

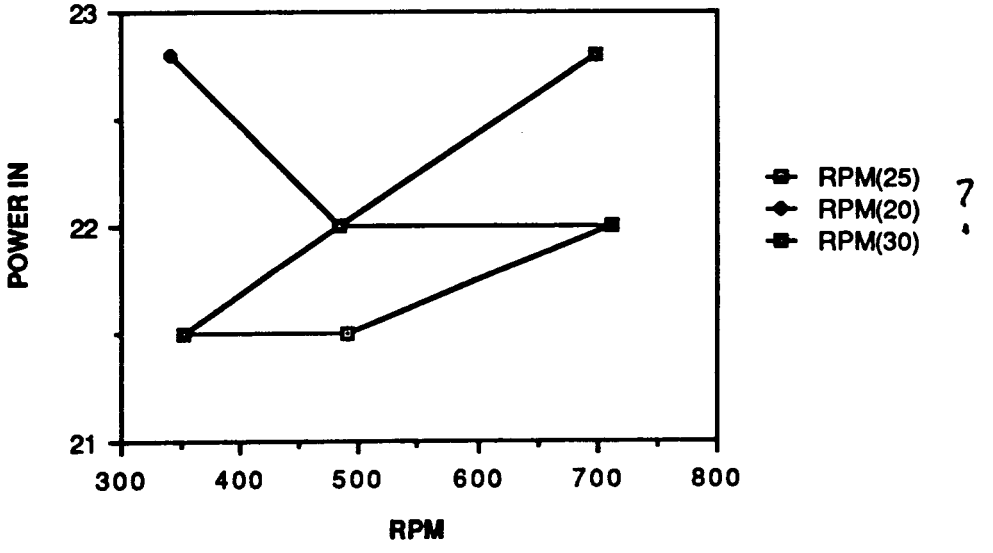

CHART 3-4

STRUCTURES

Glen W. Brown

Successful flight of an aircraft in the Martian atmosphere requires a vehicle of minimal structural mass. A wing composed of partially solid and partially flexible materials was a preliminary concept. However, upon further investigation a more conventional solid wing structure has now been chosen. High-strength advanced composite materials will comprise the main load-bearing structures of this vehicle. Composite materials have been selected due to their higher strength and higher stiffness qualities and due to their significant reduction in structural weight. A discussion of material selection will be discussed later in this text.

The computation of wing loadings was the starting point for structural analysis of this aircraft. The following variables must first be defined.

V = Shear (Newtons)

M = Bending Moment (Newton-meters)

Mac = Torsional moment about the aerodynamic center (Newton-meters)

Y = Station along wing semi-span (meters)

After receiving the lift distribution and structural weights from corresponding design areas loadings, shears, and bending moments were calculated. For analysis, the lift distribution

was segmented into two parts: the constant upward lift along the wing added to the remaining elliptical lift. The wing weight was divided into five meter sections (except for the outermost ten meters which was analyzed in its entirety) as it was reasonable to assume each of these as constant loads. This is because the main spar is the principle component of wing weight and each five-meter section of spar is of constant thickness. These thicknesses continually decrease along the wing towards the tip, thus making each five meters a very nearly constant load. (The last two five-meter sections of spar are the same thickness, thus analyzed as one ten-meter section.) Each wing also supports a tailboom, one-half the empennage, and landing gear and a small pod to house them during flight. All are located at the five-meter station. The structural weights are summed and idealized as a point load. Shear and bending moments due to the above loadings were calculated. Summing the appropriate shear and bending moments and plotting the results, corresponding diagrams are obtained for 1-g Martian loading (see Figs. 5.1, 5.2, and 5.3) and for 4-g (critical) Martian loading (see Figs. 5.4, 5.5, and 5.6). For on-ramp conditions, the landing gear of each wing has been determined to support 41% of the gross weight of the aircraft. Corresponding loading, shear and bending moment diagrams have been plotted (see Figs. 5.7, 5.8, and 5.9). Bending due to torsion was also calculated using the equation $(1/2)qc^2Cmac$. (q is atmospheric Martian density multiplied by maximum cruise

velocity squared, C is the chord length and Cmac is the pitching moment about the aerodynamic center). The torsional moment about the aerodynamic center as a function of wing semi-span can be seen in Fig. 5.10.

The structural design of the H.I.F. II Martian aircraft is expected to experience a variety of loadings. The wing of this vehicle is designed to endure bending and torsional loadings associated with 4-g Martian flight. 4-g flight is the ultimate strength load factor that has been selected. To endure such loading, the primary load-bearing structures of the wing will be constructed out of longitudinal layers of graphite-epoxy tape (4.8 x 10" $^{N}/m^{2}$ modules) overlaid at $^{+}60$ degrees and -60 degrees. Overlaid layers of this graphite-epoxy material will easily withstand the most severe bending and torsion encountered. The structures to be comprised of this material are the cylindrical primary and secondary wing spars, the tail spar, the tailbooms, and the fuselage frame. The cylidrical spars and tailbooms can be made by wrapping pre-impregnated graphite-epoxy strips on appropriate aluminum tube diameters and curing in an oven. The aluminum can then be removed by chemically etching it out. Some other materials will be discussed shortly.

From loadings, shears, bending moments and material selection, minimum thickness of the main spar at various wing stations were calculated. This was done by employing the net maximum moment from 4-g flight (My), the ultimate yield stress of graphite-epoxy composite material ($\sigma = 9.8 \times 10^8$ N/m^2), incorporating a safety factor of 1.5, and the geometric moment of inertia of the cylindrical tube cross-section ($I = \pi r^3 t$). Using the equation $\sigma y = My/I$, the moment of inertia was calculated. Equating this value with the geometric moment of inertia of the cylindrical tube, the minimum material thickness at various stations along the wing were computated. These minimum thicknesses were then generously bolstered so as to achieve absolute safety in the design. The support of the wing is seen in a cross-sectional view of the wing airfoil and the geometry at various stations is summarized in Fig. 5.11.

A schematic top view (Fig. 5.12) of the H.I.F. II shows rib placement in the wings and tail to preserve a constant airfoil shape. Wing ribs (see Fig. 5.13) placed at 0.5 meter stations along the wing (1.0 meter stations in the tail) are made of sitka spruce wood as it is of very low density (550 kg/m^3) and will keep the airfoil shape constant along the wing. These ribs are five millimeters thick. Also, cylindrical wooden disks or plugs (Fig. 5.14), five millimeters in thickness are placed in the main spar of the wing every 0.5 meters and between each rib. In the spar of the tail, the disks are

placed at one-meter intervals and again between each rib. There will be four one-centimeter thick plugs inserted in each tailboom at the two, four-, six- and eight-meter stations. These disks preserve the cylindrical shape and deter local deformation of the aforementioned structures. The wing and tail airfoil skin as well of the skin of the fuselage will be made of one millimeter thick wooden panels attached to the ribs and airframe skeleton. Once attached, the wooden skin will be wrapped in overlaid sheets of kevlar fabric and this thickness will be approximately two tenths of one millimeter. Kevlar was chosen to wrap the skin as it will add much strength and is extremely lightweight.

As already mentioned, the fuselage skin will be made of several layers of kevlar wrap. This skin will surround a graphite-epoxy frame shown in a three-view sketch (Fig. 5.15 a,b,c). A battery of substantial size and weight and a pilot and crewman will be located in the forward forty percent (2.5m) of the fuselage pod. The beefed-up framework in this section is a result of these loads that must be supported. A five millimeter thick angled floor with a rear "lip" of aluminum 7075 will support and secure the battery. This floor extends from the nose to approximately 1.5m horizontal distance. Then, a two centimeter thick birch plywood level floor extends to the three-meter station. This floor will support the crewman and equipment. Further equipment may be placed on a "wedge" of birch ply located behind the crewman, from the three-to four-

meter stations. (See Fig. 5.15b). A bulkhead at the far anterior of the fuselage secures the propellar. The pilot seat will be supported by angled aluminum supports jutting from the sides of the pod (secured in a frame support) and secured to aluminum runners under his seat. (See Fig. 5.16). The crewman will be supported by vertical aluminum supports bolted to runners both on the plywood floor and under his seat. The fuselage pod, the battery, and the pilot and crewman and equipment are all well supported.

The H.I.F. II is a structurally sound aircraft that was kept relatively simple yet quite durable. It is a reliable Martian aircraft capable of carrying out a range of missions. The materials selected are very high-strength and lightweight, which was an absolute must design criterion. From an analytical standpoint, this aircraft will support all the loads it will encounter on Mars. With adequate testing this vehicle should be proven reliable and structurally sound. With the other design criteria in capable hands the H.I.F. II will certainly be able to achieve successful Martian flight.

REFERENCES

Armstrong, Henry H. and Johnson, Robert R. "Organic and Metal Matrix Composites for Spacecraft Applications." SAMPE Quarterly, 1978.

Burke, James D., "The Gossamer Condor and Albatross: A Case Study in Aircraft Design." Report No. AV-R-80/540, June 16, 1980

Nicolai, Leland M., Aircraft Design, Published by Mets Inc., 1975

Roskam, Jan, Airplane Design Part III: Layout Design of Cockpit, Fuselage, Wing and Empennage: Cutaways and Inboard Profiles. Published by Roskam Aviation and Engineering Corp., 1986.

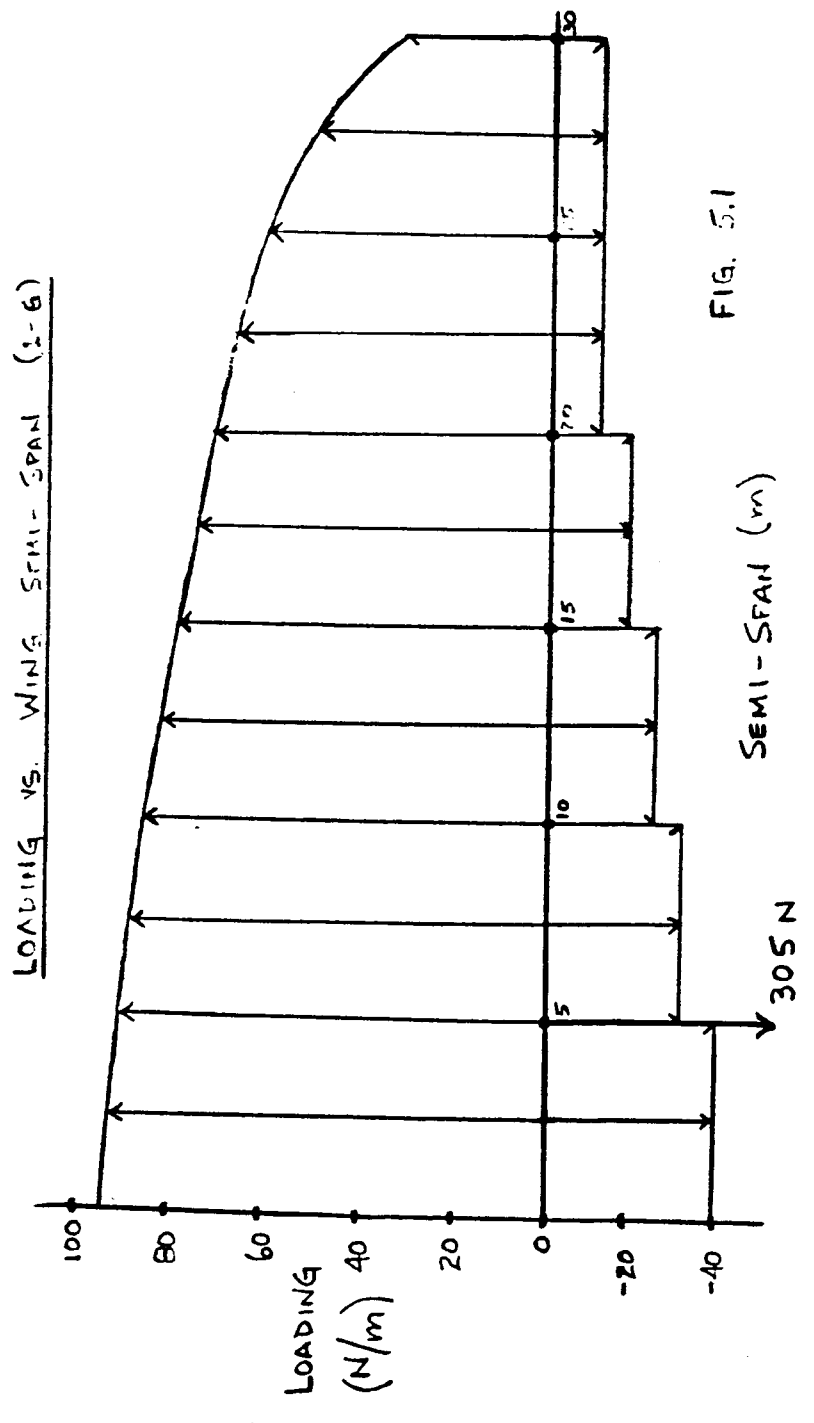

FIG. 5.1

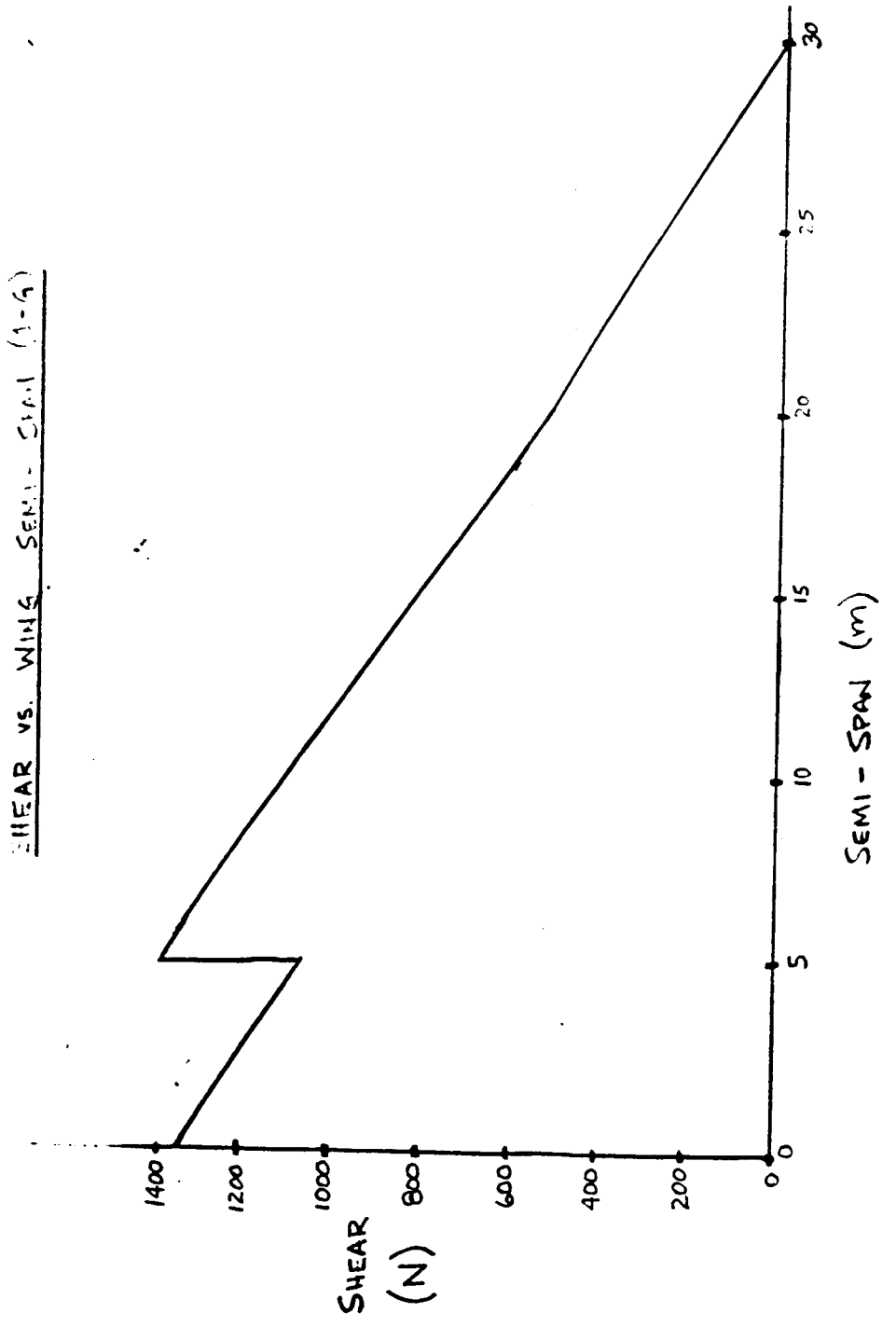

FIG 5.2

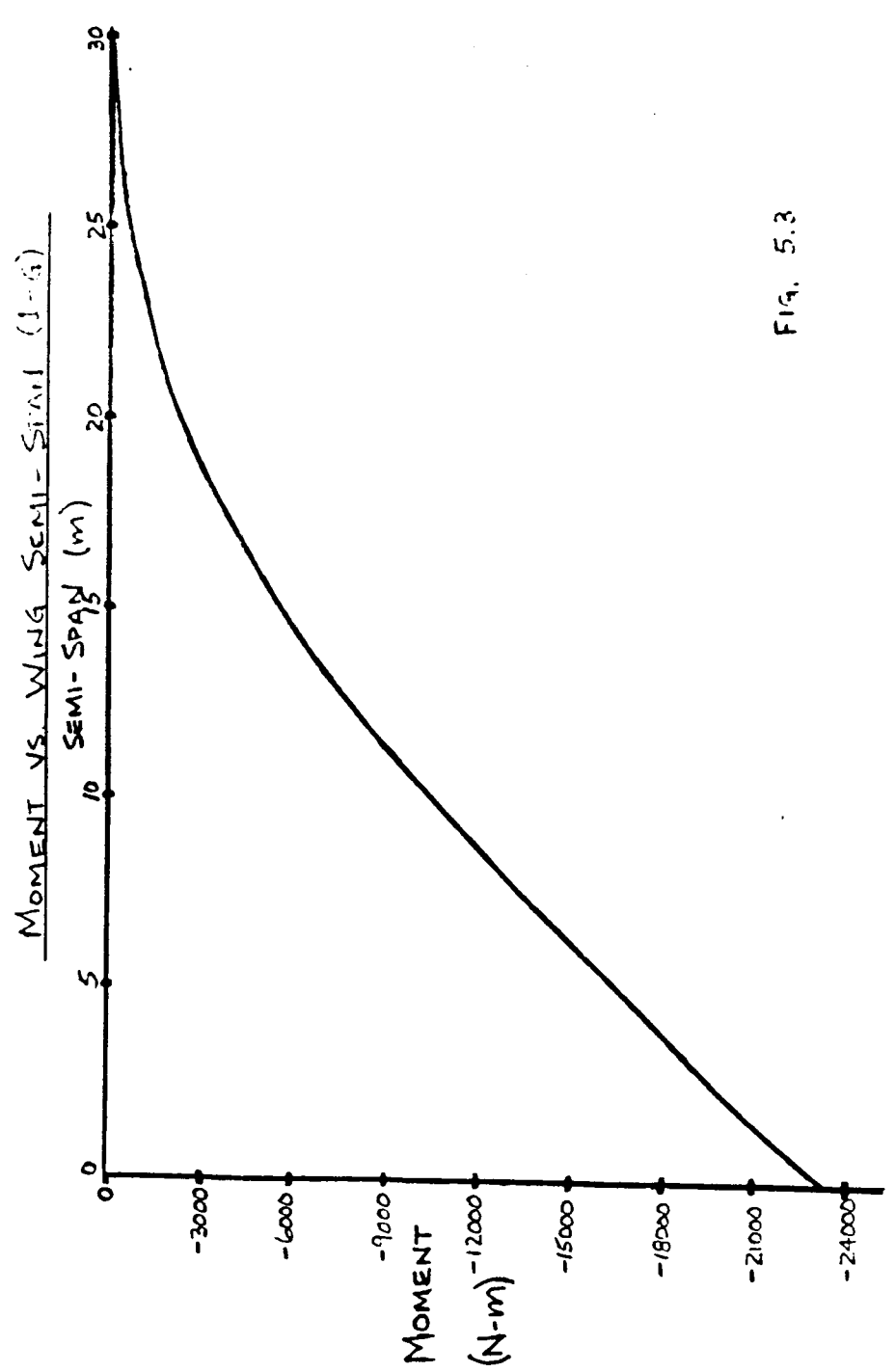

FIG. 5.3

LOADING VS. WING SEMI-SPAN (1-G)

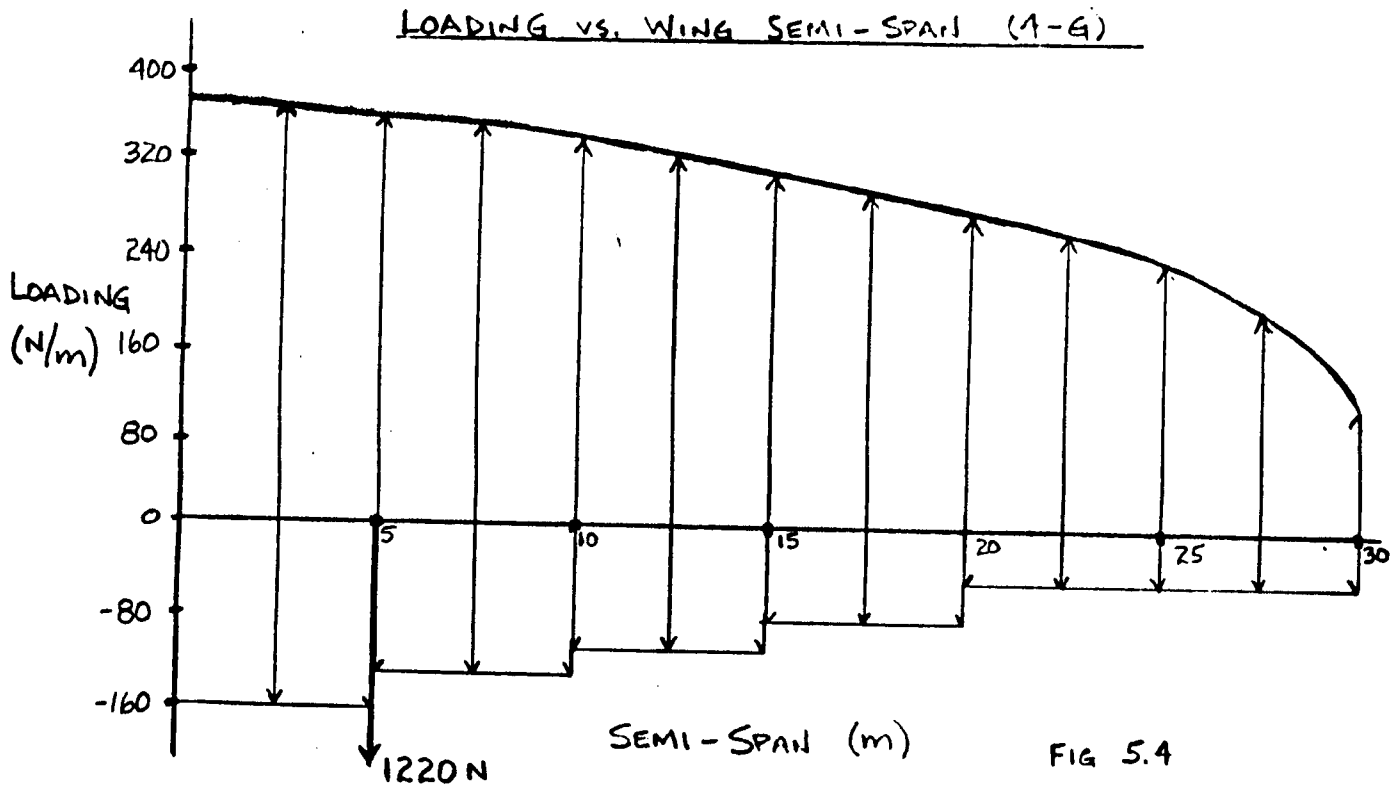

FIG 5.4

SHEAR VS. WING SEMI-SPAN (1-G)

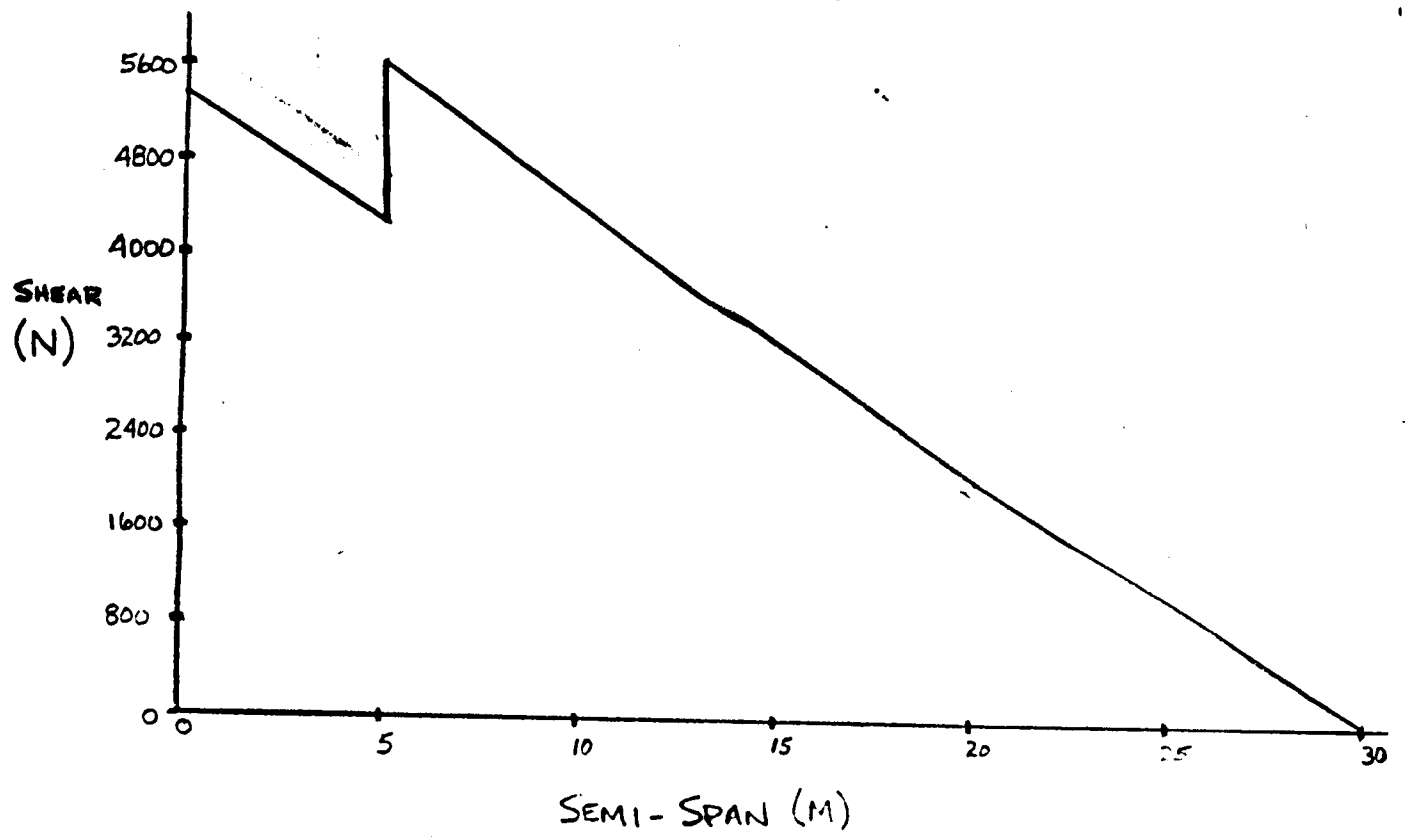

FIG. 5.5

MOMENT VS. WING SEMI-SPAN (1-G)

SEMI-SPAN (m)

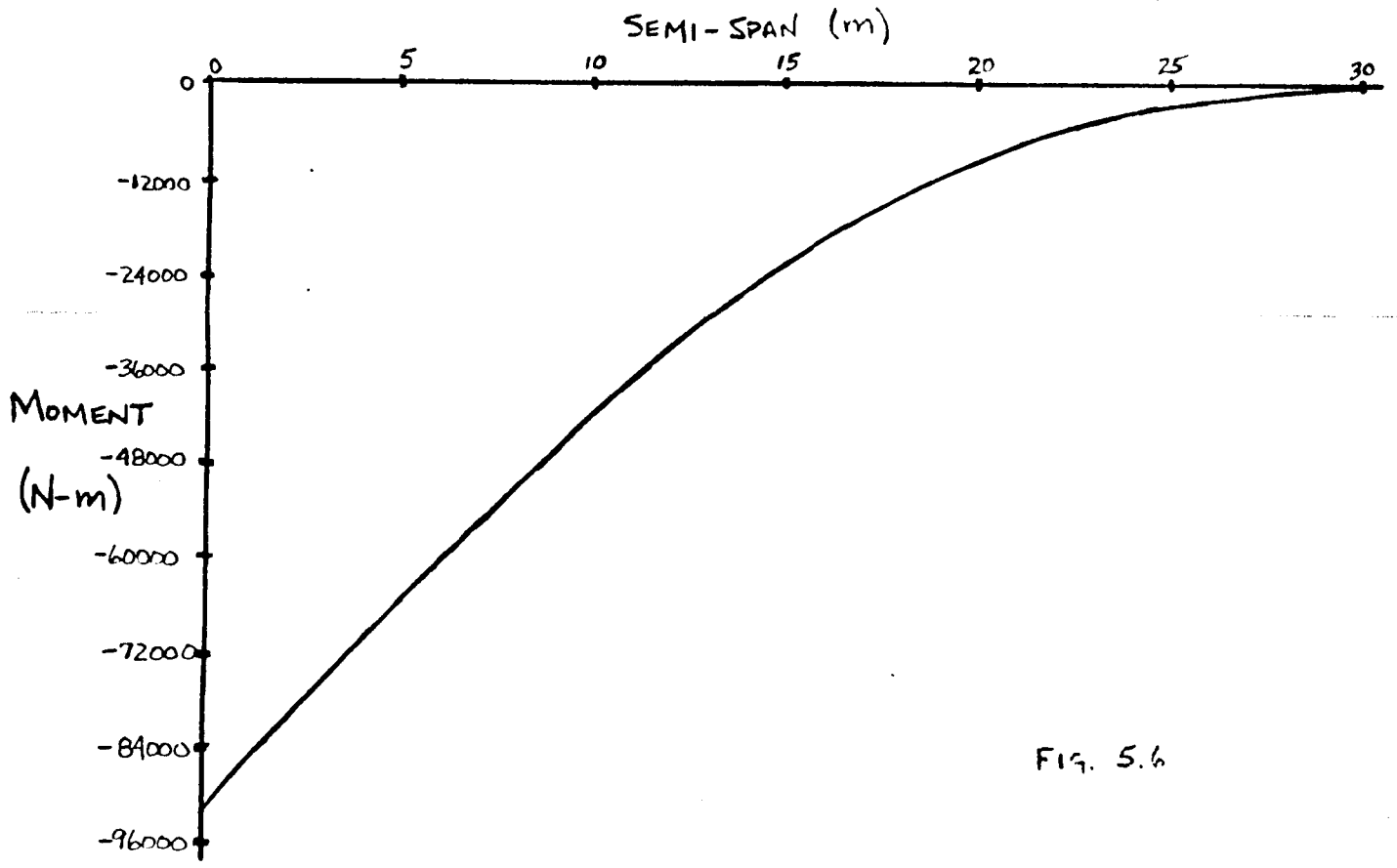

FIG. 5.6

FOLDOUT FRAME

LOADING VS. WING SEMI-SPAN (ON RAMP)

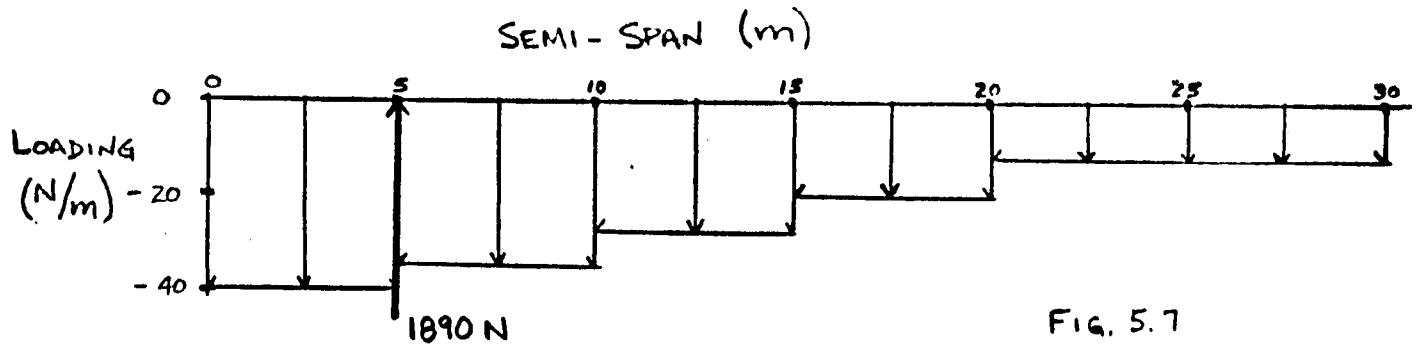

FIG. 5.7

SHEAR VS. WING SEMI-SPAN (ON RAMP)

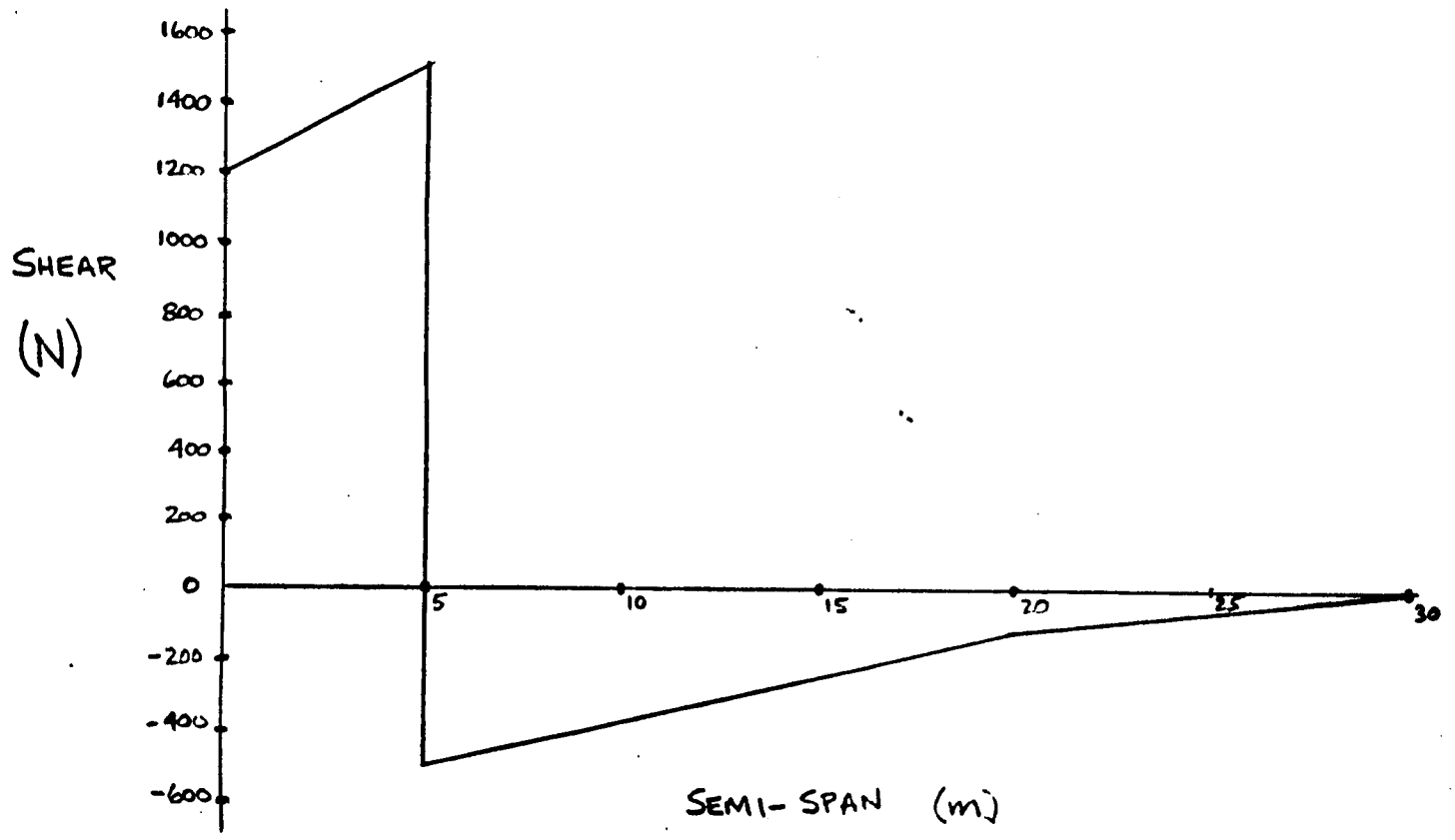

FIG. 5.8

MOMENT VS WING SEMI-SPAN (ON RAMP)

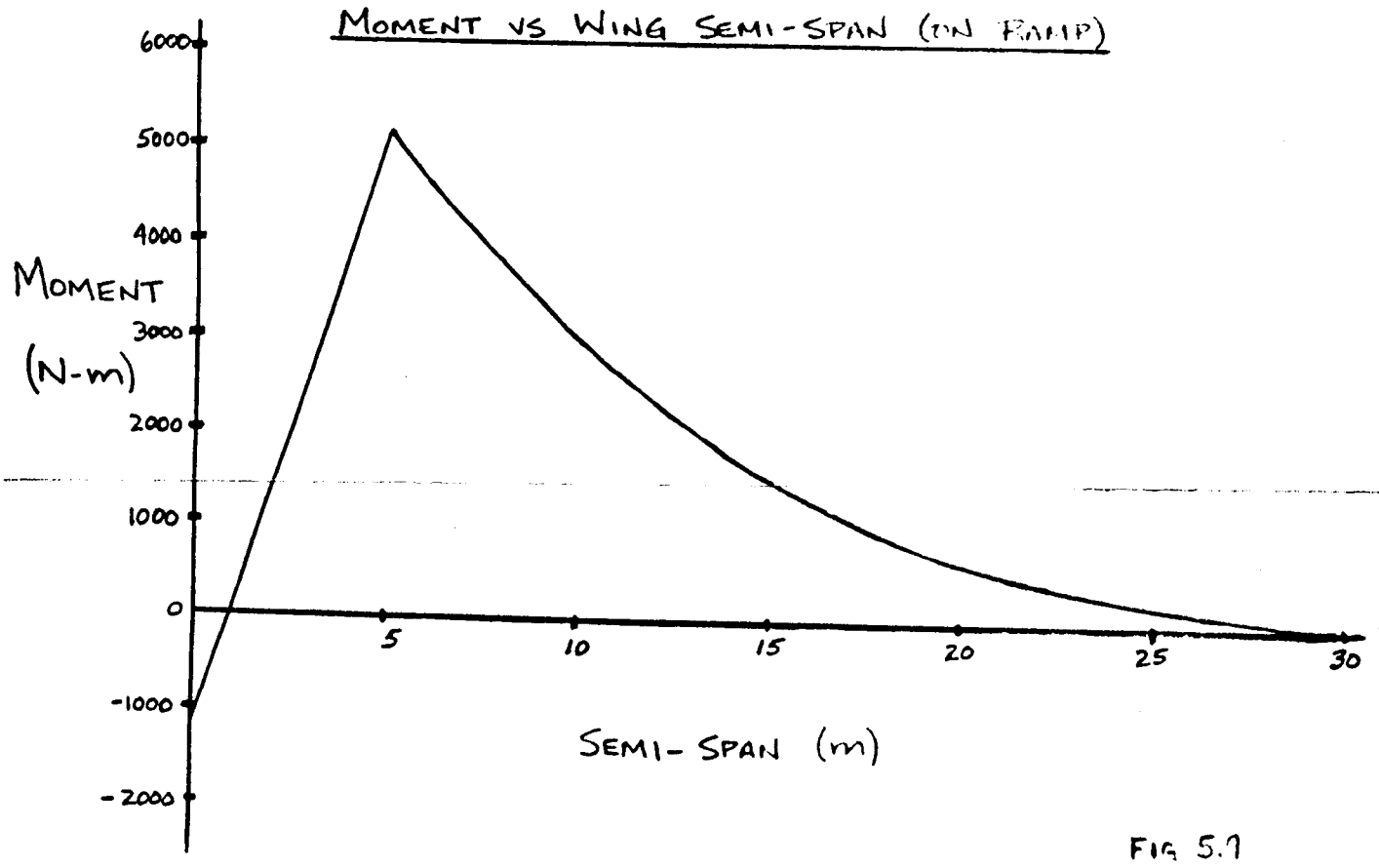

FIG 5.9

FOLDOUT FRAME

5-10

ORIGINAL PAGE IS OF POOR QUALITY

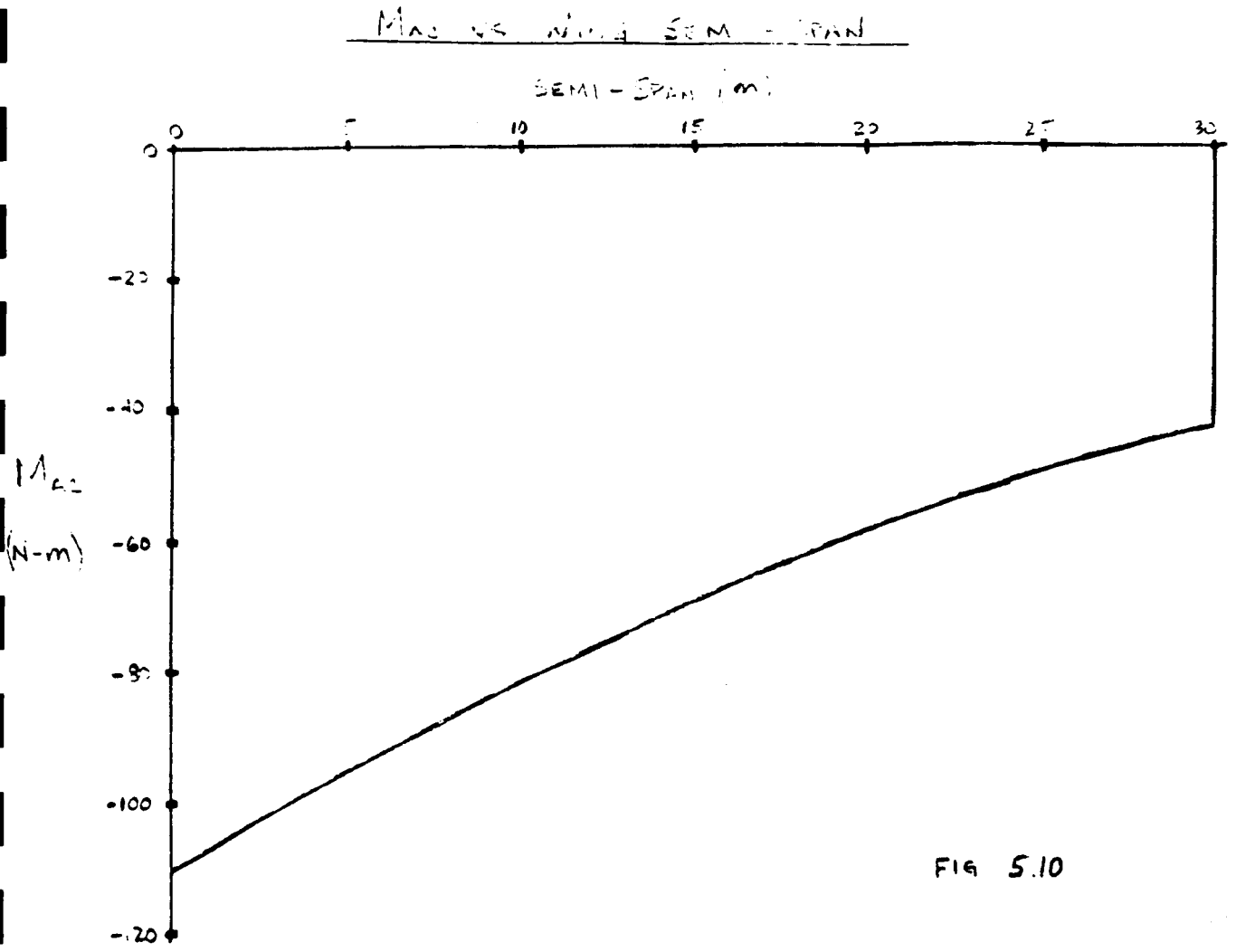

FIG 5.10

AIRFOIL CROSS-SECTION

ORIGINAL PAGE IS OF POOR QUALITY

(WING AND HORIZONTAL TAIL)

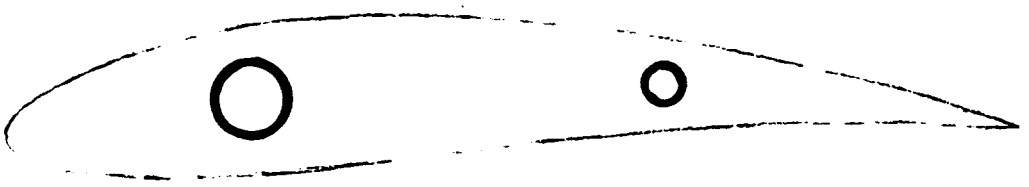

FIG 5.11

SUMMARY:

WING

LEADING SPAR

STATION (m)	0-5	5-10	10-15	15-20	20-25	25-30
OUTER RADIUS (m)	0.18	0.17	0.16	0.15	0.14	0.13
THICKNESS (m)	0.004	0.0035	0.003	0.0025	0.002	0.002
X/S ORIGIN (m) - FROM LEADING EDGE -	0.75-0.71	0.71-0.67	0.67-0.625	0.625-0.58	0.58-0.54	0.54-0.5

SECONDARY SPAR

STATION (m)	0	5	10	15	20	25	30
* AIRFOIL LENGTH (m)	3.0	2.83	2.67	2.5	2.33	2.17	2.0
OUTER RADIUS (m)	0.10	0.10	0.10	0.10	0.10	0.10	0.10
THICKNESS (m)	0.002	0.002	0.002	0.002	0.002	0.002	0.002
X/S ORIGIN (m) - FROM LEADING EDGE	2.0	1.89	1.78	1.67	1.56	1.44	1.33

HORIZONTAL TAIL

STATION (m)	ALL (0-14)
* AIRFOIL LENGTH (m)	2.0
OUTER RADIUS (m)	0.13
THICKNESS (m)	0.002
X/S ORIGIN (m) - FROM LEADING EDGE -	0.5

(NO SECONDARY SPAR)

SKELETAL TOP VIEW

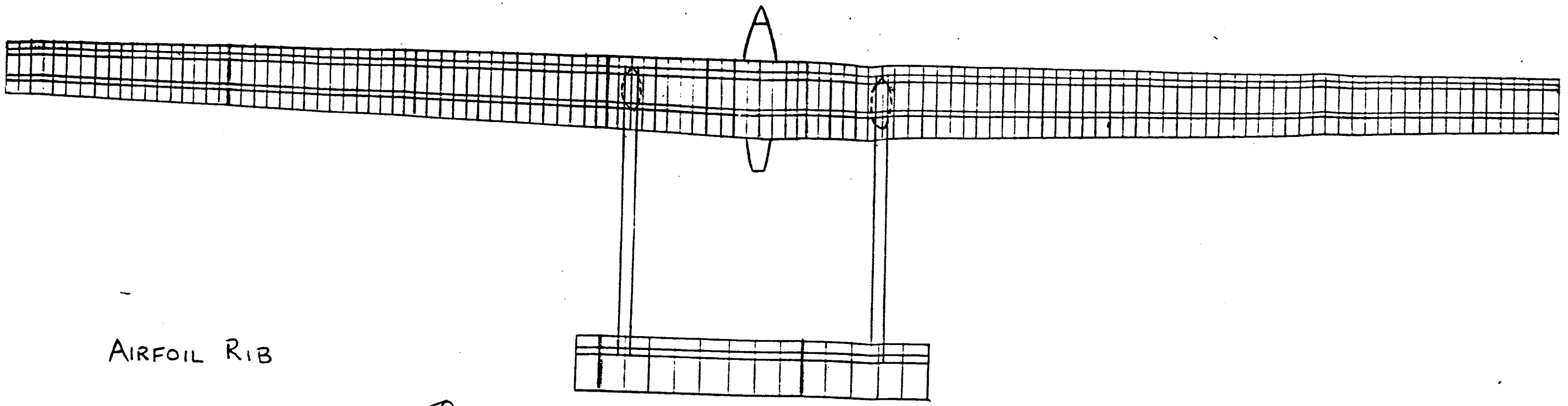

FIG. 5.12

AIRFOIL RIB

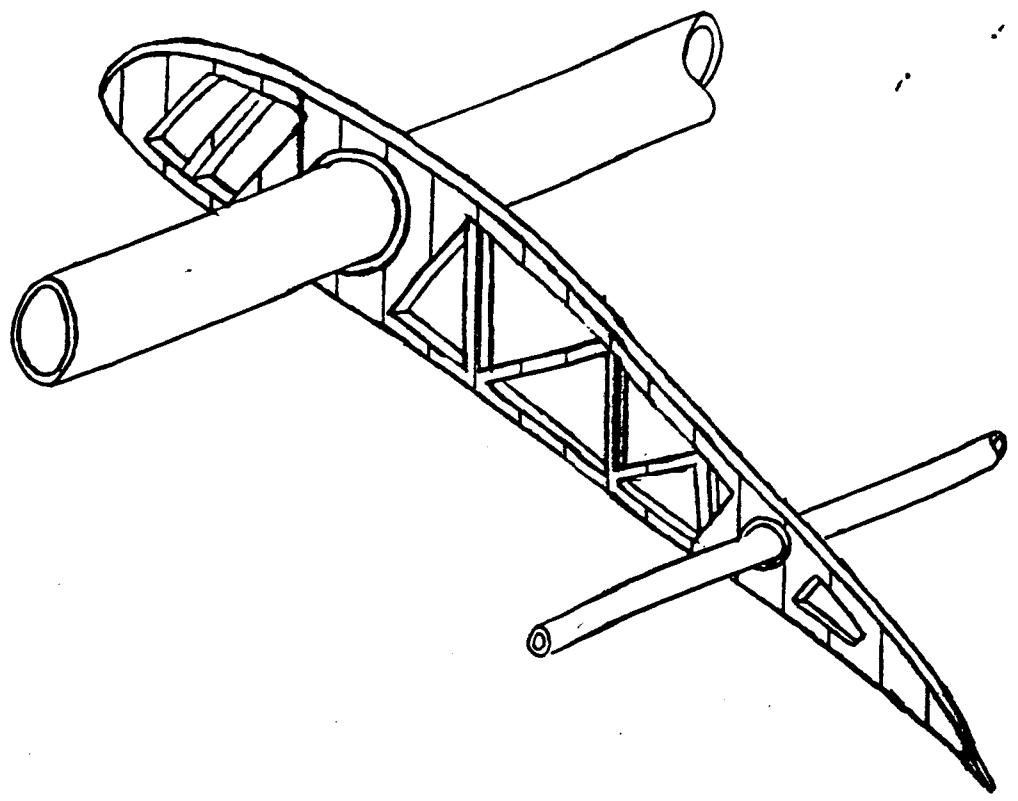

FIG 5.13

DISK INSERTION

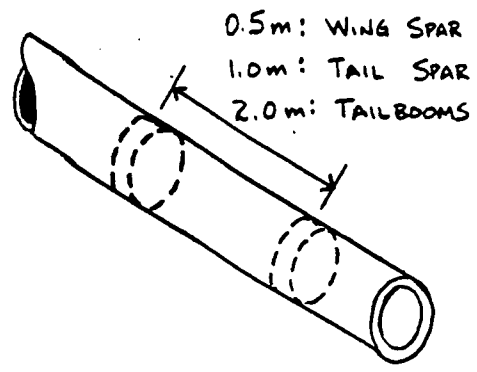

FIG 5.14

FOLDOUT FRAME

FOLDOUT FRAME

FUSELAGE

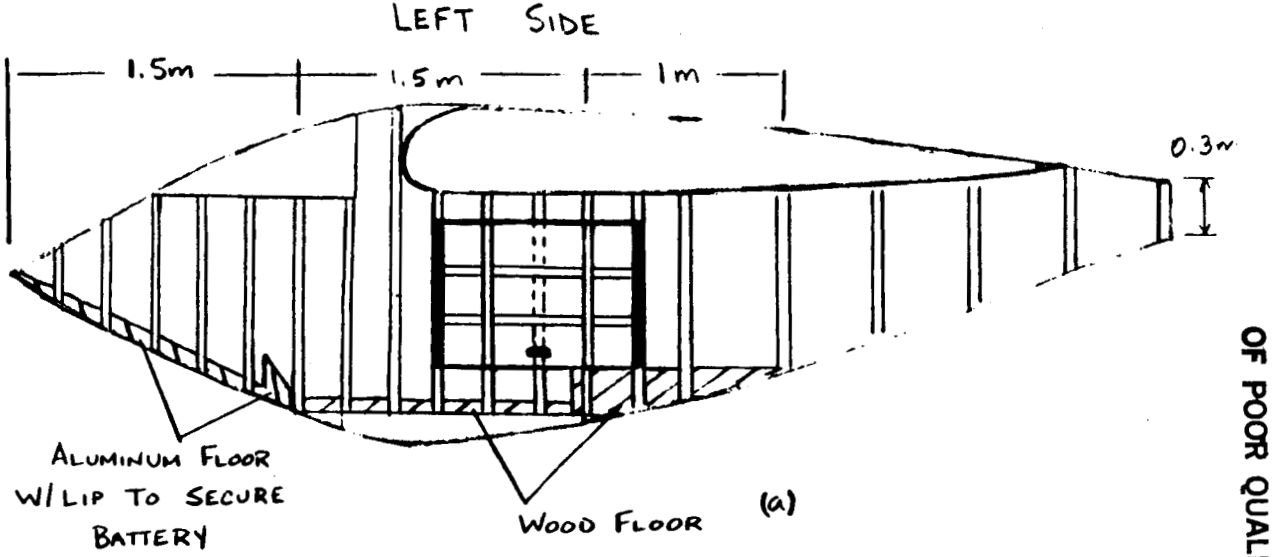

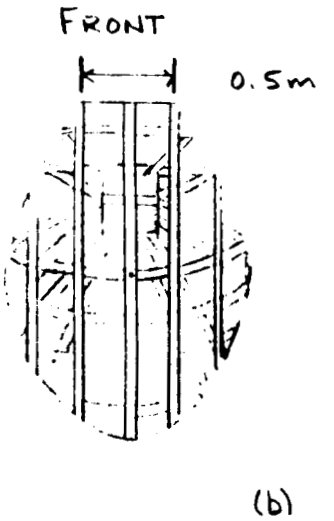

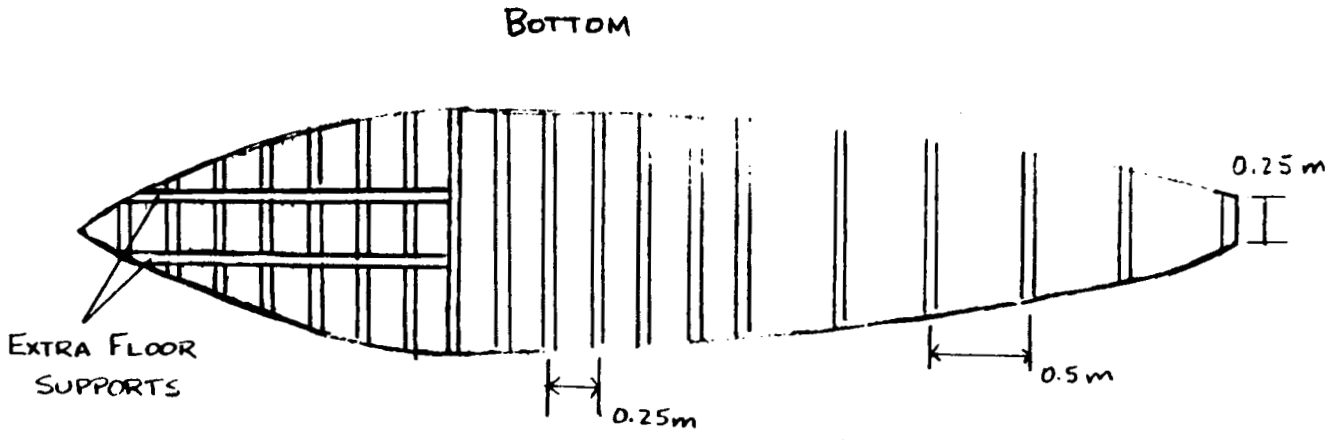

LENGTH: 6m
WIDTH (MAX): 1.25m
HEIGHT: 1.75m

FIG. 5.15

SUPPORT OF PILOT SEAT

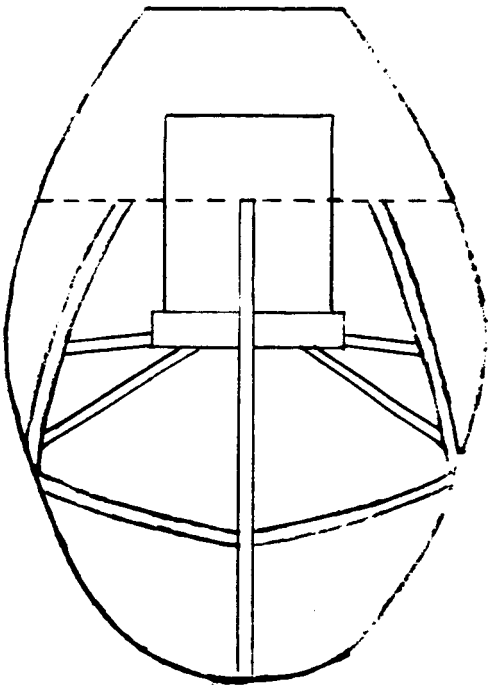

FIG 5.16

STABILITY & CONTROL

Richard R. Monke

The text that follows is split into two parts. First, essential data and calculations are presented. Then, stability and control is demonstrated at three different flight conditions. Throughout the calculations, all stability and control derivatives were calculated using methods presented by Jan Roskam, Professor of Aerospace Engineering at the University of Kansas. (1)

The stability and control of an aircraft is dependent upon the geometry. Control surface areas as % of wing area (150 meters squared) were chosen as follows; horizontal tail - 18%, vertical tails - 12%, and ailerons - 10%. The flap chord to total chord ratio for both the horizontal and vertical tails was chosen to be .25. Full span plain trailing-edge flaps were used. For the ailerons the flap chord to total chord ratio was chosen to be .375, with the inboard location of the aileron 20.72 m from the centerline and the outboard location at the wing tip. The above configurations are shown in Fig. 1. Distance between the aerodynamic center of the wing and aerodynamic center of the tail was set at 10 .$\frac{1}{0}$

With the geometry set, the neutral point was then located. In order to obtain its value, the lift curve slopes of the wing and the tail were calculated to be 6.57/rad and 4.75/rad, respectively. (2) Also, the derivative of the downwash angle with

respect to angle of attack was found to be .17. For these values, the neutral point was located 3.58 m from the nose of the aircraft.

In order to trim at cruise the tail was fixed at an angle of incidence with respect to the horizontal. This angle was found to be -5.3 degrees.

Next the center of gravity (c.g.) range was calculated. A static margin of 10% was to be demonstrated at all flight conditions. Using this value, the most aft position was found to be 3.33 m from the nose of the aircraft. The maximum static margin was then calculated to be 60%. Corresponding to this value, the most forward c.g. location was found to be 2.09 m from HIF 2's nose.

In order to assure the stability and control of HIF 2, several criterion had to be met during takeoff, cruise, and landing.

In takeoff, it was necessary to lift the nosewheel at 90% takeoff speed (51.3 m/s). To satisfy this requirement, the summation of the pitching moments about the nosewheel was set equal to zero. Fig. 2 shows the various forces acting on the aircraft and their respective moment arms. Using this static analysis, the necessary lift coefficient on the horizontal tail was found to be -.057, which corresponds to an elevator deflection of -2 degrees.

At cruise conditions (V=70 m/s & altitude=1.5 km), one of the requirements was to show sufficient lateral and longitudinal

control and power to sustain a 30 degree banked coordinated turn. For a roll angle of 30 degrees, the corresponding load factor was 1.155. With this value, an iteration was performed to find the necessary angle of attack. Its value was found to be 5.7 degrees. At this angle of attack, the drag was calculated to be 107 N. The power consumed was then 7.5 kW. This is 42% of the maximum power available.

The second requirement at cruise was to develop a bank angle of 30 degrees in 2.0 s after control application. A step change in aileron deflection was assumed. The formula used in ths calculation and an approximation formula for the moment of inertia about the x-axis are found on page 8 of the text. The former was solved for the product of variation of rolling moment coefficient with aileron angle and the aileron deflection. Solving this expression, the necessary aileron deflection was found to be -3.91 degrees. This is an antisymmetrical deflection with right aileron up 3.91 degrees.

In landing approach, it was necessary to trim at the maximum lift coefficient (Cl=1.72) with the c.g. location at the forward limit. From Fig. 3 it can be seen that a control moment coefficient of .50 was needed. The elevator deflection needed to produce this moment was found to be 12.9 degrees.

A roll response of 30 degrees in 2 s was also a requirement for landing. Using the same procedure as before, the aileron deflection was found to be -4.36 degrees. Again, this is an antisymmetrical deflection with right aileron up 4.36 degrees.

Crosswind landing is another requirement. Enough directional control was needed to develop a steady sideslip angle of 10 degrees. A NACA 0006 vertical tail cross section was chosen.(3) Using the criterion found on page 8, the rudder deflection was calculated to be greater than or equal to -20.8 degrees.

The final criterion was to mantain wings-level flight in a full rudder sideslip. The equation to satisfy this requiement is found on page 8. An upper limit was placed on the available lateral control power. It was 75%. For a maximum rudder deflection of 30 degrees, the sideslip angle was found to be 14.4 degrees. Only 38% of the available lateral control power was required.

(1) Methods for Estimating Stability and Control of Conventional Subsonic Airplanes

Jan Roskam

University of Kansas

(2) Airfoil Design at Low Reynolds Number with Constrained Pitching Moment

R. H. Liebeck and P. P. Camacho

Douglass Aircraft Company

(3) Theory of Wing Sections

Ira H. Abbot and Albert E. Von Doenhoff

NASA

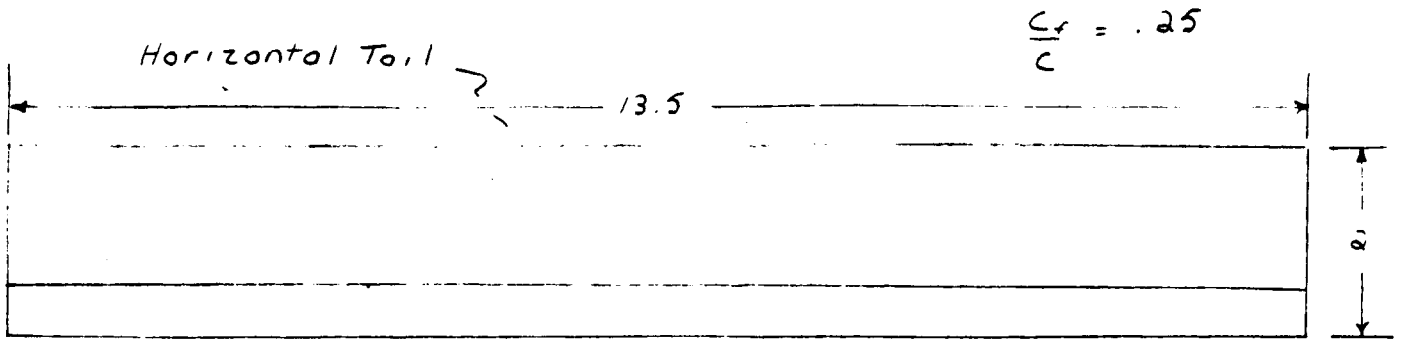

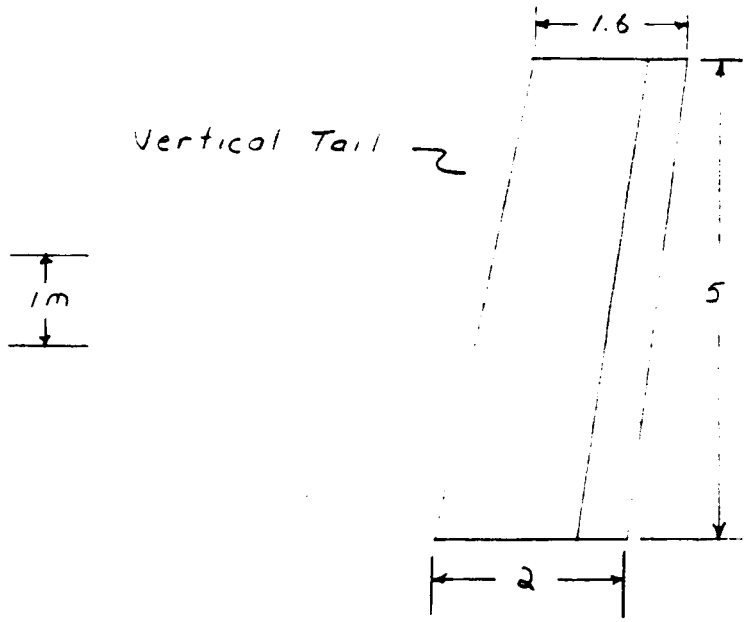

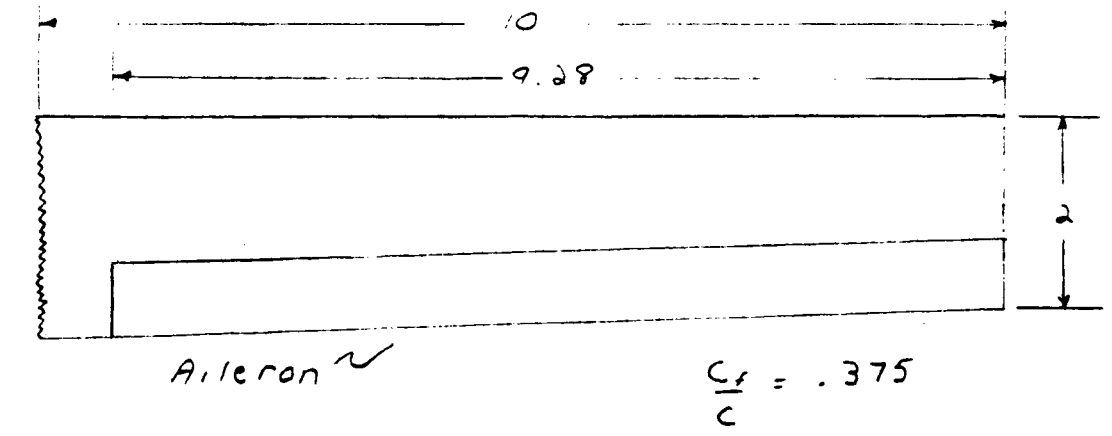

Fig. 1

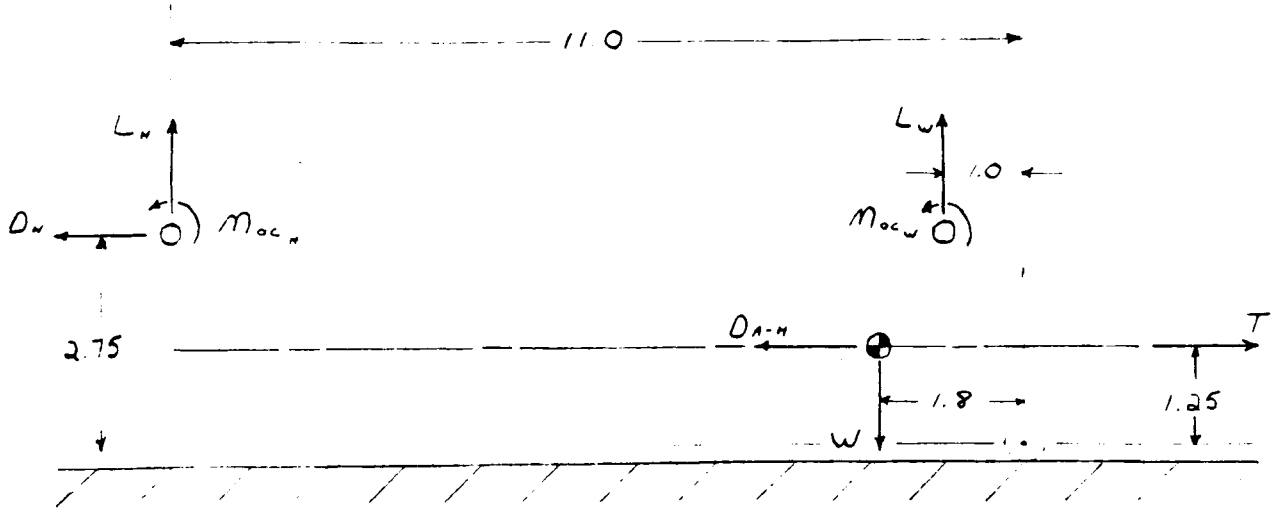

Fig. 2

$D_{A-H} = 46.5\ N$ $\quad T = 5000\ N$ $\quad L_W = 2758.3\ N$

$D_H = 7.5\ N$ $\quad W = 4618\ N$ $\quad m_{ac_W} = -1306.9\ N \cdot m$

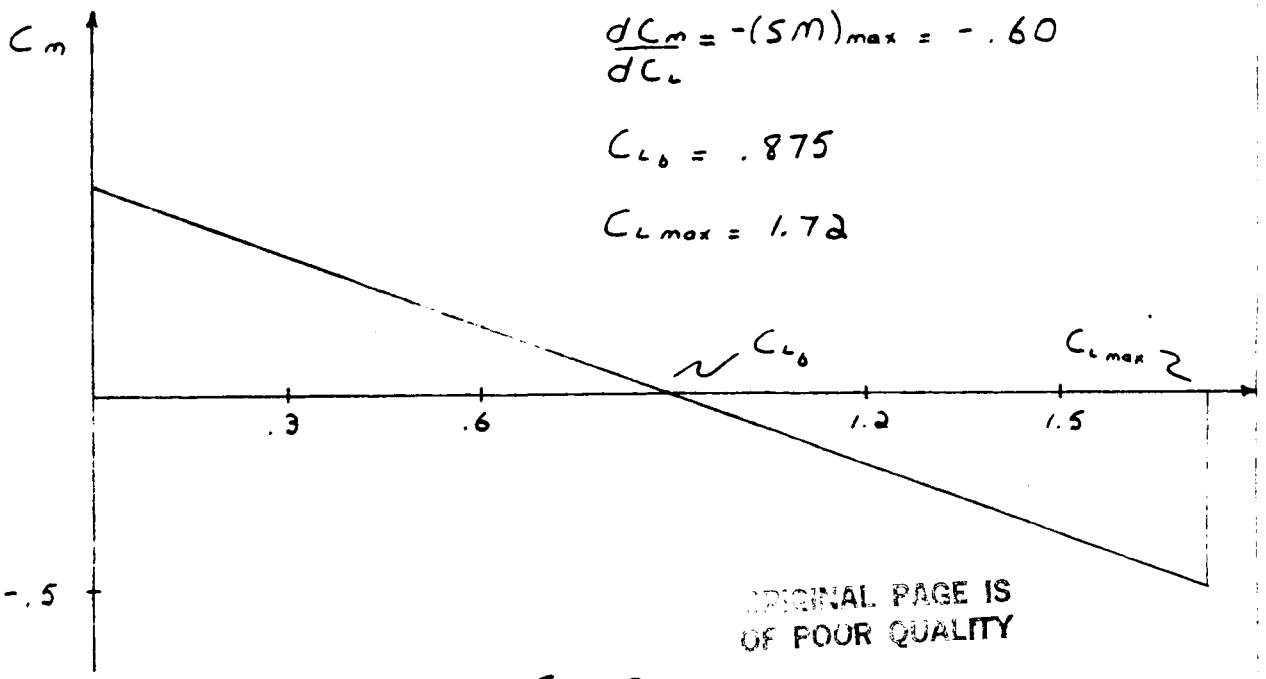

Fig. 3

ROLL RESPONSE

$$\phi = \frac{2V}{b}\left(\frac{C_{l_{\delta_a}}}{C_{l_p}}\right)\Delta\delta_a\left\{\frac{2J_x\tau}{C_{l_p}}\left[\exp\left(\frac{C_{l_p}}{2J_x\tau}t\right)-1\right]-t\right\}$$

$$I_x = \exp(1.7782\log W - 2.9365)$$

CROSSWIND LANDING

$$\delta_r \geq \frac{C_{n_\beta}}{C_{n_{\delta_r}}}\beta$$

FULL RUDDER SIDESLIP

$$(C_l)_{.75\delta_{a_{max}}} = C_{l_{\delta_a}}(.75\delta_{a_{max}}) \geq (C_l)_\beta$$

where $(C_l)_\beta = C_{l_\beta}\beta$

$C_{n_\beta} = .069$

$C_{l_p} = -.642$

$C_{L_{\delta_E}} = .553$

$C_{m_{\delta_E}} = -2.22$

$C_{l_{\delta_a}} = .179$

$C_{n_{\delta_R}} = -.033$

$(SM)_{max} = .60$

$h_{min} = 2.08\ m$

$(SM)_{min} = .10$

$h_{max} = 3.33\ m$

$h = 3.30\ m$

$l_w = 10\ m$

$\bar{c} = 2.5\ m$

$\epsilon_\alpha = .17$

$l_v = 10.8\ m$

$Z_v = 3.58\ m$

Surface Ops -- Landing Gear

The design, sizing, and placement of the landing gear for the HIF II is somewhat of a reasonable guess and an estimation due to the loss of the surface operations design member. However some effort by the design team was undertaken to help shore up this design srea. The nose gear is located 1.5 meters back of the front edge of the fuselage and centered underneath. Its length is 0.5m from the bottom of the fuselage to the center of the wheel. The wing landing gear are located 4.25m behind the front edge of the fuselage (2m behind the wing leading edge) and five meters out from the wing root. A length measured from the bottom of the wing to the center of the wheel is 1.75m.

The diameter of the nose wheel and both wing wheels is 0.5m. The thickness of all three tires is approximately twenty centimeters. The wing tires are normal, grooved and wear-resistant while an anti-shimmy tire will be used on the nosewheel. The inflation pressure of all three should be approximately $2.5 kg/cm^2$. As the wing wheels will be located towards the anterior portion of the wing airfoil, they will retract in a forward manner and into a small pad under the wing during flight. The nosewheel will retract in a backward fashion. It will be housed in a small compartment under the wood floor of the fuselage, but will have to be rotated over (i.e. the side of the wheel will be parallel to the ground) to accomodate the small housing. All retractions and/or deployment will be accomplished by electrically powered hydraulics. Due to limited knowledge

assumed the landing gear can be handled in the above manner in all respects.

The take-off and landing analysis of the surface operations report is included in the perframance section of this design report.

Weights and Balances

by Art Fletcher

Throughout the design, Weights and Balances has made many changes in the weight and configuration of the aircraft. However, the basic weight history can be easily summarized into the initial sizing, the midterm weight (HIF 1), and the final weight (HIF 2), all of which can be found in table 7.1. As can be expected, the operational empty weight (OEW) increased as the design progressed.

The HIF 2 weight was arrived at by performing a manual iteration with an HP-15C on an equation in terms of W_{to}. This equation was found by the summation of all the component weights. The result was given in lb_m and then changed to Newtons on Mars.

The weights and center of gravities (C.G.'s) of the components of the HIF 2 were arrived at by several different means. For the landing gear, fuselage, empennage, surface controls, nacelle, and electrical system, weight equations given in Roskam's[1] book were used. Also, weight reductions for use of advanced composites in the fuselage, empennage, and nacelle were taken from Niclai's[2] book.

Weights for the wing, tail booms, and air brake were found by mass density calculations taken on each individual part of the component. These individual weights were then summed over the component to get the weight of the entire component. For example, the wing weight was found by summing the individual weights of the spars, ribs, and coverings.

The weights for all components in the propulsion group (engine, power conditioner, battery, solar cells, propeller) were given to Weights and Balances by the Propulsion group, which got the information

from Hall's[3] and Clarke's[4] books.

Weights for the seats and the instruments and navigation equipment were arrived at by close estimation of what the weights and Balances felt was needed. The instruments and navigation eqpt. is only enough to fly the aircraft. With 2 pilots, there is approximately 100 N of lift availiable for added electronic and survellance equipment. With only 1 pilot, the payload weight can be increased to approximately 700 N, when distributed properly.

The C.G. locations for each component, table 7.4, again were arrived at from equations in Roskam's book. Fore and aft limits were provided by Stability and Control. As shown in figure 7.1, not all flight conditions, namely 1 pilot without payload, fall within the allowed range. This problem is easily overcome by use of ballast. This ballast,which could range from electronic equipment to a bag of rocks (or extra rockets in the rescue scenario), would be on or in place of the crew seat. Recommended ballast weighs 295 N and would place the aircraft's C.G. well within the allowed range. In minimizing the weight of the ballast, in order to maximize the weight of the payload (which would be placed on the aircraft's C.G.), as low as 210 N of Ballast could be used. The aircraft, however, would be on the edge of instability.

During normal flight, there will not be any C.G. movement. The battery will not lose any weight while draining and the rockets used for takeoff will be centered on the C.G. so when they are dropped, they will have no effect on the C.G..

A problem that also exists is that the empty aircraft's C.G. lies behind the rear wheels. This problem can be corrected easily by use of ballast (in the case of a rescue scenario) or by tying the craft down and supporting it with an outside stand (when on the ground at the home base).

Stage	Operational Empty Weight
Initial Sizing	1300 N
Midterm HIF 1	3016 N
Final HIF 2	3442 N

Table 7.1

Useful Load Fraction	25.4%
Maximum Takeoff Weight	3582 N
CEW	3442 N
Maximum Landing Weight	4616 N
Maximum Fuel Fraction	0

Table 7.2

Component Weight Breakdown For HIF 2

Component	Weight (N)	% of O.E.W.
Wing	1488.4	43.2
Fuselage	219.6	6.4
Empennage-Hor.	157.3	4.5
Empennage-Ver.(2)	112.9	3.3
Tail Booms (2)	231.9	6.7
Landing Gear-Nose	31.7	0.9
Landing Gear-Main (2)	109.1	3.2
Nacelle	10.8	0.4
Surface Controls	77.5	2.2
Airframe Totals	2437.4	70.8
Engine,Controller & Gearbox	83.6	2.4
Power Conditioner	50.0	1.4
Battery	522.8	15.2
Solar Cells	12.5	0.5
Propeller	136.9	4.0
Power Plant Totals	805.8	23.5
Instruments & Nav. Equipment	8.4	0.2
Seats (2)	67.2	1.9
Electrical System	98.0	2.8
Air Brake	25.0	0.8
Miscellanuous Totals	198.6	5.7
Total Operational Empty	3441.8	100.0

Table 7.3

Component Center of Gravity Locations for HIF 2

Component	C.G. Location (m.)
Wing	3.75
Fuselage	[illegible]
Empennage	[illegible]
Tail Booms	7.80
Landing Gear-Nose	1.50
Landing Gear-Main	3.40
Nacelle	5.70
Surface controls	2.20
Engine, Controller & Gearbox	5.70
Power Conditioner	2.20
Battery	0.75
Solar Cells	3.20
Propeller	6.15
Instruments & Nav. Equipment	0.70
Pilot Seat	1.50
Crew Seat	1.80
Electrical System	2.50
Air Brake	0.50
C.G. for Operational Empty Aircraft	3.736
C.G. for 1 Pilot & 295 N of Ballast	3.300
C.G. for 2 Pilots	3.205

Table 7.4

The ballast needed for the 1 pilot configuration is located directly on the crew (rear) seat.

All locations are measured from the nose of the craft.

Center of Gravity Locations and Allowed Ranges

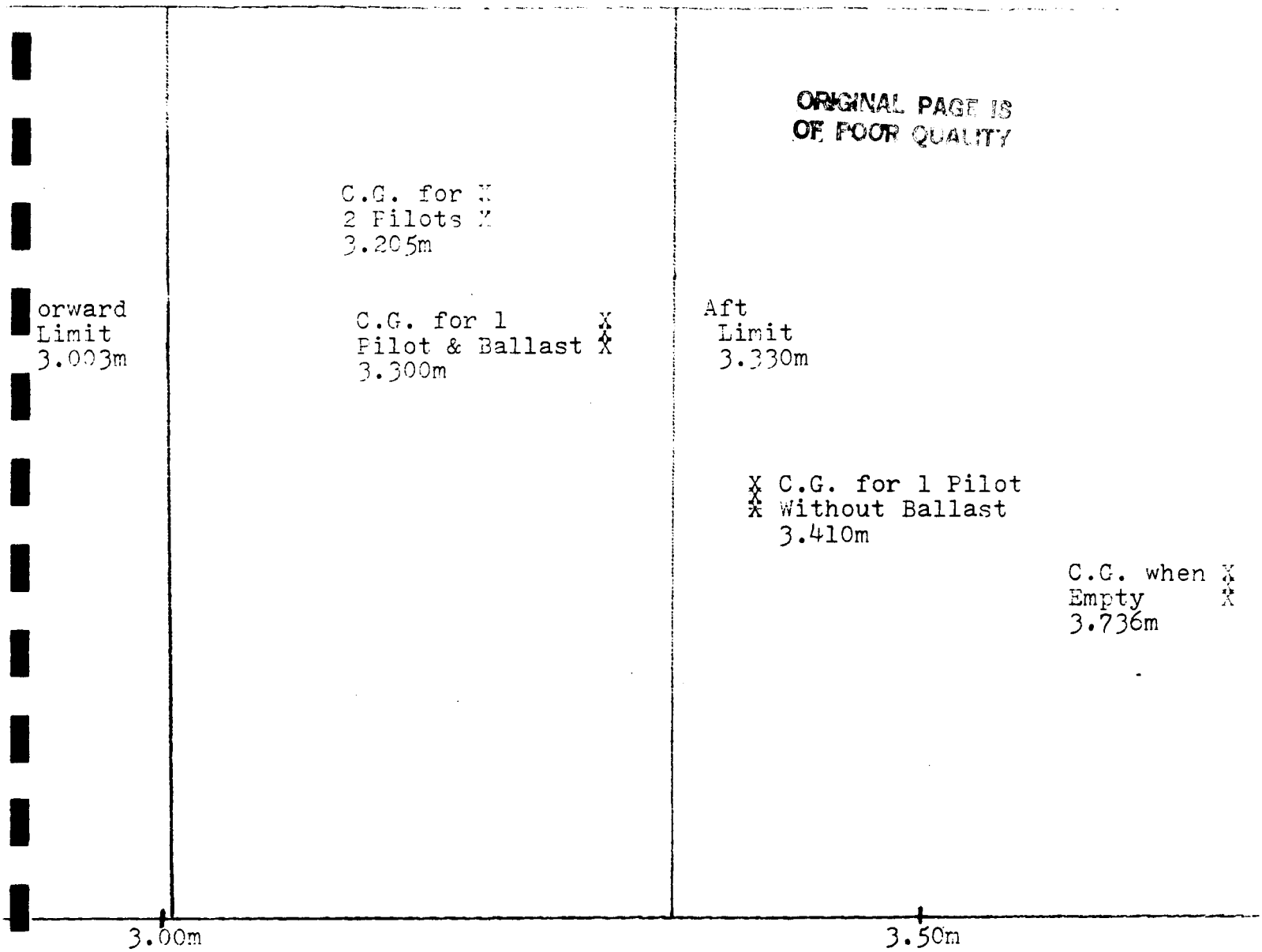

Note: The ballast in the above chart is taken to be 295 N (80 kg) and is positioned directly on the rear seat.

The above limits were established by Stability and Control.

Figure 7.1

REFERENCES

[1]Roskam, Dr. Jan : Airplane Design Part 5, Component Weight Establishment. Roskam Aviation and Engineering Corp. Eqns. 5.14, 5.15, 5.25, 7.1, 7.12. 1985.

[2]Nicolai, Leland M.: Fundementals of Aircraft Design. METS Inc. 1975.

[3]Hall, David W., Charles D Fortenbach, Emanual V. Dimickele, and Robert W. Parks: A Preliminary Study of Solar Powered Aircraft and Associated Power Trains. NASA Contractor Report 3699, December 1983.

[4]Clarke, Victor C., Abraham Serem and Richard Lewis: A Mars Plane?. American Institute of Aeronautics and Astronautics. 1979.

Auxiliary Systems

There are only two auxiliary systems needed on the HIT 2. The first is the landing gear retraction system. This system only affects the plane just after takeoff and just before landing. The second is the control surface system. This system is needed throughout the entire flight, for obvious reasons. Both systems are hydraulic and are driven by electric motors.

The added weight of these two systems is only 142.1 N (surface controls- 77.5N, landing gear retraction- 64.6N), which is only 3% of the total takeoff weight. The locations of these systems (surface controls- 2.2m, landing gear- above the respective gear) helps move the aircraft's C.G. up, something that Weights and Balances has been working toward.

At cruise, there are 14.9 availiable kilowatts to be used for auxiliary systems and whatever electronic devices are being used for experiments. This is plenty of power to run the control system and the experiments (landing gear retraction is not needed during cruise). During takeoff, the excess power is cut to 7.9 kilowatts, due to the extra power that the engine requires. Since during takeoff, the electric experiments wouldn't be running, all of this power may be used for the control surfaces and landing gear. Again, this would be sufficient power to get the job done.

COST ANALYSIS

DION L. BUZZARD

The cost of the HIF2 has an estimated value of 245.3 million dollars from the program used. This analysis assumes that there is a strong relationship between mass and cost. It has also been developed for costing of spacecraft not airplanes therefore the result at best is an approximation. The power systems of the HIF2 are based on future technological improvements which will add to the costs in research, development and testing. The structure is made of advanced composites with more detailed surfaces than that of a typical spacecraft. This alone could raise the cost to over a billion dollars since the plane's weight is mainly structural. A final note is that cost is hard to determine especially for the future.

COSTS FROM THE PROGRAM ANALYSIS

	DDT & E	FHA	TOTAL
STRUCTURES	44.0	12.9	56.8
ATTITUDE CONTROLS	21.8	4.9	26.7
ELECTRICAL POWER	7.7	0.1	7.9
PROPULSION	0.5	0	0.5
SUBTOTAL	73.9	17.9	91.9
SYSTEM TEST HARDWARE	28.6	0	28.6
SYSTEM TEST OPS	16.8	0	16.8
GSE	14.3	0	14.3
SE & I	15.6	3.8	19.4
PROGRAM MANAGEMENT	9.7	1.6	11.3
SUBTOTAL	158.9	23.3	182.2
CONTINGENCY	31.8	4.7	36.4
FEE	19.1	2.8	21.9
PROGRAM SUPPORT	4.2	0.6	4.8
TOTAL	214.0	31.3	245.3

DDT & E : DESIGN DEVELOPMENT AND TEST
FHA : MANAGEMENT AND PRODUCTION

Packaging and Assembly of the HIF 2

The transport of the HIF 2 to Mars begins with the packaging of the components here on Earth. A total of five boxes and the fuselage will be transported to the space station. These boxes contain the broken down tail booms, the main wing broken into nine parts, the two rudders, and the rest of the airplanes components in their final states.

After transport to the space station, the boxes containing the wing and elevator sections are broken down. The remaining two boxes, fuselage, and airfoil sections are placed in the transport as shown in fig. 10.1. The two remaining boxes are equal in weight so that the transport cargo bay is symmetrically weighted.

After arrival on Mars, the HIF 2 has been designed so that the broken down structures may be assembled easily. The cylindrical graphite-epoxy spars will have short extensions that will slide inside the next spar. They will then be locked together with three bolts: two vertical and one horizontal, as shown in fig. .2. The landing gear is then bolted to the wing spars and the extra supports. Next, plywood panels are attatched over the bolt openings and preliminarly secured by wood glue. Then Kelvar is wrapped over these plywood panels and sufficiently secured to the skin. The tailbooms can then be bolted to the spars of the tail and wing through the skin. The fuselage is then secured to the wings by large bolts through both spars of the wing and the beefed-up fuselage roof frame. The landing gear storage pods are also bolted through the skin to the wing spars. Next, the internal components are bolted into their assigned positions. Finally, the propeller is bolted onto the transmission drive that runs through the rear bulkhead of the fuselage.

Packaging Layout for the Transport to Mars

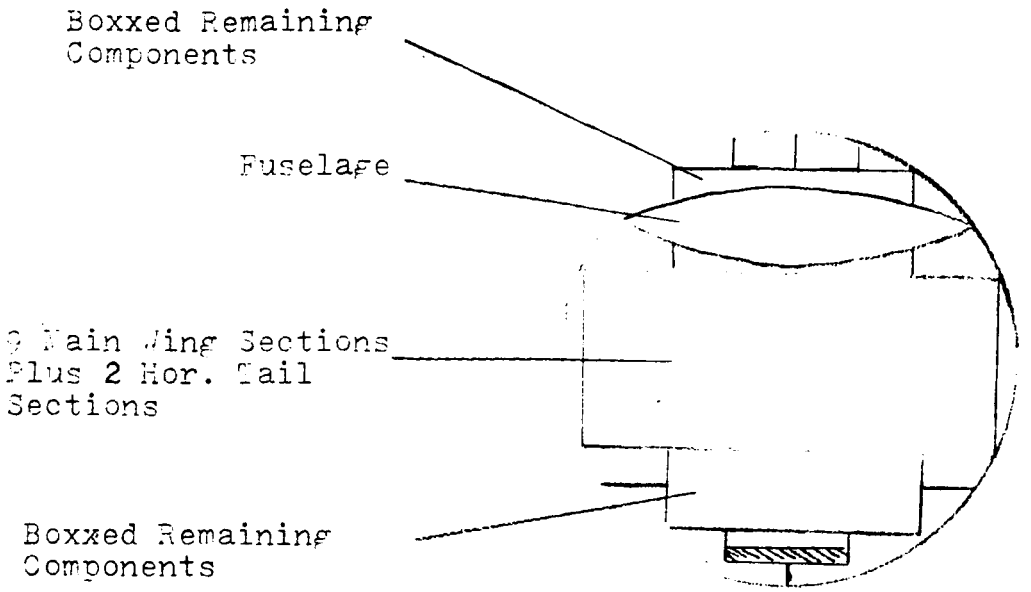

Top View of Cargo Bay

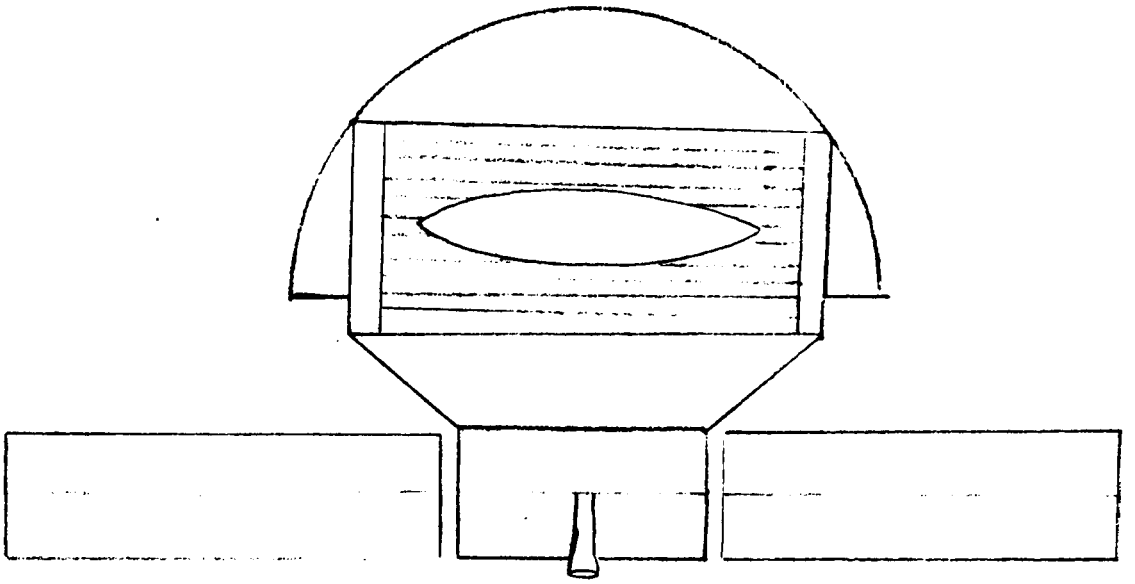

Side View of Transport Craft

Fig. 10.1

SPAR AND TAILBOOM ASSEMBLY

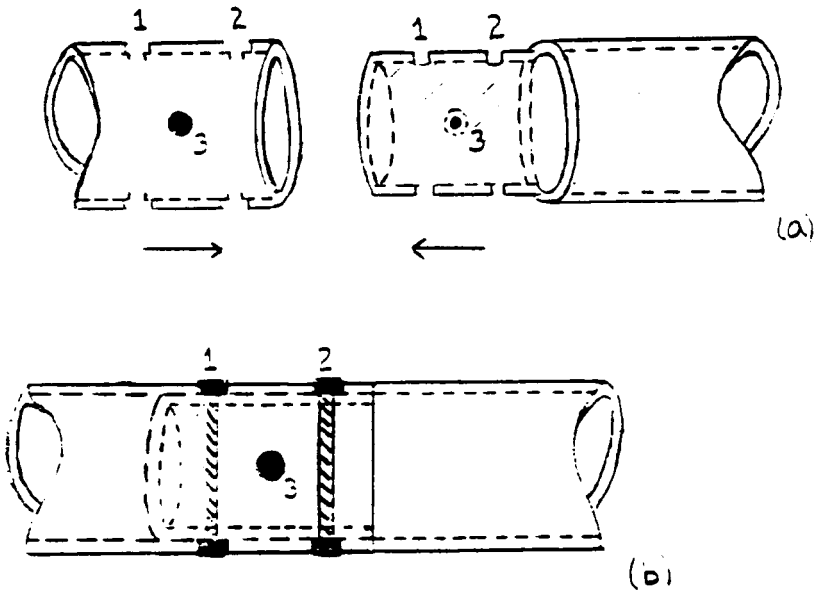

FIG. 10.2

RESCUE SCENARIO

Richard R. Monke

A rescue operation is to be provided for a survivor of a crash. With the survival kit, the stranded pilot will locate himself near a plain and radio in his coordinates. The rescue plane will then land at this location. Next, the solid rocket thrusters and ballast are removed from the second seat. The thrusters are then attached to the fuselage at the assigned location. With pilots aboard takeoff is commenced. Due to lack of surface operations personnel, this rescue scenario is uncertain.

Internal Configuration Layout

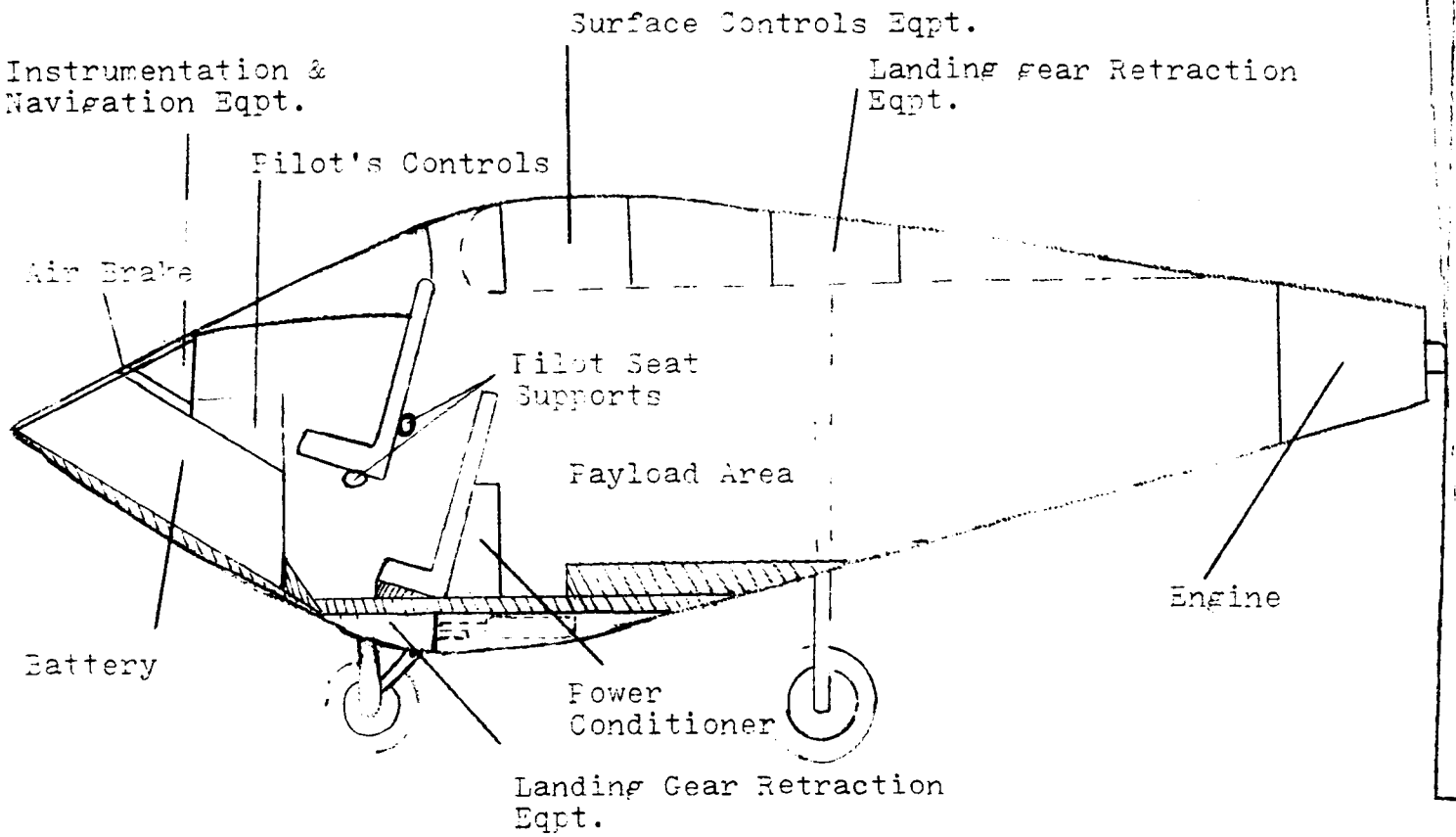

Side View

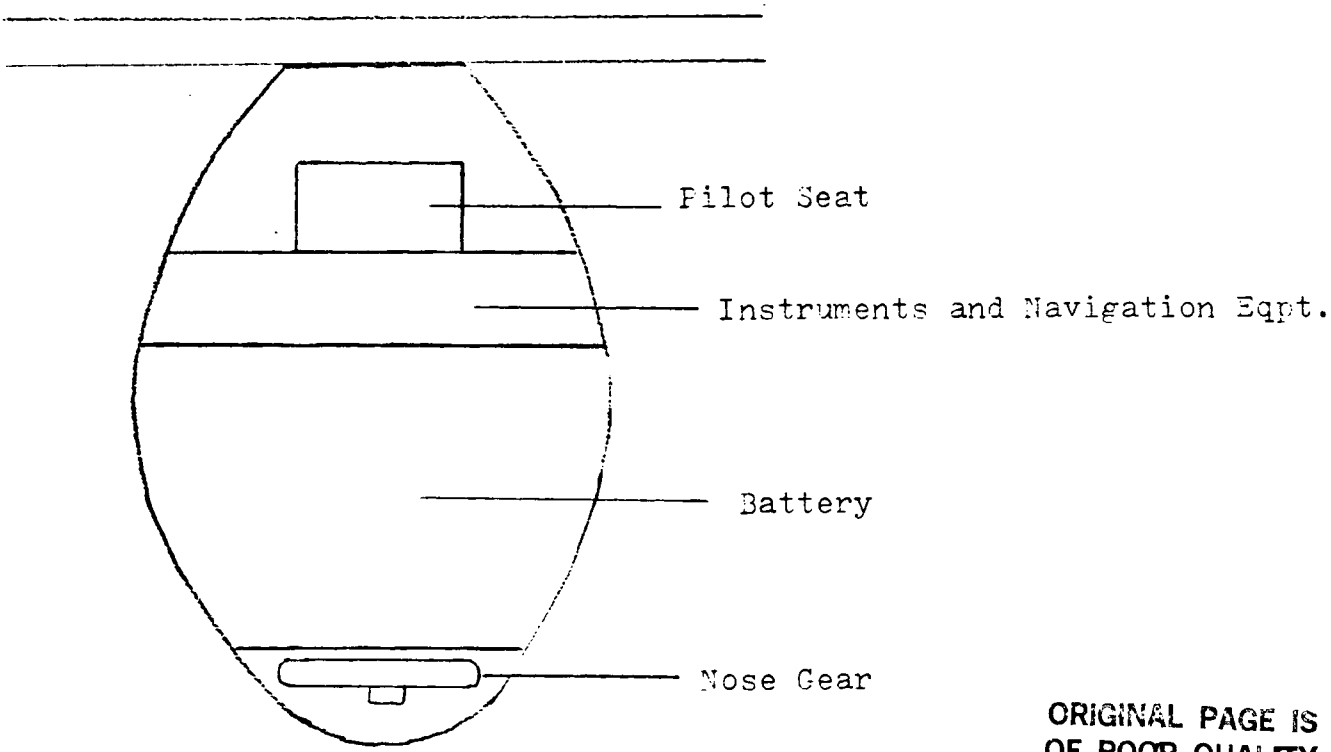

Front View

FIG. 11.1

87 PAGES
JAH
DA

THE MARS RECONAISSANCE AIRCRAFT

AAE 241

Group 3

April 28, 1988

Aerodynamics	Pat Moroney
Performance	Karen Forest
Power and Propulsion	Jim LeRoy
Stability and Control	Philip Lange
Structural Analysis	Michael Enright
Surface Operations	Nick Jasper
Weights and Balances	Patricia Perkins

INDEX

PROJECT OVERVIEW

The objective of the Mar's aircraft project was to generate a preliminary design for a manned vehicle capable of extended flight in the Martian atmosphere. The main design criteria were as follows:

1) Capable of being packaged into a compact unit for transfer to Mars via spacecraft.
2) Easily assembled after delivery to the Martian surface.
3) Ability to sustain two pilots aloft for a target endurance of eight hours.
4) VTOL capabilities to allow the aircraft to operate from desolate areas and to provide grounds for a useful rescue scenario.
5) Reasonably within the grasps of present or near-future technology.
6) Pilot procedures similar to those of a standard airplane for the normal flight regime.
7) Pilot procedures similar to a helicopter for VTOL operations.

Because of the requirement for the airplane to fit inside of a transport vehicle, the design was made as small as possible. However, the wing and canard spans (37.5 m and 25 m) were required to be quite large due to the extremely low viscosity of the Martian atmosphere. This also mandated the use of airfoils specifically designed for low Reynolds numbers for both the wing and the propellers.

Construction materials consist mainly of composites with Boron epoxy making up the spars and webs, while the wing "skin" is made of graphite.

The large wing span and the requirement to minimize weight made the structural design and choice of material a very critical one.

The gross weight of the aircraft is 7500 Newtons (Mar's Newtons), and it is stable for all configurations and possible weight loadings. It has excellent rescue capabilities due to its VTOL abilities - greater single pilot rescue radius then the normal two pilot radius since the second pilot can be replaced with fuel.

The aircraft, which is powered by three rocket driven propellers (separate from the VTOL propulsion system) provides a large safety factor by having the ability to achieve excellent climb performance utilizing only two of its engines. Hydrazine powers both the cruise and VTOL propulsion systems and is stored in the fuselage.

The design of the Mar's airplane does not rely on speculation of future technology nor does it rely on complicated concepts. By virtue of its simplicity it is hoped that reliability and actual feasibility of the project will be increased.

AAE 241
Spring 1988
INITIAL SIZING DATA SUMMARY

Gross Weight:	7000 N		
Wing Loading:	93.3	Maximum Take-off Power	1000 kW
Fuel Weight:	3500 N	Power Loading:	1.0
Useful Load Fraction:	0.671	Fuel Fraction:	0.5

Geometry

Ref. Wing Area = 75 m^2

AR = 35

Propulsion

Engine/Motor Type: propeller rocket

No. of Engines/Motors = 2

$P_{o_{max}}$ /engine = 3500 W

c_p at cruise = 15.0 N/kW (Mars N)

Aerodynamics

Cruise; C_{D_o} = 0.0300

e_o = 0.80

C_L = 1.5

$(\frac{L}{D})_{max}$ = 5.0

Cruise Performance

h = 600 m

V = 85 m/s

Take-off; C_L = not known

$C_{L_{max}}$ = not known

Landing; C_L = not known

$C_{l_{max}}$ = not known

PRECEDING PAGE BLANK NOT FILMED

AAE 241
Spring 1988
DESIGN DATA SUMMARY

Gross Weight:	7502 N	Maximum Take-off Power	1000 N
Wing Loading:	66.7	Power Loading:	1.124 kW
Maximum Fuel Weight:	2500 N	Fuel Fraction:	0.333
Useful Load Fraction:	0.493		

Geometry

Ref. Wing Area	=	75 m^2
AR	=	18.75
Λ_{LE}	=	0°
λ	=	1
t/c	=	0.157

Propulsion

Engine Description: rocket driven p

Number of Engines	=	3
$P_{O_{max}}$ /Engine	=	4000 W
Weight/Engine	=	100 lb
c_p at Cruise	=	18.2 N/kW
Prop. Diam.	=	5 m
No. of Blades	=	2
Blade Cruise R_e	=	0 - 200,0

Performance

Cruise R_e = 2.0244×10^5
Cruise h = 1500 m
Cruise M = .35
Cruise V = 85 m/s

Take-off Field Length	=	1.56 km
Take-off Speed	=	79 m/s
Landing Field Length	=	1 km
Landing Speed	=	57 m/s
Maximum Landing Weight	=	7502 @ 80 m/s
OEI Climb Gradient (%):	=	
2nd Segment	=	
Missed Approach	=	
Sea Level $(R/C)_{max}$	=	4.35 m/s

Aerodynamics

Airfoil: LA 203A
High Lift System: none

Cruise;	C_{D_o}	=	0.0215
	e_o	=	0.080
	C_L	=	1.1830
	(L/D_{max})	=	7.3849
Take-off;	C_L	=	1.5425
	$C_{L_{max}}$	=	2.15396
Landing;	C_L	=	1.784
	$C_{L_{max}}$	=	2.3275

Stability and Control

Static Margin Range	=	0.325 - 0.10
Acceptable C.G. Range	=	9.35 - 9.8
Actual C.G. Range	=	9.359 - 9.798

FOLDOUT FRAME

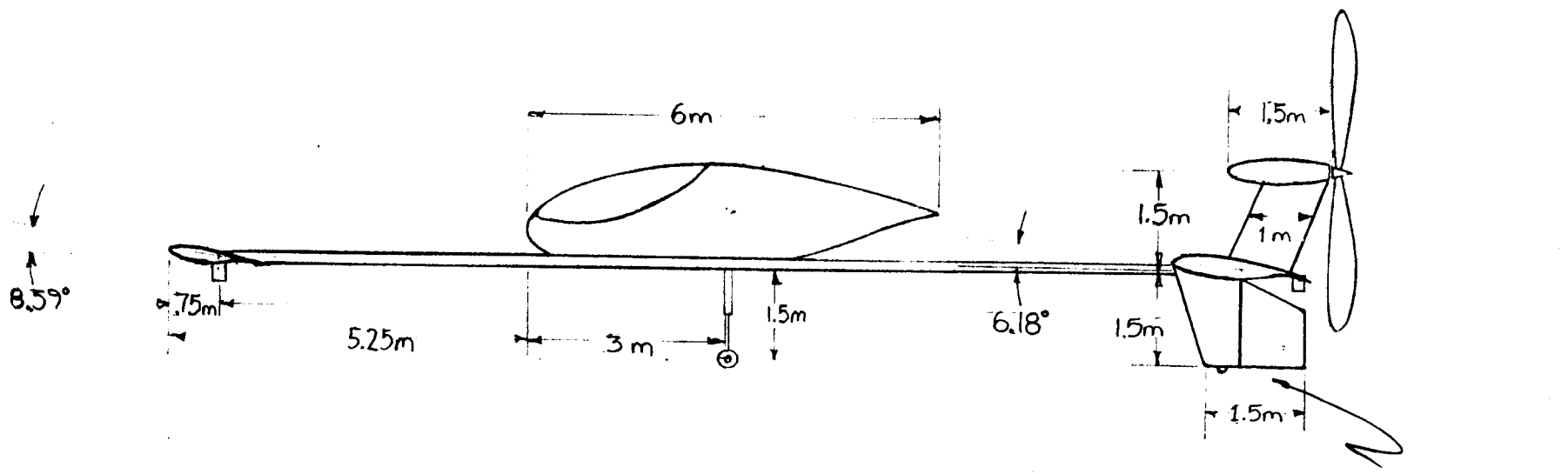

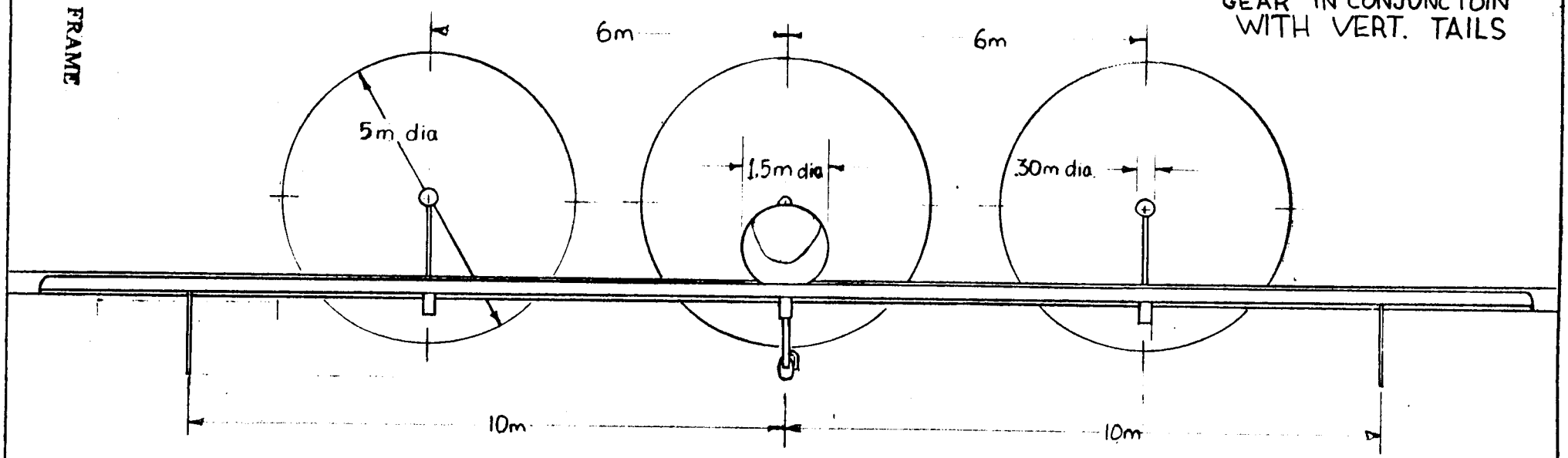

SCALE: 1cm = 1m

FOLDOUT FRAME

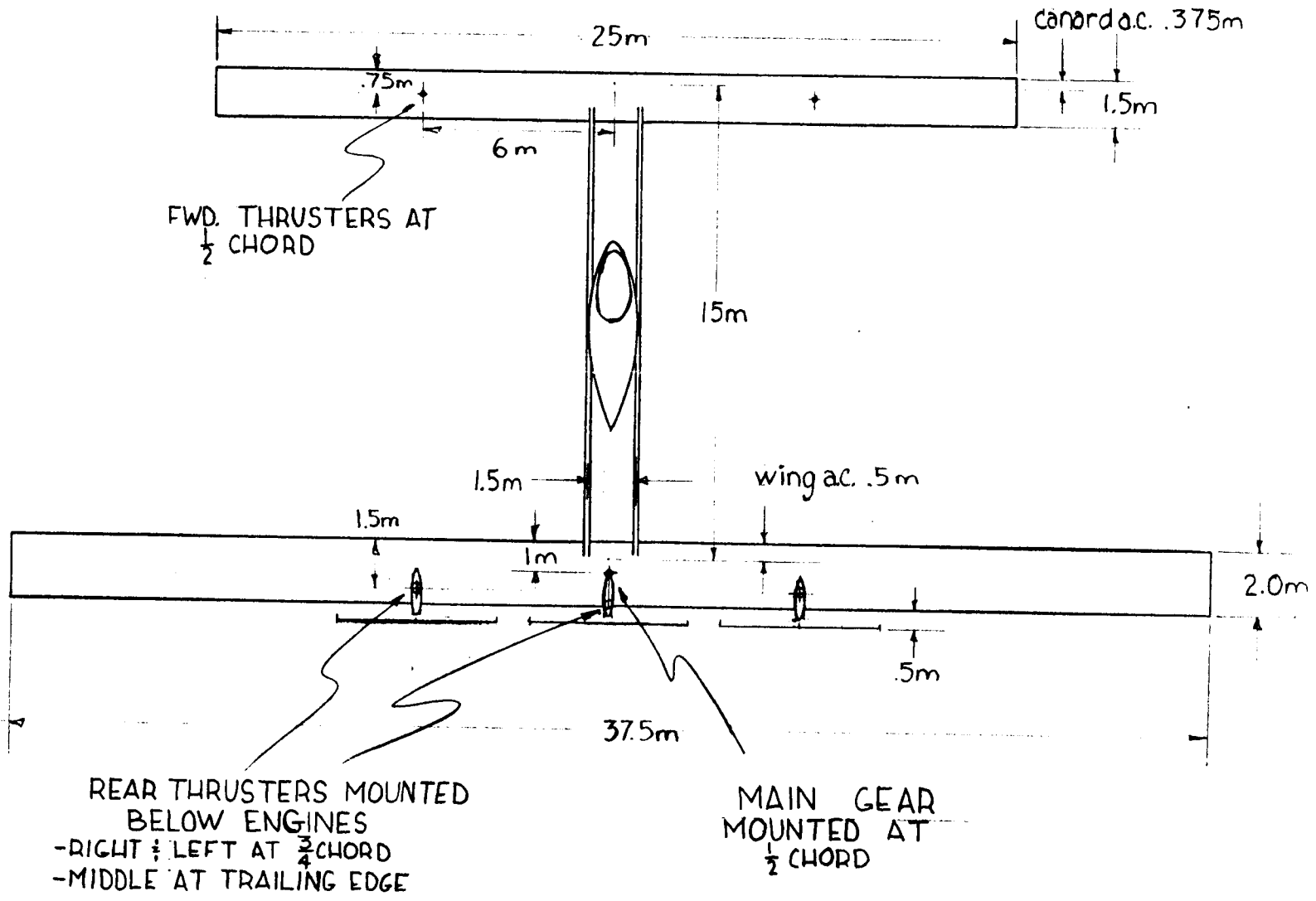

SCALE: 1cm = 2m

AERODYNAMICS

PAT MORONEY

Before presenting the airfoil selected for the Mars aircraft, it is necessary to discuss the Reynolds number calculated for the wing and canard sections. Because accurate coefficient of viscosity data is not readily available, a value of μ is estimated using the following procedure. Accurate atmospheric pressure, temperature, and density data obtained from Ref. 1 is plotted and compared to other values of pressure, temperature, and density from Ref. 2. The values from Ref. 2 are based upon a NASA,1967 model of the Martian atmosphere; however, when the curves of the maximum, minimum, and mean values from the model are matched with the actual atmospheric data, the mean model data is coincident with the actual values. Consequently, mean values of μ from Ref. 2 are chosen for the Re calculation. A plot of the maximum, minimum, and mean μ values appears in Fig. 1. At sea level:

$$\mu = 1.31 \times 10^{-5} \quad \text{(kg/m-s)}$$

$$Re_{wing} = 2.0244 \times 10^{5} \quad \text{and} \quad Re_{canard} = 1.5183 \times 10^{5}$$

When designing airfoils to fly at the very low Re calculated above, the formation of a laminar separation bubble and its effects on boundary layer separation are of primary concern. This bubble is formed when the laminar boundary layer separates from the upper surface of the airfoil and then

attaches itself once more as a turbulent boundary layer. According to Ref. 3, as the Re number decreases, the length of the bubble increases. The bubble can become long enough so that it breaks and causes flow separation over the remaining downstream portion of the airfoil's upper surface. Because of this separation, pressure drag is increased and lift is decreased. In order to achieve high lift at low Re, a gradual transition from laminar to turbulent flow needs to be achieved so that the condition of flow separation due to the bursting bubble does not occur. Although there is an increase in skin friction drag, if the flow is systematically transformed into a turbulent boundary layer, separation and stall are delayed. For high lift and very low speed flight regimes, turbulent boundary layers are desired.

The airfoil selected for the Mars aircraft is the LA 203A and is a member of the Liebeck class of subsonic, high lift airfoils designed for use in low Reynolds numbers. These airfoils achieve an orderly transition to turbulent flow by incorporating a "transition ramp that will destabilize the laminar boundary layer and induce transition ahead of a severe pressure gradient where laminar separation is expected" (Ref. 4). More specifically, the Liebeck airfoils consist of an, "'optimum' design pressure distribution comprised of a laminar 'rooftop', a Stratford pressure recovery, and a transition ramp between the two" (Ref. 4). From data on the LA 203A, the laminar bubble is practically non-existent at Re numbers of 6.5×10^5 to 5×10^5. The bubble is first noticed at $Re = 2.5 \times 10^5$. Additional data from Ref.

3 shows the flow not separating before stall throughout the entire Reynolds number test range of 2.5×10^5 to 6.5×10^5. Other reasons which justify the selection of a Liebeck class airfoil are mentioned in Ref. 5. Liebeck airfoils typically , "approach the upper limit of lift coefficient achievable with a single-element section without mechanical boundary layer control....(and) also exhibit commendably low drag coefficients in the region of the design lift coefficient and low pitching moments." For ease in calculations during this preliminary study, the same airfoil is used for both the wing and canard. Although the Re of both the wing and canard are less than the lowest design Re for the LA 203A, it is assumed that Liebeck will develop another advanced airfoil with similar sectional characteristics to operate at a lower Re (i.e. 1.5×10^5) in the near future. Data for the LA 203A was obtained from Ref. 3.

For the Mars airplane, the efficiency of a canard configuration is most beneficial from a stability point of view. Trimming the aircraft with an upload on a canard instead of a download on an aft tail makes possible a lower wing loading, delay in stall, and probably a decrease in drag. A rectangular planform (i.e. λ=1.0) is employed for both the wing and canard. Because the spar and rib sections are constant across the span, there are cost benefits to this simple design. In addition, an untapered planform will probably keep the aircraft's total weight low. Since the Re at the wing tips is already 2×10^5, any further decrease in chord will most likely lead to

flow separation near these tips (if it has not occurred already). An ideal taper ratio (for minimizing induced drag) will increase the root chord of this aircraft by a few meters in order to maintain approximately 2 meters of chord at the tips; therefore, the weight of the wing would be much greater than it is now. As stated in Ref. 6, "the simplest way to obtain a satisfactory wing from the standpoint of stalling is to force the stall to occur first at the root, with a relatively slow rate of progress toward the tips....the problem of delaying stall near the tips with a tapered wing is more difficult than with a rectangular wing because of the lower Reynolds number at the tips, which favors early tip stall." Therefore, in the low Re flight regime of the Martian atmosphere, a rectangular wing should have more favorable stalling characteristics. A final reason supporting rectangular planforms is that the possibility of the aircraft going into a spin is minimized because, as mentioned in Ref. 6, both wings are likely to stall simultaneously. The wings are also unswept and have no dihedral for simplicity in design and because these stabilizing contributions are not needed. All calculations in this preliminary study neglect the effects of wing and canard twist; however, these factors and the effects of the canard vortices on the wing should be accounted for in a future iteration.

Airfoil sectional data, wing data, V_{cruise} and C_{LA} vs. α values, and a drag polar with parasite drag breakdown are given below:

AIRFOIL SECTIONAL DATA:

$c_{l_{max}}$ =1.7 $c_{mc/4}$ = -0.17 α_{OL} = -6.0°

c_{l_α} = 0.1000/° t/c $_{max}$ =15.7%

Figures 2,3,4, and 5 at the end of the aerodynamics section show the geometry of the LA 203A, a graph of c_l vs. α, c_l vs. c_d, and c_l vs. $c_{mc/4}$ respectively.

WING DATA:

b_{wing} = 37.5 m	b_{canard} = 25 m
c_{wing} = 2.0 m	c_{canard} = 1.5 m
S_{wing} = 75 m^2	S_{canard} = 37.5 m^2
AR_{wing} = 18.75	AR_{canard} = 16.67
Λ_{wing} = 0°	Λ_{canard} = 0°
λ_{wing} =1.0	λ_{canard} =1.0
a_{wing} = .0895/°	a_{canard} = .0884/°
	η_c = .95

CRUISE VELOCITY & C_{LA} vs. α

The stall speed of this aircraft was one of the first calculations made in the design; consequently, it is based on the cl_{max} of the airfoil section and not the aircraft because the incidences of the wing and canard were unknown at the time. Using the relation:

$$V_{stall} = (2(W/S)/\rho\, c_{l_{max}})^{1/2}$$

the stalling velocity was computed to be 70.92 m/s. Therefore, to provide

the pilot with a comfortable envelope in the event of OEI, the cruise speed was determined to be:

$$V_{cruise} = 1.20(V_{stall}) = 85.0 \text{ m/s}$$

which also corresponds to a:

$$C_L = 1.1830 .$$

Once Stability and Control computed the incidence angles of the wing and canard, the C_{LA} (aircraft) vs. α (body) was calculated using the relation:

$$C_{LA} = C_{LWB} + \eta_c(Sc/Sw)C_{Lc}.$$

From the plots of C_{LA} vs. α, C_{Lc} vs. C_{LA}, and C_{Lc} vs. C_{LWB} shown in Figs. 6,7,and 8 respectively, the following values were determined:

$a_{aircraft} = .1315/°$

C_{Lmax} aircraft = 2.3132 (when C_{Lc} = 1.7, i.e. canard stalls)

V_{stall} of aircraft = 60.79 m/s

Therefore, at V_{cruise} = 85 m/s, there is a comfortable velocity margin above the aircraft's stalling speed.

DRAG POLAR

Using methods in Ref. 7, a drag polar for the Mars aircraft was calculated. A graphical illustration of this drag polar is presented in Fig. 9. Since this aircraft does not utilize flaps in the take off or landing configuration, the same drag polar shown below is used throughout the

design. The drag polar includes the following contributions:

$$C_D = (C_{Do})_W + (C_{Do})_B + (C_{Do})_V + (C_{Di})_{WB} + \Delta C_{Dmisc}$$

where:

$(C_{Do})_W$ = zero lift drag coefficient of the wing

$(C_{Do})_B$ = zero lift drag coefficient of the body (fuselage)

$(C_{Do})_V$ = zero lift drag coefficient of the dorsal and ventral fins

$(C_{Di})_{WB}$ = induced drag coefficient of wing-body combination

ΔC_{Dmisc}= estimation of miscellaneous zero lift drag contribution

and the calculated drag polar is:

$$C_D = .0215 + .0331C_L^2 + 3.0001\alpha^3.$$

The parasite drag is broken down into the following components:

$(C_{Do})_{wing}$:	.0106	
$(C_{Do})_{canard}$:	.0053	
$(C_{Do})_{wing + canard}$:	.0159	
$(C_{Do})_{body}$:	.0022	
$(C_{Do})_{booms}$:	.0017	
$(C_{Do})_{nacelles}$:	.0003	
$(C_{Do})_{ventral\ fins}$:	.0004	
$(C_{Do})_{dorsal\ fins}$:	.0006	
ΔC_{Dmisc}:	.0004	
$(C_{Di})_{WB}$:	.0463	(at cruise and assuming $\alpha = 0°$)

Note that α is the angle of attack of the fuselage. A graphical percentage distribution for the parasite drag components is given in Fig. 10.

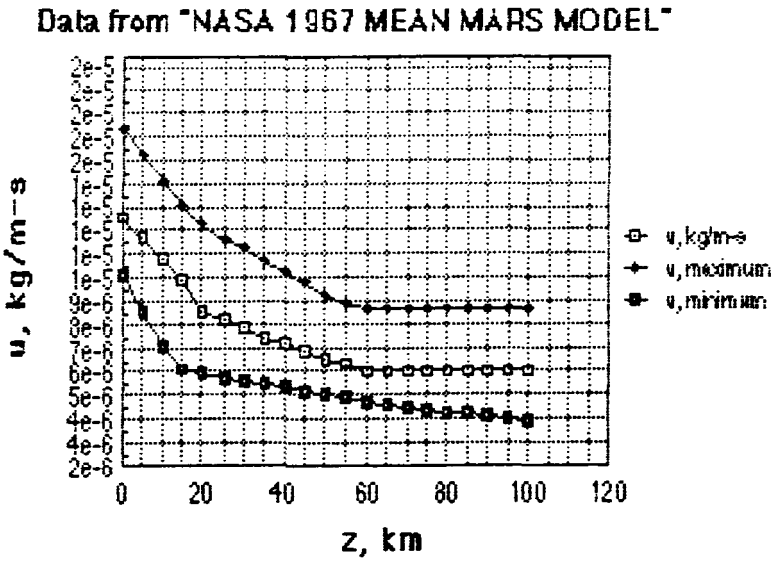

(Figure 1)

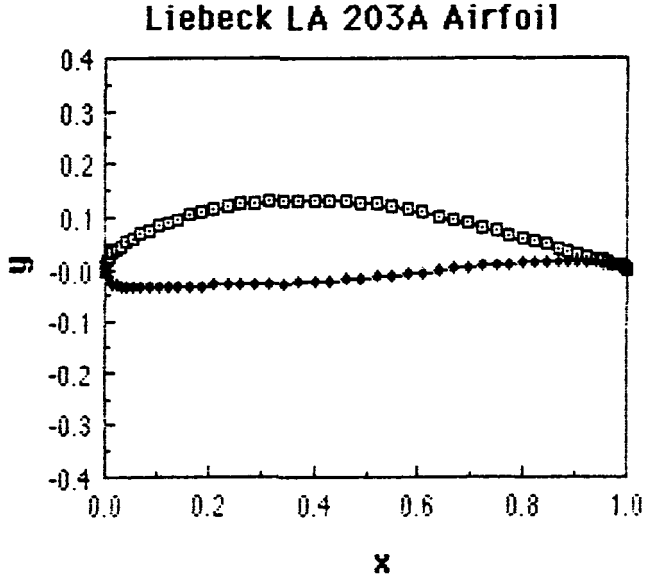

(Figure 2)

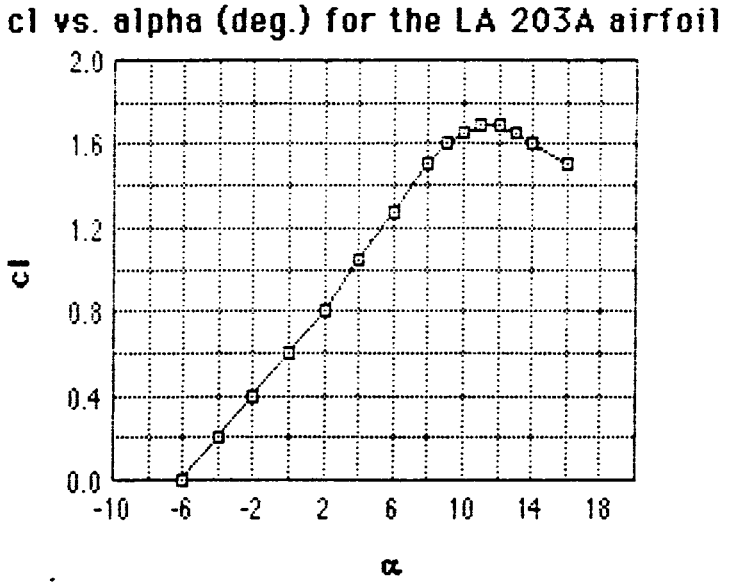

(Figure 3)

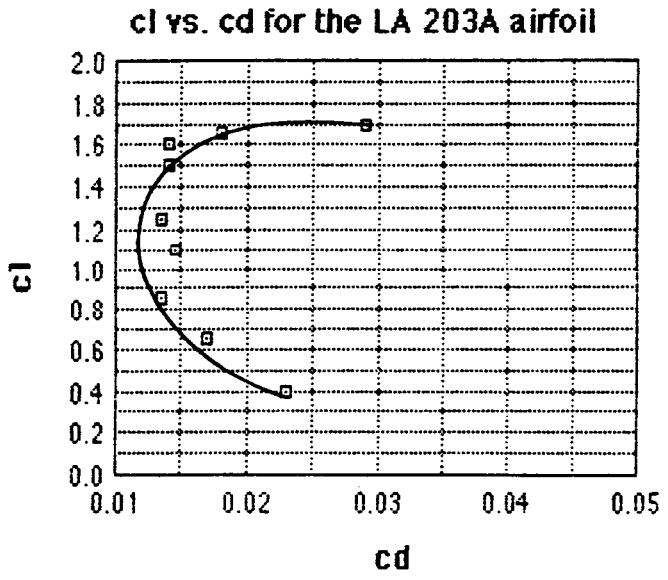

(Figure 4)

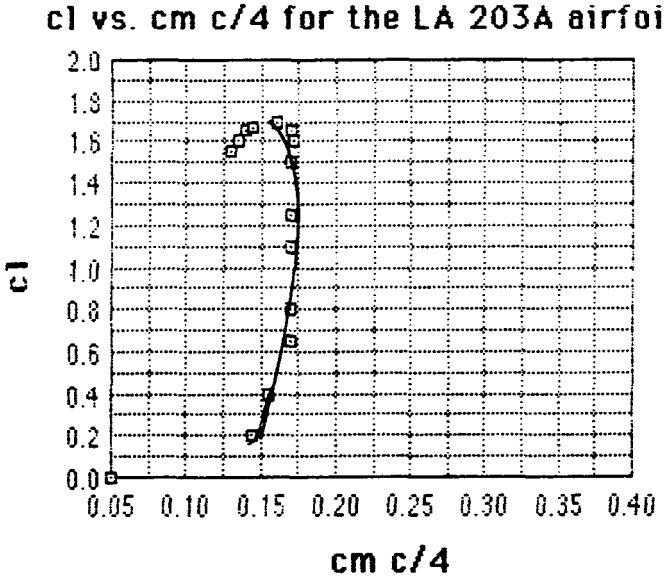

(Figure 5)

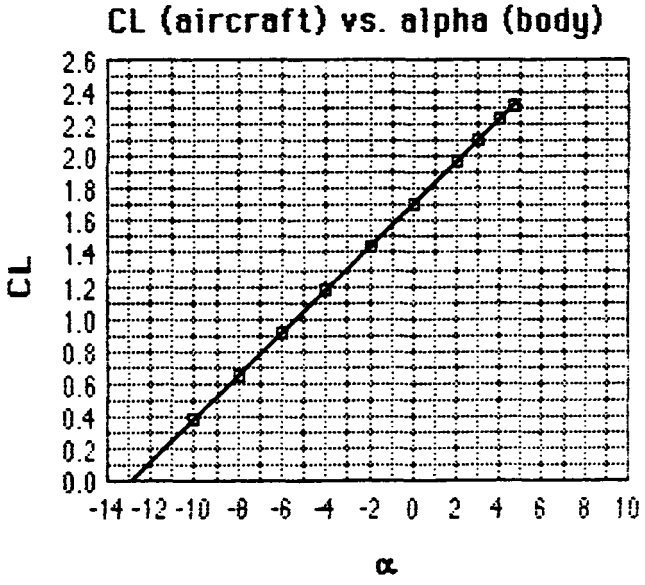

(Figure 6)

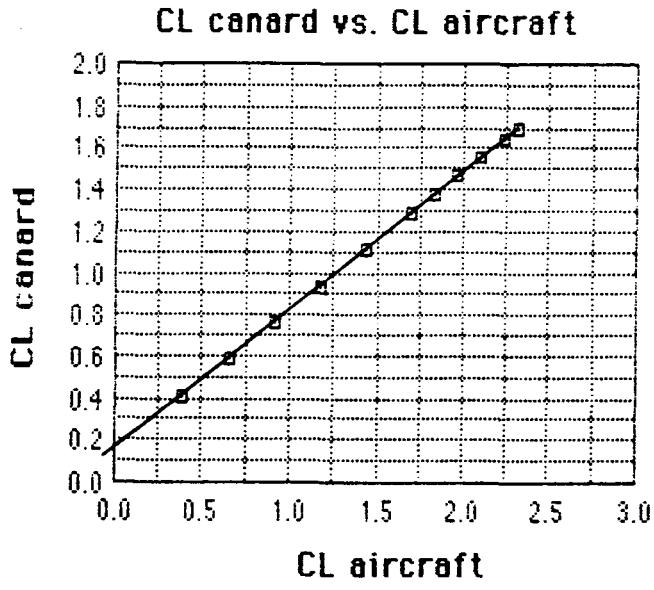

(Figure 7)

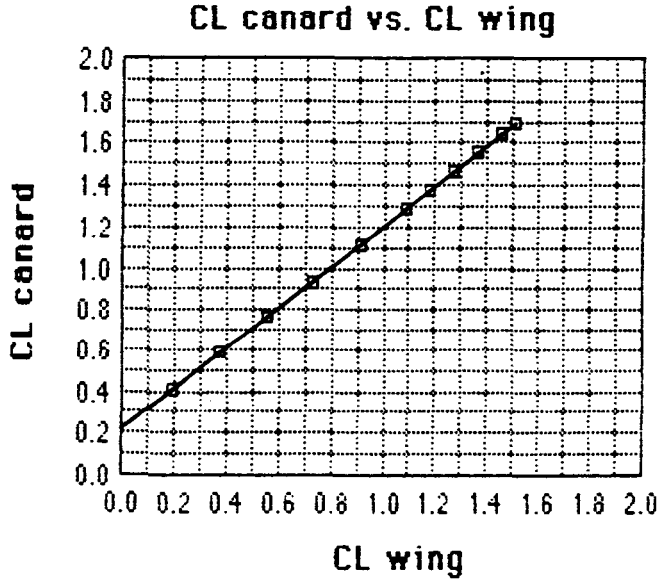

(Figure 8)

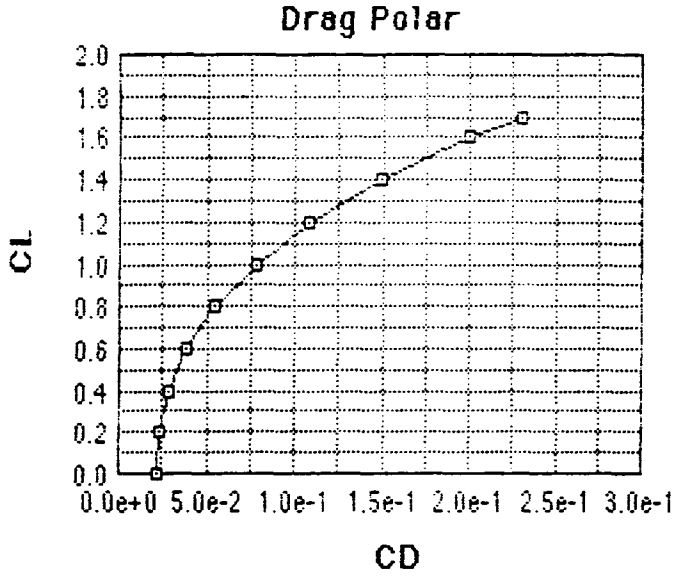

(Figure 9)

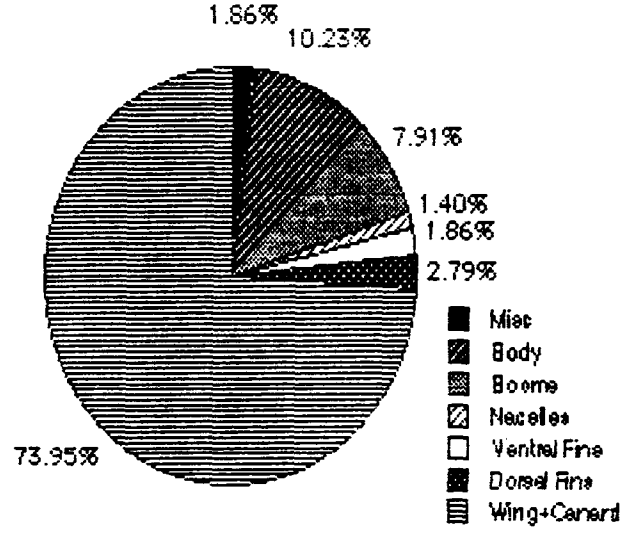

Parasite Drag Comparison

(Figure 10)

REFERENCES

1. Smith, R.E., and West, G.S., Space and Planetary Environment Criterion Guidelines for Use in Space Vehicle Development, NASA TM-82478, 1982.

2. _____. Models of Mars Atmosphere, NASA SP-8010,May 1968.

3. Liebeck, R.H. and Camacho, P.P.: "Airfoil Design at Low Reynolds Numbers with Constrained Pitching Moment", Proceedings of the Conference on Low Reynolds Number Airfoil Aerodynamics, University of Notre Dame UNDAS-CP-77B123, June 1985.

4. Evangelista, R., et al, "Design and Wind Tunnel Test of a High Performance Low Reynolds Number Airfoil", A87-2349, AIAA, 1987.

5. McMasters, J.H. and Henderson. M.L., "Low-Speed Single-Element Airfoil Synthesis", NASA-SSA Third International Symposium on the Science & Technology of Low-Speed & Motorless Flight, NASA-Langley Research Center, March 1979.

6. Dommasch, Sherby, & Connolly, Airplane Aerodynamics, 4th Edition, Pitman, 1967.

7. Roskam, J., Methods for Estimating Drag Polars of Subsonic Airplanes, 3rd Printing, University of Kansas, 1977.

PERFORMANCE

Karen E. Forest

When reviewing the performance of an aircraft, the first things to look at are the power curves. The Power available and Power required versus velocity curves are shown in Figure 2.1 and 2.2. In Figure 2.1, along with the Power curves, is the Power available with one engine inoperative. In this case, the available power is reduced by one third (this aircraft is operated with 3 propellers). As can be clearly seen, a missed approach is not a problem since there is still plenty of excess power. It is necessary at this point to comment on the seemingly infinite Power available. The numbers on the graph are accurate in the flight regime that this aircraft will be performing (i.e., cruise velocity of 85 m/s). However, once above our cruise velocity, the propeller tips will reach a velocity such that the Mach number will approach one. At this point, transonic drag effects will begin to reduce the shaft power. Because the loss of power is beyond this aircraft's requirements, these effects were ignored. (This discontinuity will be discussed further in Power and Propulsion.) There is a slight problem with using inaccurate data for the Power curves, even above our area of interest. Because the Power data is not computed correctly above cruise velocity, the maximum excess Power cannot be determined. However, the rate of climb can be found with a given velocity, which is done in this case.

A mission profile is given in Figure 2.4. The conditions for both conventional and VTOL take-off and landing are given. The conventional take-off will place the aircraft at 15 meters altitude with a velocity of 79 m/s. During climb the plane will ascend the remaining 1485 meters (cruise altitude is 1500 meters) and reach a velocity of 85 m/s (cruise velocity). The maximum amount of fuel that can be used during cruise is 2236 N (as shown in Figure 2.4). The next 2 values for fuel weight (2615 N and 2836 N) are instances where there is only one passenger with no equipment. The weight that is allowed for a second person can be used to carry fuel, thereby increasing the endurance of the aircraft by approximately twenty percent. This would be very useful in the rescue scenario. Only one passenger without equipment would be flying to reach the injured or stranded party. The extra fuel that could be carried (600 N) minus the fuel needed for VTOL would allow the aircraft to rescue someone 154 km outside the normal radius of the aircraft.*Figure 2.5 shows a summary of aircraft characteristics, including the absolute ceiling. The level flight performance envelope which also shows the absolute ceiling is given in Figure 2.3.

*It should be noted that the total amount of fuel allowed was used in the endurance calculations. In reality, those values would be less to allow for a safety factor.

This aircraft has very reasonable performance characteristics. However, it has not reached the eight hour endurance required. There have been suggestions made to increase the endurance by carrying extra fuel instead of equipment or an extra passenger. If the purpose of this Mars plane is to investigate the planets surface, then six hours endurance is not only reasonable but practical. A person would not function well in a small aircraft for eight hours. The original reason for the Mars plane was to carry men and materials to distant sites that could not be reached by land vehicles. In this case, the range of 1854 km (927 km radius) is sufficient.

Fig. 2.1

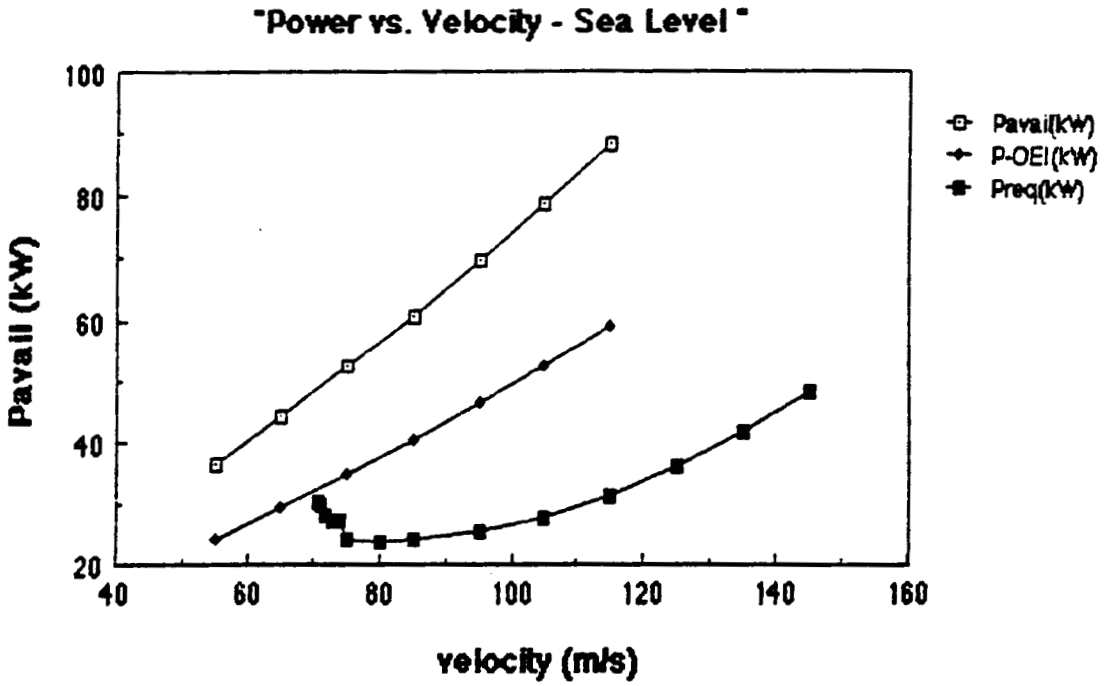
"Power vs. Velocity - Sea Level "
Pavail (kW)
velocity (m/s)
Pavail(kW)
P-OEI(kW)
Preq(kW)
100
80
60
40
20
40
60
80
100
120
140
160

Fig. 2.2

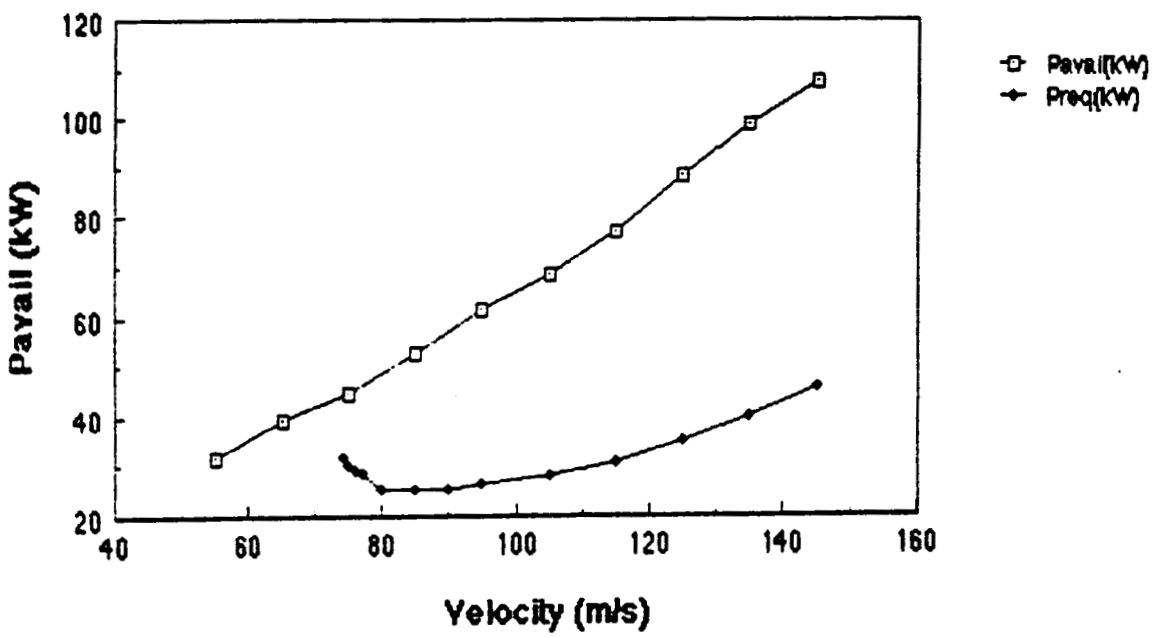
"Power vs. Velocity - 1.5 km"
Pavail (kW)
Velocity (m/s)
Pavail(kW)
Preq(kW)
120
100
80
60
40
20
40
60
80
100
120
140
160

Fig. 2.3

this isn't a conventional representation of LFE.

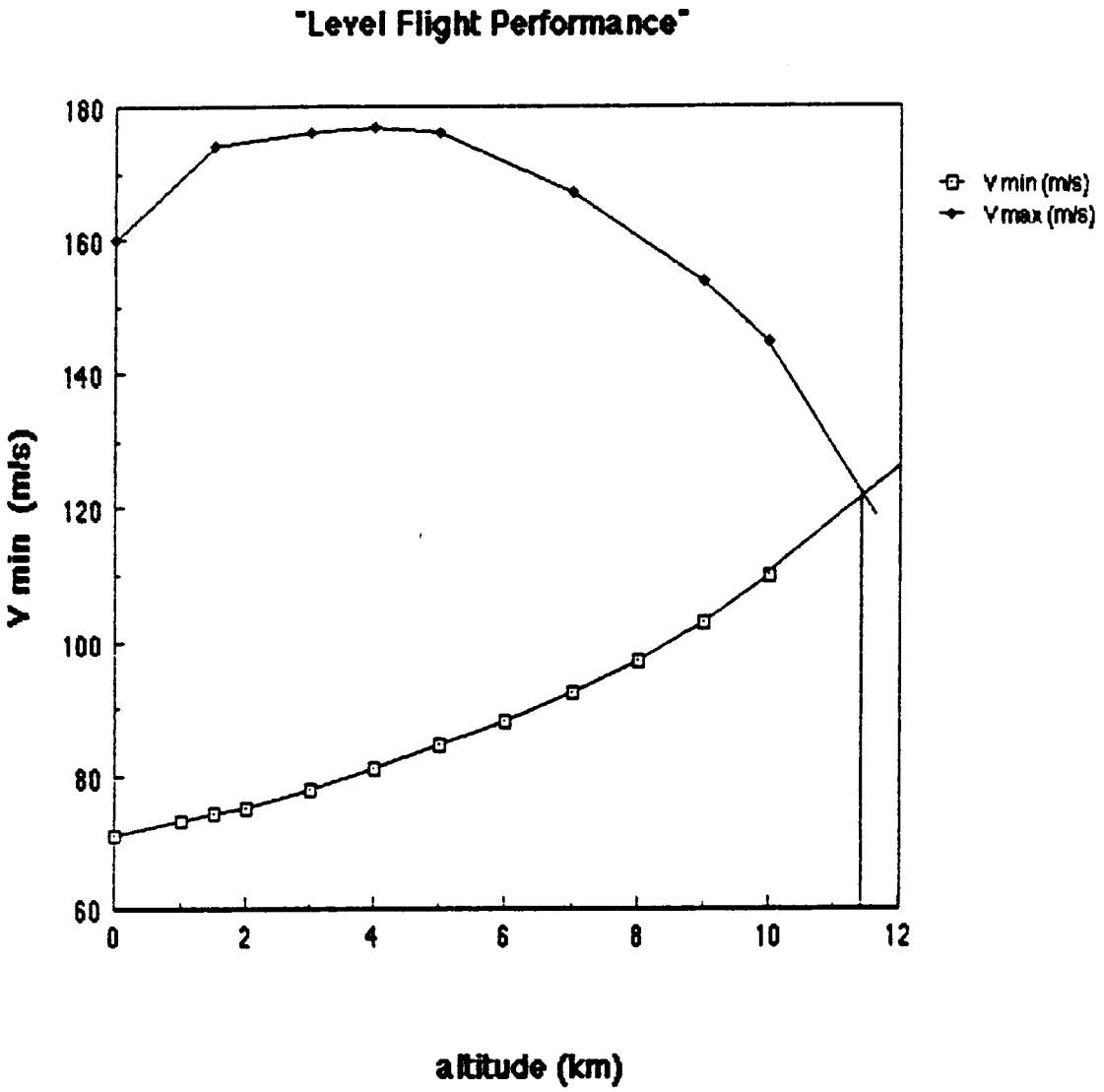

FIG 2.4

CONDITION	FUEL USED (N)	RANGE (km)	ENDURANCE (sec)
CONVENTIONAL			
Take-off	168.0	-	-
Landing	32.0	-	-
VTOL			
Take-off	159.0	(at W = 6252 N)	-
Take-off	230.0	(at W = 7502 N)	-
Landing	62.0	-	-
CLIMB	38.7	26.4	322.70
DESCENT	25.2	17.8	209.70
CRUISE			
Normal	2236.0	1810.0	21295.0 (5.9 hr)
Rescue (carry fuel)	2615.0	2118.0	24912.0 (6.9 hr)
1 Pass (carry fuel)	2836.0	2295.0	27000.0 (7.5 hr)
TOTALS	conventional, normal		
	2499.9 N	**1854.2 km**	**6.1 hours**

C-3

Fig. 2.5

CHARACTERISTIC	CLIMB	CRUISE ALT	DESCENT
R/C	4.35 m/s	4.96 m/s	-7.15 m/s
Angle of attack	3.16 deg	3.35 deg	~~-4.83 deg~~
Preq	24.1 kW	24.4 kW	24.4 kW
Pavail	56.0 kW	60.6 kW	60.0 kW ← will this be cut? otherwise no descent
Velocity	79.0 m/s	85.0 m/s	85.0 m/s
Vstall	71.0 m/s	74.0 m/s	61.0 m/s ?

POWER AND PROPULSION

JAMES V. LEROY

General Discussion

The Martian atmosphere, as can be seen from figure 1, is such that the options for propulsion systems are quite limited. Because of the extremely low oxygen content, any type of "air breathing" engine would be required to carry its own supply of oxygen. The on-board storage of the oxygen and the weight of the storage system thus add complexity which may or may not be feasible depending on the aircraft's design function.

Another possible option is that of a solar/battery powered system. However, with this design the need arises for heavy batteries and solar arrays which may require that the aircraft be "built around" the propulsion system. In other words, the entire aircraft may have to be designed in such a manner as to accomodate the propulsion system (for example - the use of an unnecessarily large wing in order to carry all of the solar panels required). Also with this system, the design team would probably be forced to rely heavily upon the speculation of future technology.

Martian Atmosphere Composition

CO_2	95%
N_2	3%
Ar	2%
water vapor, oxygen, neon, CO, krypton, xenon, ozone	1%

Figure 1

Rocket power has the definite advantage of being available with today's technology, relatively simple and easily capable of providing the requirec power. The main drawback of the rocket system is the associated massive fue consumption. This factor alone makes rocket power inadequate for a

lightweight, extended endurance aircraft.

After analyzing the formentioned possiblitites and associated drawbacks, a decision was made. Instead of designing the aircraft around a propulsion system, a somewhat unusual system was designed which takes advantage of the benefits of several concepts.

The Propulsion System Chosen....

The propulsion system chosen for the Mar's reconaissance aircraft consists of three, rocket powered, controllable pitch, dual bladed propellers mounted in the pusher configuration. In short, the system consists of a propeller which is driven by small rockets built into the extreme tips of the propeller blades.

The system thus combines the advantages of rocket propulsion (i.e. simplicity, reliability, high thrust) with the fuel efficiency advantages associated with the concept of a high bypass turbofan engine. In addition it is simple in construction and in concept. The technology required to design and develop such an engine is well within the grasp of present technology.

The main disadvantage of this system is a somewhat larger fuel consumption, however, this is balanced out by the elimination of large bulky machinery - the rocket prop requires no engine to drive it other than the small rockets in the propeller tips. In addition, with the elimination of the engine hardware there is a elimination of the required cooling systems. (Since the Martian atmosphere is so thin, an aircooled internal combustion engine would possibly suffer overheating problems.)

Because of its extreme simplicity, the rocket-prop system might easily prove to be more trouble-free and thus more reliable. This is a great advantage since maintanance and replacement parts on Mars will be extremely limited.

Description of the Rocket Propeller System

As previously stated, the rocket propeller propulsion system consists of three, rocket powered, controllable pitch, dual blade propellers mounted in the pusher configuration. The system yields a fuel consumption rate which is lower than that of a conventional rocket propulsion system by a factor of 2.25. Specific fuel consumption remains approximately constant over the entire operating range: c_p = 18.2 N/Kw·hr (Mar's newtons) both at sea level and at cruise altitude (h = 1500 m).

Figure 2 shows a front and side view of the engine as well as the associated dimensions. As can be seen, the system is quite simple consisting of a rather large propeller (5 m diameter) with two small rockets built into the tips. The propeller is mounted on a 10 cm diameter hollow steel drive shaft. The shaft is then mounted into three support bearings. Each bearing is enclosed and is bathed in a lubricating fluid. A fuel pump and an alternator are also geared to the drive shaft. The propeller pitch is controlled by a small hydraulic system which automatically feathers the propeller should the rotation rate decrease below a specified limit.

The cockpit engine controls associated with this system consist of a throttle (fuel flow control), and an RPM control (blade pitch control). The pilot simply sets the RPM control for the desired rotational rate and then applies throttle as needed. Because of the increased efficiencies obtainable with higher propeller rotation speeds, a design RPM of 812 RPM was chosen. At this rotation rate, the transonic effects at the tips are negligible but are approaching unnegligible limits due to critical Mach.

Fuel is pumped through the hollow engine crankshaft into the hub of the propeller. It is then fed radially outward through fuel ducts located inside the propeller blades to the small rockets located at the tips.

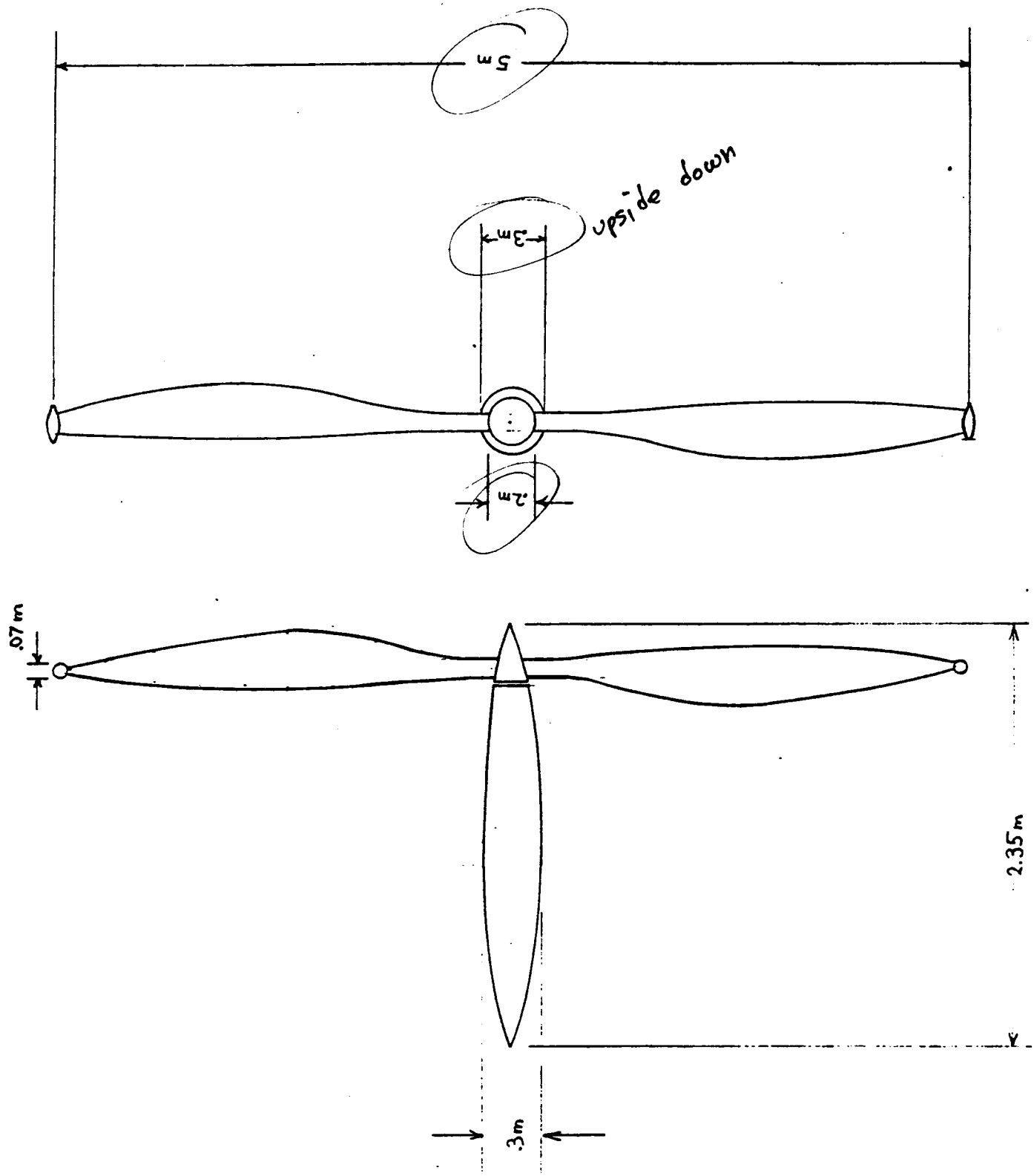

Figure 2

The propeller blades are detachable from the hub which will allow access to the fuel ducts. The rockets are also detachable to accomodate servicing and/or replacement and contain ceramic sleeve inserts which serve as combustion chambers. Since the required rocket thrust is so low (5 lb_F/rocket at cruise) the rockets are expected to last for at least several flights. After rocket deterioration has progressed beyond a safe limit, the ceramic insert is simply replaced.

It was first thought that an attempt should be made to keep the heat produced by the rockets contained at the tips of the propellers. However, after further consideration it has been determined that the heat should be allowed to conduct itself through the propeller. In this way the propeller serves as a large cooling fin and thus operating temperatures are reduced considerably.

Rocket Prop Performance

NOTE: All engine performance numbers and graphs are relative to one engine thus to obtain "total values" it is necessary to multiply by a factor of three.

Because of the rather low thrust required by the rockets at the propeller tips (5 lb_F/rocket at cruise) , the limiting factor in terms of performance is considered to be the propeller (propeller design will be discussed later). Thus in determining the various engine performance graphs it was assumed that the rockets were capable of providing the required thrust at all conditions. This is of course an extreme assumption but for the flight regime of the aircraft in question, it is acceptable.

From figures 3 and 4, extrapolation yields a static maximum thrust and a static maximum shaft power of 175 N and 4.3 Kw at sea level. Figures 5 and 6 give the identical parameters at cruise altitude (1500 m) to be 155 N and 3.0 Kw.

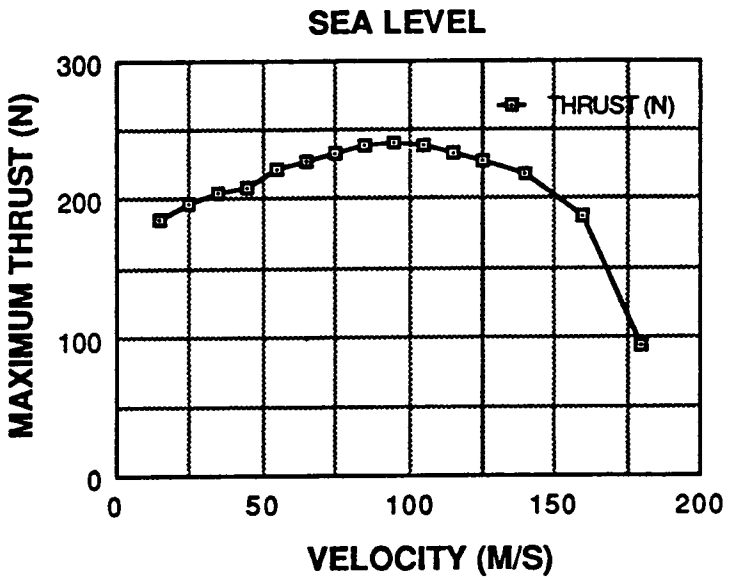

Figure 3

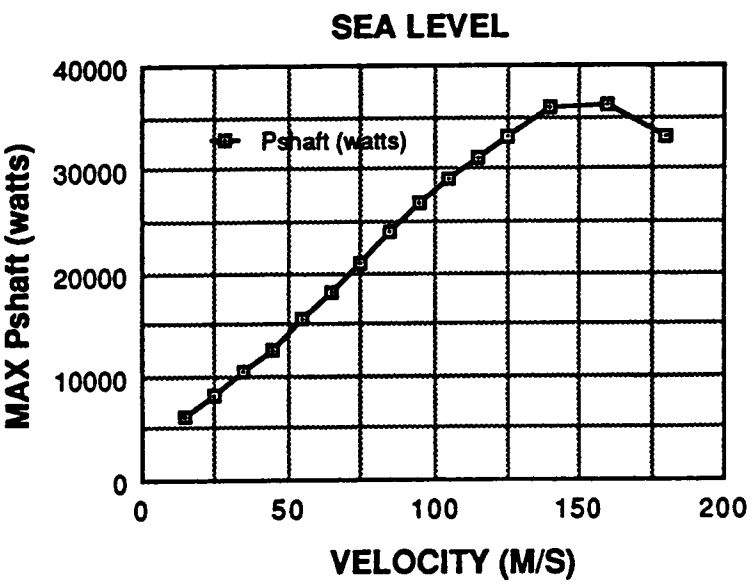

Figure 4

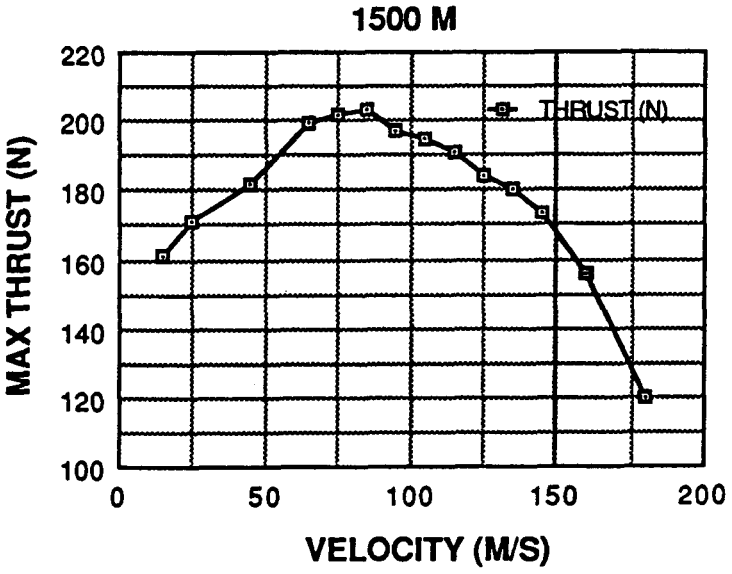

Figure 5

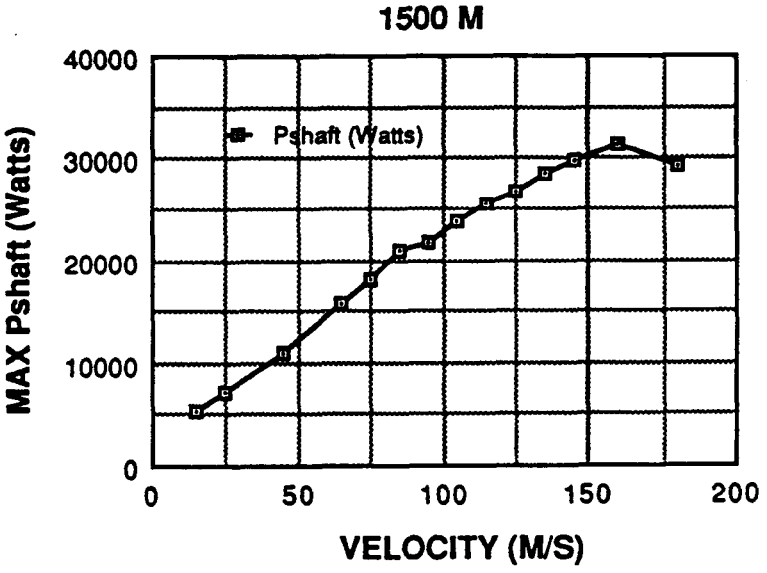

Figure 6

As vehicle flight velocity is increased it is necessary to decrease the rotational speed of the propellers to avoid large drag increases due to transonic effects at the tips. Rotation rate is kept constant at 812 RPM (85 rad/s) except when it becomes necessary for a reduction. The design Mach number for the tips is .95 and all transonic effects at the speed are ignored. Once again, the propeller blade itself (not the tip - rockets) is consider to be the limiting factor for engine performance in all calculations.

Figures 7 and 8 show fuel flow data per engine at sea level and 1500 m respectively (V = 85 m/s). Although fuel burn rates increase steadily with airspeed, specific fuel consumption remains approximately constant: c_p = 18.2 N/Kw·hr.

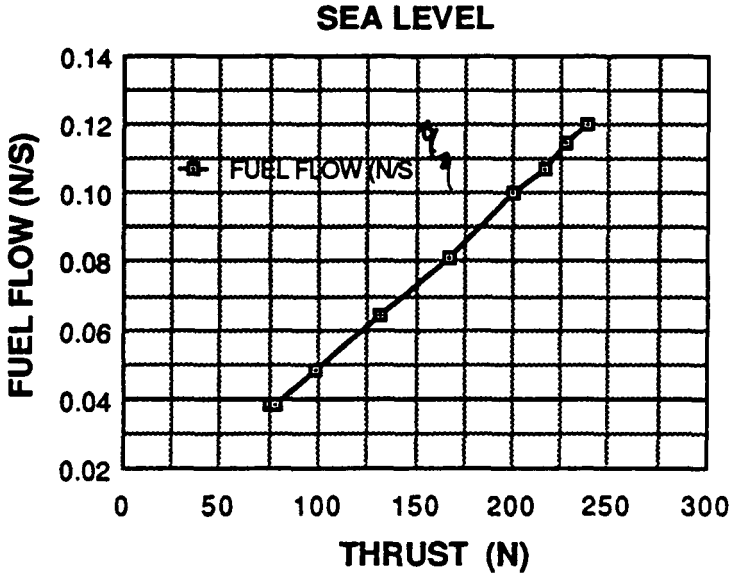

Figure 7

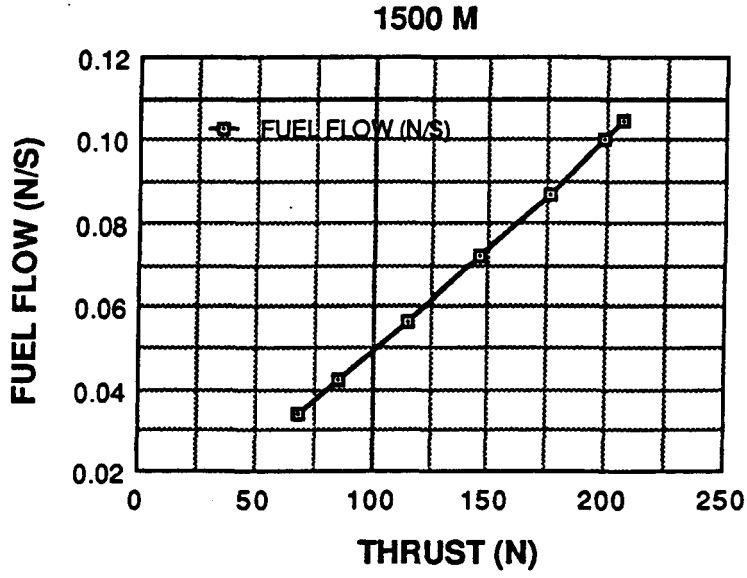

Figure 8

Propeller Design

The design of an efficient propeller was considered to be the single most important feature of the report, since propeller performance influences total engine performance more than any other single feature.

Because of the extremely low Reynold's numbers associated with the Martian atmosphere, standard propellers containing standard airfoil designs are unacceptable at best. Proper propeller design includes selecting airfoils which are appropriate for the low Reynold's numbers (0-200000) and which also provide acceptable structural margins (i.e. thick near the hub and thin at the tip).

Three airfoils were chosen for the design:

Airfoil		Location
1)	LA203A	Inner third of radius
2)	LNV109A	Middle third of radius
3)	Eppler 387	Outer third of radius

All three of the above are specifically designed for low Reynold's numbers. The LA203A is a thicker airfoil thus it was selected for use near the hub where the stress concentration will be the greatest (1). The Eppler 387 is a relatively thinner airfoil section thus it is adequate for the outer regions near the tip (2). The LNV109A is an "in between" thickness and thus allows for a smooth geometric transition from the hub to the tip (1).

An algorithm was obtained from a paper written by Eugene Larrabee (3) for determining optimum propeller design and "off-design" performance. The algorithm, which utilizes Goldstein's solution, was then incorporated into a computer program which proved to be instrumental in determing the best design for the given conditions.

The lift and drag curves for each of the three airfoils were plotted and modelled mathematically. The resulting equations were then incorporated into the propeller design program. An optimal angle of attack was selected for each airfoil (based on maximum L/D) as well as the associated drag vs. lift ratios. These values were also included in the program. A design point was then decided upon (design criteria - engine out climb capabilities at cruise velocity) and a propeller design was specified by the program.

The propeller was then analyzed utilizing momentum theory and modified blade element theory (4),(5). Both methods verified the design and thus support the computer procedure. The resulting geometry is shown in figure 9 where "r" is the distance from the hub, "R" is the propeller radius, and beta is the angle between the chord and the plane of rotation.

Propeller Geometry (V = 85 m/s; T = 200 N)

r/R	.1	.2	.3	.4	.5	.6	.7	.8	.9
beta (deg.)	85	74	64	56	49	44	39	36	33
chord (m)	.1	.17	.26	.40	.42	.39	.35	.29	.20

Figure 9

As can be seen from figures 10 and 11, efficiency at cruise (roughly 100 N/engine) is around 88%. Figures 12 and 13 show the necessary change in beta (beta prescribed by figure 9) necessary for a given thrust when at cruise velocity (85 m/s).

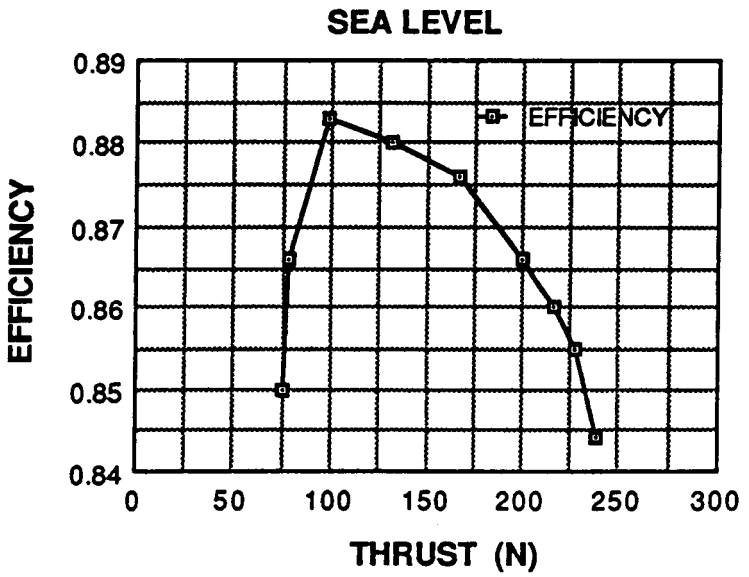

Figure 10

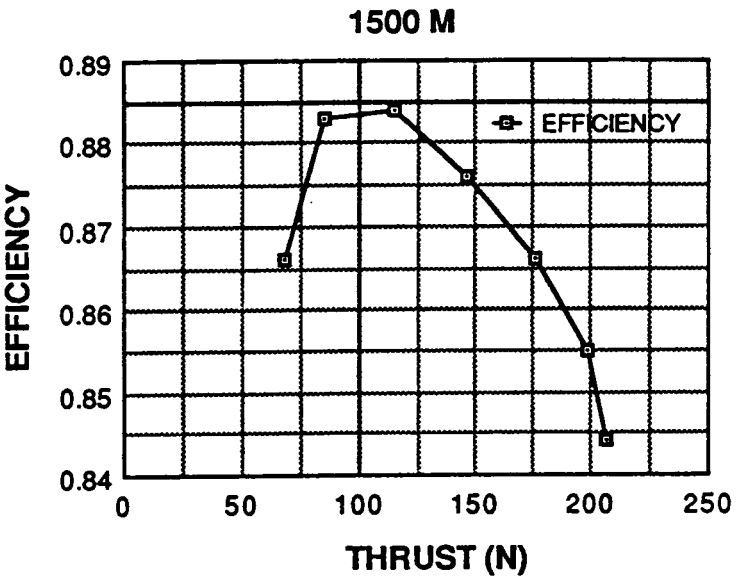

Figure 11

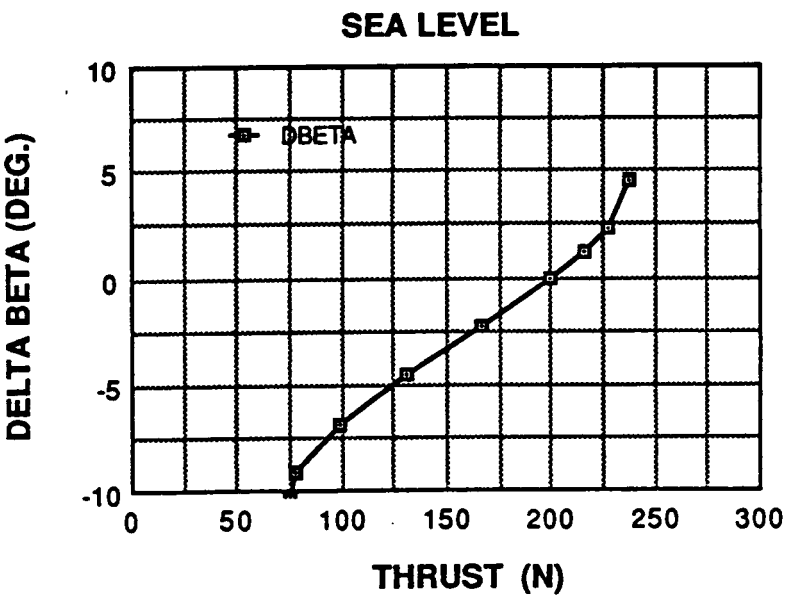

Figure 12

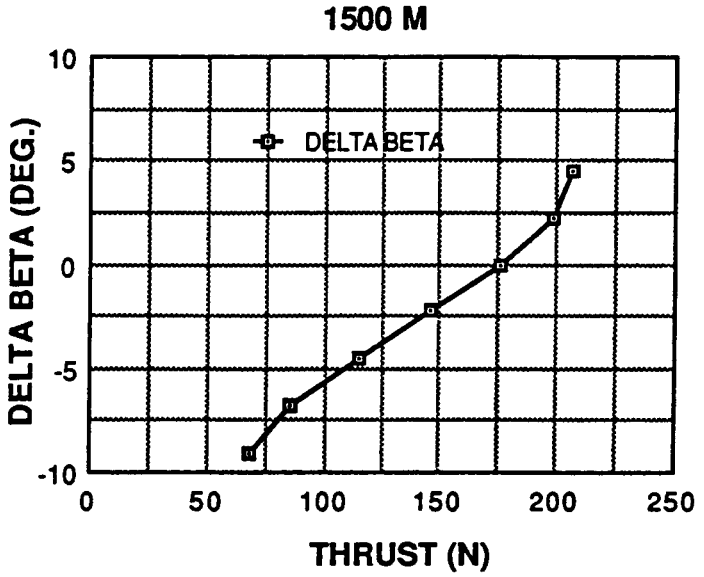

Figure 13

Fuel Selection

The ideal fuel would be a monopropellant that offers no storage or stability problems, is liquid at the operational temperatures and affords a high specific impulse. The fuel found to match this description most closely is hydrazine (6), however a somewhat optimistic value for specific impulse was used to attain the present fuel consumption data (assumed specific impulse = 350 s).

The advantages of hydrazine (monopropellant) are:

1) Can be decomposed by a suitable solid catalyst (Iridium)
2) Reliability and simplicity of a single feed system
3) Stable up to 530 ^{o}K
4) Easily stored for long periods of time

The hydrazine will be pumped into the rocket and ignited via a catalyst mesh. For starting, the mesh will require pre-heating.

Engine Inoperative Drag

All three engines have feather capabilities such that beta is increased by 40^{o} over the values specified in figure 9. The result of this is an engine out drag of: Drag = .0195 Rho $(Vel)^2$ Newtons, where Rho is expressed in Kg/m^3, and Vel is expressed in m/s. For cruise conditions this results in a drag of 2.2 N for a feathered inoperative (not turning) propeller.

In Conclusion...

In conclusion, it should be emphasized that although this system may not be as fuel efficient as various other types of propulsion syustems, it offers extreme simplicity and eliminates the need for heavy machinery. By virtue of the fact that there are less moving parts the rocket-prop could quite possibly prove to be more reliable and easier to maintain.

1. Liebeck, R.H. and Camacho, P.P. "Airfoil Design at Low Reynolds Numbers with Constrained Pitching Moment", Proceedings of the conference on Low Reynolds Number Airfoil Aerodynamics, University of Notre Dame UNDAS-CP-77B123, June 1985

2. Mcghee R.J., et al "Performance Characteristics from Wind-Tunnel tests of a Low-Reynolds-Number Airfoil", AIAA 26th Aerospace Sciences Meeting, AAIA-88-0607, January 1988

3. Larrabbee, E.E., "Propeller Design and Analysis..."

4. McCormick, B.W. "Aerodynamics, Aeronautics, and Flight Mechanics", 1979, pp. 343-358

5. Sivier, K. "Applied Aerodynamics", Lecture Viewgraphs, 1987, pp. 293-328

6. Sutton, G.P. "Rocket Propulsion Elements", 1986

Stability and Control

Philip Lange

This section covers the information pertaining to the stability and control of the aircraft. The development of the various control components will be examined. First, the sizing of the canard and elevator is presented, followed by the vertical tail and rudder selection. Next, the proper aileron size is calculated, followed by a discussion of the aircraft's ability to meet the listed design requirements.

Sizing the canard consists of determining the best combination of canard area and distance between wing aerodynamic centers. After numerous iterations, the combination chosen for this aircraft is a canard area of 37.5 m^2 and a distance of 15 m between wing aerodynamic centers. This results in the neutral point being located 10 m behind the canard's aerodynamic center. (See figure 1) Using a cruise weight of 6252 N (aircraft weight with only half fuel), a cruising altitude of 1.5 km and speed of 85 m/s, the wing incidence is set at 6.18° to enable the fuselage to be level at this configuration. The corresponding canard incidence is then 8.59°. (See reference 1 and 2)

Next, the area of the elevator is chosen to be large enough to provide sufficient control of the aircraft, yet small enough so the

canard is not overloaded. Since the elevator span is equal to the span of the canard, an overly large elevator would cause much torsion in the canard, thus necessitating more structure and weight. Hence, the chord of the elevator remains at 0.30 m, corresponding to an elevator effectiveness of 0.30 ($\delta_{e\ max}$= 30°). The structure group confirms that such a small elevator would pose no structural problems. As shown by Table 4.1, the elevator is of adequate size to furnish ample control power.

In order to keep the aircraft sufficiently stable, the smallest allowable static margin must be equal to 0.10. In following this constraint, the most rearward center of gravity is restricted to 9.8 m behind the aerodynamic center of the canard. Using the above configuration, the center of gravity range is equal to 2.47 m. Such a large theoretical range is desirable for weight and balance, but is unfortunately inconsistent with the flying requirements outlined in Table 4.1. When confined to these requirements, the most forward center of gravity is limited to 9.35 m aft of the canard's aerodynamic center. The limiting condition, namely the canard power needed for take-off rotation, is itself constrained by the take-off velocity. The center of gravity range is thus limited to only 0.45 m. This range corresponds to a maximum static margin of 0.325 and a minimum static margin of 0.10. Wing sweep is not incorporated in this design due to the possibilty of wing damage from the exhaust of the rocket

propellers.

With the above configuration, the aircraft exhibits sufficient longitudinal control power for the flying requirements, and it has adequate stability. In addition, the actual center of gravity range is consistent with the allowable range as outlined in Weight and Balance.

After the canard is sized, the various stability and control derivatives are calculated according to reference 3. (See Table 4.2) The vertical stabilizers are then sized, and checked against the control requirements found in Table 4.1. Due to the area of the required structure to raise the engines, the vertical stabilizers, which contain the rudders, needed to be smaller than expected. The rudders are placed beneath the main wing in order to prevent disturbing the flow to the propellers. (See figure 4.1 for exact placement) Two rudders, each of 1.5 m^2 , are sufficient to provide directional control as defined by the flying requirements outlined in Table 4.1.

The remaining requirement is for roll control. Spoilers, desirable because of their design simplicity and proverse yaw effects, are unacceptable due to the possibility of separating the flow from the wing when deployed. Because of the undesirable spoiler effects, ailerons are used for roll control. The initial choice of aileron dimensions of 3 m by 0.50 m is unchanged. This size provides the aircraft with adequate roll control for all flying requirements. In order to avoid performance problems encounterd from producing turbulence

forward of the propellers, the ailerons are positioned lateral to the propellers. The proximal end of the ailerons are 8.5 m from the centerline. (See figure 4.1) A maximum aileron deflection angle of 20° is sufficient to conform to all the flying requirements found in Table 4.1.

The various control, surfaces outlined in this report will be controlled by electric servos. This system is designed to be dependable, easily maintainable, and simple enough for the fabrication of the aircraft in space. Since such servos are now used extensively on military aircraft, they are already proven to be reliable. The ease of maintenance is accomplished by having only three systems in the control loop. These divisions are the pilot's controls, the signal-carrying wires, and the servos, each of which are easily accessed. Since the servos are mounted and calibrated at the factory, and the wires are disconnected at the aircraft's seams, the fabrication is trivial. One last characteristic is that since the servos are electrically activated, they can also serve as trim tabs since they may be moved during flight to correspond to a neutral stick position. As discussed above, this system is well suited for the design requirements.

In conclusion, the designed control surfaces and overall configuration are consistent with, and frequently perform better than the design requirements.

Flying Requirements:

Condition	Requirement	Performance
Take-off rotation	The ability to rotate at $0.9V_{TO}$.	Rotation velocity is $0.95V_{TO}$ sufficient
Engine-out control	The ability to maintain a straight flight path at $0.9V_{TO}$ with OEI, $\beta = 0$, and $d_{r\ max}$.	At V = 70 m/s, with OEI only 2.4° of rudder deflection is needed to maintain a straight path.
Engine-out control	The ability to maintain a straight flight path at $1.10V_{TO}$, $0.75d_{r\ max}$, and f = 5°	At V = 85 m/s only 72% (18°) of rudder deflection is needed while f = 1.70°.
Banked turn	Sustain a 30° banked, coordinated turn at V_{cruise} and h_{cruise}.	A 40° banked turn is possible at these conditions.

Roll response	Roll 30° within 2 sec. of a maximum aileron deflection at V_{cruise}	Only 11° of aileron deflection is needed to roll 30° in 2 s.
Stall	Sufficient control power to hold $C_M = 0$ at $C_{L\ max}$ at landing conditions	See explanation*
Roll response	Roll 30° within 2 seconds of full aileron deflection at $V_{approach}$	Same roll response as previously stated since the velocities are similar.
Crosswind landing	Sufficient directional control to hold $\beta = 10°$	A 10° sideslip can be maintained using only 4.89° of rudder deflection.
Full rudder sideslip	Maintain wings level in a full rudder sideslip using only 75% of the lateral control power	A 51° sideslip is maintained with a full rudder deflectionof 25°. This requires a 67% aileron def.(13.6°)

* Due to the canard configuration , it is impossible to stall the aircraft unless the center of gravity is located 0.31 m behind the neutral point. At landing, $C_L = 0.89C_{L\ max}$ is attainable with an aircraft angle of attack equal to 4.84°.

Table 4.1

Stability and Control Derivatives

Sideslip angle,ß

$C_{y\beta} = -0.765/rad$ $C_{l\beta} = 0.0517/rad$ $C_{n\beta} = 0.089/rad$

Rolling velocity, p

$C_{yp} = 0.041/rad$ $C_{lp} = -0.622/rad$ $C_{np} = -0.185/rad$

Aileron deflection, da

$C_{yda} = 0.0/rad$ $C_{lda} = -0.195/rad$ $C_{nda} = 0.0063/rad$

Rudder deflection, dr

$C_{ydr} = 0.0512/rad$ $C_{ldr} = -0.0344/rad$ $C_{ndr} = -0.182/rad$

Angle of attack, a

$C_{La} = 7.506/rad$ $C_{Ma} = -3.15/rad$

Table 4.2 (Ref 3)

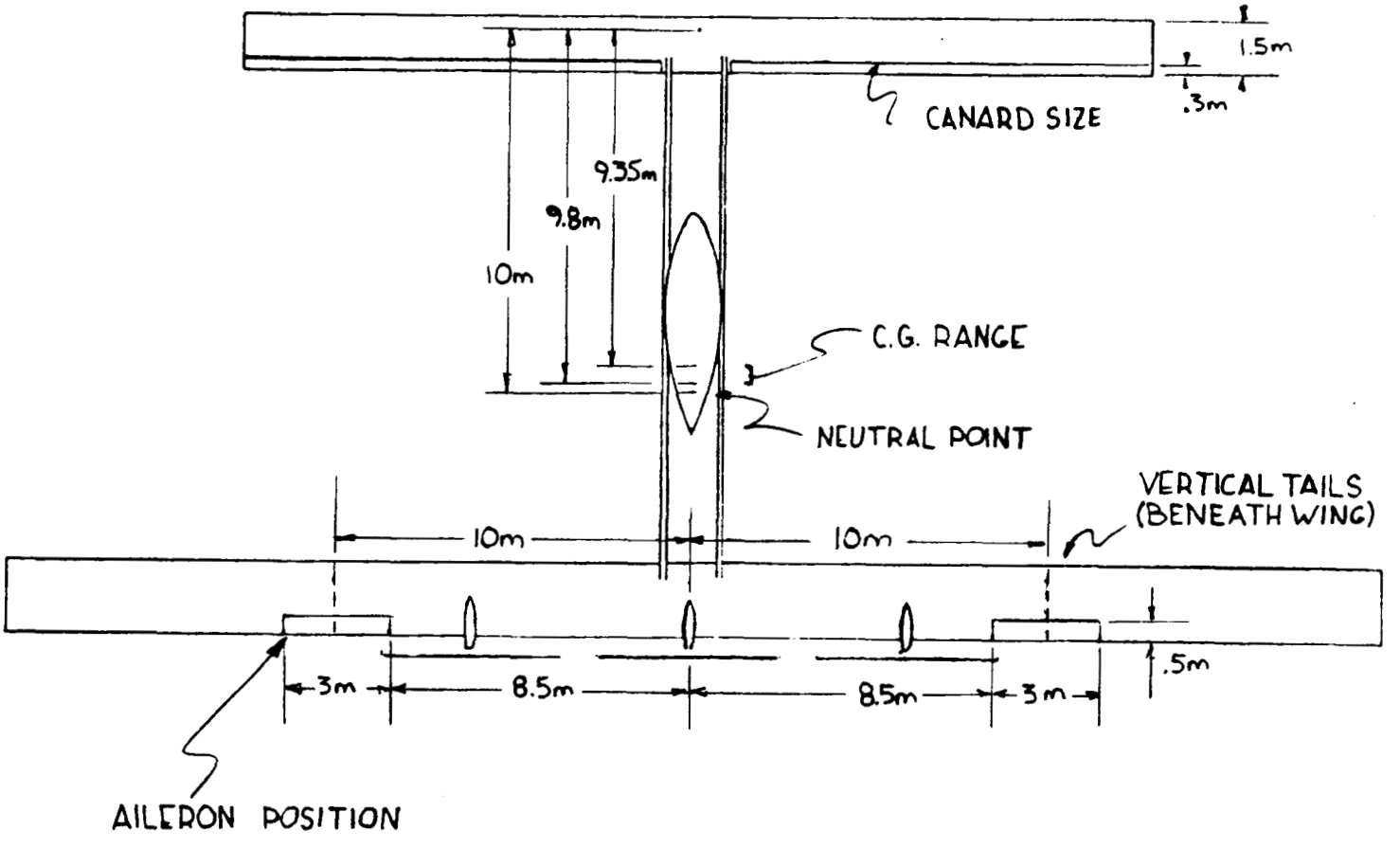

Figure 4.1

References

1 Sivier, K.R., "Lecture Viewgraphs for AAE 319 Aircraft Flight Mechanics", Spring 1988

2 Sivier,K.R., "Canard Longitudinal Stability and Control", Spring 1988

3 Roskam, J., Methods for Estimating Stability and Control Derivatives of Conventional Subsonic Airplanes, 1977

STRUCTURAL ANALYSIS

MICHAEL ENRIGHT

The structure of the Mars aircraft is a relatively simple structure consisting of spars, weps, and skin covering, in addition to the engines, landing gear,etc. Figures 5.1 throough 5.7 illustrate the moments, shears, and loads acting on various parts of the wing. The loads for the wing lift and the wing weight were done using Shrenk approximations. From these loads it then becomes necessary to design a structure that will support these loads. The maximum moment the wing experiences occurs at the root and has a value of 20,292 N-M in 1G flight. This number was then multiplied by 4.5 to accomodate a maximum 3G flight and a safety factor of 1.5. From this value, other parameters had to be incorporated to find the dimensions of the spar that would support it, these being where along the chord should the center of the cross section be placed, and which type of material, due to it's ultimate yield strength, should be used. Because of the high moment on such a thin wing it became necessary to abandon the idea of a circular cross section, and try ones of a different shape. After experimentation with several types, an elliptical cross section was chosen, which will be centered at the quarter chord length. Figure 5.8 illustrates the wing cross section at the root, where the maximum thickness is .36 meters. Following are the dimensions for the spar:

semi-horizontal axis = 0.30 meters

semi-vertical axis = 0.15 meters

thickness = 4.5 x 10E-4 meters

Because certain parts of the aircraft experience greater stresses than others, the aircraft will be made out of two different Advanced Composite Materials, Boron/Epoxy and Graphite/Epoxy. Some characteristics of each are shown below:

	Density (lb/in3)	Ultimate Strength (ksi)
Boron/Epoxy	0.070	276
Graphite/Epoxy	0.055	214

Boron/Epoxy was chosen for the spars and webs on the main wing and the canard. It will also be used for the frame of the fuselage, which will consist of two spars, one on each side of the pod, and cross-fasteners with a Mylar covering over the top. The pod will be made out of Graphite/Epoxy except for the clear plasticpanel which will also serve as an entrance into the pod. The rest of the aircraft which consists of mainly skin coverings will be made out of Graphite/Epoxy.

This one was done for two reasons, the first being that the skin doesn't need to be as strong as the webs and spars, and secondly, Graphite/Epoxy composite material is 75% that of Boron/Epoxy.

The Load vs. Span diagrams for 1G flight and on the ground illustrate a non-constant wing weight. This is due to the fact that the number of webs and size of the spar decrease past the 7 meter point along the span, which can be seen in figures 5.1 and 5.4. This was done to save weight since the heaviest weight

other than the wing itself past the 7 meter point is outrigger gear, which has negligible weght. At six meters along the span both the engine and the thruster are located, which again can be seen in figures 5.1 and 5.4, in addition to figures 5.9 and 5.10. The engine and the thruster weigh 150.33 N and 28.6 N, respectively. Because of the weight concentration at this point webs were put directly on each side of the engine and thruster. The spacing for the remaining webs is as follows:

0.50 meters	0 < span < 7 meters
0.75 meters	7 < span < 18.75 meters

The canard consists of only a thruster located at 6 meters, which like on the main wing will have a web directly on either side, but other than these, they will also be spaced by 0.75 meters. Figure 5.7 describes the loads acting on the canard for 1G flight, the lift, the canard weight, and the thruster wight. As was done for the main wing, the canard's lift and weight
were derived using Shrenk approximations.

Lastly figures 5.9 and 5.10 show all the important structural dimensions and the 8 points were the structure will be disassembled for transport. This along with a more in depth discussion of the fuselage will be discussed in the section on Packaging and Assembly.

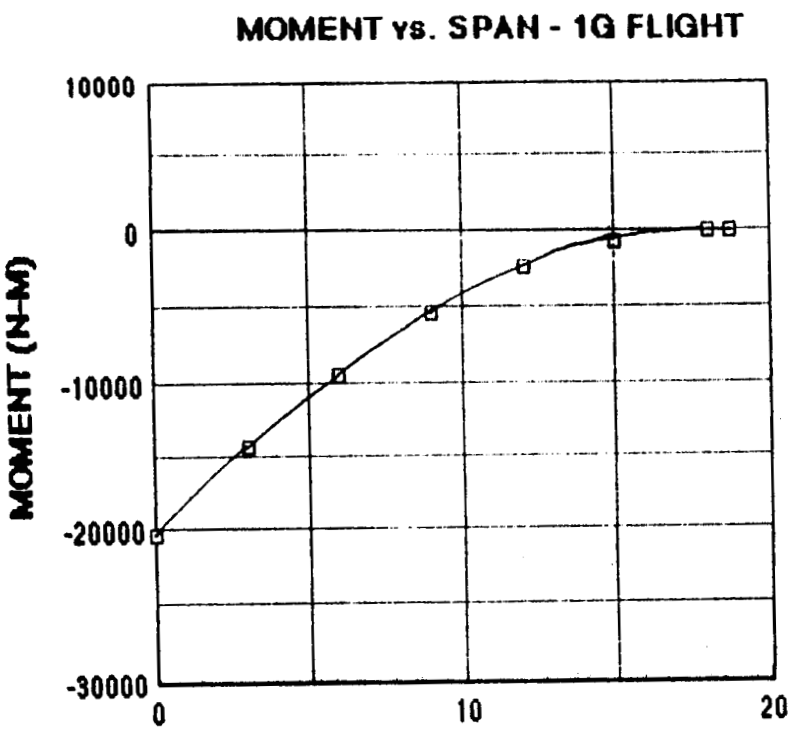

FIGURE 5.3

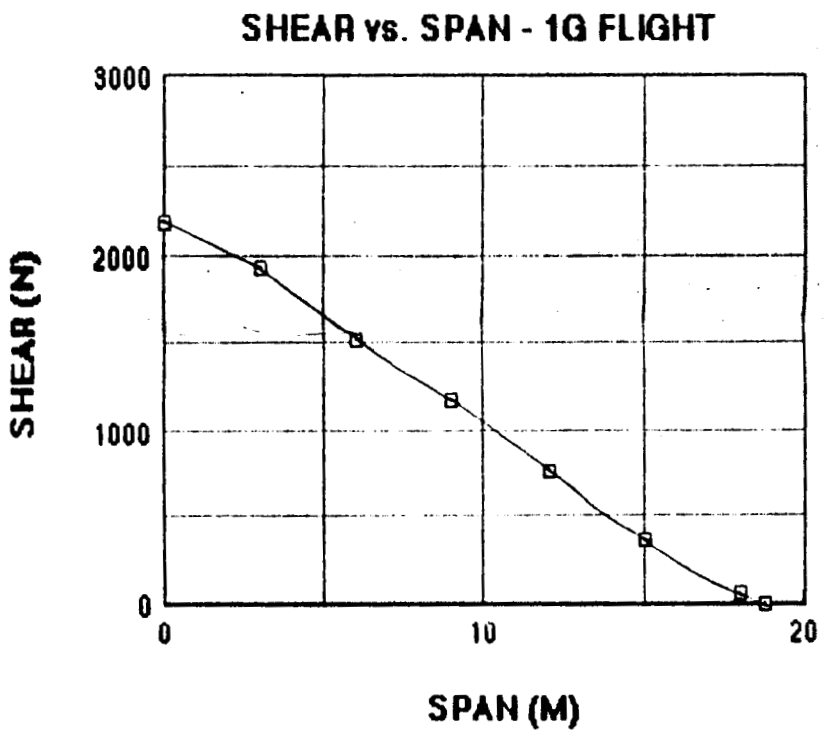

FIGURE 5.2

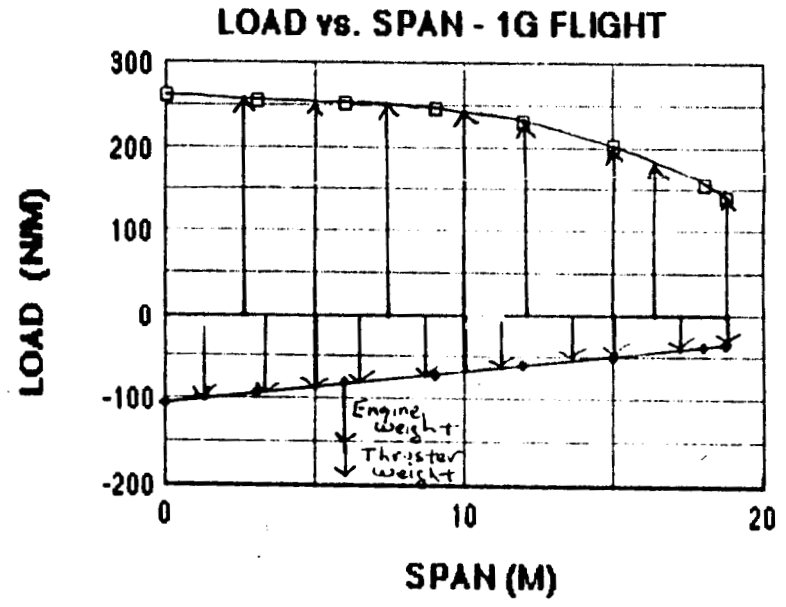

FIGURE 5.1

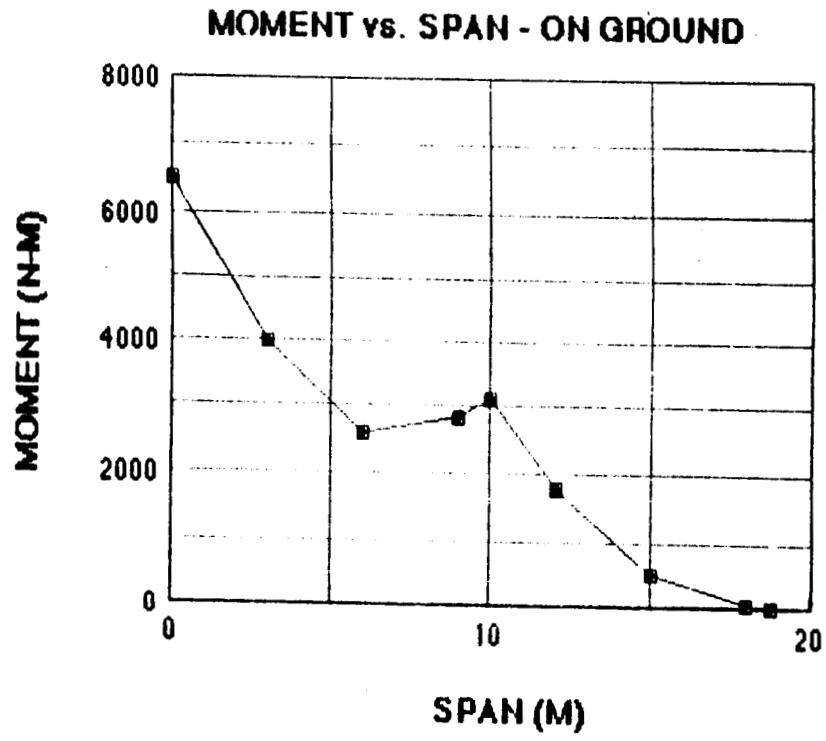

FIGURE 5.6

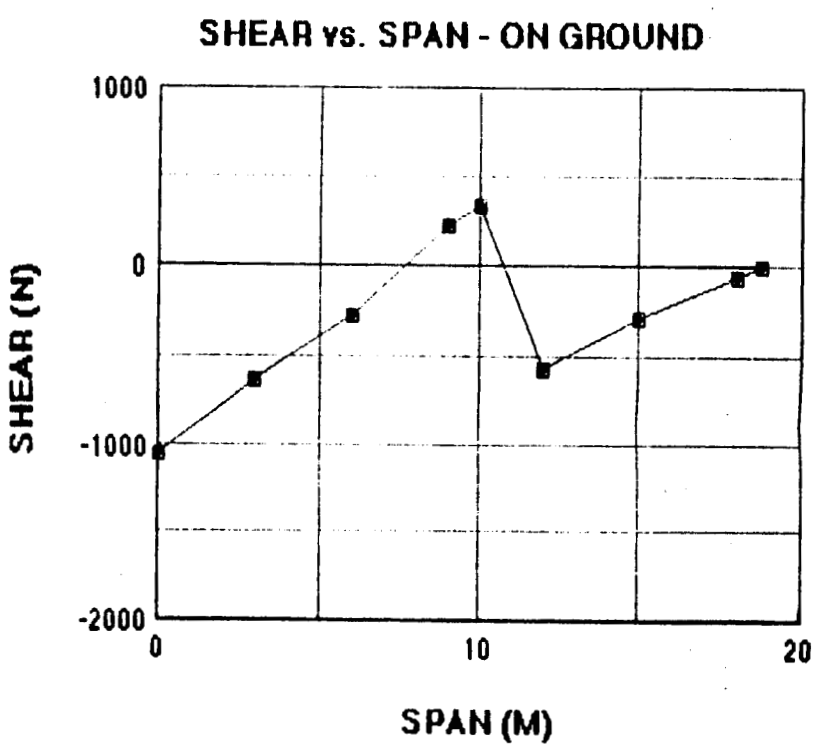

FIGURE 5.5

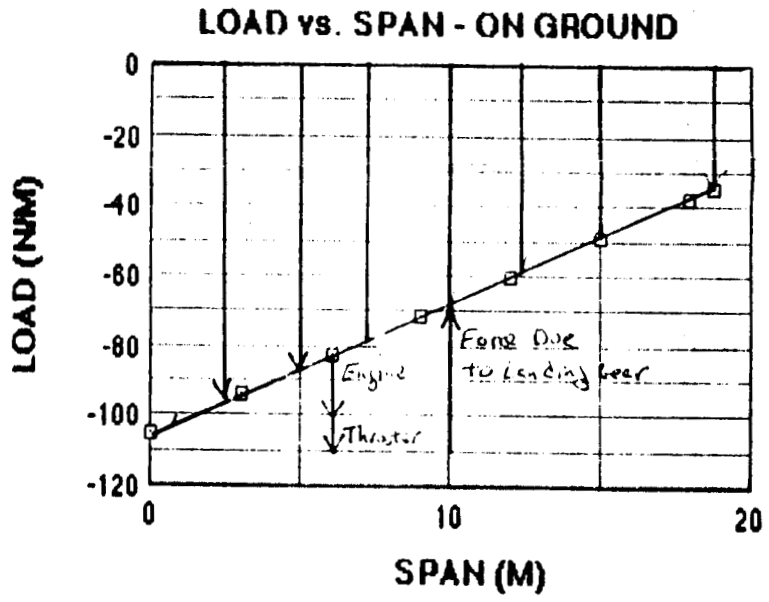

FIGURE 5.4

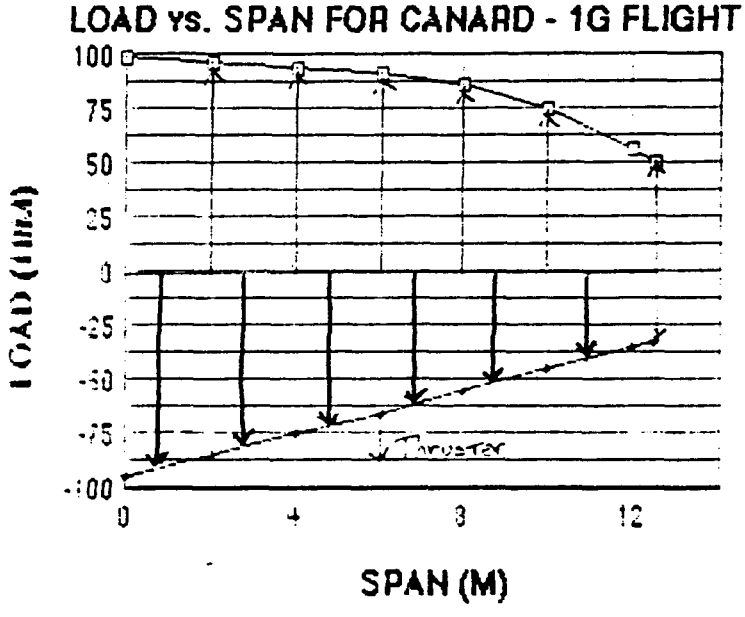
LOAD vs. SPAN FOR CANARD - 1G FLIGHT
100
75
50
25
0
-25
-50
-75
-100
0
4
8
12
SPAN (M)

FIGURE 5.7

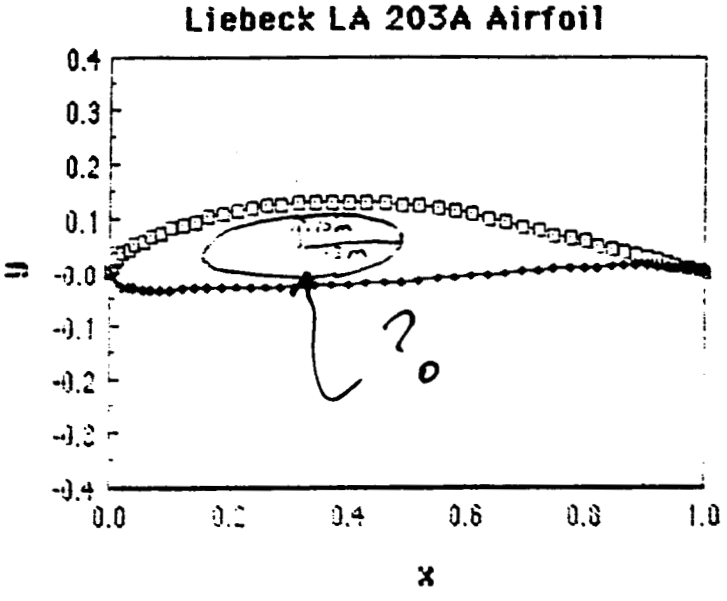
Liebeck LA 203A Airfoil
0.4
0.3
0.2
0.1
-0.0
-0.1
-0.2
-0.3
-0.4
0.0
0.2
0.4
0.6
0.8
1.0
x

FIGURE 5.3

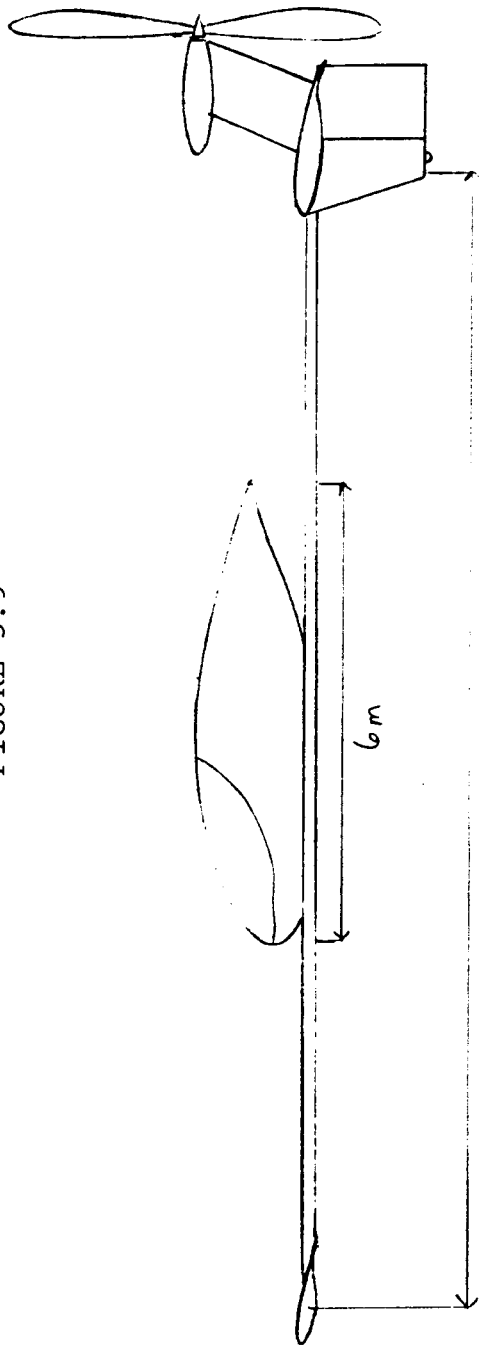

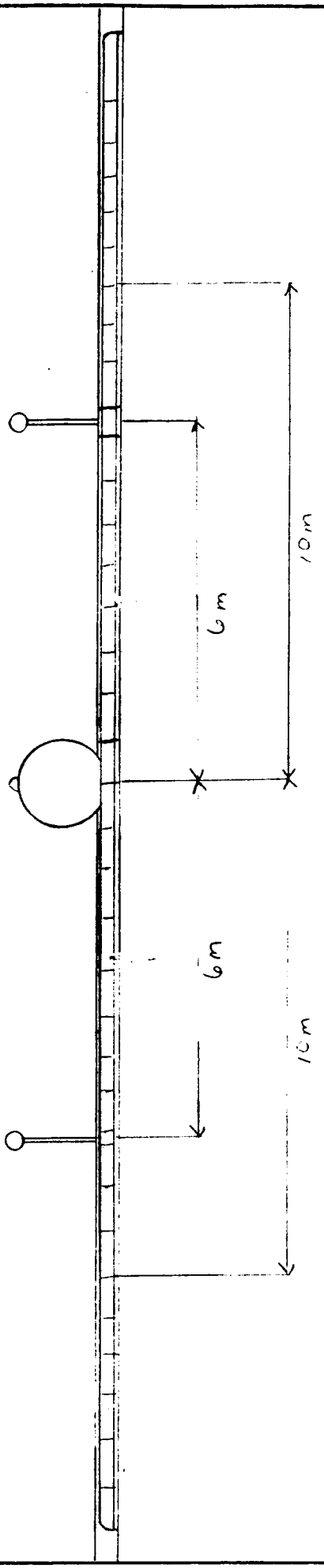

FIGURE 5.9

FIGURE 5.13

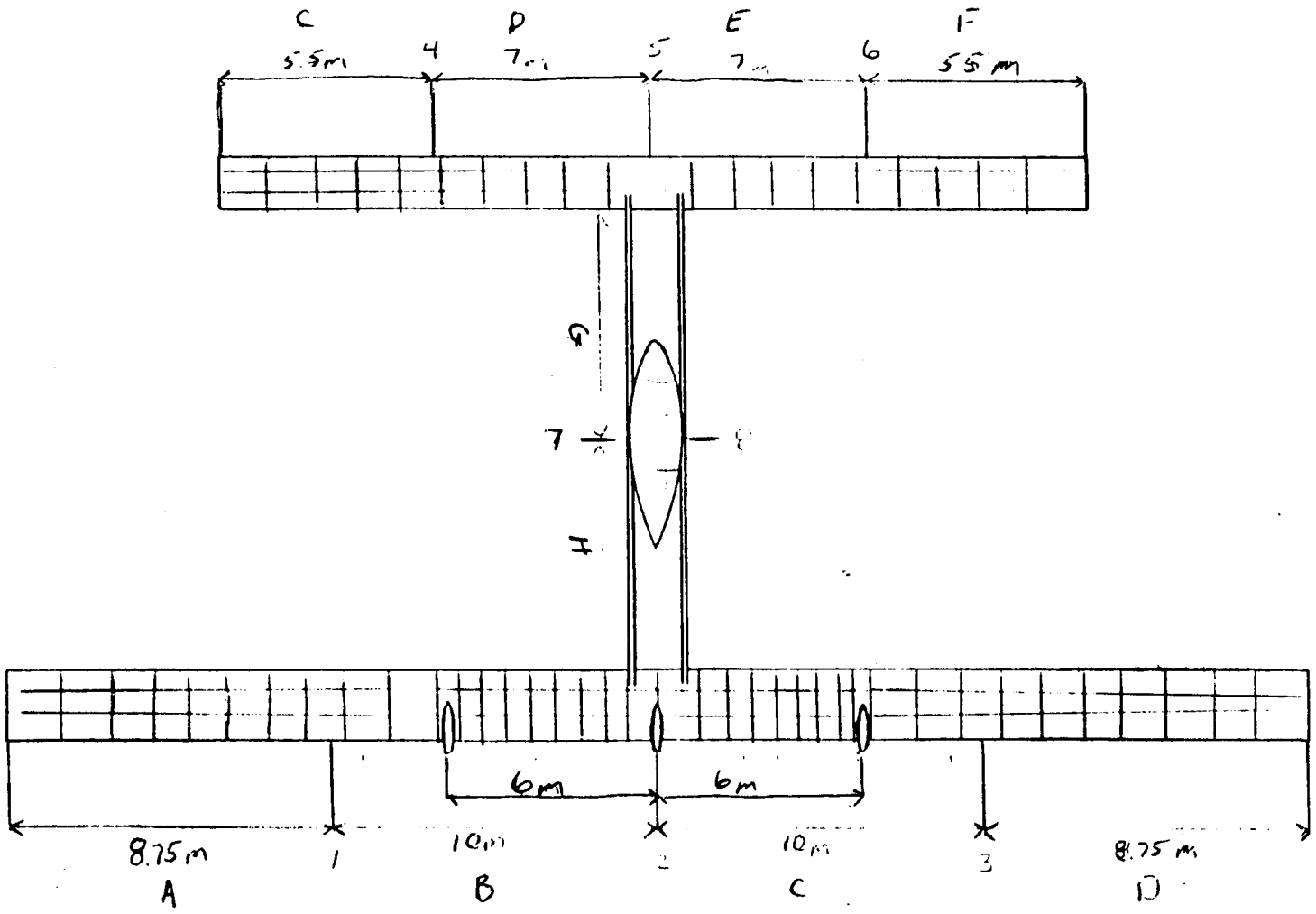

Surface Operations:

Nick Jasper

The landing and take off systems in this aircraft offer a large degree of variability in how the aircraft is operated. The systems are designed to provide both conventional landing and take off and vertical landing and take off. It is intended to be used primarily in a conventional mode due to the fuel limitations imposed by VTOL maneuvers. The VTOL capability enables the craft to perform rescue missions and operate from unprepared sites. This make's it useful for ferrying personnel and small payloads to remote outposts. Also because of the VTOL capability, the aircraft can be delivered to Mars and put into operation before a landing strip is completed for it. It would, however, suffer an endurance penalty if it had to VTOL at all times.

The VTOL System:

The VTOL system consists of five, vectorable, 2500 N thrusters based on the design used for Viking lander's main engines. The possibility of just taking them "off the shelf," and making the necessary modifications makes their use all the more attractive. They are hydrozine fueled and share a common fuel system with the main propulsion system. They have a length of 23 cm and a diameter of 22 cm. (1) In order to allow them to be swept 95° from the vertical in any direction without striking the aircraft, they are mounted with a ball-in-socket joint at the end of an 13 cm, rotating shaft. The ball-in-socket joint pivots 95° from the vertical and the shaft can rotate 360°; in this manner the thrusters are fully vectorable. The extra 5° is to allow the thrusters to be vectored horizontally regardless of the body angle of attack, which is always less than 4.9°, according to Stability & Control.

The layout of the thrusters relative to the aircraft can be seen in figure 1. There are three thrusters on the rear wing, two of which are 6 m off the center line and at .75 chord and the third is along the center line at the trailing edge of the fuselage. The two thrusters up front are also located 6 m off the center line and are at the half chord of the canard. The spacing off the center line of 6 m corresponds to the same longitudinal axis as the propellors. This makes tying them into the fuel system simpler, and, by displacing them from the center axis, provides better control. The center aft thruster is positioned further back than the others due to a space conflict with the rear landing gear. Also due to the gear location, its range of motion is limited from facing forward at all. This does not cause any difficulty. The three back-two up configuration works out very well for the center of gravity location. At gross take off weight, to hover with no nose up or down moment, the two front and one center line rear thruster must put out max thrust while the two outer thrusters in the back need only provide 81.2% of their total thrust in the vertical direction. This corresponds to a yaw moment capability of 17.5 kN-m or 2.8 kN-m of roll moment. These moments would be higher at lower weights but the percentage of thrust provided by the two outlying rear thrusters compared to to the other thrusters remains approx. 81%.

The choice of five 2500 N thrusters instead of four larger thrusters also provides survivability should one thruster fail. It can be seen from fig. 1 that if any one of the thrusters were to fail, the cg would remain inside the trapezoid formed by the other four. This indicates that the aircraft could maintain an even keel and not roll off on a wing as it descends. If any one of the thrusters off the center line were to fail, then the pilot should immediately shut down the thruster which is across the diagonal from it and go to full vertical thrust on the remaining

two diagonal thrusters. He then needs to add enough vertical thrust from the aft center thruster to counteract the resulting roll. When a worst case, computer aided, analysis is done (2) (3) (thruster failure after a 15 m VTOL from maximum take off weight) the weight at failure (due to a minimum required fuel burn) is 7454.6 N. The single rear thruster applies 32.5° of its total thrust and this leaves the thrust short of the weight by 1641.7 N. After the craft drops 15 m, taking into account the decreasing weight due to fuel burn and drag, it strikes the ground with a velocity of 5.255 m/s. This corresponds to dropping the plane from a height of 3.67 m with no thrusters. It was with this in mind that the landing gear was designed, and it should be survivable with no damage.

The only other, single thruster, failure which would result in a situation other than that just discussed, would be if the single center line thruster were to fail. If this were to happen, then the vertical component of thrust in the remaining rear thrusters would have to be increased, and, other than that, it would not present any severe problems. The pilot in the heaviest load scenario described above would still have 1250 N of excess thrust to either complete his maneuver, or make a regular VTOL landing.

The Landing Gear:

The landing gear design has many criteria which it must satisfy, and it has done so reasonably well. The general configuration of the gear can be seen on the 3-view at the beginning of the paper, and consists of two main gear, located along the center line (Fig 2), and two outrider gear, to keep the plane from tipping, located 10 m off the center line along the main wing. It should be noted that the nose gear is exceptionally close to the cg. This is due to a communication problem before the freeze date. Believing the cockpit to be located directly above and

extending to just behind the canard, the nose gear was to be placed below the middle of the cockpit. Later, when the cockpit was moved further aft, the nose gear inadvertently got moved with it, and this change was not noted until after the freeze date. The nose gear was not intended to be so close to the cg. It would be preferable for it to be approximately as far from the cg as the rear gear. The rest of the gear design has been affected by this change. Although it is not optimum, the gear configuration appears to be adequate.

First of all, as mentioned above, the landing gear must survive an impact of 5.255 *m/s*. There is a direct relationship between impact velocity and shock absorber stroke in the gear, and that is given by (ignoring wheel displacement under impact): (4)

$$S = \frac{1}{\eta_s}\left\{\frac{w^2}{1.84g\lambda}\right\}$$

where:

- S total shock displacement, all gear
- η_S efficiency of shock absorber
- w impact velocity
- g gravitational acceleration on Earth
- λ reaction factor of the aircraft

By choosing the impact velocity to be 5.255 m/s, the shocks to be liquid springs with an efficiency of .85, and the frame to have the same reaction factor as a transport (2.5), it is found that the total shock displacement needed is 721 cm. The design chosen, as seen in figure 2, can easily displace up to 60 cm apiece and, if forced to maximum deflection, may even displace as much as 85 cm apiece.

This maximum displacement just keeps the middle section of the gear leg from moving between the wheels. This is because there may not be enough clearance due to flattening of the tire under such a heavy impact. This gives a total deflection of 1.7 m and, theoretically, could withstand an impact of 8.07 m/s, or, in other words, a free fall from 8.66 m. More than likely though, such an impact would overstress the wing roots, since it is highly questionable that the wings could deflect sufficiently 10 m away, where the outrigger gear are located. Even if the wings could deflect enough, since the outrigger gear contain no shock absorbing mechanism, they, along with the vertical stabilizer built around them, would probably be crushed. The 1.5 m length of the landing gear, in addition to being able to take a high impact, also serves the purpose of keeping the thrusters away from the ground. With the thrusters pointing straight down, this keeps them 1.14 m above the ground. This elevation is necessary to keep the rockets from throwing up excessive amount of debris, which could cause damage to the aircraft.

Normally, landing gear struts are about three times the shock absorber stroke. (4) This problem is avoided by the use of liquid springs as mentioned before. Instead of keeping all the liquid in the strut, as is usually the case, there is a liquid reservoir above the shock in the fuselage. When the shock deflects, the fluid goes into the fuselage, and back out again as the shock extends. There are also small electric pumps in the fuselage that allow the gear to be pumped up or bled off to whatever length desired. The purpose for this will be discussed in more depth later.

The tire size choice for the gear was based on observation of tire sizes on comparably sized aircraft (Leer Jet, Aztecs, Dornier commuter aircraft) rather than empirical formula since the formula do not appear to interpolate to other

gravities (4). The tires are at a differential pressure of approx. 4.2 kg/cm^2 (60 psi). This falls into the range of what is used for operation from hard desert sand, hard grass, and tarmac with a poor foundation (4). These conditions seem to be most like that which exists on Mars. Therefore construction of the runway is less expensive, since it needn't be concrete. The braking coefficient of the system is equal to .6.

The two main gear are retractable. They don't tuck into the fuselage, however. They merely move up out of the way as much as possible to lay lengthwise along the fuselage. They utilize an electrically driven, four bar link and the front gear fold rearward, while the rear gear, to avoid the center thruster, fold forward. The two outrigger wheels, which are part of the vertical stabilizer structure, do not retract, but are obviously streamlined by the stabilizer.

Conventional Landing & Take off:

For a conventional take off, the aircraft's gear must all be pumped up so that the plane sits high and level. If the aircraft is not level, (angle of attack = 0) then the canard cannot generate enough lift to rotate the plane around the rear gear, which is substantially further back than the cg (the normal point of rotation). The pilot then applies full thrust to the props and however much rocket thrust as he desires. The amount depends upon how much fuel he wishes to use in a tradeoff for how short he wishes the ground roll. When the plane reaches 80 m/s, he rotates to 2.5° and lifts off. As soon as he leaves the ground, the thrusters are cut in order not to waste any more fuel, and the aircraft climbs up and out.

For a conventional landing, the pilot flies in over the 15 m obstacle (the prospects of actually finding a 15 m obstacle on Mars are very poor and therefore

in doing the landing and take off analysis it would've been more reasonable to use a height of 7.5 m or 10 m) at approximately 71 m/s and flares before touchdown killing most of his vertical velocity. As soon as the tail gear touches, the plane will rotate down and the nose gear will touch right away, since the canard will not be able to hold the nose up against the moment about the rear wheel. As soon as the impact is absorbed, the pilot will bleed the nose gear down to a length of .925 m. This will cause an angle of attack of - 3.5° and lower the C_L. (This amount of down angle will still leave the front thrusters 21.5 cm clearance.) By spoiling as much of the lift as possible in this manner (the plane has no flaps or other such high lift system), the downforce on the gear is as large as possible allowing more effective breaking. The pilot must also apply a certain amount of forward thrust from the rear thrusters in order to stop before running off the end of the runway. Thrust is applied in the rear only to keep from stirring up dust around the cockpit and obscuring the pilot's view. Obviously, the more fuel he has left aboard, the more inertia he has and the more thrust he must apply.

Take Off and Landing Performance:

In order to analyze the landing and takeoff performance for both VTOL and conventional maneuvers, four computer programs were written. All four have the same basic structure with only the necessary changes made for which maneuver is actually being looked at. The programs take into account the following: the varying thrust of the propellors, the drag of the aircraft in both the vertical and horizontal directions, the sweep rate of the thrusters, the fuel burn rate of the propellors, the fuel burn rate of the thrusters with varying thrust output, the reduction in weight as fuel is burned, the varying of thruster output as is needed to support the aircraft, and the in flight variance of the body angle of attack with

its effect on lift and drag. All of the above is read in from the keyboard as is: specific impulse, maximum values of the vertical and horizontal velocities, obstacle height, headwind, surface area of the plane, drag polar, coefficient of lift, and how small of a time increment to integrate over. The only thing which the programs does not to take into account are the ground effects on lift and drag.

For take off at a fully loaded weight of 7502 N, the fuel burns, ground rolls, total takeoff lengths over 15 m obstacle and time required for maneuverare as follow:

	time	ground roll	total distance	fuel burned
Conventional:				
$T_{thrusters}$ = 12500	19.56 s	.47 km	1.1 km	171.8 N
$T_{thrusters}$ = 6000	31.62 s	.98 km	1.6 km	168.3 N
$T_{thrusters}$ = 0	318. s	12.3 km	13.4 km	95.4 N
VTOL	15.3 s		.6 km	214.2 N

As can be seen, if the distance traveled in flight before clearing the obstacle is included, then, even with maximum thrust, take off cannot be achieved in less than 1 km. If however, the ground roll only were to be considered then with 6000 N of added thrust, the 1 km goal would barely be reached for what seems a good compromise fuel consumption. It is also interesting to note that without the aid of the thrusters, the propellors alone would be totally inadequate.

Landings at just under full load will not be examined since there would be no need to try to conserve fuel and the pilot could chose to land vertically or horizontally at his option.

Landing with just enough fuel left to get on the ground and stopped requires 49 N when using VTOL. When landing conventionally the optimum landing parameters turn out to be using 1500 N of reverse thrust upon touchdown. This will use 32 N of fuel and have of ground role of .616 km. If an approach speed of 70.9 m/s and sink rate of 5 m/s is used along with a touchdown speed of 57 m/s and sink rate of .5 m/s, and the velocities are assumed to be linear in between; then the distance between crossing over the obstacle and touching down is .384 km for a total landing length of 1.00 km.

The fuel burn for VTOL at less than full load and greater than no load will be discussed in the Rescue Scenario discussion.

Ground Support & Conclusions:

The only real difficulty posed by the current landing gear system is that since the bottom of the fuselage is 1.5 m off the ground then the top of the cockpit is 3 m high. How does the pilot get into something that is 9 ft high? When the craft is at a prepared base with refueling capability, this poses no problem. The fueling point is in the back of the cockpit beside the rear seat. Therefore, the pilot can get in and out when they bring over the refueling equipment, which must obviously include a ladder. When landing at a remote sight the pilot will have to use the backup system. This consists of a simple rope and stick ladder with a foldable frame to hold it about .3 m away from the fuselage. Although climbing a rope ladder in a pressure suit on Earth might be difficult, it should be comparable

on Mars to doing it without the suit on Earth.

In trying to asses what type of airfield would be needed for this aircraft one has to consider the high take off speeds and approach speeds. This is offset by the fact that with the low pressure tires it can operate on cleared and compacted Mars soil. It would be best therefore to construct a 2 km runway of compacted dirt or perhaps crushed rock. This length would give the pilot room to shut down and come to a halt even if he's going 75 m/s when he makes the abort decision.

The VTOL, assisted conventional take off and landing system looks to be a very feasible and versatile way to meet the design requirements. Without the dual capability, either the endurance goal or the rescue capability would have had to been sacrificed.

References:

1) Class handout on Viking Main Engine
2) Vertical take off program
3) Vertical landing program
4) Class handout: Chapter 10: The undercarraige layout

Fig. 1

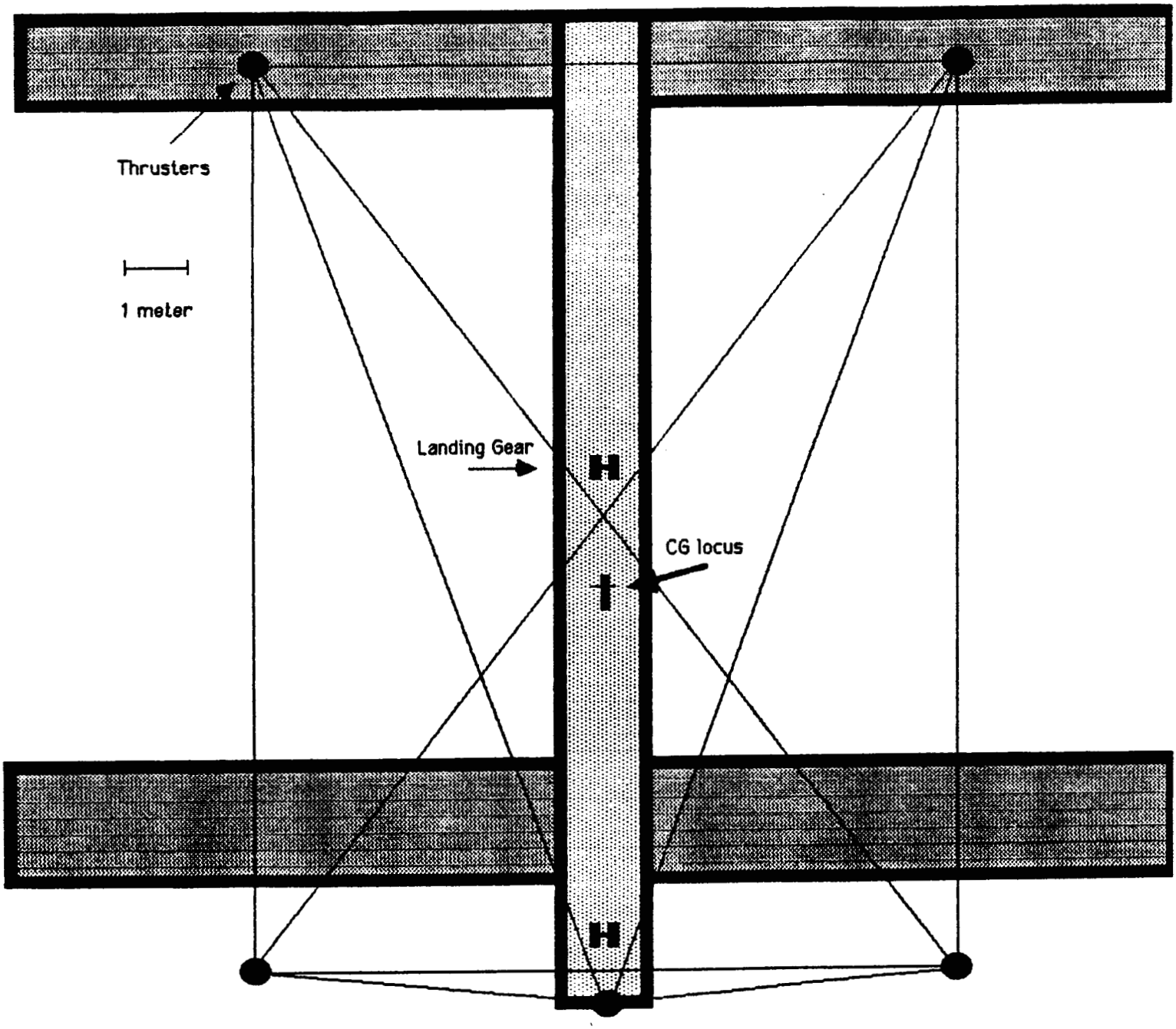

Fig. 2

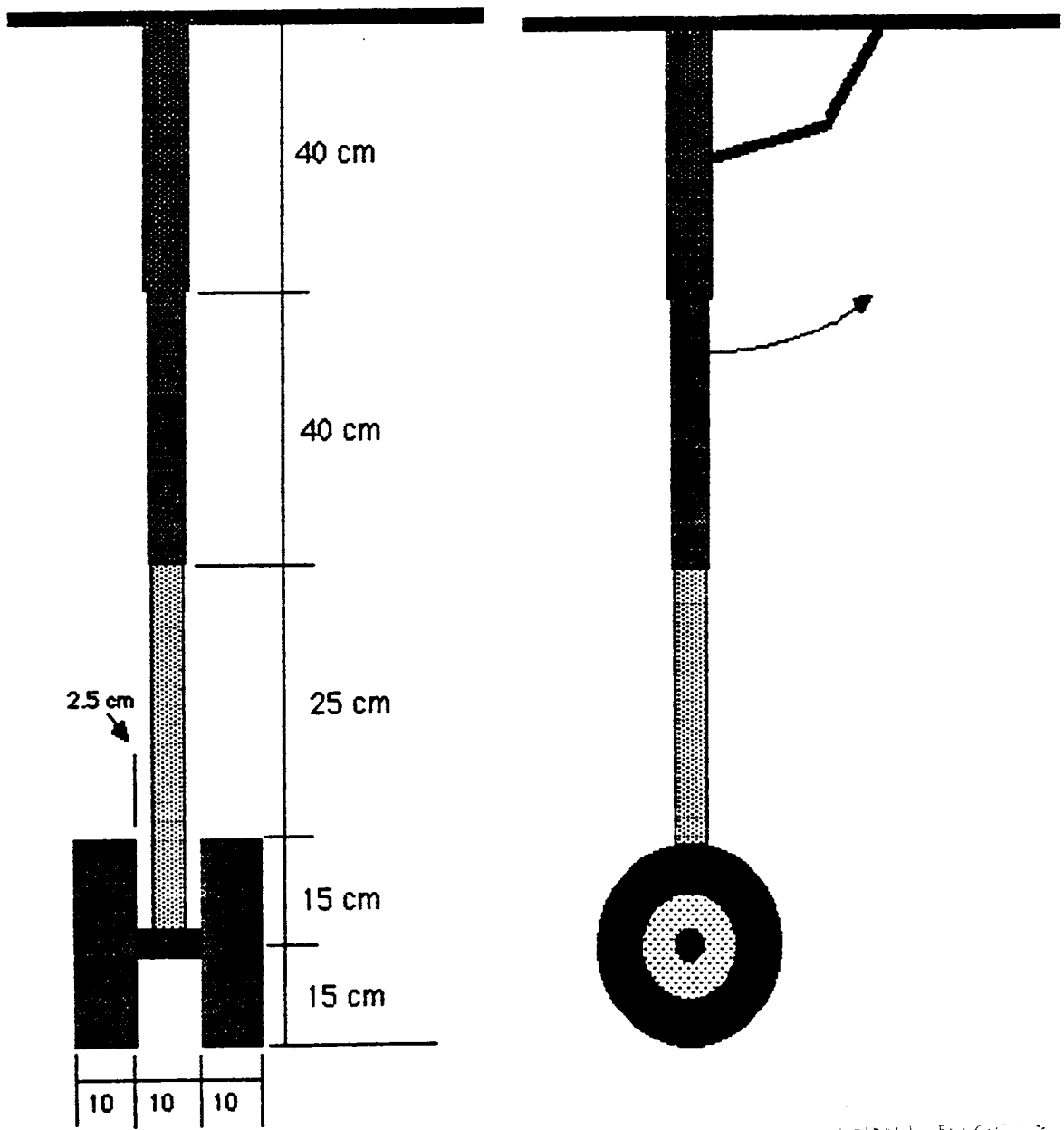

WEIGHTS AND BALANCES

PATRICIA PERKINS

From the original sizing example, Group 3 had an estimated weight of 7000 Newtons on Mars (Nmars). As the design process progressed, the goal weight changed to 7400 Nmars. Component weights were calculated using a number of equations compiled by Jan Roskam (Ref 1). At the preliminary design stage, the gross take off weight was 7953 Nmars, with the majority of weights being approximations. Presently, few component weights remain estimates. The majority are known. As can be seen on the detailed weight breakdown (Fig 7-1), the final gross take off weight is 7502 Nmars. The final weight iteration to be run produced the following results:

INPUT	OUTPUT
2893.5	4053.5
4053.5	4349.7
4349.7	4419.0
4419.0	4435.0
4435.0	4438.7
4438.7	4439.4

4439 lbs Earth = 7502 Nmars

Maximum Take Off Weight	7502 Nmars
Operating Empty Weight	3802 Nmars
Maximum Landing Weight	5002 Nmars
Useful Load Fraction	0.493
Maximum Fuel Fraction	0.333

Stability and Control provided a final center of gravity range of 9.35 to 9.8 meters from the canard aerodynamic center. Although this range decreased considerably from that given at the preliminary design stage, no problems were encountered. All center of gravities fall within the range as can be seen from figure 7-2 except that for the "1 passenger, zero fuel" situation. This does not present a problem, however, because the aircraft would not be flown in such a situation. The center of gravity does fall between the landing gear, so the aircraft will sit steady on the ground.

WEIGHT BREAKDOWN

Group Indication	Wt*	% Wt	Moment Arm X(m)**	Z(Nm)
Airframe Structures	2747	36.6		26426.0
Wing	1300	17.3	15.300	19890.0
Canard	795	10.6	0.225	178.9
Tail	37	0.5	15.800	584.6
Fuselage	395	5.3	7.875	3110.6
Landing Gear	117	1.6	7.875/15.5	1456.7
Nacelles	49	0.6	16.000	784
Struts	54	0.7	7.800	421.2
Propulsion Group	746	10.0		10241.4
Propeller Rockets	20	0.3	16.000	320.0
Fuel System	118	1.6	8.500	1003.0
Engine System	34	0.5	5.375	182.8
Propeller	431	5.7	17.000	7327.0
Thrusters	143	1.9	.375/16.0/16.5	1408.6
Airframe Equipment	292	3.9		2670.1
Instruments	17	0.2	5.375	91.4
Hydraulic Group	108	1.4	7.875/15.500	1262.3
Electrical Group	100	1.4	8.875	887.5
Electronics Group	17	0.2	5.375	91.4
Furnishings	50	0.7	5.875/7.625	337.5
Basic Empty Weight	3785	50.5		39337.5
Oil, Residual Fuel	17	0.2	16.000	272.0
Operational Empty Weight	3802	50.7		39609.5
Fuel	2500	33.3	9.000	22500.0
Payload	1200	16.0	5.875/7.625	3525/4575
Gross Take Off Weight	7502	100.0		70209.5

* All weights in Nmars
** All moment arms in meters from canard aerodynamic center

Fig 7-1

Flight Condition	Wt (Nmars)	cg* (m)
A. Gross Take Off	7502	9.359
B. 2 Pass, Zero Fuel	5002	9.538
C. 1 Pass, Full Fuel**	6902	9.509
D. 1 Pass, Zero Fuel**	4402	9.798
E. Operational Empty Weight	3802	10.418

* All center of gravities measured from canard aerodynamic center

** For "1 Passenger" flight conditions, passenger must be in front seat

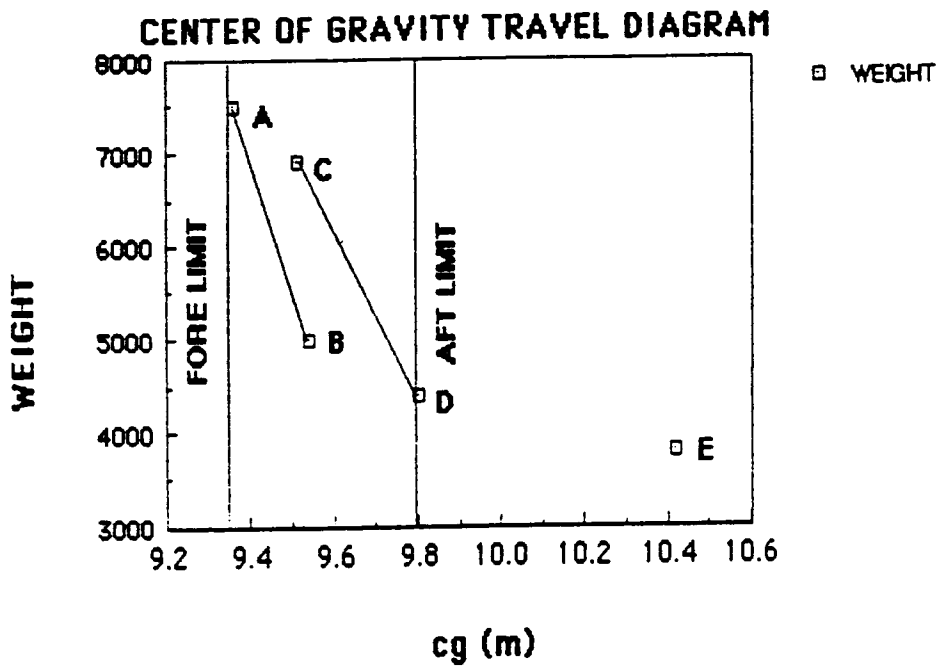

Fig 7-2

References

1. Roskam, Jan, Airplane Design V: Component Weight Estimation, Roskam Aviation and Engineering Corp., 1985.

AUXILIARY SYSTEMS

Controls for the auxiliary systems are explained in the corresponding technical areas.

COST ANALYSIS

PAT MORONEY

Utilizing the SAI Planetary Cost Model, a very rough estimation of the costs to design, engineer, test, and operate the Mars aircraft was determined. Shown below are the weights of various components of the aircraft entered under categories provided in the cost estimation software. The resulting costs are general amounts since the software was designed for spacecraft. A complexity factor of 1.0 was assumed throughout the analysis. The weights of the fuel and payload were not included in the analysis. Hard copies of the spreadsheets containing the totals follow this section.

CATEGORY	WT. (kg)	TOTAL COST (millions of $)
STRUCTURES	757	"
THERMAL	110	"
ATTITUDE CTRL	100	"
REACTION CONTROL	37	"
COMMUNICATIONS	5	"
ELECTRICAL POWER	18	"
PROPULSION	194	"
		$596.3

If 150 kg is removed from structures.....**$567.6**

If 50 kg is removed from propulsion.....**$586.2**

If 150 kg is removed from structures and
50 kg is removed from propulsion.....**$567.5**

As shown, the most likely solution to reducing costs would be to build the aircraft out of a lighter material instead of decreasing the weight of the

propulsion system.

MSFC PROTOFLIGHT COST MODEL

VEHICLE CONFIGURATION : PLANETARY COST MODEL
MARS AIRCRAFT PCM
APRIL 26,1988 ********* 08:46 PM

STANDARD ANALYSIS

	DDT&E	FHA	TOTAL
STRUCTURES	$46.7	$14.2	$60.9
THERMAL	$8.1	$15.6	$23.7
ATTITUDE CTRL & DETERMINATI	$81.1	$18.7	$99.8
REACTION CONTROL	$13.4	$3.2	$16.6
COMMUNICATIONS & DATA HANDL	$3.3	$0.4	$3.7
ELECTRICAL POWER	$5.8	$0.0	$5.9
PROPULSION (AKM)	$0.4	$0.0	$0.4
SUBTOTAL	$158.7	$52.2	$210.9
SYSTEM TEST HARDWARE	$99.9		$99.9
SYSTEM TEST OPS	$28.4		$28.4
SOFTWARE	$0.0		$0.0
GSE	$23.9		$23.9
SE&I	$35.5	$9.1	$44.6
PROG. MGT	$21.7	$6.0	$27.7
SUBTOTAL	$368.2	$67.3	$435.5
CONTINGENCY	$73.6	$13.5	$87.1
FEE	$44.2	$8.1	$52.3
PROGRAM SUPPORT	$9.7	$1.8	$11.5
TOTAL	$495.8	$90.6	$586.3

MSFC PROTOFLIGHT COST MODEL

VEHICLE CONFIGURATION : PLANETARY COST MODEL
MARS AIRCRAFT PCM
APRIL 26,1988 ********* 09:10 PM

STRUCTURES MINUS 150 KG

	DDT&E	FHA	TOTAL
STRUCTURES	$42.6	$12.2	$54.8
THERMAL	$8.1	$15.6	$23.7
ATTITUDE CTRL & DETERMINATI	$81.1	$18.7	$99.8
REACTION CONTROL	$13.4	$3.2	$16.6
COMMUNICATIONS & DATA HANDL	$3.3	$0.4	$3.7
ELECTRICAL POWER	$5.8	$0.0	$5.9
PROPULSION (AKM)	$0.4	$0.0	$0.4
SUBTOTAL	$154.6	$50.2	$204.8
SYSTEM TEST HARDWARE	$95.5		$95.5
SYSTEM TEST OPS	$27.8		$27.8
SOFTWARE	$0.0		$0.0
GSE	$23.5		$23.5
SE&I	$34.5	$8.8	$43.3
PROG. MGT	$21.1	$5.7	$26.8
SUBTOTAL	$356.9	$64.7	$421.6
CONTINGENCY	$71.4	$12.9	$84.3
FEE	$42.8	$7.8	$50.6
PROGRAM SUPPORT	$9.4	$1.7	$11.1
TOTAL	$480.5	$87.1	$567.6

MSFC PROTOFLIGHT COST MODEL

VEHICLE CONFIGURATION : PLANETARY COST MODEL
MARS AIRCRAFT PCM
APRIL 26,1988 ********* 09:15 PM

PROPULSION MINUS 50 KG

	DDT&E	FHA	TOTAL
STRUCTURES	$46.7	$14.2	$60.9
THERMAL	$8.1	$15.6	$23.7
ATTITUDE CTRL & DETERMINATI	$81.1	$18.7	$99.8
REACTION CONTROL	$13.4	$3.2	$16.6
COMMUNICATIONS & DATA HANDL	$3.3	$0.4	$3.7
ELECTRICAL POWER	$5.8	$0.0	$5.9
PROPULSION (AKM)	$0.3	$0.0	$0.3
SUBTOTAL	$158.7	$52.2	$210.9
SYSTEM TEST HARDWARE	$99.9		$99.9
SYSTEM TEST OPS	$28.4		$28.4
SOFTWARE	$0.0		$0.0
GSE	$23.9		$23.9
SE&I	$35.5	$9.1	$44.6
PROG. MGT	$21.7	$6.0	$27.7
SUBTOTAL	$368.1	$67.3	$435.4
CONTINGENCY	$73.6	$13.5	$87.1
FEE	$44.2	$8.1	$52.2
PROGRAM SUPPORT	$9.7	$1.8	$11.5
TOTAL	$495.7	$90.6	$586.2

MSFC PROTOFLIGHT COST MODEL

VEHICLE CONFIGURATION : PLANETARY COST MODEL
MARS AIRCRAFT PCM
APRIL 26,1988 ********* 09:13 PM

STRUCTURES MINUS 150 KG & PROPULSION MINUS 50 KG

	DDT&E	FHA	TOTAL
STRUCTURES	$42.6	$12.2	$54.8
THERMAL	$8.1	$15.6	$23.7
ATTITUDE CTRL & DETERMINATI	$81.1	$18.7	$99.8
REACTION CONTROL	$13.4	$3.2	$16.6
COMMUNICATIONS & DATA HANDL	$3.3	$0.4	$3.7
ELECTRICAL POWER	$5.8	$0.0	$5.9
PROPULSION (AKM)	$0.3	$0.0	$0.3
SUBTOTAL	$154.5	$50.2	$204.7
SYSTEM TEST HARDWARE	$95.5		$95.5
SYSTEM TEST OPS	$27.8		$27.8
SOFTWARE	$0.0		$0.0
GSE	$23.4		$23.4
SE&I	$34.5	$8.8	$43.3
PROG. MGT	$21.1	$5.7	$26.8
SUBTOTAL	$356.8	$64.7	$421.5
CONTINGENCY	$71.4	$12.9	$84.3
FEE	$42.8	$7.8	$50.6
PROGRAM SUPPORT	$9.4	$1.7	$11.1
TOTAL	$480.4	$87.1	$567.5

FUSELAGE CUTAWAY

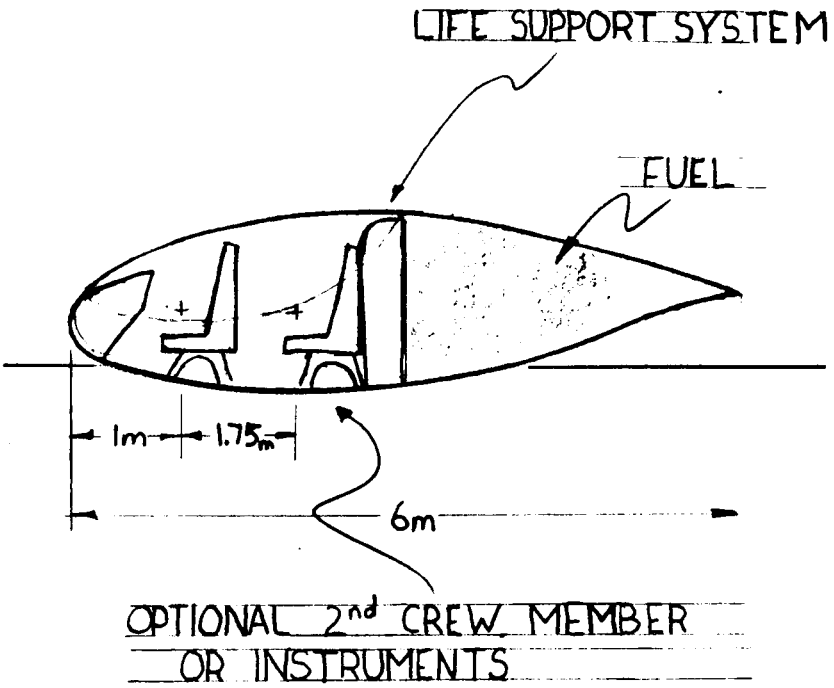

PACKAGING AND ASSEMBLY

MICHAEL ENRIGHT

As was stated in the previous structure section, the aircraft will be divided at 8 separate points which are shown and numbered in figure 5.10. The first three points will be along the main wing. Point 1, just as point 3, will divide the wing into two sections. Point 2 is where the two wings will meet and be attached to the fuselage. This will break the wing into four sections, A, B, C, and D. Sections A and D will have lengths of 8.75 meters, and sections B and C will have lengths of 10 meters. The engines will be easily disassembled and the propellors will also come off the engines. Points 4 and 5 act the same as points 1 and 3 , and point 5 acts as point 2. By this design the canard is also broken into four sections C, D, E, and F. Sections C and F will be 5.5 meters in length, and sections D and E will be 7 meters in length. The next part of the aircraft to disassemble is the pod, it will disattach from the fuselage. The fuselage will consist of two bars, which will be connected by cross stiffeners and have a Mylar fabric covering. These bars will break up at points 7 and 8. They will attach by screwing into each other and then locking into place, then the cross fasteners would be connected and the covering put back in place. The fuselage length will be approximately 13 meters, therefore there will be two pieces of 6.5 meter length, and two of 7 meter length (there is an extra have meter since the pipes will have to screw onto each other. These pipes or tubes will made out of Boron/Epoxy (as stated in structures) of which the dimensions are given in stability and control. We were given by the spacecraft

group a tube in which the materials will be stored the dimensions of the tube are a 4 meter diameter by a 14 meter length. This will be more than enough since our largest length is 10 meters and our largest diameter is a 2 meter chord for the wing.

Rescue Scenario: **Nick Jasper**

Due to the VTOL capabilities of this aircraft, it is ideally suited for rescue missions. In the event that it becomes necessary to perform a rescue, the mission will consist of a conventional take off, a vertical landing, a vertical take off, and finally, a conventional landing again. The mission will be performed with only one man aboard and in the second seat an expendable 600 N fuel tank will be strapped. Since hydrazine is much denser than a man in a pressure suit, it will fit in easily. This tank will attach directly into the main fuel supply via the refueling point in the back of the cockpit. It was for this purpose that the refueling point was placed there. Upon reaching the downed man the plane would have to execute a vertical landing, and then a vertical take off again. The flight out to the downed airman could consume a large amount of fuel, if the downed airman had been operating near the radius of operations when he went down. A sample fuel burn for a vertical landing at a weight of 6252 N (half a normal fuel load burned off) would require 62 N. To execute a vertical take off at a weight of 6790 N (6252 N minus the fuel burned landing plus the 600N man) would require approximately 190 N. Notice that while it takes only 252 N for the VTOL cycle, the plane originally took on 600N more fuel than it usually flys dual seat missions with. The difference of 348 N means that in the rescue scenario, it can fly well beyond its normal two man operating radius. It can exceed its normal range by almost 300 km. It is therefore an ideal rescue vehicle.

No. 4

THE SPIRIT OF CHAMPAIGN

AAE 241 AIRCRAFT DESIGN SPRING 1988

FINAL DESIGN REPORT OF THE MARTIAN AIRCRAFT 1995-2010

By

Michael Brody - Surface Operations
Timothy Ehmke - Structures
Kurt Heier - Aerodynamics
Daniel Ramshaw - Performance
Kentaro Sugiyama - Power and Propulsion
John Walter - Weights and Balances
Arlene Zander - Stability and Control

Submitted for Aeronautical and Astronautical Engineering 241
at the University of Illinois Urbana/Champaign
Professor K. Sivier
28 April 1988

PROJECT OVERVIEW

Dan Ramshaw

The task of designing a manned aircraft for use in the Martian atmosphere has proved to be a very challenging activity. However, the success of this project appears to have been reached. The main goal of the project is to be able to fly an aircraft safely over the surface of Mars while gathering geological data mainly from the use of photograpy and radar. Specifically, the aircraft must accomodate the equivalent of a 12000 N payload on Mars and be airborne for eight hours.

To accomplish this goal, the biggest obstacle to overcome in the preliminary design configuration had to be attacked directly. The extremely low density (1.42×10^{-2} kg//m^3 on Mars, or about 1 percent of Earth's) was a prime factor in sizing the aircraft to a rather large wingspan of 50 meters. Since keeping the aircraft's overall weight to a minimum was also a major concern, it naturally followed that a suitable layout for the craft would resemble a "flying wing". It was this design philosophy of low weight and large wingspan that lead to the configuration shown in detail in the Three View Drawing. A canard, which is nearly a "scaled down" version of the wing, was added for increased stability and control.

The intial analysis of the objectives and specifications of this project led to the use of solar energy as a means to propel the aircraft. The decrased gravity, colder temperatures, and thinner atmosphere of Mars as compared to Earth, combine to give the solar power effectiveness of the former's twice as great as the latter's. Also include "unlimited" endurance, constant weight, flexible choices in the types of cruise, the

ever-increasing improvements in the use of solar power, and one can see how this choice appears optimal. However, it was determined that the use of solar power would give better performance results if it was complimented with the addition of fuel cells. Due to the cells' low weight and high power output characteristics, the rate of climb of the aircraft, for instance, would increase about 50 percent. The combination of these power sources has been optimized with gross weight to yield the best performance possible, although a power sled must be used to get the craft airbourne due to a lack of large excess power.

Nonetheless, the design criteria for this aircraft ~~has~~ have been met and the goal of Martian air travel quite realistic. In this light, the details concerning the aspects involved in the Major Technical Areas will now be presented.

AAE 241
Spring 1988
DESIGN DATA SUMMARY

Gross Weight	: 6118 N	Maximum Take-off Power	: 26.4 kW
Wing Loading	: 25.18 N/m^2	Power Loading	: 231.7 N/kW
Maximum Fuel Weight	: 391.9 N	Fuel Fraction	: 64.1 %
Useful Load Fraction	: 0.256		

Geometry

Ref. Wing Area	= 243 m^2
AR	= 10
Λ_{LE}	= 19.87 deg.
λ	= 0.30
t / c	= 0.15

Performance

Cruise R_e	= 7.84 E4
Cruise h	= 1.5 km
Cruise M	= 0.327
Cruise V	= 81 m/s
Take-off Field Length	= 400 m
Landing Speed	= 45.3 m/s
Max. Landing Weight	= 6118 N
OEI Climb Gradient (%)	= 0.0
2nd Segment	= Not Applicable
Missed Approach	= - 0.71
Sea Level (R/C)	= 1.53 m/s

Stability and Control

Static Margin Range	= 0.10 to 0.30
Acceptable C.G. Range	= 3.93 to 5.653 m
Actual C.G. Range	= 3.97 to 5.647 m

Propulsion

Engine Description	: Sm-Cb DC Brushless Electric Motor
Number of Engines	= 2
$P_{o\ max}$ / Engine	= 15.35 kW
Weight / Engine	= 15 kg
c_p at Cruise	= 0.063
Prop. Diameter	= 6.9 m
No. of Blades	= 2
Blade Cruise R_e	= 7.128 E6

Aerodynamics

Airfoil		:	LA 203 A
High Lift System		:	Simple Trailing Edge Flaps
Cruise;	C_{Do}	=	0.0191
	e_o	=	0.75
	C_L	=	0.57
	$(L/D)_{max}$	=	17.3
Take-off;	C_L	=	0.71
	$C_{L\ max}$	=	1.32
Landing;	C_L	=	1.04
	$C_{L\ max}$	=	1.64

AAE 241
Spring 1988
Initial Sizing Data Summary
Group #4

Gross Weight: 6559 N mars

Wing Loading: 28.8 N/m

Fuel Weight: No Fuel

Useful Load Fraction: 0.16

Maximum Take Off Power: 26 kw

Power Loading: 188.1 N/kw

Fuel Fraction: 0 - not computed yet

Geometry

Ref. Wing Area = 243 m3

AR = 10

Propulsion

Engine/motor type: Brushless DC,with rare earth magets
No. of engines/motors: 2

P_o max/engine: 17.44 kw

C_p unknown at this time

Aerodyanamics

Cruise; $C_{Do} = 0.0161$
$e_o = 0.75$
$C_L = 0.516$
(L/D)max = 18.6

Take-off; C_L = Unknown at this time.
$C_L$max = Unknown at this time.

Landing; C_L = Unknown at this time.
$C_L$max = Unknown at this time.

Cruise Performance

h = 1500 m

V = 82 m/s

The Spirit of Champaign

Drawn by Kentaro Sugiyama 4/28/88 for AAE 241

1: 200 Scale

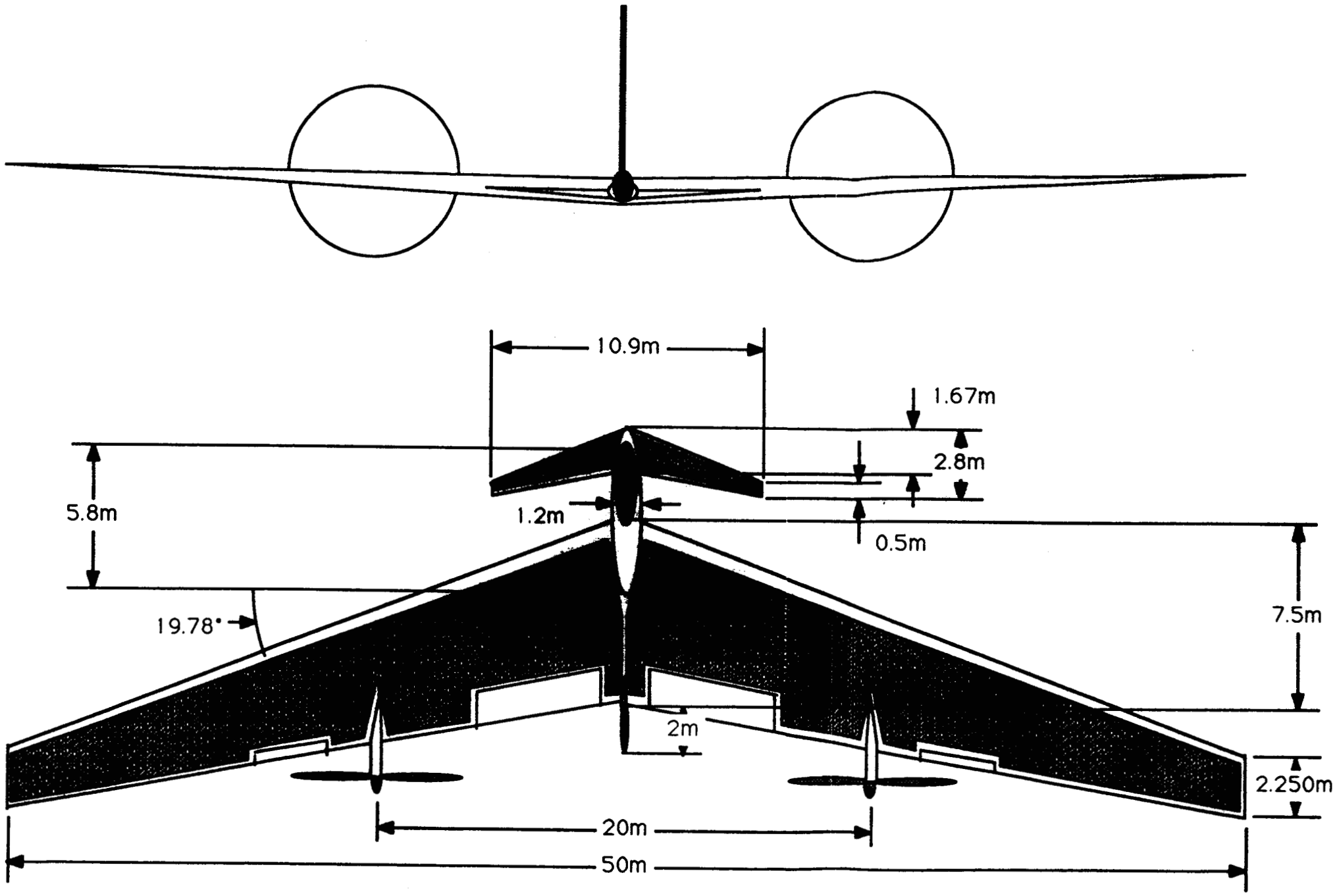

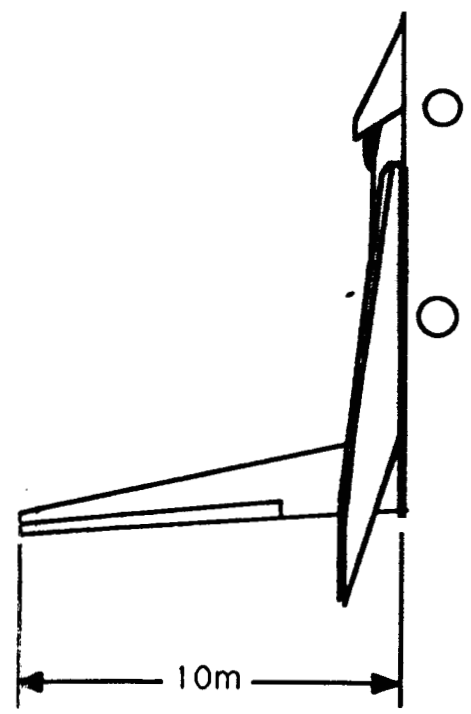

FOLDOUT FRAME

FOLDOUT FRAME

Aerodynamics

Kurt Heier

In this section aerodynamic data are presented, including sectional airfoil characteristics, parasite drag data, drag polars, and an analysis of the canard. The aircraft is essentially a flying wing with a canard attached by a short fuselage boom. In this analysis, some effects of the boom, such as body induced drag, will be neglected because of its small size (1.2 meters in diameter) relative to the rest of the aircraft.

Because of the low density of the Martian atmosphere (approximately one percent of Earth density), an airfoil had to be chosen which could operate at low Reynolds numbers, on the order of $2.5*10^5$. Recently, there has been a renewed interest in low Reynolds number airfoil research. Most of this research has been aimed at reducing some of the losses due to laminar separation and the resulting high pressure drag and loss of lift. Low Reynolds number conditions occur when there is a low air density, a low freestream velocity, or small airfoil chord lengths. Some examples of this flow can be seen in high altitude aircraft, low speed gliders, and small model aircraft. The actual Reynolds numbers in this Martian aircraft in cruise will range from $1.1*10^5$ at the wing root to $3.2*10^4$ at the wing tip. No airfoils could be found that could meet this requirement and also have a $c_{l_{max}}$ of 1.5 or greater. With this in mind, the LA203A airfoil was chosen (Ref. 1). This airfoil has a maximum thickness to chord ratio of 15.7%, a sectional pitching moment of -0.170, a $c_{l_{max}}$ of 1.7, and an angle of attack for zero lift of -6.00 degrees (see Fig. 1 and Fig. 2). Using reference 2, the data given for the aircraft were then used to determine and derive the necessary properties of the wing.

From initial sizing iterations, an aspect ratio of 10 was chosen, and from this a planform area of 243 square meters and a wingspan of 50 meters was calculated (see Table 1). This gives a wing loading of 25.2 Newtons per square meter. A taper ratio of 0.30 and a leading edge sweep angle of 19.78 degrees were chosen to meet stability requirements. One of the main problems involved with a tailless airplane is to achieve lift and moment equilibrium simultaneously. In this aircraft a canard is used in

neutralizing the large nose down moment produce by the wing. Another method of neutralizing this nose down moment is by using wing sweepback to place outboard control surfaces behind the center of gravity (cg), but the lever arms of the moments are very short compared to a conventional tail.

The canard also uses airfoil section LA203A. It has a planform area of 11.81 square meters and a span of 10.89 meters (see Table 1). The canard is a "scaled down" version of the wing, having the same wing properties, such as taper ratio and leading edge sweepback angle. In order to satisfy trimmed and stable flight the canard will operate at a higher lift coefficient than the wing. With this condition the canard will stall before the main wing and create a nose down pitching moment. This nose down moment will decrease the angle of attack and cause the canard to regain lift, thus keeping the wing from stalling. Because the aircraft is not designed to climb or descend at an angle of more than one or two degrees, stall will only occur if the aircraft's speed drops below stalling speed, the aircraft encounters vertical gusts, or if inadvertant control inputs occur.

The aircraft will cruise at a lift coefficient of 0.51 for the wing and 1.13 for the canard, producing a total lift coefficient of 0.567 for the aircraft. These coefficients correspond to a cruising speed of 81 meters per second. In order to meet these cruising requirements the wing will be mounted on the aircraft at an angle of attack of -1.10 degrees with respect to the horizontal while in cruise. The canard will be mounted on the aircraft at an angle of attack of 4.40 degrees, also with respect to the horizontal. In cruise, the fuselage will be at zero degrees angle of attack. All of these conditions are met for minimum trim requirements. Figure 3 shows a plot of canard lift coefficient vs. wing lift coefficient. It can be seen from this graph that the canard will stall at a C_{Lmax} of 1.72, and this corresponds to C_L of 1.23 for the wing. Figure 4 is a plot of C_{LTOT} vs. angle of attack of the aircraft (fuselage). C_{LTOT} is calculated from the equation $C_{LTOT} = C_{Lwing} + 0.05C_{Lcan}$, where 0.05 is a constant assuming the center of gravity is not moving while the aircraft is in flight. The aircraft will stall at a C_{Lmax} of 1.32, corresponding to an angle of attack of 6.80 degrees. As the aircraft approaches the stall angle, the drag coefficient increases drastically. Table 2 relates changes in sectional lift coefficient to the changes in the sectional drag coefficient, beginning with a lift coefficient of 1.50 up to 1.72 (also see Fig. 1 and Fig. 5). This data was supplied to the performance section and used in plotting power vs. velocity.

The drag decomposition breakdown can be seen in Table 3 (see also Fig. 5 for

sectional drag coefficient vs.. sectional lift coefficient). The parasite drag, C_{Do}, consists of five separate contributions: the wing, canard, fuselage, vertical tail, and miscellaneous drag (Ref. 3 and Ref. 4). Because the aircraft essentially has no main fuselage (a flying wing with a canard), the body induced drag can be considered negligible compared to the induced drag of the wing. Even when the aircraft is climbing or descending, the angle of attack is less than two degrees for the fuselage, so induced effects can be considered negligible. The drag polar for cruise, climb, and descent and the drag polar for the landing configuration can be seen in Figure 6. The drag polar for the takeoff configuration is the same as that of cruise because the aircraft is carted to takeoff speed without flaps deflected or landing gear lowered. Table 4 shows incremental parasite drag and lift coefficients for various flap deflections. The aircraft will land with a 40 degree flap deflection, resulting in an increase of C_{Do} from 0.0191 to 0.0670, including landing gear drag. Figure 4 shows the lift coefficient vs. angle of attack for the aircraft with flaps deflected 40 degrees. C_{Lmax} is increased from 1.32 to 1.64. This increase of 0.32 is two thirds of the incremental C_L increase of 0.474. This is a valid approximation. An Oswald's efficiency factor of 0.75 was assumed when calculating the drag polar for the aircraft in cruise, and a decrease in Oswald's efficiency factor of -0.15 was assumed when calculating the drag polar for landing.

Another assumption made in the design is that a laminar boundary layer is maintained and boundary layer transition should be prevented as long as no separation is present. For Reynolds numbers between 50,000 and 500,000, it is much easier to maintain a laminar boundary layer than to achieve a transition far enough forward (Ref. 5). When calculating parasite drag coeffecients for some of the surfaces, the skin friction coefficient was calculated assuming laminar flow over a flat plate.

The wing lift vs. span distribution can be seen in Figure 7. A Schrenk approximation was used, averaging the elliptical lift assumption with the linear lift of the tapered wing. These data were supplied to the structures section along with the quarter chord pitching moment of -0.170.

REFERENCES

1. Liebeck, R.H., and Comacho, P.P., Airfoil Design at Low Reynolds Number with Constrained Pitching Moment, Proceedings of the Conference on Low Reynolds Number Airfoil Aerodynamics, UNDAS-CP-77B123, June, 1985, p. 27-49.

2. McCormick, Barnes W., Aerodynamicss, Aeronautics, and Flight Mechanics, John Wiley and Sonss, 1979.

3. Hall, David W., Fortenbach, Charles D., Dimicell, Emanual V., and Parks, Robert W., A Preliminary Study of Solar Powered Aircraft and Associated Power Trains, NASA Contractor Report 3699, p. 96-103.

4. Roskam, Jan, Methods of Estimating Drag Polars of Subsonic Airplanes, University of Kansas, 1977.

5. Eppler, Richard, and Somers, Dan M., Airfoil Design for Reynolds Numbers Between 50,000 and 500,000 , Proceedings of the Conference on Low Reynolds Number Airfoil Aerodynamics, UNDAS-CP-77B123, June 1985, p. 2-3.

Properties	Wing	Canard
Aspect Ratio	10.00	10.00
Area (m^2)	243.00	11.81
Span (m)	50.00	10.87
Root Chord (m)	7.50	1.67
Tip Chord (m)	2.25	0.50
Taper Ratio	0.30	0.30
Leading Edge Sweep	19.78^0	19.78^0
Thickness to Chord-Max	14.73%	14.73%
Wing Tip Twist	0.0	0.0

Table1

Incremental c_l	Incremental c_d
0.05	0.0001
0.05	0.0001
0.05	0.0029
0.05	0.0070
0.02	0.0046

Table2

Component	C_{Do}	Percent
Wing	0.0139	72.8%
Canard	0.0014	7.3%
Fuselage	0.0012	6.3%
Vertical Tail	0.0023	12.0%
Miscellaneous	0.0003	1.6%
Total	0.0191	100.0%

Table 3

Flap Deflection Angle	Incremental C_{Do}	Incremental C_L
10 degrees	0.0053	0.197
15	0.0122	0.289
20	0.0184	0.338
25	0.0232	0.357
30	0.0309	0.400
35	0.0387	0.435
40	0.0474	0.474

Table 4

Sectional Lift Coefficient vs. AOA

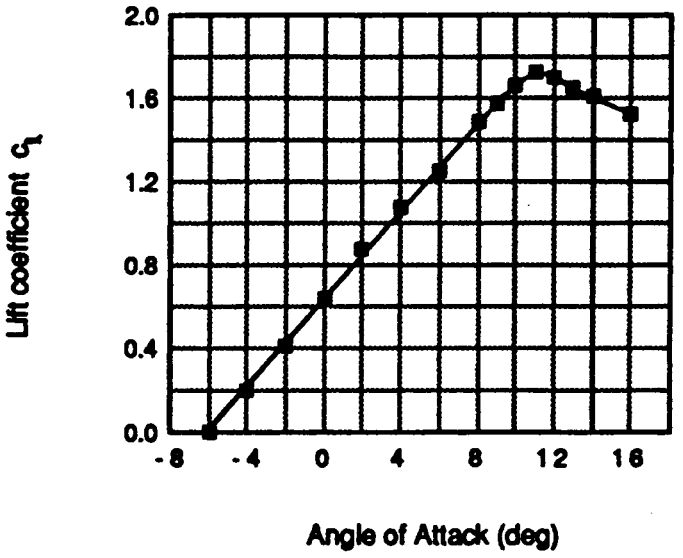

Figure 1

Pitching Moment (c/4) vs. Angle of Attack

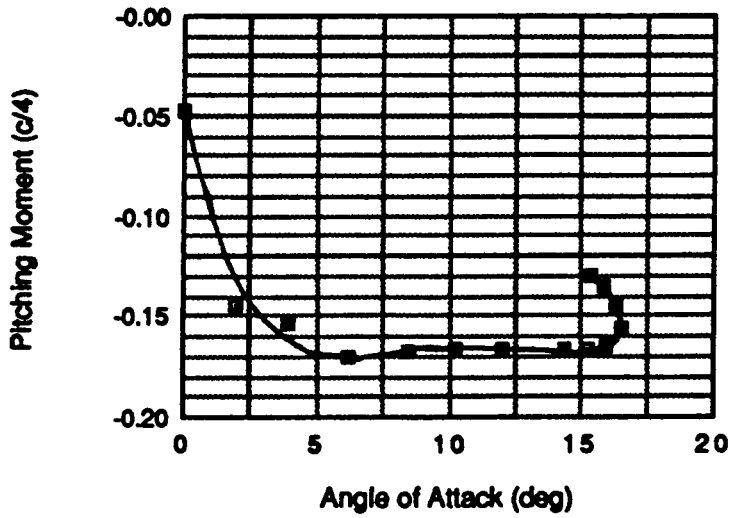

Figure 2

$C_{L_{canard}}$ vs. $C_{L_{wing}}$

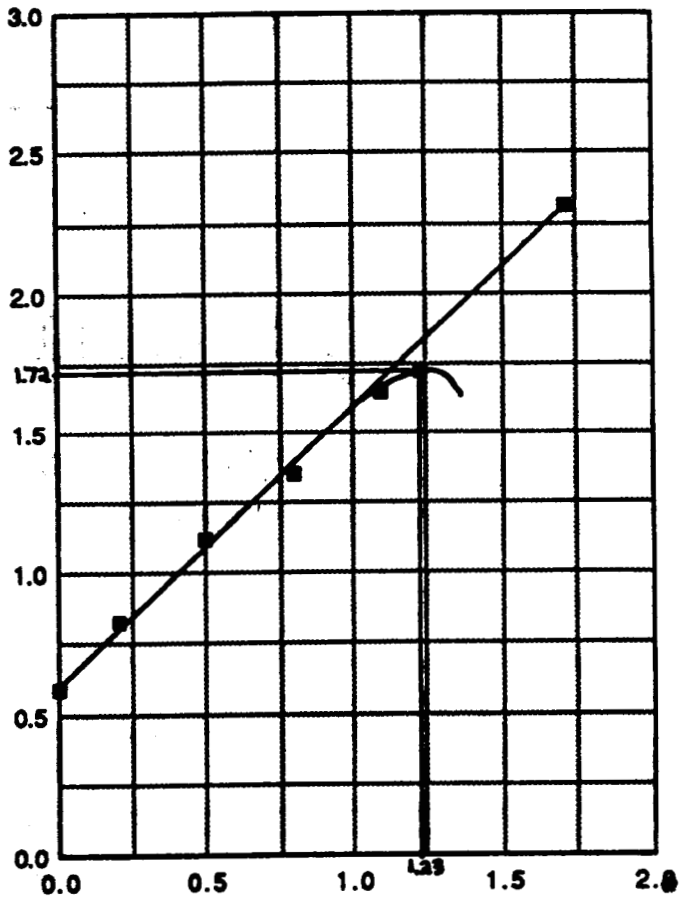

$C_{L_{canard}}$

$C_{L_{wing}}$

Figure 3

Lift Coefficient vs. Angle of Attack

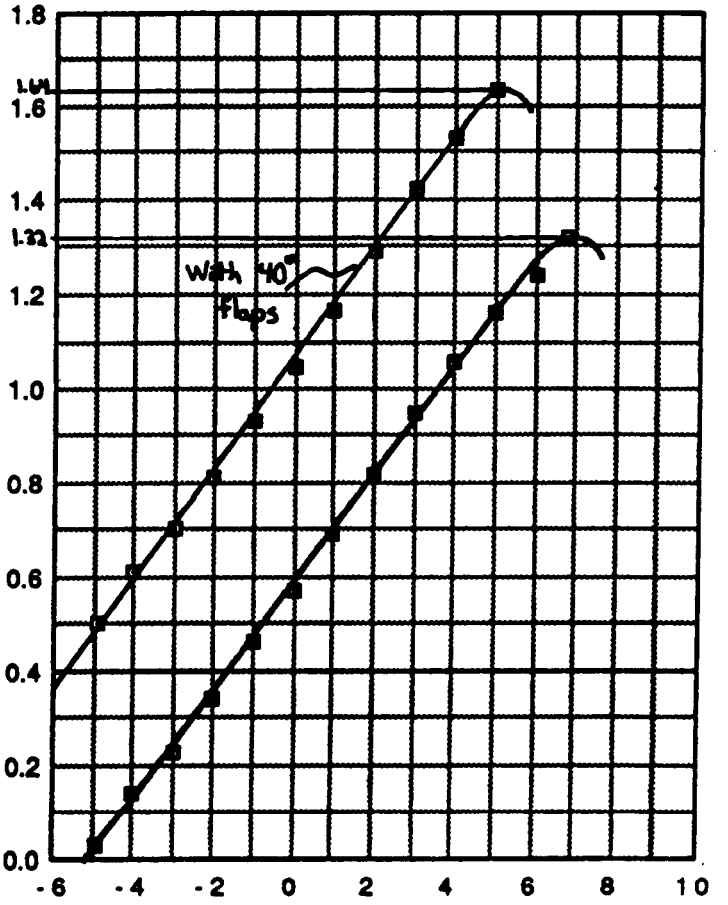

$C_{L\ TOT}$

Angle of Attack of Aircraft (deg)

Figure 4

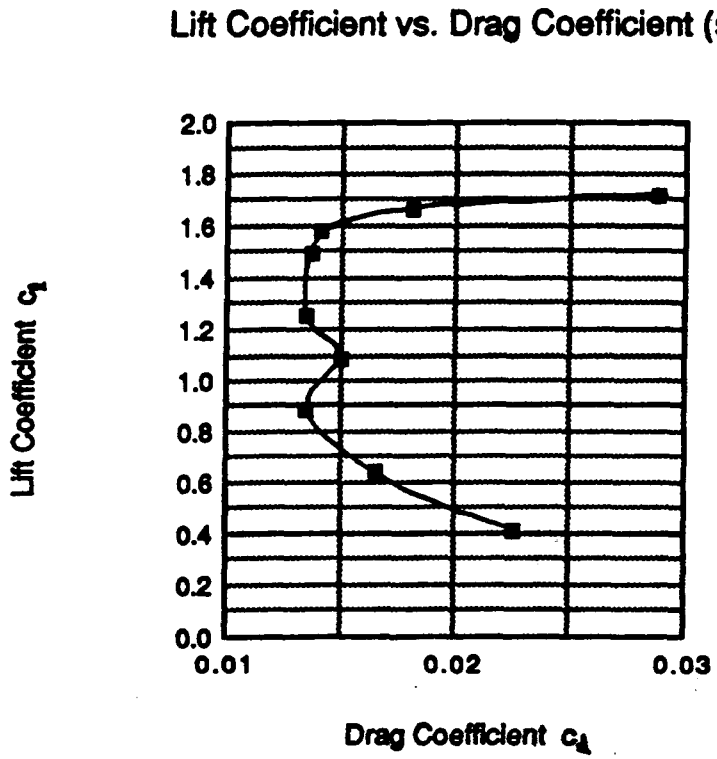

Figure 5

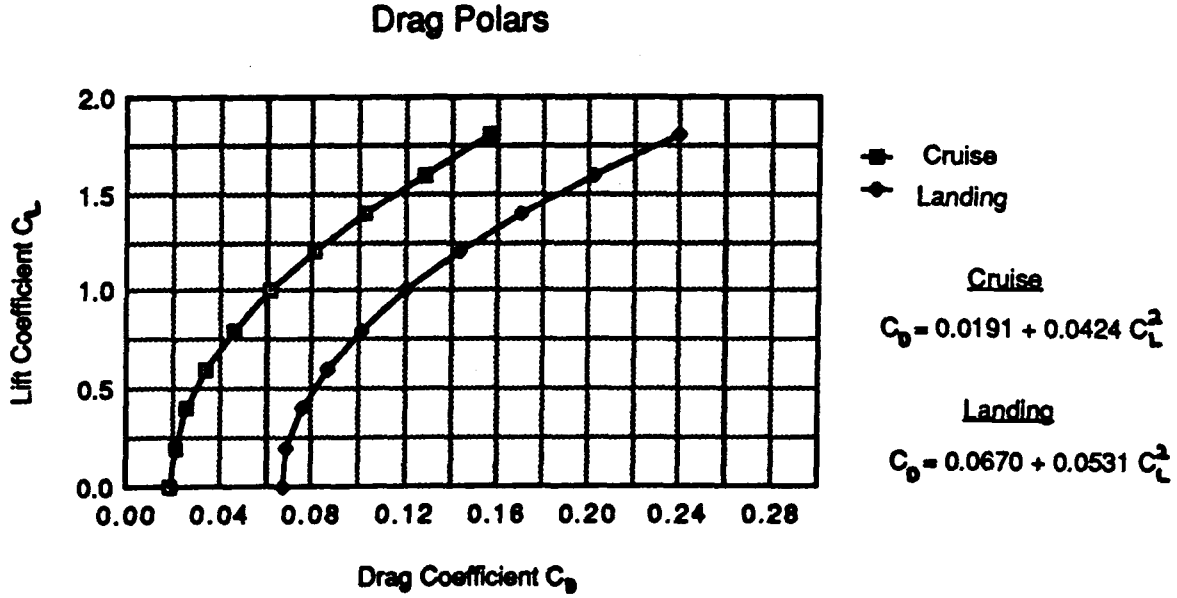

Figure 6

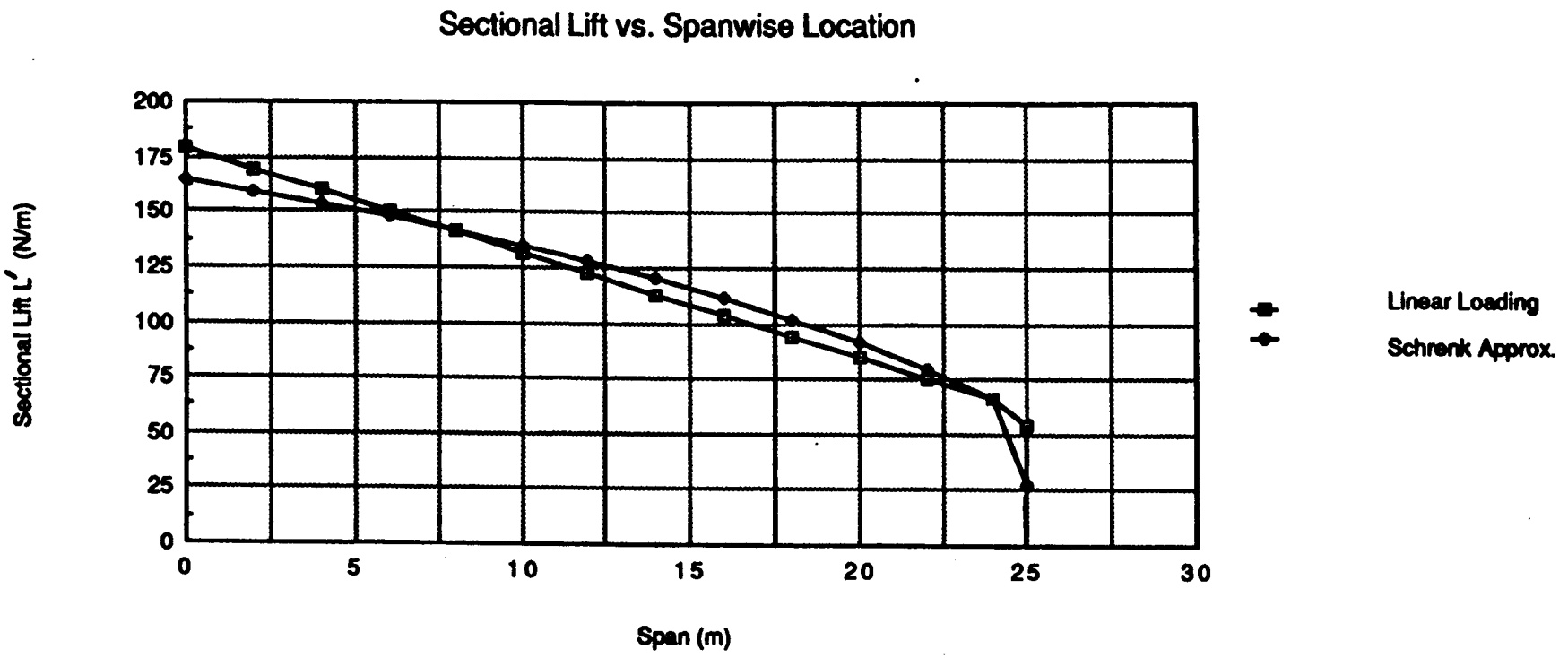
Sectional Lift vs. Spanwise Location
Sectional Lift L′ (N/m)
200
175
150
125
100
75
50
25
0
0
5
10
15
20
25
30
Span (m)
Linear Loading
Schrenk Approx.

Figure 7

PERFORMANCE

Dan Ramshaw

Data used in Performance calculations:

Does not agree with Aero.

$W = 6118\ N$ $e_0 = .90$

$S = 243\ m^2$ $C_{Do} = .018$

$AR = 10$ $P_{available} = 26.5\ kW$

$h_{cruise} = 1500\ m$

The analysis of the performance of the Mars aircraft reveals satisfactory results. The original solar design was complimented with the addition of fuel cells to provide the necessary power for adequate performance. Specifically, the time to climb to the cruise altitude of 1500 m was reduced from 26 munutes to 17 minutes. However, the overall weight of the aircraft did not change significantly, but it was considered in the iteration process of maximizing performance characteristics with trade-offs between engine size and gross weight. Due to this, the aircraft will be able to meet its given requirements with a resonable amount of ease and safety considerations. The results of the evaluation of the performance characteristics are as follows:

Climb

Again, the rate of climb has been increased significantly mainly due to the addition of fuel cells. This results in an increase of power available (26.5 kW) while holding the gross weight almost constant. The consequence of this can be seen in Graphs 1 and 2 where the power available and power required are plotted against velocity at sea level and at 750 m. The latter is shown because the rate of climb is linearly and inversely proportional to altitude, so the climb rate at 750 m will be the average climb rate over the entire range from sea level to the design cruise altitude of 1500 m.

For safety reasons of avoiding abstacles, the climb rate is chosen to be the maximum possible climb rate of 1.5 m/s. The time, then, for the aircraft to climb to cruise altitude is 17 minutes. This climb rate is achieved by flying at 51 m/s which will result in a ground distance travel of 52.4 km. The climb speed's "cushion" above the stall speed of 44 m/s is not large, but nonetheless, comfortable if the plane's speed is monitored well. Since the endurance of 8 hours was set as an input parameter to the selection of engine size, weight etc., the amount of fuel used will be the fraction of the amount of time required to climb, to the total amount of flying time available, or 3.5 percent.

Cruise

The power available and power required as a function of velocity can be seen in Graph 3. This graph corresponds to an altitude of 1500 m as specified by the design criteria. Since the sun is obviously the energy source for the solar

portion of the propulsion system, and the by product of the fuel cells (i. e. water) is collected, the weight of the plane will not vary in flight. This allows the type of cruise to be chosen as both constant altitude and constant velocity. Simplicity and ease in the gathering of information from the surface of Mars are two main benefits resulting from this choice of cruise type. Instruments used to take data from the surface do not have to be adjusted nearly as much if the altitude and velocity remain constant.

Since the purpose of the missions of the Mars flights is to explore the surface, it would seem appropriate to cover as much distance as possible. This is achieved by cruising at the maximum speed allowed by the propulsion limitations of 81 m/s. It should be noted that climb is impossible at this speed but this will not prove to be a problem for safety since the plane is cruising nearly a mile above sea level. The time allowed for cruise conditions will be the remaining time from the given 8 hours endurance after the climb and the descent times have been allotted. Consequently, the cruise will cover about 2000 km (1200 miles) and take 6 hours 45 minutes. A design safety factor of having 10 percent fuel remaining has been built in to this analysis and has cut the cruise time and range slightly. Therefore, the cruise condition will use 84.2 percent of the total fuel available.

Descent

Assuming a cut-back in power of 85 percent and a flying speed of 51 m/s, the rate of descent will be 2.3 m/s. The speed of 51 m/s is chosen because if, by chance, one of the engines should fail, this is the speed which will permit the

aircraft to descend at the lowest rate. No precious time will be lost adjusting the craft's speed to the slowest rate of descent of .71 m/s. This one major flaw in the aircraft's performance is illustrated in Graph 4 showing power vs. velocity with One Engine Inoperative. However, assuming a normal descent, the aircraft will reach the surface of Mars from cruising altitude in 11 minutes and cover a range of 33 km. Thus, descent will use 2.3 percent of the fuel available.

Level Flight Envelope

In order to insure that the aircraft can cruise at 1500 m, the LFE must be constructed. This is shown as Graph 5. From this, it is evident that the cruise altitude is clearly possible with the maximum altitude being 9750 m.

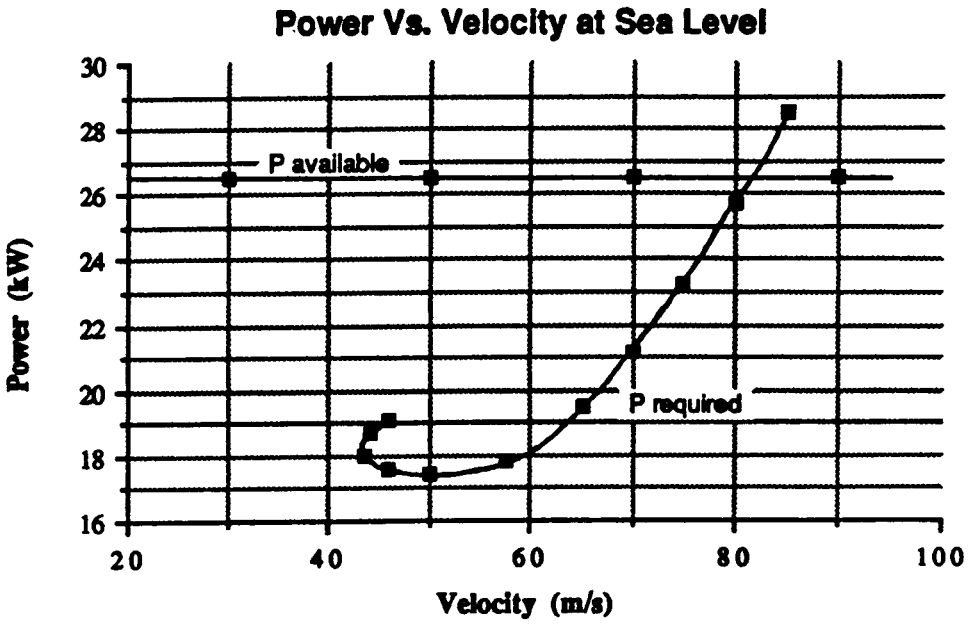

GRAPH 1

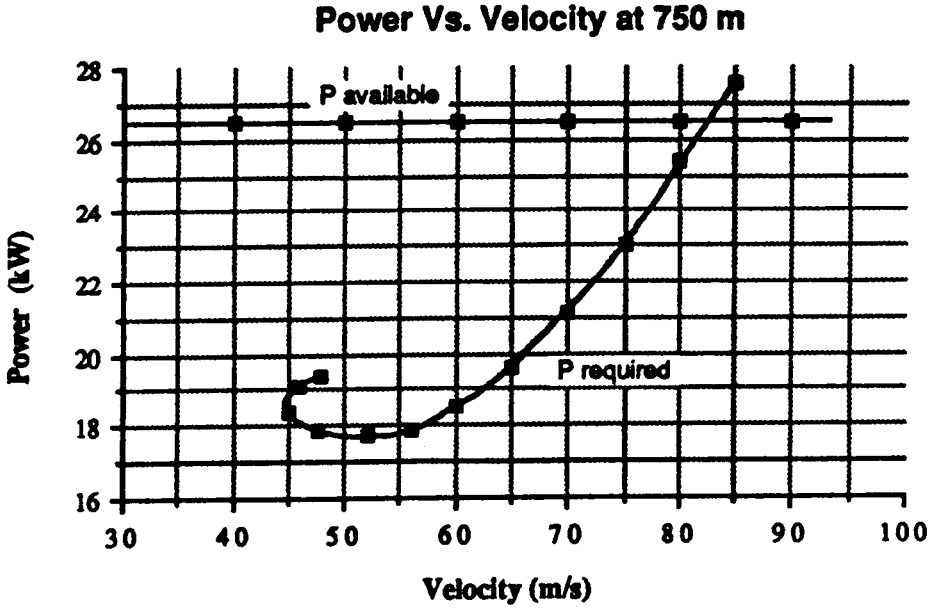

GRAPH 2

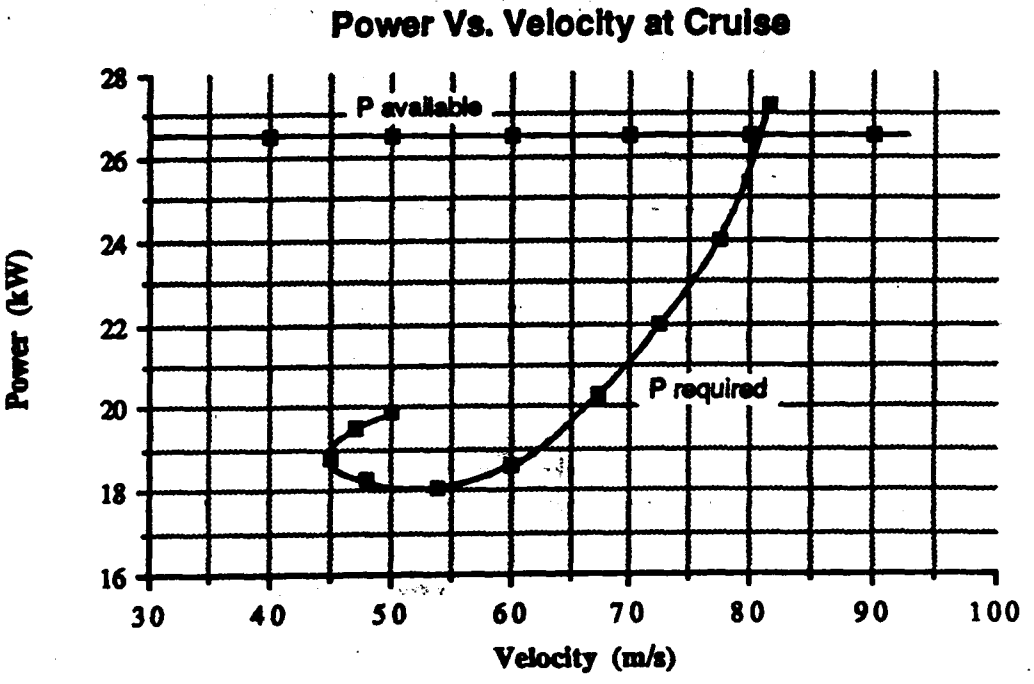

GRAPH 3

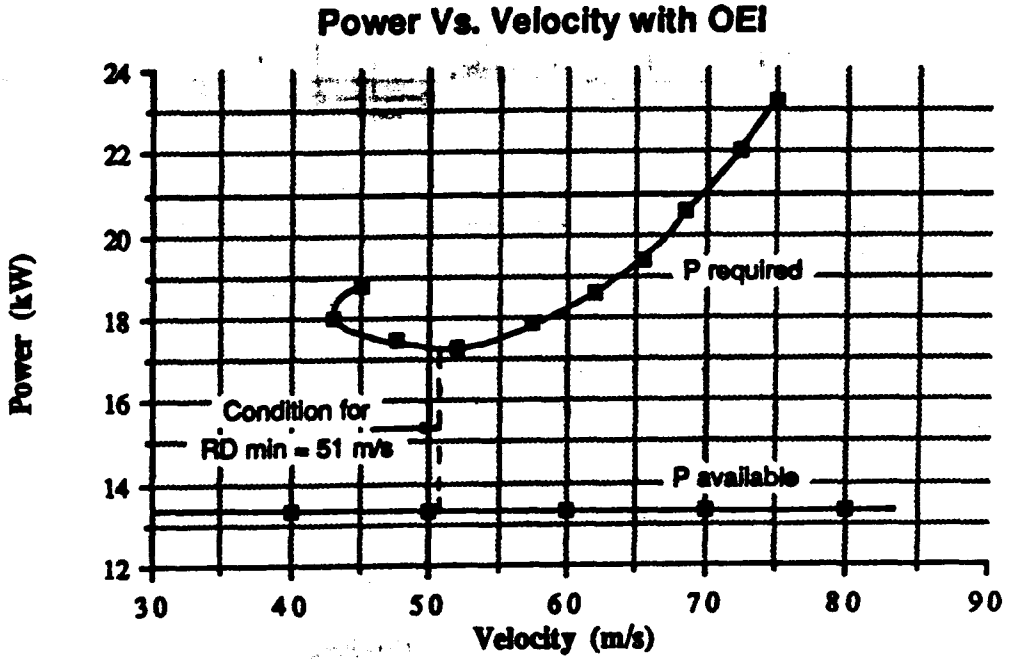

GRAPH 4

Level Flight Envelope

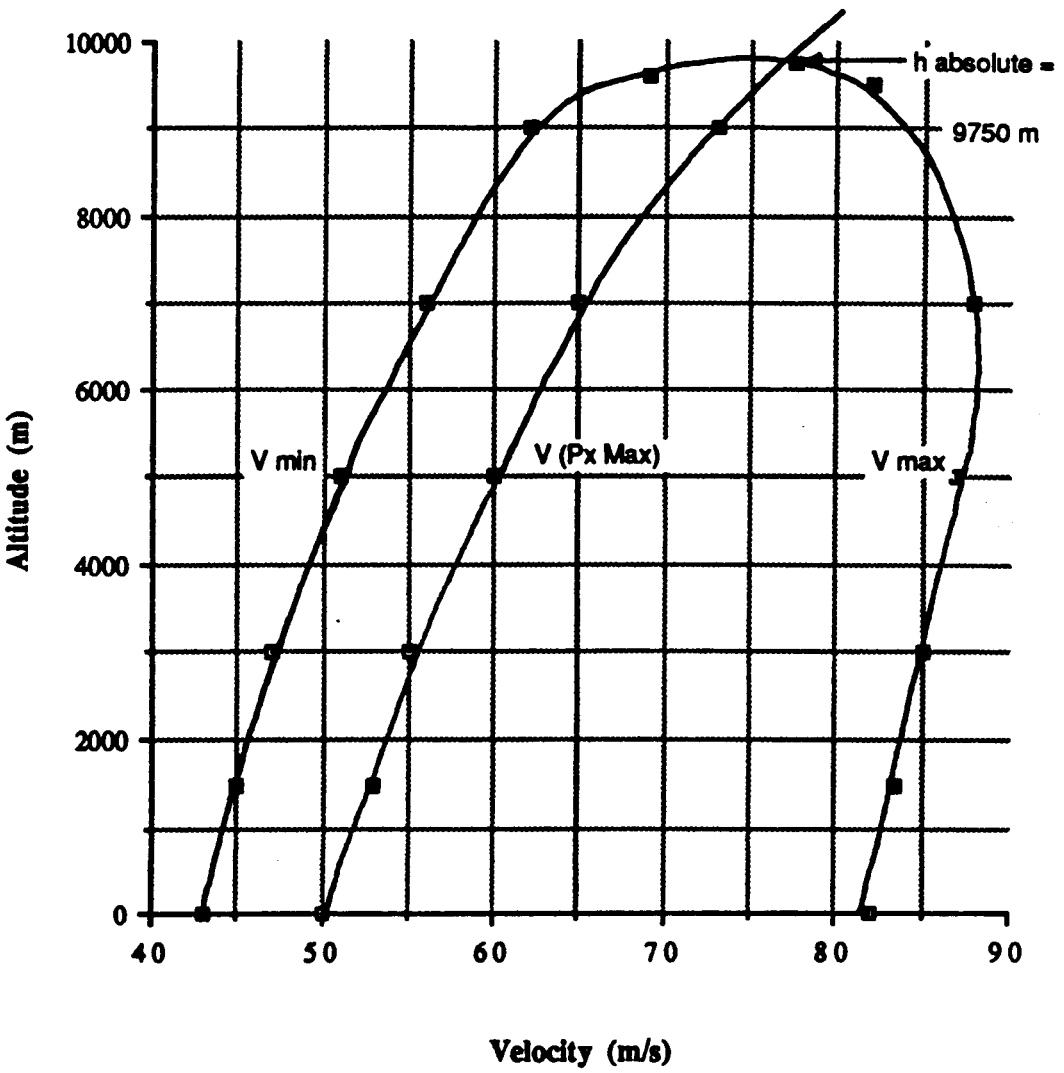

GRAPH 5

POWER AND PROPULSION

Kentaro Sugiyama

The final configuration of the power train system has been determined for the Martian aircraft. The preliminary power train system design relied completely upon solar power for propulsion. The final system design provides roughly 25 kw of power from solar photovoltaic arrays while 42.4 kw-hrs (5.3 kw for 8 hours) of supplemental power is provided by regenerative fuel cells and associated reactant tanks. In short, the system at design conditions will produce approximately 26.4 kw of power available (P_{av}) after aerodynamic losses (due to propeller efficiency). Also, since the power output of the solar arrays is totally dependent upon the solar flux intensity and operating temperature, the P_{av} may flucuate according to attitude, atmospheric, and seasonal conditions.

In selecting a candidate power train configuration, several factors were considered: simplicity, technological feasibility, and technological outlook. Two power train configurations were examined with these factors in mind: closed combustion and solar power (a more detailed discussion of other configurations appear in (1), p. 48). It was immediately apparent that solar power was the configuration of choice due primary on technological outlook. It happened to also be simple (as far as photovoltaic collectors are concerned) and technologically feasible, with only some limitations. It is the author's opinion that solar is the power source of the future, and that it still has much untapped potential. Besides, one cannot ignore the natural association of space exploration with solar technology. With solar power, two collection technologies were considered: Solar Thermal and Solar Photovoltaic (PV).

The selection of solar PV arrays as a basis for the power system is clearly obvious. This is due to the prohibitive weight of the solar thermal system, as well as aerodynamic drag created by the awkward placement of the collecters. Complicated tracking and collection subsystems further condemn solar thermal technologies for the time being. (1) Despite the fact that solar PV efficiencies are somewhat lower than solar thermal, technological advances have allowed Silicon (Si) PV cells to increase from base efficiencies of around 14% in the late 70's to 20% in the mid 80's. (2)(3)(4)(5)

The barriers limiting Si PV efficiencies have been identified and suggestions have been made to improve the quality of Si, where the projected efficiencies could be as high as 25% or more depending on technological advancement. (2)(3)(4)(5) Clearly, at the present rate, it would be justifiable to predict that 25% efficient Si PV cells will be available around the turn of the century, which is nearly within the same time frame of the Martian aircraft.

Gallium Arsenide (GaAs) PV cells presently have higher base efficiencies (20-25%) than Si, but tend to be heavier than Si per unit area and are prohibitively expensive. (6) Still, they remain a reasonable contender for PV array material if costs go down sometime in the future. For this report though, Si PV cells will be used assuming projected efficiencies.

Electrical motor designs were looked over very briefly, resulting from the choice of solar power. After some examination, it has been decided that two Rare-Earth Samarium-Cobalt Permanent Magnent DC Brushless electric motors would be employed. (1) Such motors have been projected to produce 22.4 kw of maximum continous power, and 11.23 kw normal. They have been scaled from present designs to have a mass of 18 kg each and shaft speed of 10000 RPM. (1) It is assumed that by the turn of the century, such motors will be lighter and more powerful. For this study, a motor mass of 15 kg and gearbox mass of 7.5 kg.

In order to determine power train sizing requirements, a preliminary power and weight optimization study was conducted using a Macintosh SE computer and Microsoft Excel spreadsheet software. The study was conducted with Power and Propulsion interacting exclusively with Weights and Balances and supplemental consultation from Performance. Three spreadsheets were programmed to calculate the following: Power train mass as a function of power desired by Performance, as well as performance characteristics as a function of weight; Weights and associated Center of Gravity values as a function of power train mass; and a propeller designer as a function of performance characteristics.

All three were integrated in order to compute optimum weight, as well as regenerative fuel cell (RFC) sizing under specified conditions. With this calculated information, a propeller was selected from the 40+ designs created by the spreadsheet, with careful attention given to diameter and efficiency. The interested reader will find the detailed equations, and sample spreadsheet outputs in the appendix following this section. Spreadsheet values may be slightly off from reported values.

To begin the study, the desired P_{av} was input as the primary variable, along with other secondary variables, into the power train mass spreadsheet. The power produced by the solar PV arrays was immediately calculated as a function primarily of solar flux intensity, which was held constant. Thus, since P_{av} and endurance were given quantities, the remaining power (in kw-hrs) needed to be generated by the RFCs (P_{RFC}) was found. The masses of the RFC, reactants, and their respective tanks could then be calculated.

The RFC mass was calculated by dividing the P_{RFC} by the specific power rating of the RFC. The reactant masses then were calculated by dividing the kw-hrs required (P_{RFC} times endurance) by the specific energy rating of the RFC. The result represented the total mass of the product. Working backwards, using basic chemistry, the respective masses of the reactants were calculated. Spherical reactant tank sizing using Kevlar with a safety factor of 2 and 15% attachments was considered and

calculated.

Calculating the mass of the PV array was simply the area of the array times the array density. After considering miscellaneous items and electric motor masses, the total power train mass was calaculated. This power train mass was input into the Weights and Balances spreadsheet to compute the optimum airplane weight. The weight was immediately input into the Power required (P_{reqd}) equation supplied by Performance. The resulting P_{reqd} was then immediately input into the propeller design spreadsheet which generated over 40 different 'sets' of propeller specifications. (Data from (7)) A suitable propeller was selected from this so called 'shopping list' with regard to best compromise between efficiency, diameter, and shaft speed. The selected propeller specifications indicated the shaft power needed, which was then input back into the power train mass spreadsheet. It is noted that the propeller selection process was the only portion of the study that required human judgement.

This iterative process continued until a consistent propeller design emerged. No appreciable convergence in optimum weight occurred, but the relative behavior of the model under different given conditions (e.g. solar flux, temperature, velocity, altitude, etc.) was mentally noted. Finally, a weight was decided upon which would reasonably satisfy Performance, Power and Propulsion, and Weights and Balances (as to C.G. location). At this point in the study, the P_{av} value was fixed as well as the mass of the RFC and reactants.

The three spreadsheets were then combined, modified, and finally truncated into a single spreadsheet where the weight and propeller diameter were held constant. Fine adjustments and corrections were made resulting in the Power and Propulsion's final version of its respective spreadsheet, thereby concluding the optimization study.

As a result of the optimization study, a P_{av} of 26.4 kw was agreed upon consulting Performance. In order to generate that amount of power, approximately 31.2 kw of shaft power must be generated. Of this requirement, 5.3 kw will be generated for 8 hours by RFCs (42.4 kw-hrs). The remaining 25.9 kw will be easily generated by the PV arrays if

the following conditions are met: that solar flux intensity is 0.450 kw/m^2; that operating temperature at a given altitude is 214 °K; and that Si PV array efficiency is 25% with thermal coefficient of 0.05 $\partial\%/\partial°K$ at 298 °K (Si PV efficiency goes up as the temperature goes down).

It is clear at this point to emphasize that shaft power, and thus P_{av} will be directly affected by intensity and temperature, assuming technology has provided us with 25% efficiency by the time frame of the Martian aircraft. Figure 1 gives the P_{av} as a function of intensity, at three different operating temperatures. For this report, it is assumed that temperature will vary from 200 to 228 °K, with 214 °K being the average value. As it can be seen, small variations in temperature make only a small contributions to P_{av}. Taken in this light, examining P_{av} as a function of altitude assuming a 2 °K/km temperature lapse rate (4) would bear insignificant results.

Because of the unpredictable nature of intensity and temperature, the actual power available may fluctuate along a range of values during the course of the actual flight. It will also surely vary according to the latitude, the time of day, and the season. Since very little useful data was found pertaining to this facet, such affects on P_{av} have been dismissed. However, a rough estimate of "good" flying conditions as far as Power and Propulsion is concerned would be ideally around noontime, at perihelion, during the spring or summer season (when dust storms occur less frequently (4)). By inspection of the Power Required vs. Velocity graph in Performance (Specific Reference needed), a generous amount of excess power is available for operating avionics, payloads, controllers, or other devices. However, this will be at some sacrifice to climb performance and/or cruising speed.

For most practical purposes, it is assumed that no more than 0.5 to 1 kw will be needed on a continual basis. This is partly due to the decision by Weights and Balances to actuate a majority of control surfaces with wires and pulleys in order to save weight. In the worst case up to roughly 8 kw of power can be available (again varying with intensity) to meet any contigency, but at almost total degradation of all performance specifications. In this manner, payloads with higher power requirements

may be flown infrequently, waiting for suitable days where sufficient intensity and cold weather are available. Another solution may be to 'pulse' the available power to all the devices that need it. This would be in a sense distributing the power, but such a configuration is beyond the scope of this report.

As far as fuel consumption is concerned, the one significant advantage of using solar PV arrays as a foundation of the power train is constant weight. The supplemental power delivered by the RFCs will also have constant weight. The water produced by the reaction of H_2 and O_2 was to be dumped into the athmosphere to reduce weight, but it has been decided that the water will be stored on board in a closed cycle system. This will benefit Weights and Balances with constant C.G. and Performance with constant P_{reqd} (no weight loss) resulting in easier calculations. Also, such water can be used for drinking, cooling, or refueling purposes. The closed cycle system was designed to pump the water to an electrolyzer where water would be broken down, using surplus P_{av}, into its respective reactants for future use. This would, depending on electrolyzer efficiency and production rate, effectively increase the range and endurance of the plane (not counting the endurance of the pilots). It was decided though, that the benefits of the electrolyzer may not prove to be significant with regard to additional weight. Refueling therefore, will be accomplished with an external land based electrolyzer. All that is required is for the aircraft to "sit in the sun" for a day or two to break down the onboard water into useful fuel.

The regenerative RFCs have a specific energy rating of 0.4 kw-hrs/kg using the $2H_2 + O_2 = 2H_2O$ reaction at 66% efficiency. (8) This is the highest energy density available. The production of 42.4 kw-hrs, using H_2 and O_2 as reactants in the RFCs, will result in 106 kg of water product. This means constituent masses of 11.8 kg H_2 and 94.2 kg O_2, and tank masses of 5.4 and 43 kg respectively. Water will take up 10.6 m^3, while the reactants occupy 0.168 and 0.083 m^3 respectively. The RFCs also have a specific power rating of 0.217 kw/kg resulting in a RFC mass of 24.4 kg. (9) Miscellaneous masses are listed in the sample output of the POWER-WEIGHTS FINAL spreadsheet in the

appendix.

As stated before, the final propeller design was selected as the best compromise between efficiency, diameter, and shaft speed, from a list of propeller designs generated by the optimization study (a sample page is in the appendix). It was decided in the preliminary design report that two engines with counter-rotating propellers would be used. It was desired to keep the diameter within an acceptable range of values, for the study showed that single engine propeller designs had very large diameters. The final physical parameters for the propeller are as follows:

Diameter of 6.9 m
Pitch Blade Angle of 25°
Advance Ratio of 0.9

Performance Parameters are as follows:

Efficiency of 84%
Shaft Power Requirement of 15.52 kw/engine at cruise
Shaft Speed of 782.6 RPM at cruise
C_p of 6.30×10^{-5} at cruise
C_p of 1.44×10^{-4} at climb
Static Thrust of 1177 N

A higher efficiency of 86% could be used, but only at a significant increase in diameter.

Finally, the engine inoperative drag of the propeller design is roughly 45.6 N/engine or 91.2 N total, assuming that pitch blade angle is 17.5° at 70% blade span, that the blade planform is 1.1218 m^2 per blade, and velocity at 81 m/s.

In conclusion, the final power train system will consist of a mixture of two power

sources. Approximately 25 kw of power will be provided by the solar photovoltaic arrays covering 85% of the wing, while the remaining 5.2 kw will be sustained for 8 hours by a regenerative fuel cell system with associated reactant tanks. As promised by Power and Propulsion to Performance, 26.4 kw for 8 hours endurance will be available to for consumption in the manner Performance sees fit. This availability is subject to flucuations due to variations of temperature, solar flux intensity, altitude, latitude, time of day, time of year, weather, and other imponderables, not to mention unscheduled miscellaneous power consumption. What Performance gets in return for lack of predictability is constant weight, and therfore consistant range, which means no variation of C.G. locations for Weights and Balances. Also, solar power is free. Initial cost will probably give better returns than other comparable systems, plus the possibility for better performance always exists.

APPENDIX

Power available and Power produced by PV array equations for P_{RFC} sizing:

1) $P_{av} = (P_{PV}+P_{RFC})Eff_{prop}$

2) $P_{PV} = Int(S_{wing}+S_{canrd})A\%(Eff_{PV}+(298-T)\partial\%/\partial°K)Eff_{Pcnd}$

where: Eff_{prop} = Propeller efficiency

Int = Solar Flux intensity (kw/m^2)

S_{wing} = Area of wing (m^2)

S_{canrd} = Area of canard (m^2)

A% = Percentage of wing and canard area used for PV array

Eff_{PV} = PV array efficiency at 25°C Air Mass Zero

T = Absolute Temperature (°K)

$\partial\%/\partial°K$ = Thermal Coefficent of efficiency

Eff_{Pcnd} = Power conditioner efficiency

Reactant Tank Sizing equation for Kevlar with safety factor 2 and 15% attachments (1):

$$Mass_{tank} = Mass_{reactant}(2.13E\text{-}03)\ T$$

Equation as supplied by Performance for Power required:

$$P_{reqd}=(0.5\ rho\ V\text{^}3\ S_{wing}\ C_{Do} + 2W\text{^}2/(S_{wing}\ \pi\ e_o\ AR\ rho\ V))/1000$$

where: rho = Air density at specified altitude (kg/m^3)
V = Velocity (m/s) at climb or cruise
C_{Do} = Aircraft class
W = Aircraft total weight
e_o = Oswald's efficiency factor
AR = Wing aspect ratio

Propeller Sizing Equations as used for Propeller Design Spreadsheet:

$$P_{reqd} = P_{shaft}\ (Eff_{prop})$$
$$n = ((V\text{^}5\ rho)/(C_s\text{^}5\ P_{reqd}))\text{^}0.5$$
$$D = V/(n\ J)$$
$$N = 60n$$

where: n = shaft revolutions per second
C_s = Speed Power Coefficient
J = Advance Ratio
N = shaft revolutions per minute

REFERENCES:

(1) Hall, David W., Charles D. Fortenbach, Emanual V. Dimicell, and Robert W. Parks, A Preliminary Study of Solar Powered Aircraft and Associated Power Trains. NASA Contracter Report 3699, Lockheed Missiles and Space Company, Inc. (Sunnyvale, CA: 1985).

(2) Sah, C.T. "High Efficiency Crystalline Silicon Solar Cells." Solar Cells, Vol. 17 (1986), pp. 1-27.

(4) Iles, P.A. and F. F. Ho, "High Efficiency Silicon Solar Cells." Solar Cells, Vol. 17 (1986), pp. 65-73.

(3) Wolf, M. "The Influence of Heavy Doping Effects on Silicon Solar Cell Performance." Solar Cells, Vol. 17 (1986), pp. 53-63.

(5) Swanson, R. M. "Point Contact Solar Cells: Modeling and Experiment." Solar Cells, Vol. 17 (1986), pp. 85-118.

(6) Fisk, Mariam, and William Anderson. Introduction to Solar Technology. Addison-Wesly Publishing, Co., Reading MA, 1982. (Acquired from 241 notes of Daniel Dorney)

(7) "Design chart for propeller 5858-9, Clark-Y section, two blades (NACA Tech. Rept. 640)"

(8) Smith, Robert E. and George S. West, *Compilers* : Space and Planetary

Environment Criteria Guidelines for Use in Space Vehicle Development, 1982 Revision (Volume 1). NASA Technical Memorandum 82478, Marshall Space Flight Center, (Huntsville, AL:1983).

[9] Telehone conversation with NASA Marshall Space Flight Center. Huntsville, AL, Bob Giudici (Power System Design Engineer), April 8 and 20, 1988.

[10] Space Electrochemical Research and Technology (SERT). NASA Conference Publication 2484, NASA Lewis Research Center, (Cleviand, OH: April, 1987).

Other Supplemental References:

Manned Mars/Lunar Studies: Mid-Term Reviews, Marshall Space Flight Center, (Huntsville, AL: December 1987).

Clarke, Victor C., Abraham Kerem, and Richard Lewis: "A Mars Airplane?". Aeronautics and Astronautics, AIAA, January 1979, pp. 42-54.

French, J.R. The Mars Airplane. Jet Propulsion Laboratory, Pasedena, CA.

Augenstein, B.W. The Mars Plane Revived - Global Mars Surface Surveys. Rand Corporation. Presented at the "Case for Mars III Conference 1987".

The 1985 Goddard Space FlightCenter Battery Workshop. NASA Conference Publication 2434, NASA Goddard Space Flight Center, (Greenbelt, Maryland: November, 1985).

Power Train/Weights and Balances Spreadsheet

Given Conditions

I-kw/m2	0.450
T-K	214.000

Wing Characteristics

AR	10.000
Wing S-m2	243.000
Canard S-m2	11.810

Collector/motor Characteristics

PV Rho kg/m2	0.414
Array/S-%	0.850
PV Eff-%	0.250
Pwr Cond Eff-%	0.920
TC-∂%/∂K	0.050

P PV-kw	26.183
P FC Goal-kw	5.300
kwh reqd	42.400
Shaft Power-kw	31.483
Pav-kw	***26.446***

after aerodynamic losses

Fuel Cell Characteristics

SpE-kwh/kg	0.400
SpP-kw/kg	0.217

<<at 66% eff

Power Train Weights-kg		Volume-m3
1 EngW	15.000	
FC Weight	24.379	1.833
H2O	106.000	10.600
H2 Weight	11.778	0.168
O2 Weight	94.222	0.083
H2 Tnk W	5.369	
02 Tnk W	42.948	
H2O Tnk W	48.317	
Misc Pumps	20.000	
Power Cond	10.565	
HXR	10.000	
Power Dist	5.000	
Prop (x2)	40.000	
Prop Shaft (x2)	15.000	
Cont/Grbox (x2)	15.000	
Misc Total	115.565	
Total W:FC	227.013	
Total W:PV	89.668	
P&P Total	462.246	

Performance Section

Endrnce-hrs	8.000
Altitude-km	0.000
V-m/s	53.000

Characteristics

Rho-kg/m3	0.016
Cdo	0.018
eo	0.900
Clmax	1.720
Weight-N	6118.000
V stall-m/s	43.320
Excess Pwr-kw	8.154
P Reqd-kw	18.292
Range-km	1526.400
Range-miles	948.446
Climb rate-m/s	1.333

Propeller Specifications

Cs	1.500
Beta-Deg	25.000
Efficiency-%	0.840
Advance Ratio	0.900
Diameter-m	6.900

Characteristics

Shaft Power-kw	21.776
Cp	0.144
Ct	0.134
Static Thrust-N	1177.319
Thrust-N	1401.621
P Reqd/Eng-kw	10.888
n-rps	8.535
N-RPM	512.077

Power Train/Weights and Balances Spreadsheet

Given Conditions

I-kw/m2	0.450
T-K	214.000

Wing Characteristics

AR	10.000
Wing S-m2	243.000
Canard S-m2	11.810

Collector/motor Characteristics

PV Rho kg/m2	0.414
Array/S-%	0.850
PV Eff-%	0.250
Pwr Cond Eff-%	0.920
TC-∂%/∂K	0.050

P PV-kw	26.183
P FC Goal-kw	5.300
kwh reqd	42.400
Shaft Power-kw	31.483
Pav-kw	***26.446***

after aerodynamic losses

Fuel Cell Characteristics

SpE-kwh/kg	0.400
SpP-kw/kg	0.217

<<at 66% eff

Power Train Weights-kg		Volume-m3
1 EngW	15.000	
FC Weight	24.379	1.833
H2O	106.000	10.600
H2 Weight	11.778	0.168
O2 Weight	94.222	0.083
H2 Tnk W	5.369	
02 Tnk W	42.948	
H2O Tnk W	48.317	
Misc Pumps	20.000	
Power Cond	10.565	
HXR	10.000	
Power Dist	5.000	
Prop (x2)	40.000	
Prop Shaft (x2)	15.000	
Cont/Grbox (x2)	15.000	
Misc Total	115.565	
Total W:FC	227.013	
Total W:PV	89.668	
P&P Total	462.246	

Performance Section

Endrnce-hrs	**8.000**
Altitude-km	**1.500**
V-m/s	**81.000**

Characteristics

Rho-kg/m3	0.014
Cdo	0.018
eo	0.900
Clmax	1.720
Weight-N	**6118.000**
V stall-m/s	45.405
Excess Pwr-kw	0.372
P Reqd-kw	26.073
Range-km	**2332.800**
Range-miles	**1449.511**
Climb rate-m/s	**0.061**

Propeller Specifications

Cs	1.500
Beta-Deg	25.000
Efficiency-%	0.840
Advance Ratio	0.900
Diameter-m	6.900

Characteristics

Shaft Power-kw	31.040
Cp	0.063
Ct	0.059
Static Thrust-N	1177.319
Thrust-N	2142.100
P Reqd/Eng-kw	15.520
n-rps	13.043
N-RPM	**782.609**

Pav-I,T Chart 1

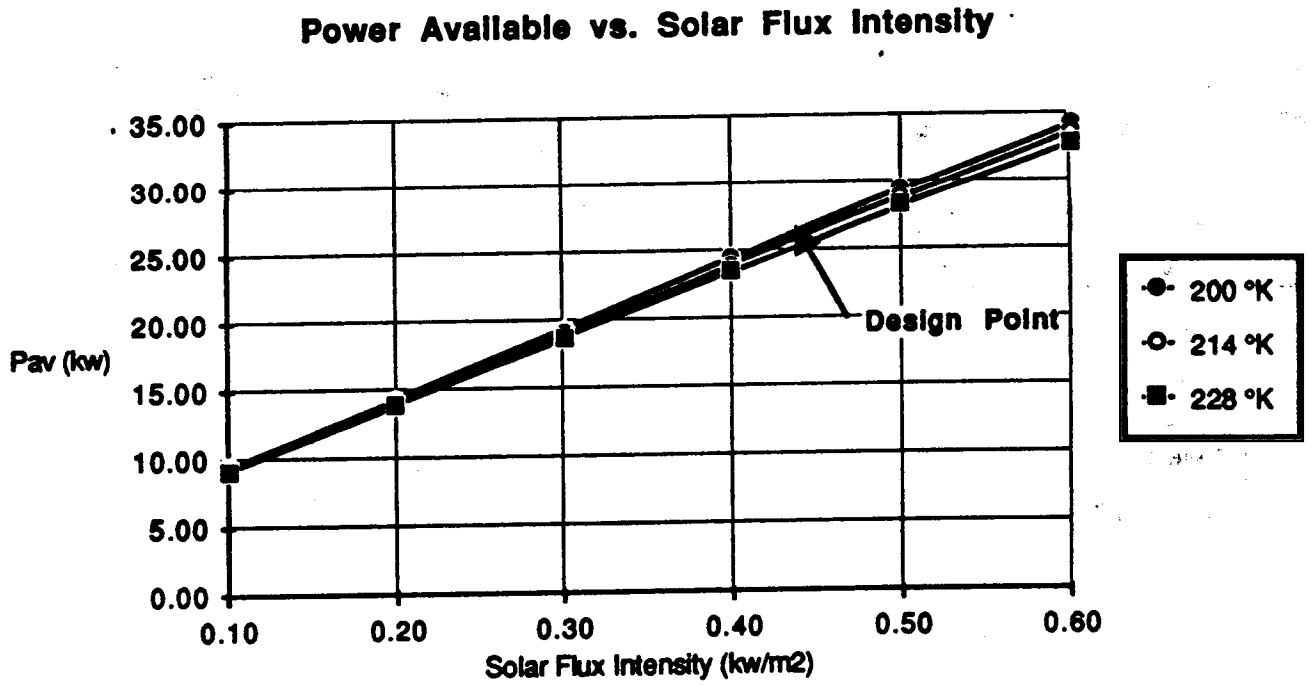

STABILITY AND CONTROL

Arlene Zander

The original design of The Spirit of Champaign consisted strictly of a flying wing configuration. But as examination of the stability and control problems began, the flying wing configuration was found to have insufficient control power. Consequently, a canard was introduced for longitudinal control and a vertical tail was added for directional stability. Additional control surfaces include elevators on the canard, a rudder on the vertical tail and flaps and spoilers on the wing. The wing also has sweep, dihedral, and twist contributions. Each of these control surfaces and contributions will be addressed individually in greater detail later in this report.

The first design problem confronted was the sizing of the canard. By examining the interdependence of center of gravity location, canard size, and canard location, graphs were obtained that showed canard sizes and locations for different center of gravity values. Due to the constraints of the weights and balances division, a most aft center of gravity range was desirable. Hence, the optimum choice for a canard had an area of 11.81m^2 and a span of 10.87m at a distance of 2.6316m from the canard aerodynamic center to the leading edge of the wing. This size and location provided the most rearward c.g. possible while still allowing a canard large enough to longitudinally trim. For further verification of these results, the graph in Figure 1 presents these data in dimensionless ratios for the desired center of gravity location. The optimum choice is indicated with an arrow. Other canard characteristics include a taper ratio of .3, an aspect ratio of 10, a quarter chord sweep angle of 17 degrees, a dihedral angle of 0 degrees, a zero lift angle of -6.0 degrees[1] and it is mounted at an angle of attack of 4.4 degrees.

At first appearance, the canard size appeared to be quite small so closer scrutiny and further investigation was necessary. After additonal calculations, the canard size was verified as satisfying requirements because with the virtual flying wing configuration, only a small amount of longitudinal control power is necessary. Thus the aforementioned canard was maintained as the truly optimum choice.

Similar considerations to those in the sizing of the canard brought about the size of the vertical tail. The optimum choice is a tail of area 20.22m^2 and a height of 10m with the leading edge located at the back of the wing. Although this tail has a relatively small moment arm and area, it still satisfies the directional stability requirements and needs only a small rudder

deflection to continue an engine-out take-off. This high capacity for directional stability with a small tail (8.32% of wing area) is due in part to the taper angle of the wing and its contribution to directional stability. This topic will be addressed in more detail later in the report. The vertical tail location also satisfies the additional constraints of the power and propulsion division that the vertical tail not cast shadows on the solar panels and thus reduce the power available. Another advantage to the small vertical tail size is that it minimizes its contribution to the gross weight.

The next topic addressed is the sizing and placement of the other control surfaces. Elevators on the canard span most of the length of the canard, except for where the pod attaches, and they have a chord that gives them an area that is 27.6% of the canard area itself. The rudder spans the upper 7m of the vertical tail and has a chord that gives it an area that is 27.2% of the tail area. Allerons are located just beyond the engines at 12m from the aircraft centerline. They are 3m long and have a chord that gives them an area that is 1.71% of the wing area. Spoilers are employed on the aircraft, but only during landing ground roll to partially destroy lift and bring the aircraft to a stop in less time. Originally, spoilers were considered for use during actual flight, but after finding that they would destroy more lift than was desired, they were used solely for landing ground roll purposes. An additional consideration is that the spoilers have no fine control mechanisms; they are limited to a spring loaded release mechanism in order to minimize the structure and weight necessary to activate them. Thus, for these reasons, spoilers will not be further addressed because they are not precision controlled and have little bearing on stability and control.

Further design considerations involve locating the neutral point of the aircraft. Based on the data used for the optimum canard size and location, the neutral point is located 2.8684m behind the leading edge of the wing during cruise (Figure 2). The changes in neutral point location for take-off and landing as defined by surface operations are negligibly small. On landing, the descent and approach angle is very small and on take-off, only elevator deflection is used which does not affect the neutral point location.

In order to achieve a certain degree of stability, a static margin of 10% was chosen. This static margin not only keeps the center of gravity a safe distance from the neutral point, but it also gives a center of gravity range that is 1.6736m long, beginning from .6602m behind the wing leading edge and extending to 2.3838m ^{2} behind the leading edge (Figure 2). This center of gravity range has a substantial length and in a climb at maximum lift coefficient, it allows for a trimmed and stable condition at a minimum elevator deflection angle of 30 degrees while the elevator deflection required to trim at zero lift coefficient is -12.9 degrees (Figure 3). This range proves to be excellent in that it not only satisfies stability and control requirements but it also provides an excellent range for weights and balances.

The next topic addressed is various aspects of the aircraft configuration that contribute to the stability and control derivatives affecting longitudinal, directional and lateral motion of the aircraft. First, the wing dihedral angle necessary to obtain the proper variation of rolling

moment coefficient with sideslip and variation of yawing moment with sideslip derivative values to satisfy specifications of the Addendum is 3 degrees[3]. Secondly, wing twist was found to be 0 degrees. Next, the canard angle of attack necessary to maintain controlled flight at cruise is 4.4 degrees. Also, a wing sweep of 19.78 degrees is determined and used for various reasons. One reason being that the initial choice to have a sweepback angle came because of the important contribution to directional stability because the asymmetric dynamic pressure distribution normal to the lines of aerodynamic centers of the wing panels produces a force that will counteract sideslip, thus helping to stabilize the aircraft[4]. Another reason is that this angle brought the desired effect of moving the wing aerodynamic center and the center of gravity range back on the wing as compared to a rectangular wing or a wing with a smaller sweep angle. The final reason being that an angle of 19.78 degrees will be quite effective during the sideslip conditions defined in the Addendum. To verify these aspects of the aircraft configuration, please refer to Figure 4 where the control derivatives are presented in tabular form. The final specifications addressed are those defined in the Addendum for required control performance of the aircraft during maneuvers. All these data are presented in tabular form in Figure 5. Note that only small rudder deflections are necessary for lateral trim because of the contribution of the wing sweepback angle.

In conclusion, it is evident from the data presented in the previous pages, The Spirit of Champaign is trimmed and stable longitudinally, directionally and laterally during take-off, cruise, landing and during maneuvers necessary.

References

1. Liebeck, R.H. and Comacho, P.P. , Airfoil Design at Low Reynolds Number with Constrained Pitching Moment, Proceedings of the Conference on Low Reynolds Number Airfoil Aerodynamics, UNDAS-CP-77B123, June, 1985, p. 27-49.

2. McCormick, Barnes W., Aerodynamics, Aeronautics, and Flight Mechanics, John Wiley & Sons, 1979, p. 111.

3. Roskam, Jan, Methods for Estimating Stability and Control Derivatives of Conventional Subsonic Airplanes, University of Kansas, 1977.

4. Sivier, Kenneth R., Aircraft Flight Mechanics, Lecture Viewgraphs for AAE 319 at the University of Illinois, 1988, p.149-255.

Figure 1: Canard Sizing Graph

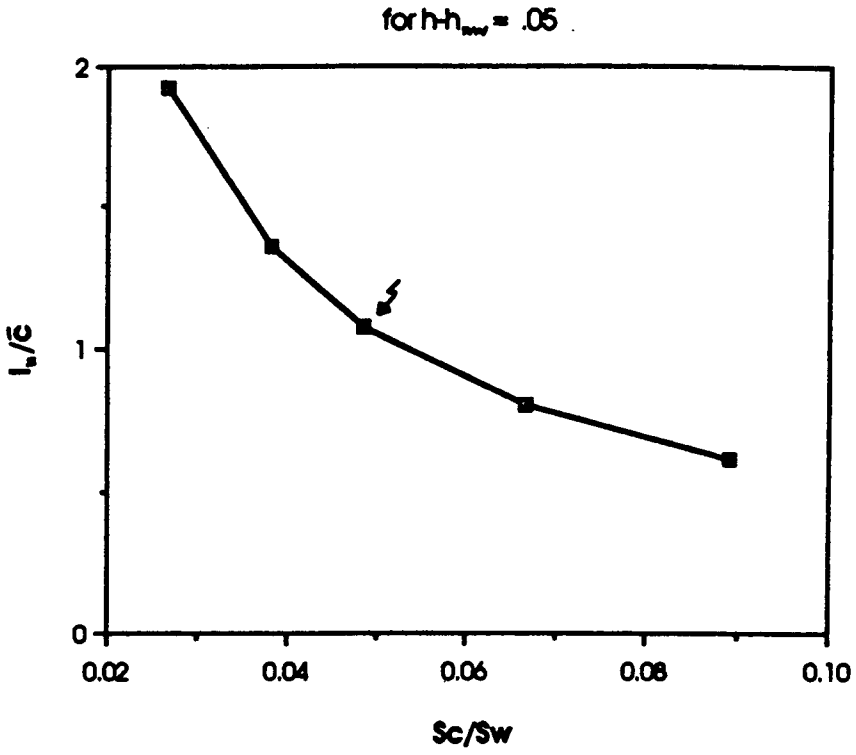

Figure 2: Diagram of Locations

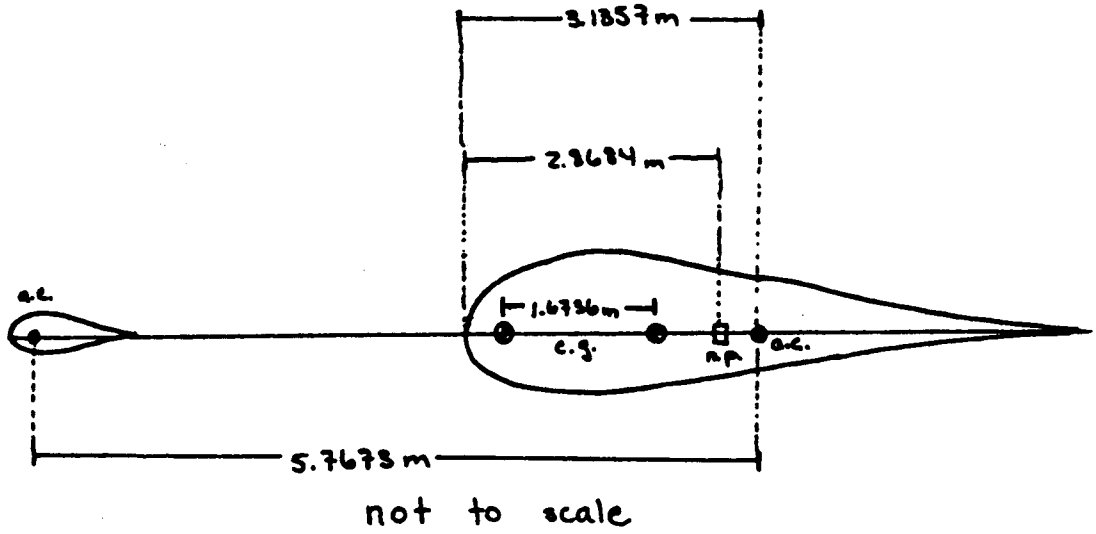

not to scale

Figure 3: Trim at max lift coefficient

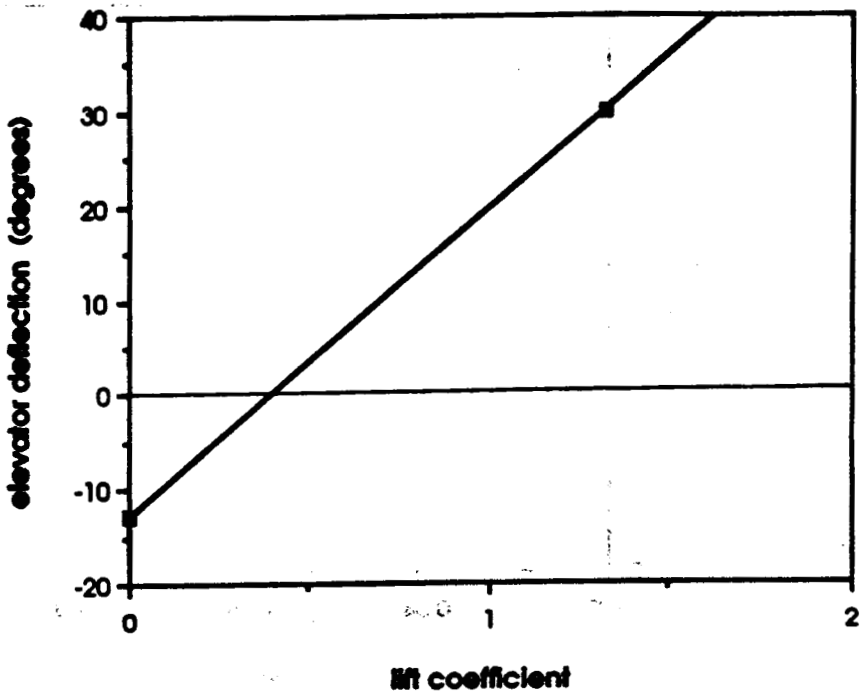

sideslip angle		rudder deflection		rolling velocity		aileron deflection		other	
C_{Y_β}	-0.1900	$C_{Y_{\delta_R}}$	0.1189	C_{Y_p}	-0.0177	$C_{Y_{\delta_A}}$	0.0000	C_{L_0}	0.10357
								C_{m_0}	-0.0133
C_{l_β}	-0.0532	$C_{l_{\delta_R}}$	0.0061	C_{l_p}	-0.9457	$C_{l_{\delta_A}}$	-0.1002	C_{L_α}	3.0426
								$C_{L_{\dot{\alpha}}}$	0.0139
C_{n_β}	-0.0222	$C_{n_{\delta_R}}$	-0.0041	C_{n_p}	-0.0039	$C_{n_{\delta_A}}$	0.0265	$C_{L_{\delta_E}}$	0.4978

Figure 4 CONTROL DERIVATIVES

	A	B	C	D
1	Figure 5: Stability and Control Requirements			
2				
3	number	description	requirement	performance
4				
5	2.1	take-off rotation	$V=.9V_{TO}$	$\delta_e=25.06°$
6	2.2	take-off	$\beta=0°$	$\delta_r=.94\,\delta_{r\,max}$
7		one engine out	full rudder	
8	2.3	cruise control	$V=1.1V_{TO}$	$\delta_r=.73\delta_{r\,max}$
9		one engine out	$\delta_r<.75\delta_{r\,max}$	$\phi=3.692°$
10			$\phi\leq5°$	
11	3.1	banked turn	$\phi=30°$	$\delta_r=.60\delta_{r\,max}$
12			cruise V & h	$\delta_a=.75\delta_{a\,max}$
13	3.2	roll response	$\phi=30°$	$\delta_a=.89\delta_{a\,max}$
14			$t\leq2s$	$\delta_a=.89\delta_{a\,max}$
15	4.1	stall	$C_m=0$	$\delta_e=.92\,\delta_{e\,max}$
16			$C_l=C_{lmax}$	
17	4.3	crosswind landing	$\beta=10°$	$\delta_r=.62\delta_{r\,max}$
18	4.4	full rudder sideslip	$\delta_r=\delta_{r\,max}$	$\delta_a=.69\,\delta_{a\,max}$
19			$\delta_a<.75\delta_{a\,max}$	

has no meaning to the reader

STRUCTURES

Timothy Ehmke

Extensive use of composite materials in all major components will help to minimize the weight of the Martian aircraft. The greater strength to weight ratio of composite materials, compared to standard aluminum, will reduce the primary structure's weight by approximately 25 percent (Ref. 1). At this time, weight reduction is the primary concern, therefore, the much greater cost of composites is not being considered during material selection.

To obtain an initial sizing of the wing's structural members, wing loading diagrams have been made for two critical flight conditions. These conditions are steady-level flight, and on the ramp (Fig. 1a and 1b). For these diagrams, weights were supplied by the weights specialist. The estimated wing weight that was provided has been assumed to be distributed as the square of the chord length. The lift load has been calculated using the Schrenk approximation.

From these diagrams, shear distributions (Fig. 2a and 2b) and bending moment distributions (Fig. 3a and 3b) have been determined. The torsional moment distribution, about the elastic axis (which has been assumed to coincide with the line of sectional aerodynamic centers), has also been determined (Fig.4).

The wing structure has been designed to withstand the maximum moment acting on it at each location, obtained from the prementioned graphs. For the sizing of the structural members, an ultimate load factor of six has been used, with a safety margin of 1.8 due to increased variance in composite material properties compared to aluminum (Ref. 2)

The basic aircraft structural layout, to now be discussed, is illustrated in Figure 5.

SPARS- Two metal matrix composites were considered for the spar. A graphite/aluminum matrix composite has been selected instead of silicon carbide (continuous)/ aluminum. Since the wings are so large, a relatively stiffer spar was desired. Even though the latter is twice as strong, its relatively low modulus made the former more desirable (Ref. 3).

The spars are comprised of six meter tubular sections, due to transportation constrants imposed by the spacecraft designers. They are located at 25 percent and 65 percent chord (Fig. 6). Each section has a constant radius and thickness to simplify fabrication. They are also sized so that each section stores inside the adjoining one to save space during transportation. Therefore, adapters will be required to join the unequal

radius sections.

Using the previously discussed design requirements, an initial spar sizing has been done. The results are given in Figure 7. The thicknesses of the sections may appear small, however, the forward spar has been independently sized to withstand the maximum sectional moment, while the aft spar has been sized to withstand one-half of this moment. Since this design should be able to withstand the maximum moments generated, no re-enforcements have been considered for these spars.

RIBS- From the center line of the aircraft to 13 meters, the spacing of the wing ribs will be 0.75 meters. Out board of this the spacing will increase to 1.0 meters (Ref. 4). Other ribs will be added as reqiured by special wing features. They will be constructed of one of two materials, depending on their requirements.

Ribs required to withstand large loads, such as control surface hinges or engine mounting, will be made of the graphite/ aluminum metal matrix composite. The five center ribs will definately be made of this material, since they must be used to attach the body and tail to the wing. More ribs may also need to be made of this material, however, the more that are, the greater the weight of the wing structure.

Therefore, as many ribs as possible will be made from a dense blue foam stripped with carbon and Kevlar-wrapped. This rib design has proven to be very strong while being almost weightless (Ref. 5). The ribs are then attached to the spars using a structural adhesive. This is also the method used to attach the skin to the ribs (Ref. 6).

SKIN- To furthur reduce the wing's structural weight, a skin of Mylar will be used on the bottom surface of the wing. This covering, however, will not be used on the top surface of the wing for two reasons. First, the solar panels require a somewhat rigid base for mounting. Second, it will also maintain the airfoil section shape better than Mylar. By using a leading edge skin thickness that is equal to the solar array thickness plus the skin thickness it is attached to, a smooth upper surface will be achieved for the airfoil. The aerodynamic performance of the wing will, therefore, be improved. This more rigid covering will also be used for the wing's leading edge.

This skin will be type HT graphite-epoxy laminate. It was chosen instead of Kevlar because its relatively large modulus will provide improved shear buckling strength (Ref. 7).

TAIL- The tail described on the freeze data sheet has proven much too tall to safely construct. Therefore, if design of this airplane is to continue, a reduction in the tail's height from ten meters, to seven meters is recommended. This will allow it to be transported in one piece, instead of two as is now planned. It is this resized tail that is represented in Figure 5a. The tail, to reduce weight, will be covered with Mylar.

The canard will be constructed similarly to the wing. It will also be a graphite/aluminum structure covered by a type HT graphite-epoxy skin. Control surfaces, except for the spoilers, will be of honeycomb design. The spoilers due to their large size will require a graphite/aluminum frame, covered by the rigid skin.

REFERENCES

1. Nicolai, Leland M., Aircraft Design, Mets, Inc., 1975.

2. Sellars, R. J., and Terry, G., "Sophisticated Aircraft Developments - Combat Airplanes," Aeronautical Journal, Sept., 1981, pp. 334 - 338.

3. DeMario, William F., "New World for Composites," Aerospace America, Oct., 1985, pp. 36- 42.

4. Roskam, Jan, Airplane Design Part III: Layout Design of Cocpit, Fuselage, Wing, and Empennage: Cutaways and Inboard Profiles, Roskam Aviation and Engineering Corp., 1986.

5. Burke, James D., The Gossamer Condor and Albatross: A Case Study in Aircraft Design, "AIAA Professional Study Series," Report No. AV-R-80/540, June 16, 1980.

6. Schreder, Dick, "Building the HP-18," Soaring, Vol. 40, March - Aug., 1976.

7. Smith, William F., Principles of Materials Science and Engineering, McGraw - Hill Book Co., 1986.

Figure 1a. Wing Loading in Steady-Level Flight

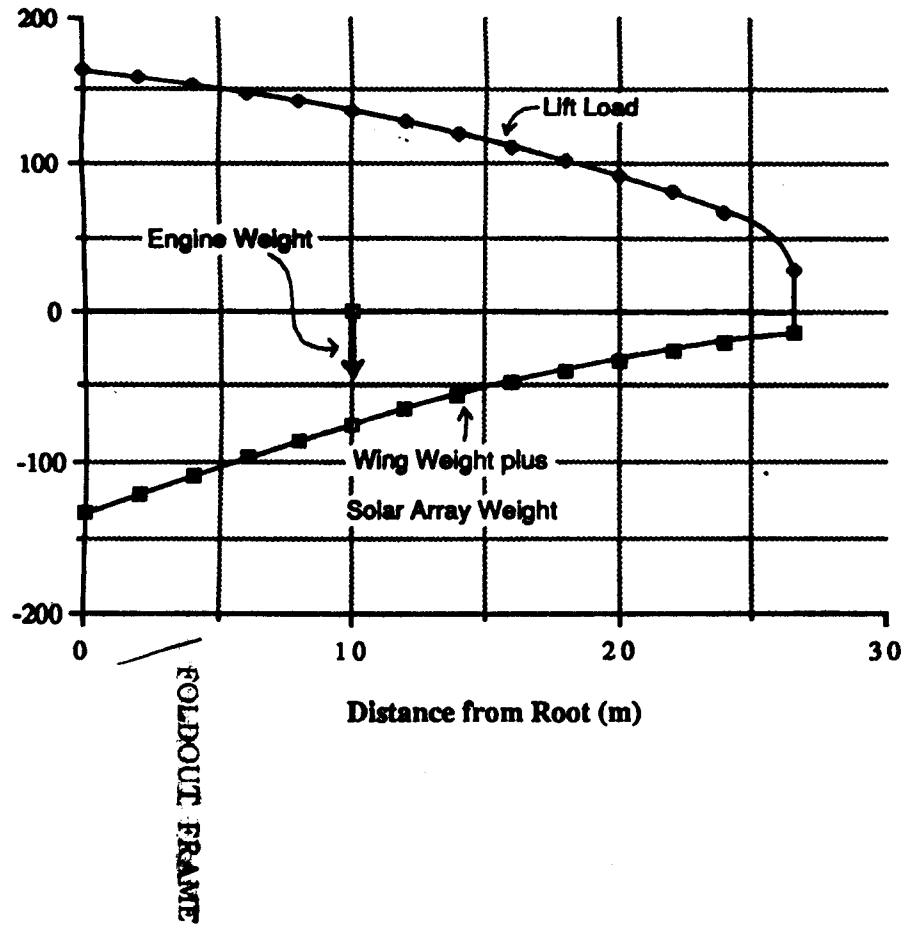

FOLDOUT FRAME

Figure 1b. Wing Loading on the Ramp

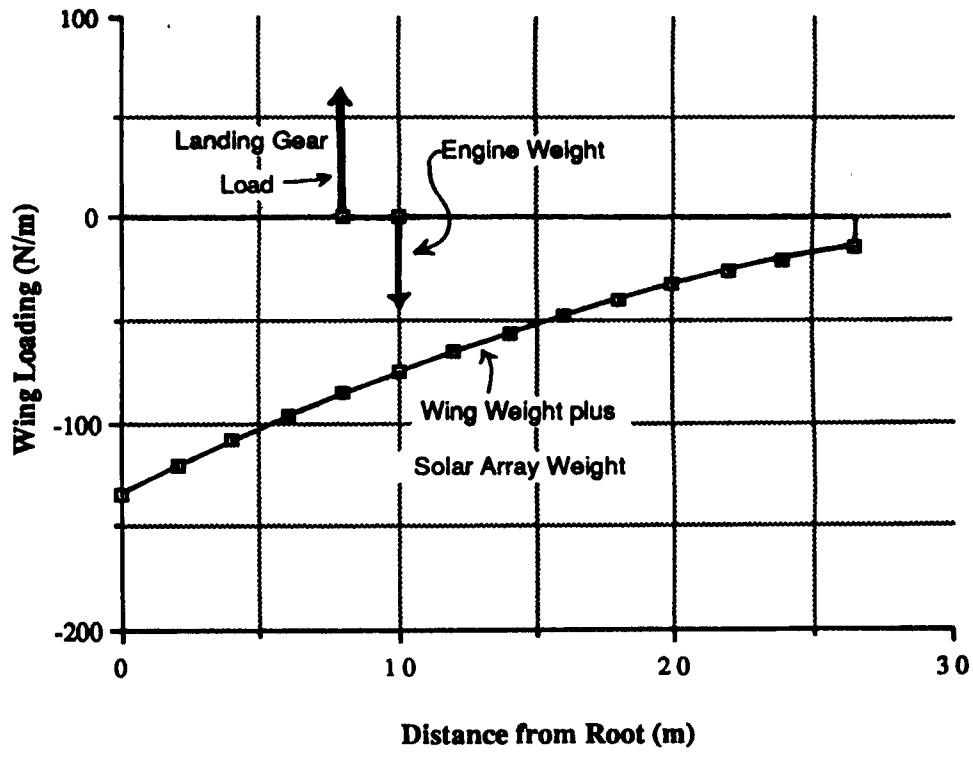

Figure 2a. Shear Distribution in Steady-Level Flight

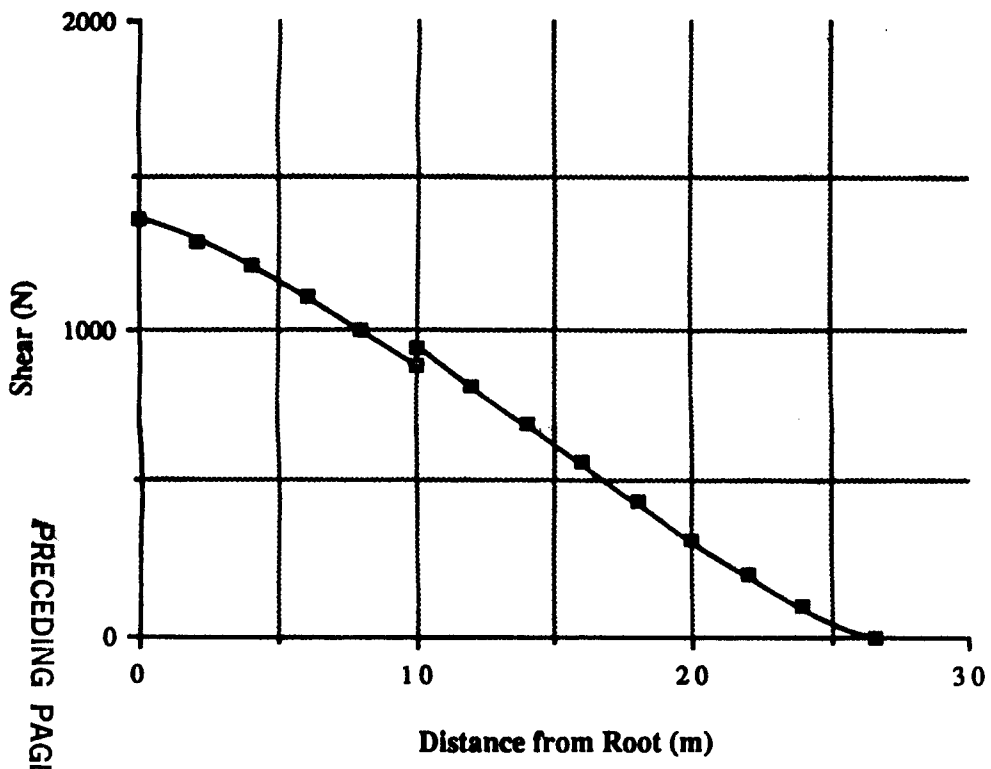

Figure 2b. Shear Distribution on the Ramp

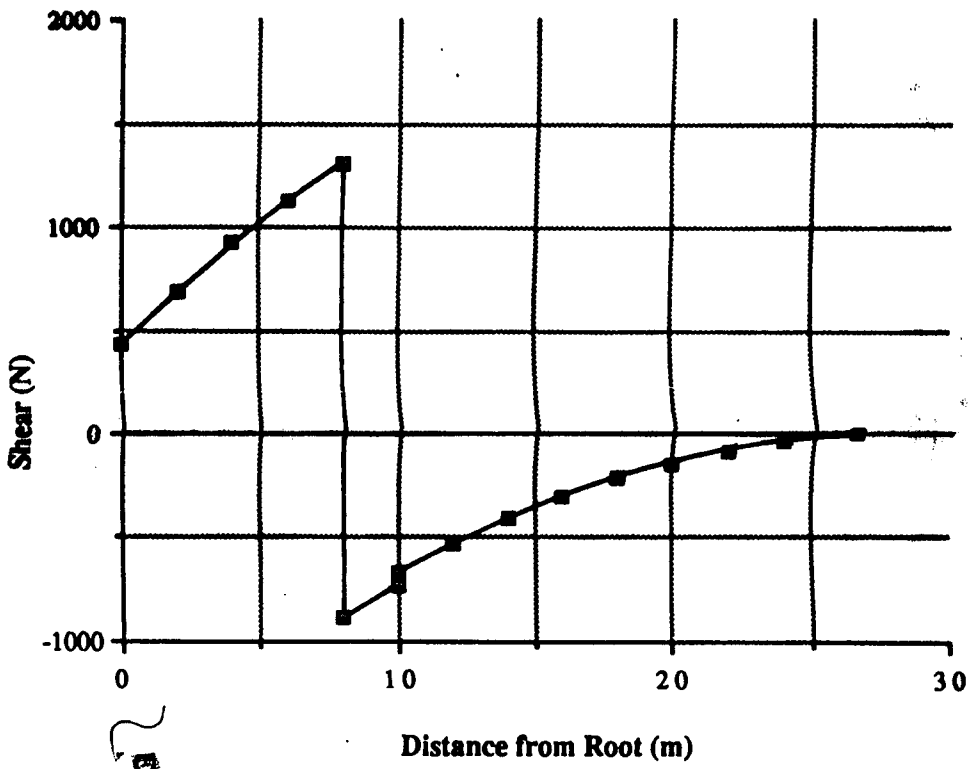

FOLDOUT FRAME

FOLDOUT FRAME

5-5

Figure 3a. Bending Moment Distribution in Steady-Level Flight

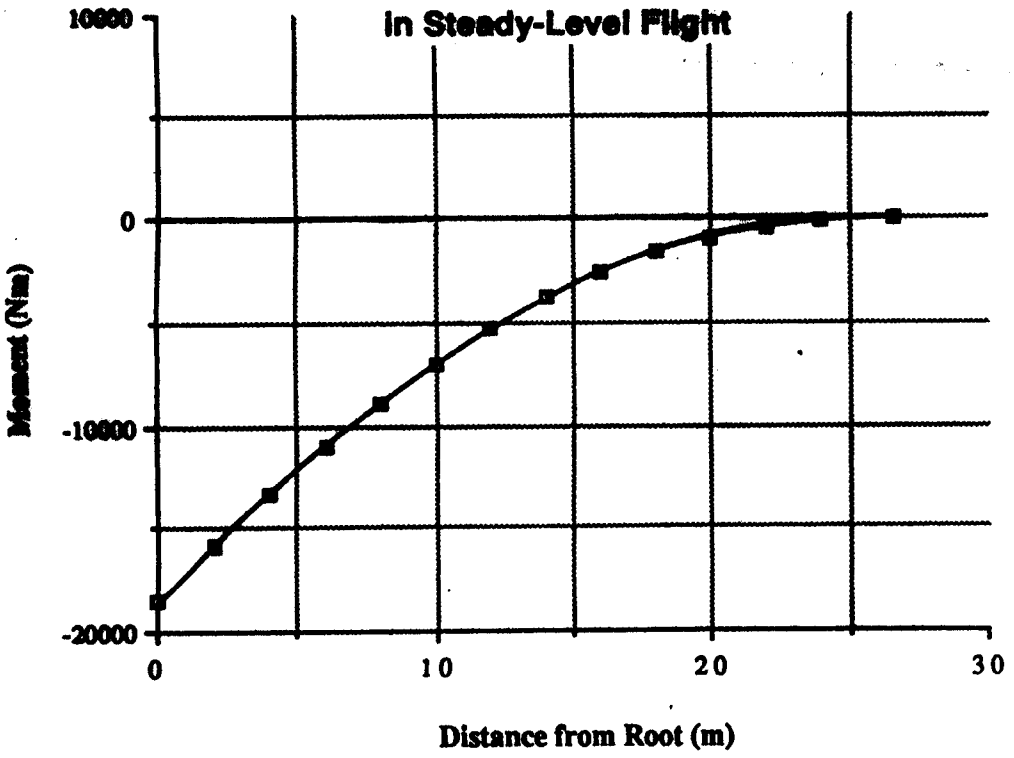

Figure 3b. Bending Moment Distribution on the Ramp

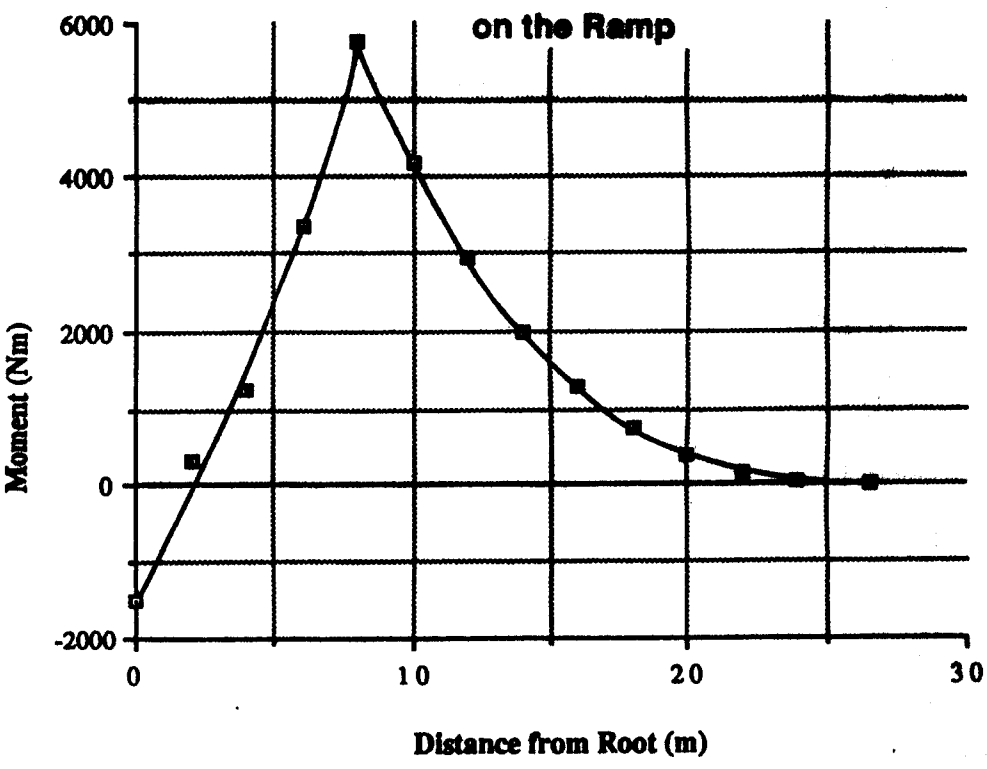

Figure 4. Torsional Moment about Elastic Axis in Steady-Level Flight

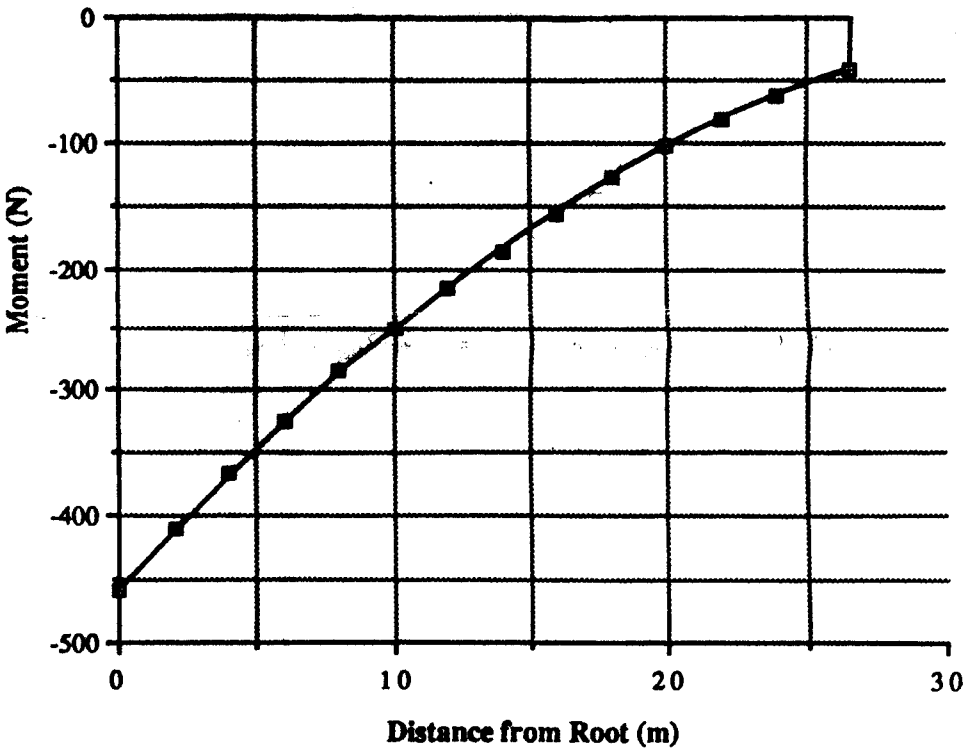

FOLDOUT FRAME

FOLDOUT FRAME

Figure 5. The Aircraft Structural Layout

The aircraft's right half has been omitted for simplicity.

For clarity, only one-half of canard's ribs are shown. Spoilers are not shown for the same reason. Their location is indicated, however, by the dashed line on the wing's upper surface (see drawing at lower left for side view of spoiler). The rib sections have been drawn as being only external frames.

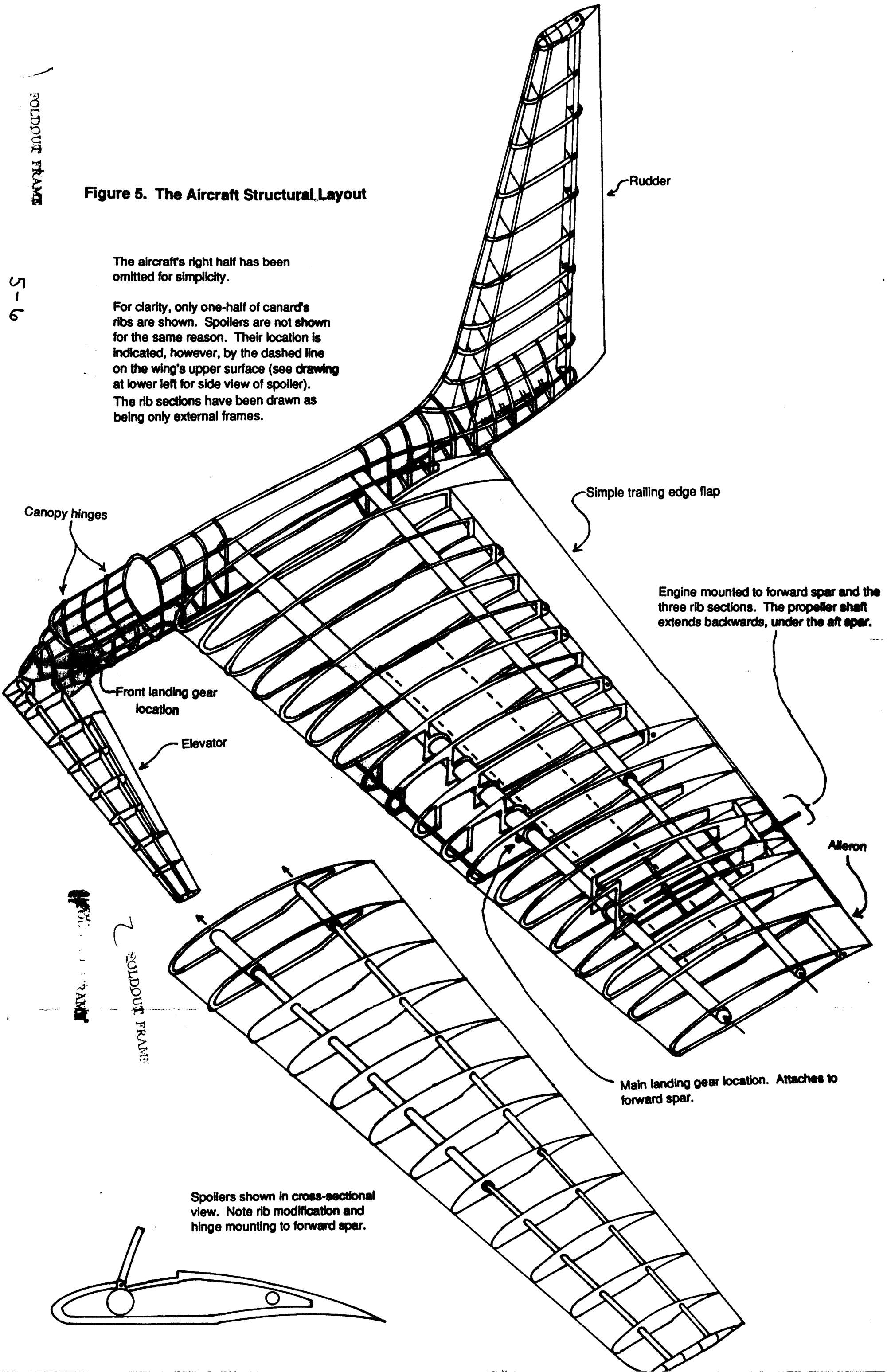

FOLDOUT FRAME

Figure 6. Cross-Section View of Airfoil Showing Spar Location

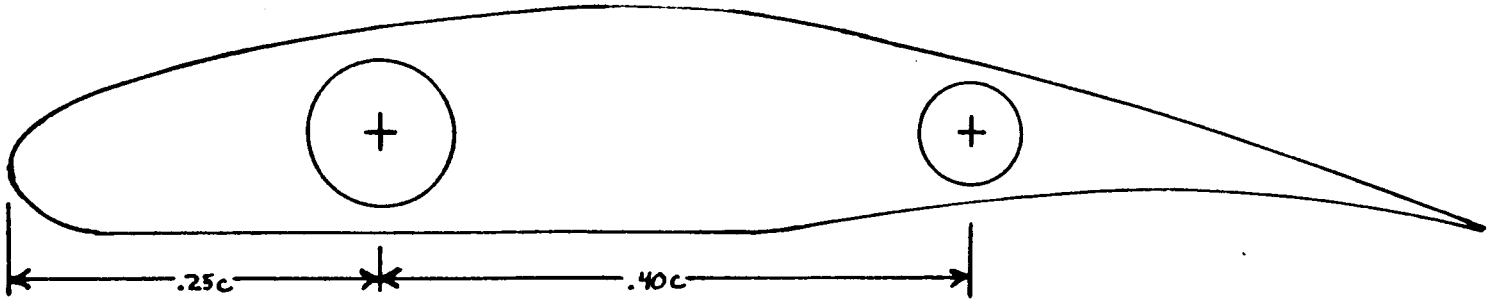

Note: each spar has been sized to be 75 percent of the rib height, at the particular chord location, of its outboard end.

Figure 7. Spar Sizing Results

Location of Spar(m)	Front Spar		Aft Spar	
	radius(m)	thickness(mm)	radius(m)	thickness(mm)
0 to 2	0.300	1.03	0.185	1.34
2 to 8	0.300	1.03	0.185	1.34
8 to 14	0.245	0.77	0.145	1.06
14 to 20	0.180	0.60	0.110	0.78
20 to 26.6	0.115	0.36	0.070	0.47

SURFACE OPERATIONS

Michael Brody

The Mars craft will take off with a ground assist sled. The sled will bring the plane to its launch speed and then release it. Then the thrust for the craft will be provided by two propeller engines. Landing will be done by throttling down the engines and gliding in for a landing. During landing, simple flaps will be deployed to provide extra lift and spoilers will be deployed to decrease the ground roll distance. The ground based facilities needed will be a hangar to store the aircraft, a refueling station, and trucks to push the craft around the runway area. The trucks will also push the craft up a ramp to elevate it to the height of the launch sled grasps (Fig. 1).

A standard take-off configuration was first considered but there was not enough power available to make it possible in a reasonable length of runway. Using the fuel cell/solar panel power system, only about 30%[1] of the needed power was available. Rocket assisted TOL (take-off and landing) was also studied. It would consist of three Viking Lander type hydrazine rocket engines to provide vertical and horizontal thrust[2]. This was discarded for several reasons. It was difficult to find places on the plane where horizontal thrust could be installed. There was also the extra weight of the fuel tanks. As the engines fired, there would be a weight decrease that would make stability and control difficult.

The ground based sled that brings the craft up to take-off speed can be powered by several methods. Rockets, similar to the Viking rockets, could be attached to the sled and fired to bring the sled and craft to launch speed. Another possibility is to use a magnetic sled that uses very powerful superconducting magnets to float on top of a guideway containing imbedded conducting coils[3] (Fig. 2). Initially, the sled will rest on wheels (Fig. 3), but when it reaches a speed of about 8 m/s, the sled's magnets will induce a current in the guideway conducting coils. The magnetic field produced by these currents will lift the sled up to 10 cm off the guideway. Electromagnetic forces will also propel the sled forward. Another set of guideway coils will be energized in a timed sequence to produce a moving magnetic wave. This magnetic wave will continuously repel the sled's magnets from behind and attract

them from in front. Accelerations of up to 20 g's have been theorized as possible using this scheme. The train's magnets would have to be superconducting, since ordinary magnets would require to much power. With the advances in superconductivity, there will be magnets that are small and strong enough to make this concept practical. To achieve the take-off speed (V_{LO}) of 46.9 m/s [1], the sled could be accelerated at 11 m/s^2 (about 1.1 earth g's) for about 100 meters (S_G=100 m). (The data calculated for TOL was derived from equations in the McCormick reference.) The guideway will be about 400 meters to allow the sled and its support towers to move ahead of the plane, out of the way of the ascending aircraft propellers. This guideway distance will also give the sled enough distance to decelerate to a stop, even with the aircraft attached (as in an aborted take-off). The plane will be held 8 meters above the ground by the sled enabling the propellers to turn without hitting the ground. The sled will hold the craft by its two wing landing gears. The third landing gear located at the nose will rest freely on a platform of the sled. When the plane reaches its launch speed, it will rotate its nose up, pivoting on the sled's landing gear grasps. This rotation will last three second (t_{rot}=3 sec). This rotation distance, S_R, will be about 141 meters. These grasps will then release the craft. The angle of climb, γ_{cl}, will be 3^0. The transition or flare manuever distance, S_{tr}, is 47 meters. At this angle of climb, the craft will clear a 15 meter obstacle in 263 meters. So, the total takeoff distance, S_{total}, is 551 meters. The craft will need about 21,900 watts of power out of the propellers to acheive this climb angle. At the beginning of the climb, all the landing gears will be retracted.

At the beginning of the landing sequence, the flaps will be deployed at a flap angle of 25 degrees ($\delta_f = 25^0$). This will decrease the craft's airspeed from its descent speed to its approach speed, V_A=45.3 m/s, in about 40 seconds. The craft will then lose attitude by gradually throttle down the engines and increase the flap angle to $\delta_f = 40^0$, keeping its approach velocity constant. The approach angle will be about $.7^0$. This corresponds to a total airborne distance, S_A, of about 1500 meters from a 15 meter obstacle to the beginning of the runway. When the plane approaches the runway, it will deploy its landing gears and totally cut off its power and align the propeller blades horizontally with respect to the ground. This will enable the plane to land on standard size landing gears without having the propellers hit the ground. When the plane is gliding a few feet above the runway the pilot will intiate a controlled stall, which will drop

the craft softly on the ground. Brakes will then be applied to the landing gears to slow the plane's ground roll. Ground spoilers (lift dumpers) will also be deployed to decrease the ground roll length. The flare manuever will cover 75 meters (S_{trans}=75 m), which includes a 2 second delay while the pilot changes from the landing to the breaking configuration. The landing surface will be made of firm, dry compacted dirt or sand with a ground resistance coefficient (μ) of .04.[4] This allows the plane to have an average wheel braking coefficient of .30. The deceleration of the craft will be 1.45 m/s^2 using both landing gear breaks and ground spoilers. Thus the ground roll distance, S_G, will be about 708 meters.

The craft will use plain flaps on the trailing edge of the wing to obtain a higher lift coefficient[5]. The length of each flap will be 6 meters, starting 1 meter away from the centerline of the plane. The percentage of the local chord that is made of flaps will be 20% (C_f/C = .20). Increments in wing lift coefficient (ΔC_L) are presented in Fig. 4. (The data calculated for the plain flaps was derived from equations in the Datcom reference.) Also, increments in drag (ΔC_D) and wing moments (ΔC_m) caused by the flaps are shown in Fig. 5 and Fig. 6, respectively. The flaps will only be used during the landing procedures. Their primary purpose is to decrease the stalling speed which in turn decreases the approach speed (V_A) and ground roll distance (S_G).

The plane will use three landing gears. Two will be located under the wing, 8 meters from the plane's centerline and 1.3 meters behind the wing's local leading edge[6]. The third landing gear will be located on the centerline trailing edge of the canard. The three landing gears will be almost identical, each weighing about 102 N. The difference between the nose and main gears is how they are retracted. The nose gear is retracted from the front while the main gears are retracted from the side. (See Fig. 7 for their specifications.) If the plane is in a standard load configuration, the wing landing gears will each encounter a static load of 2120 N, while the nose will encounter a load of 1860 N[6]. Fig. 8 shows how the two different landing gears will retract.

Spoilers are used to decrease the ground roll distance during landing. The length of each spoiler will be 8 meters, starting 4 meters from the centerline of the plane. 18% of the local chord will be the width of the spoilers. When the spoilers are deployed, they effectively destroy the lift over the part of the span they cover[1]. They also increase the parasite drag of the craft. Overall, the use of spoilers add .373 m/s^2 of deceleration[4], eliminating about 245 meters from the ground roll.

The servicing required for the craft will be general maintanence and refueling. The maintainence will be done in a hangar to protect the craft from outside elements. Refueling will consist of plugging the refueling unit into the servicing palette located on the craft. The unit will use energy produced by the solar panels on the craft to break down water into hydrogen and oxygen. Electricity will flow from the craft panels through the palette to hydrolysis electrodes in the refueling unit. Water stored in the craft will also be pumped into the refueling unit to serve as the hydrolysis reactant. The produced hydrogen and oxygen will then be fed back through the palette into storage tanks aboard the craft. The top of the hangar can also be outfitted with solar panels to assist or replace the function of the craft solar panels during refueling.

Ingress and egress will have relatively simple procedures. Before the plane is moved to the launch sled, its canopy will open up for entrance. The canopy will be hinged on the right side of the aircraft. A restraining cord will be attached to the left side of the canopy and fuselage to prevent the canopy from stressing the hinge from over-rotation. A ladder will be hooked on the open side of the fuselage for the fully suited pilot to enter or exit the cockpit.

References

1. McCormick, Barnes W., Aerodynamic, Aeronautics, and Flight Mechanics, John Wiley & Sons, 1979.

2. Thompson, Jim, Viking Lander Rocket Engine Data NASA MSFC

3. Lerner, Eric J., "Superconducters Heat Up Space" Aerospace America, AIAA, October 1987

4. Torenbeck, Egbert, Synthesis of Subsonic Airplane Design Delft University Press, 1986

5. DATACOM, Material on High Lift Wing System Copied by K. Sivier, 1988

6. Corning, Gerald, Supersonic and Subsonic, CTOL, and VTOL Airplane Design, College Park, Maryland, 1960

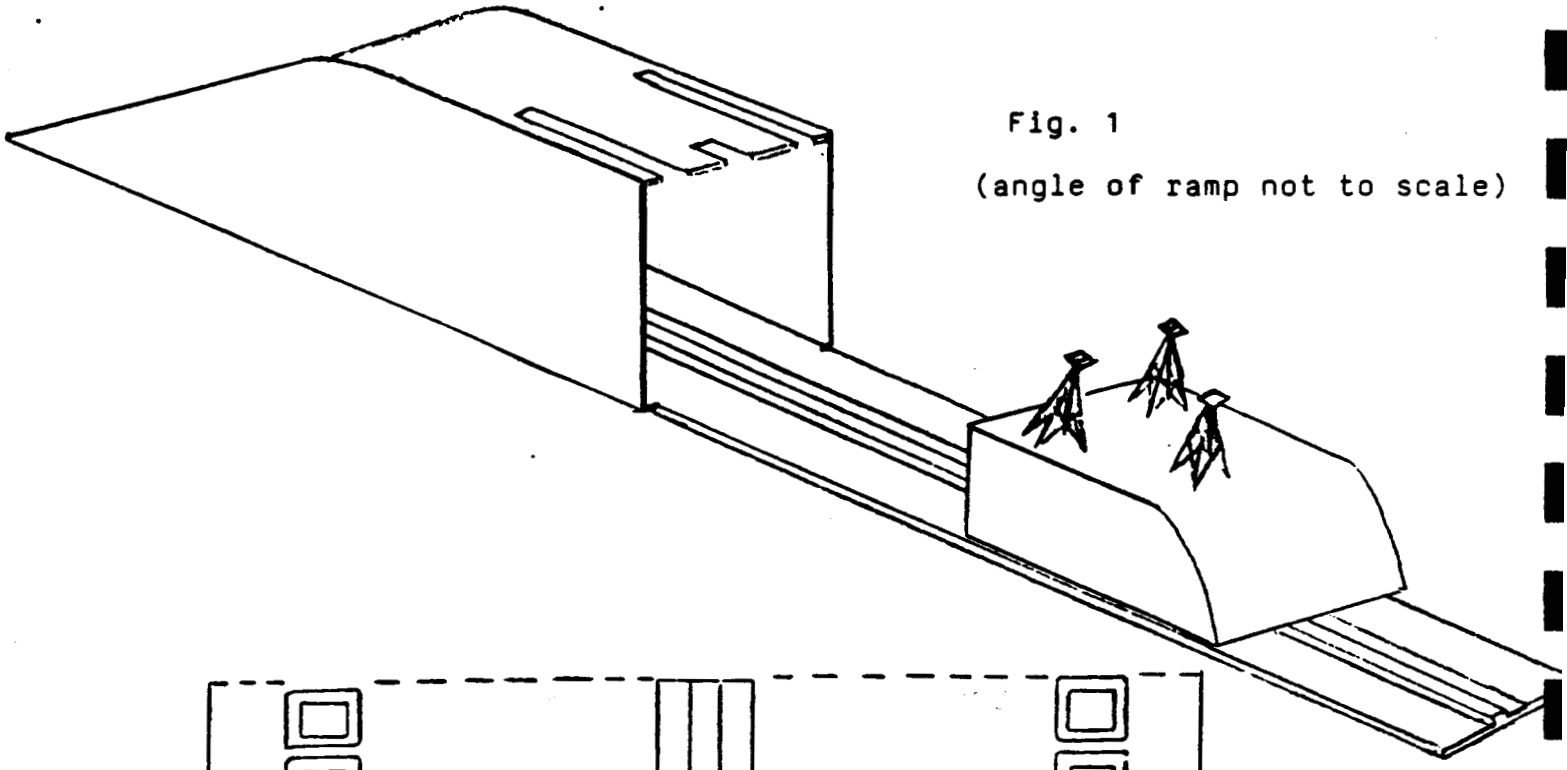

Fig. 1

(angle of ramp not to scale)

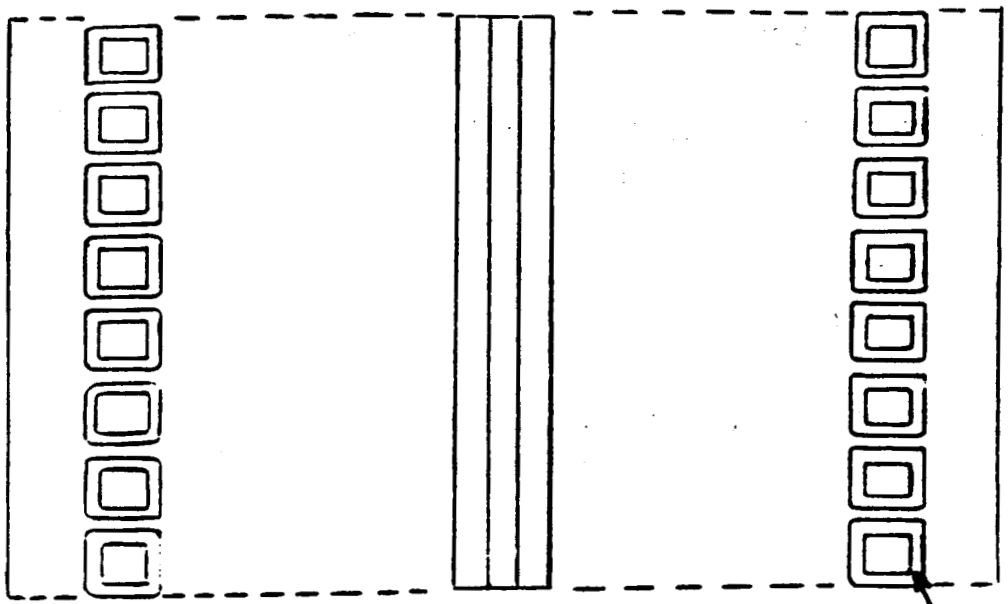

Top View

Fig. 2:

The Guideway

imbedded conducting coil

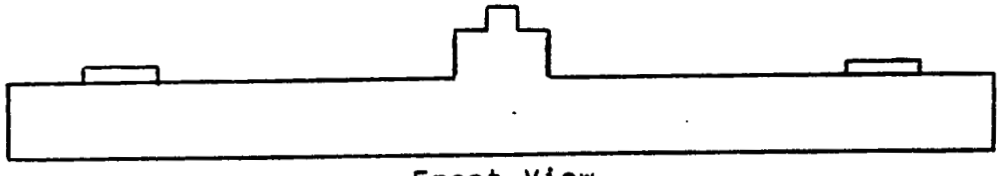

Front View

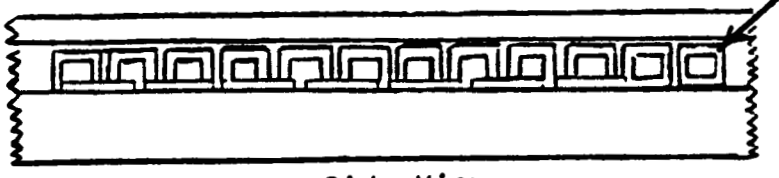

Side View

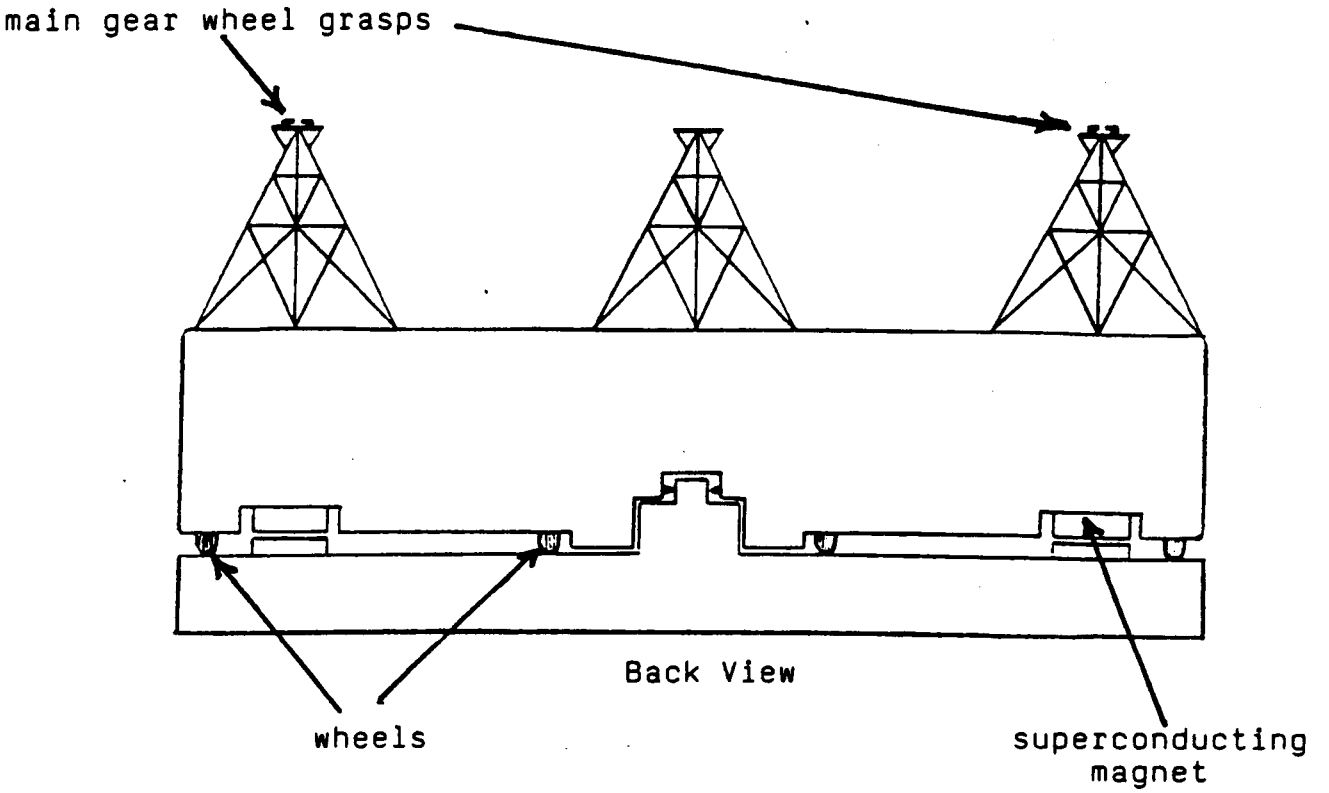

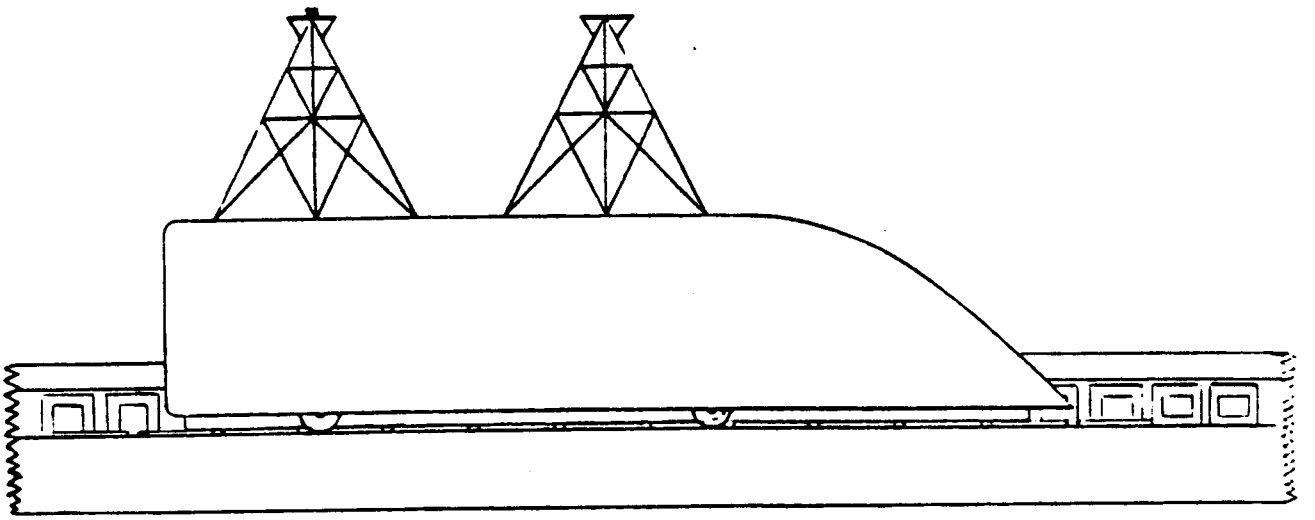

Fig. 3: Sled resting on guideway

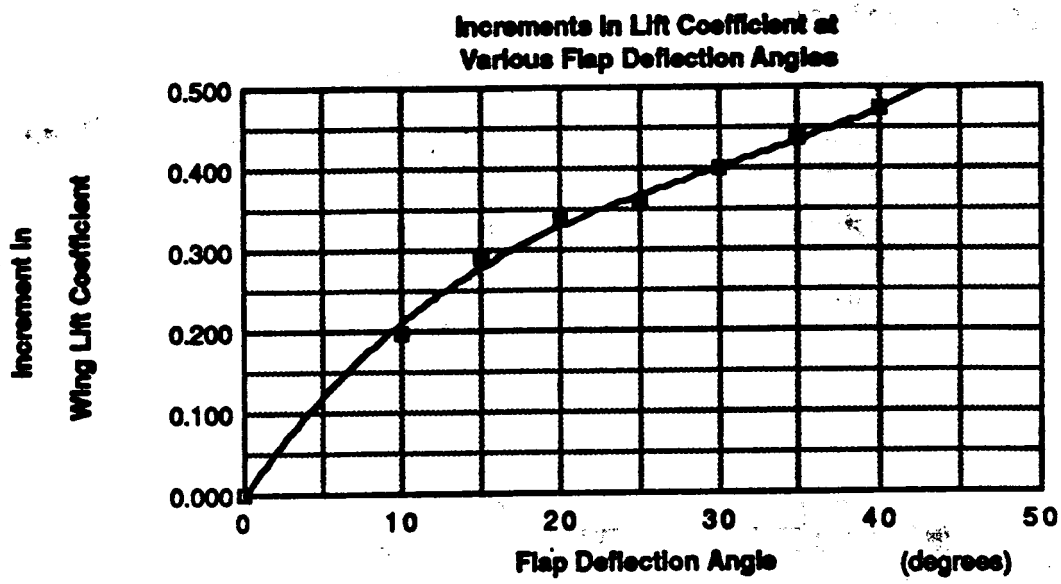

Fig. 4

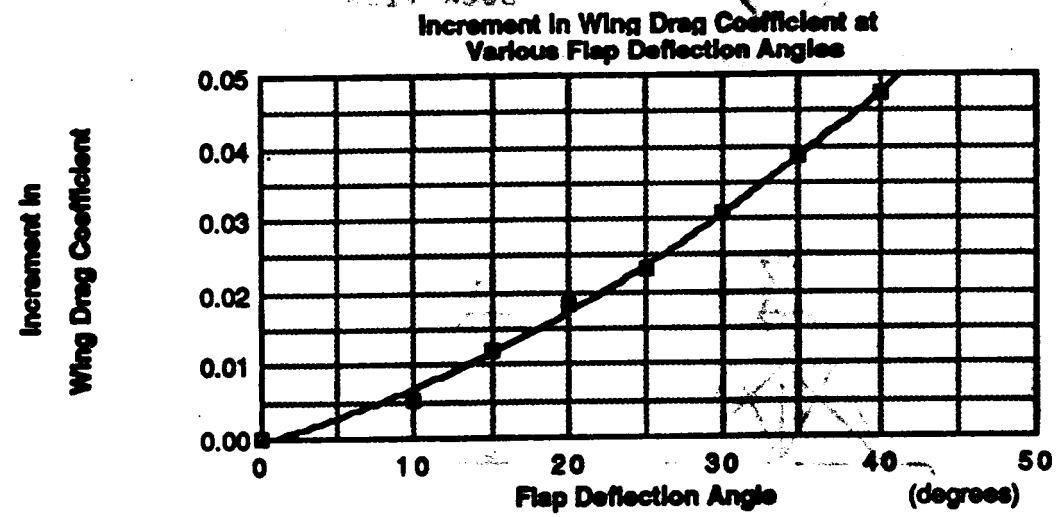

Fig. 5

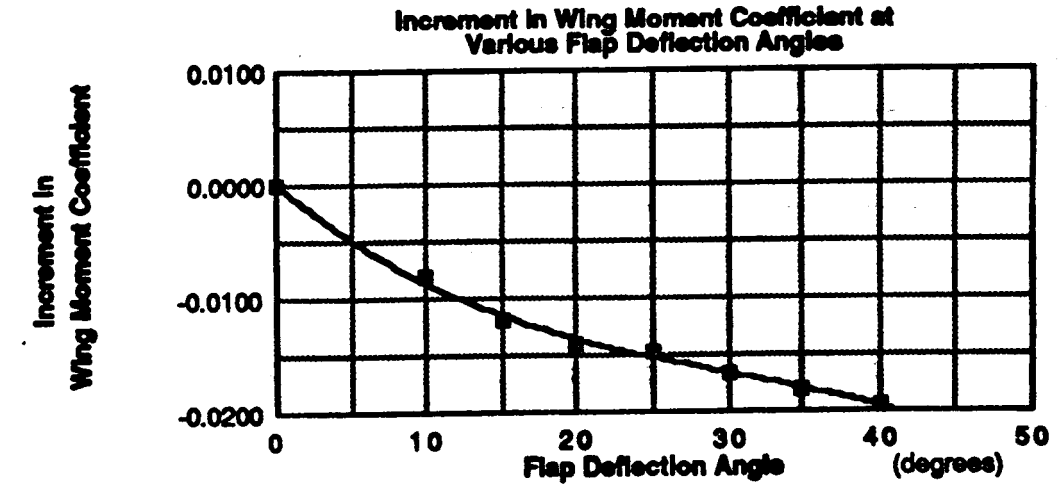

Fig. 6

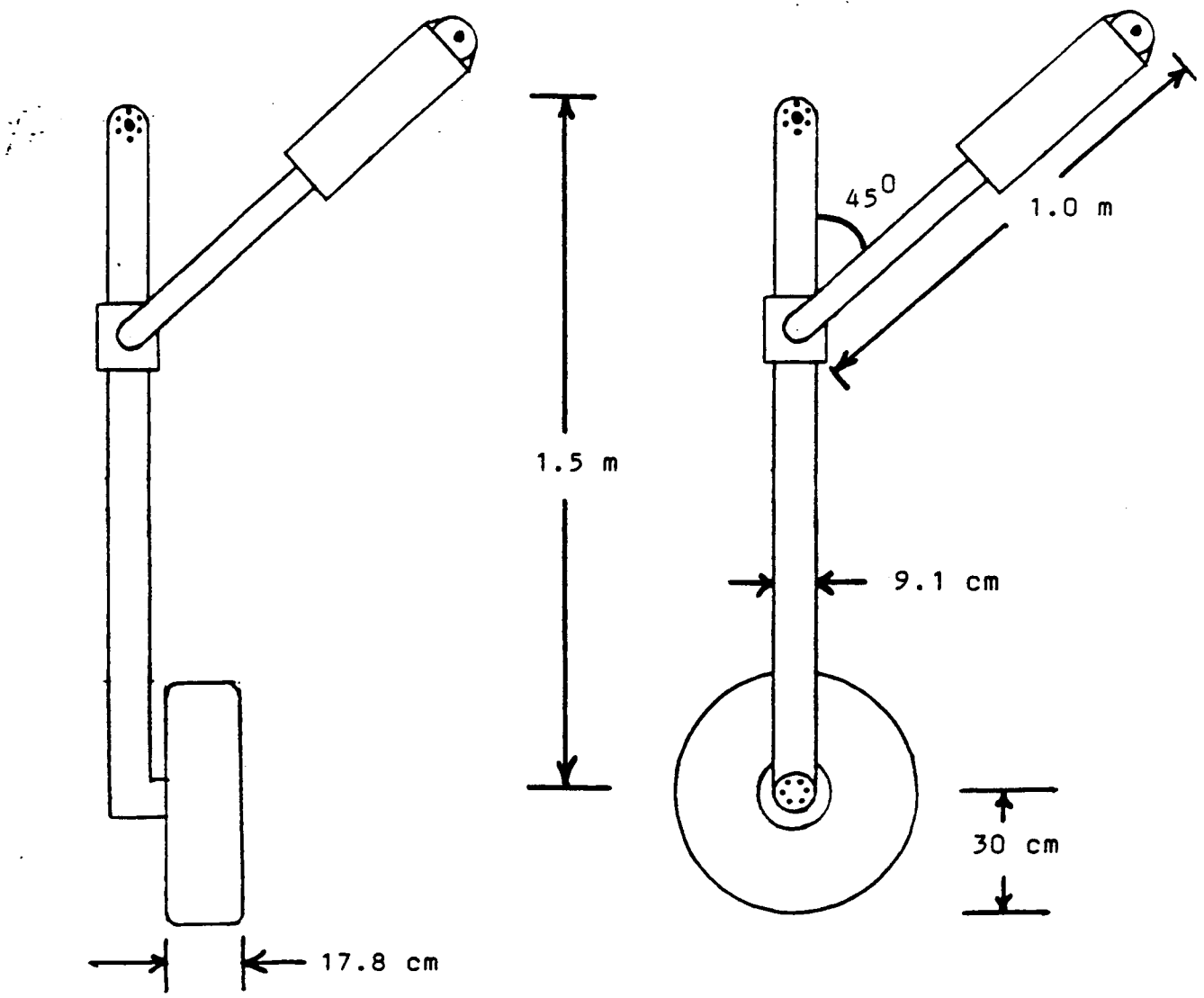

Main Gear
(left side of wing)

Nose Gear

Material of Struts: Steel (5Cr-Mo-V)

Tire Pressure : 4.2 kg/cm^3 or 60 lb/in^3

Tire Type : Normal, grooved tire

(Source: Torenbeck)

Fig. 7

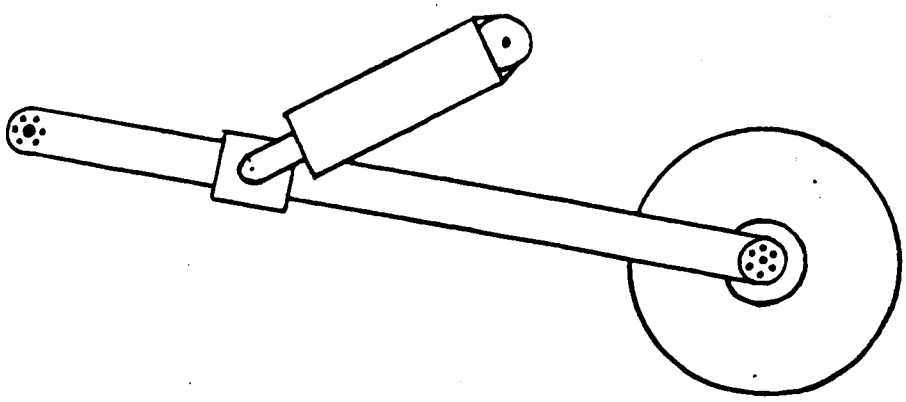

Nose Gear Retracted

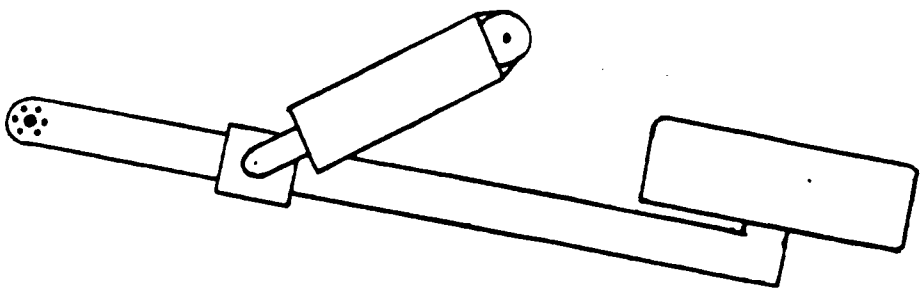

Main Gear Retracted
(left side of wing)

Fig. 8

WEIGHTS AND BALANCES

John Walter

The weight analysis was performed by using an iterative method to determine gross weight. Component weights were determined from empirical relations taken from the handout from Torenbeek[1]. These relations require the use of English units, so all component dimensions were converted before any calculations could take place.

The wing weight was calculated by using the Torenbeek method. The result is a wing weight much less than that calculated in the midterm report. The flying wing concept allows a much lighter structural weight than a conventional fuselage airplane because a large part of the weight of the wing comes from the joint between the wing and fuselage. The crew compartment in our design is not viewed as being a true fuselage because of its small size . The pod will provide approximately the same structural weight regardless of where it is placed. The forward placement is necessary in order to produce a stable configuration. Because of the structural complexity of the pod, its weight is estimated to be 10% of the gross weight. This value also takes into account the necessary piping and tubing used to connect the fuel system. A flying wing can be designed in such a way that its contents are not all concentrated at midspan. If the payload, power system and fixed equipment are distributed along the span, the bending moments on the wing can be reduced and the structure can be made lighter.

Current and future technology will allow instruments and flight controls to be made significantly lighter than present systems. Flat panel displays will weigh less and provide more room in the cockpit for the pilots. This aircraft will have a relatively low gross weight and undemanding performance characteristics so that powered flight controls are unnecessary.

A canard is being used for stability purposes and its weight has been calculated in the same manner as the wing. Because of its size, the canard is not considered to be lightly loaded.

Several power system components are located within the canard to create an acceptable center of gravity location. Therefore, the canard is being treated as a wing during the weight calculation. The vertical tail is also large in size but it will not be heavily loaded during flight. As a result, a normal vertical equation was used for estimation.

The landing gear was estimated by the surface operations group to be 5% of the gross weight. The forward gear is located under the crew pod and the aft gear is located behind the empty weight center of gravity location to guarantee ground stability. The payload consists of the crew members, their space suits, and the accessories they will use during the mission. The weight of the maximum payload was given to be 700 pounds on earth which is approximately 1174 Newtons on Mars.

The propulsion group offered the power system mass following research into electrical motors, fuel cells and photovoltaic cells. It was found that a combination of fuel and photovoltaic cells provides the most power for the least amount of weight given the span of the wing. Tanks of liquid hydrogen and liquid oxygen are located within the canard. These elements combine in the fuel cells to produce energy and water. The water will be stored in tanks located in the wings. The reason for this is to keep the gross weight constant during flight. The center of gravity, however, will not remain in a constant position and will move towards the rear of the plane. The two electric engines are located 9 meters in back of the leading edge of the canard and 10 meters out on the span of the wing.

Reductions in gross weight can be realized through the use of composite materials for structural components. The weights of the wing, and vertical tail have been reduced by 25% and the landing gear by 12% to account for the use of composite materials. The canard was not reduced but was, in fact, made heavier so that the center of gravity could be moved forward.

Table 1 gives a brief history of the gross weight calculations from the initial sizing exercise to the final design. The design goal of 6000 Mars Newtons was not reached but the final weight of 6118 Newtons is a more realistic number. If the wing area obtained in the sizing exercise

had decreased as weight decreased, a significantly lower gross weight could have been achieved.

Table 3 gives a detailed weight breakdown of the components of the final design and the locations of the centers of gravity as measured from the leading edge of the canard. The table also gives the weight of each component as a percentage of the gross weight. The values given are for the situation in which there are two pilots and full fuel tanks. The formulas and values chosen for the iteration seem to give reasonable results with a few exceptions. The weight of the vertical tail may be too low given its present dimensions. Modifications should be made to the tail to make it shorter so that the structure need not be so heavy. If the vertical dimension is decreased by about 3 or 4 meters and the horizontal dimension is increased accordingly lighter materials can be used in its construction. The wings account for roughly 23% of the gross weight and if the crew pod is included the value is 33%. Total structural weight is nearly 50% of the gross weight. These values are all feasible if future progress can bring about the development of stronger alloys which will be used in critical areas of the wing such as the spars. The propulsion system is rather complex and, therefore, will probably require the full 28% which was calculated. Masses for propulsion components were provided by the propulsion group based on data obtained from NASA. Since the plane is being designed around a payload criteria it makes sense that the payload weight should account for a large percentage of the gross weight. The value of 19% meets this requirement and yet is not unrealistic. A graphical display of the component percentages is given in Figure 1.

The weights and centers of gravity have been calculated for seven different situations and are shown in Table 2. For the sake of clarity, the hydrogen and oxygen tanks will collectively be referred to as fuel tanks. As the H_2 and O_2 combine they form water which is stored in tanks located in the wing. The first two cases (A and B) are for two pilots and either full or empty fuel tanks. The next two cases (C and D) are for one pilot and either full or empty fuel tanks. Cases E and F will occur only on the ground and they are for no pilots and either full or empty fuel tanks.

The last case (G) is the case for no pilots, fuel or water. Following the values in the table is the accepted center of gravity range as provided by the stability group. The reference letter will indicate the location for each case on the C.G. Travel Diagram (Figure 2).

The data seems to indicate that the plane is unstable for the last three cases. This is not true, however, because the rear landing gear will be located a considerable distance behind the actual centers of gravity for these cases. Although the plane is still stable for case D it is very close to being unstable. This situation can be greatly improved by placing an object of relatively large mass in place of the missing crew member. For example, the crew pod can be designed so that a rescue package along with a certain amount of ballast can be placed in the empty space. The package can be dropped through a hatch in the bottom of the pod and the ballast will remain on board to provide greater stability. For the first three cases the center of gravity locations fall well within the acceptable range and should pose no problem during flight.

The operational empty weight is that found in case G from Table 2. The maximum weight for takeoff corresponds to case A in the table. From these two values the useful load fraction can be determined.

Maximum Takeoff Weight = 6118 Newtons

Operational Empty Weight = 4552 Newtons

Useful Load Fraction = 0.256

In summary, the weight analysis indicates that very lightweight materials must be developed in order for the project to succeed. Work needs to be done in reducing the wing area so that the aircraft can become more structurally sound. The size of the vertical tail is probably the most questionable feature on the aircraft. Its enormous size creates a number of weight problems. Most importantly, it must remain very light in order for the aircraft to remain stable. Perhaps one solution is to have a number of smaller tails distributed along the wing. These smaller tails can be made very light because they will not have the large bending moment that the present design has. Because the purpose of the program is to provide a better

means to study the Martian surface, the amount of instruments on board should actually increase as a percentage of gross weight. For the most part, however, this design of a Mars airplane is not an impossibility and with further research and development in the areas mentioned above, a flight date of 2010 is a reasonable goal.

REFERENCES

1. Roskan, Jan., **Airplane Design Part V: Component Weight Estimation**. Roskan. Aviation and Engineering Corp. 1985

2. Nicolai, Leland. **Fundamentals of Aircraft Design**. **METS, Inc.** 1975

WEIGHT HISTORY

	Gross Weight (N_M)
Initial Sizing	7200
Midterm Weight	6559
Final Design Goal	6000
Final Design Weight	6118

TABLE 1

GROSS WEIGHT AND CENTER OF GRAVITY LOCATIONS FOR VARIOUS LOADING SITUATIONS

(Distances Measured From L.E. of Canard)

REFERENCE LETTER	PILOTS	FUEL TANKS	WATER TANKS	GROSS WEIGHT(N_M)	C.G. LOCATION(m)
A	2	Full	Empty	6118	5.070
B	2	Empty	Full	6118	5.339
C	1	Full	Empty	5531	5.342
D	1	Empty	Full	5531	5.640
E	0	Full	Empty	4944	5.775
F	0	Empty	Full	4944	6.108
G	0	Empty	Empty	4552	6.229

Acceptable Range During Flight: 3.973 m to 5.647 m

Range on the Ground: 1.71 m to 7.49 m

TABLE 2

WEIGHT BREAKDOWN AND CENTER OF GRAVITY LOCATIONS

Distances (X) are measured from the leading edge of the canard

Component	Mars Weight (N_M)	X-location (m)	Percentage of Gross Weight
WINGS	1416	9.045	23.14
CANARD	507	1.315	8.29
VERTICAL TAIL	136	13.234	2.22
LANDING GEAR	306	5.903	5.00
CREW POD	612	2.100	10.00
STRUCTURAL GROUP	2977	6.169	48.65
ENGINES	111	9.000	1.81
FUEL CELLS	838	1.747	13.71
PHOTOVOLTAIC CELLS	331	8.890	5.41
PROPELLERS	148	13.500	2.42
MISCELLANEOUS	279	5.450	4.56
POWER PLANT GROUP	1707	5.228	27.91
FLIGHT CONTROLS	109	9.045	1.78
FURNISHINGS	32	2.100	0.52
AVIONICS	119	1.750	1.95
PAYLOAD	1174	2.100	19.19
FIXED EQUIPMENT GROUP	1434	2.599	23.44
GROSS WEIGHT	6118	——	
CENTER OF GRAVITY	——	5.070	

TABLE 3

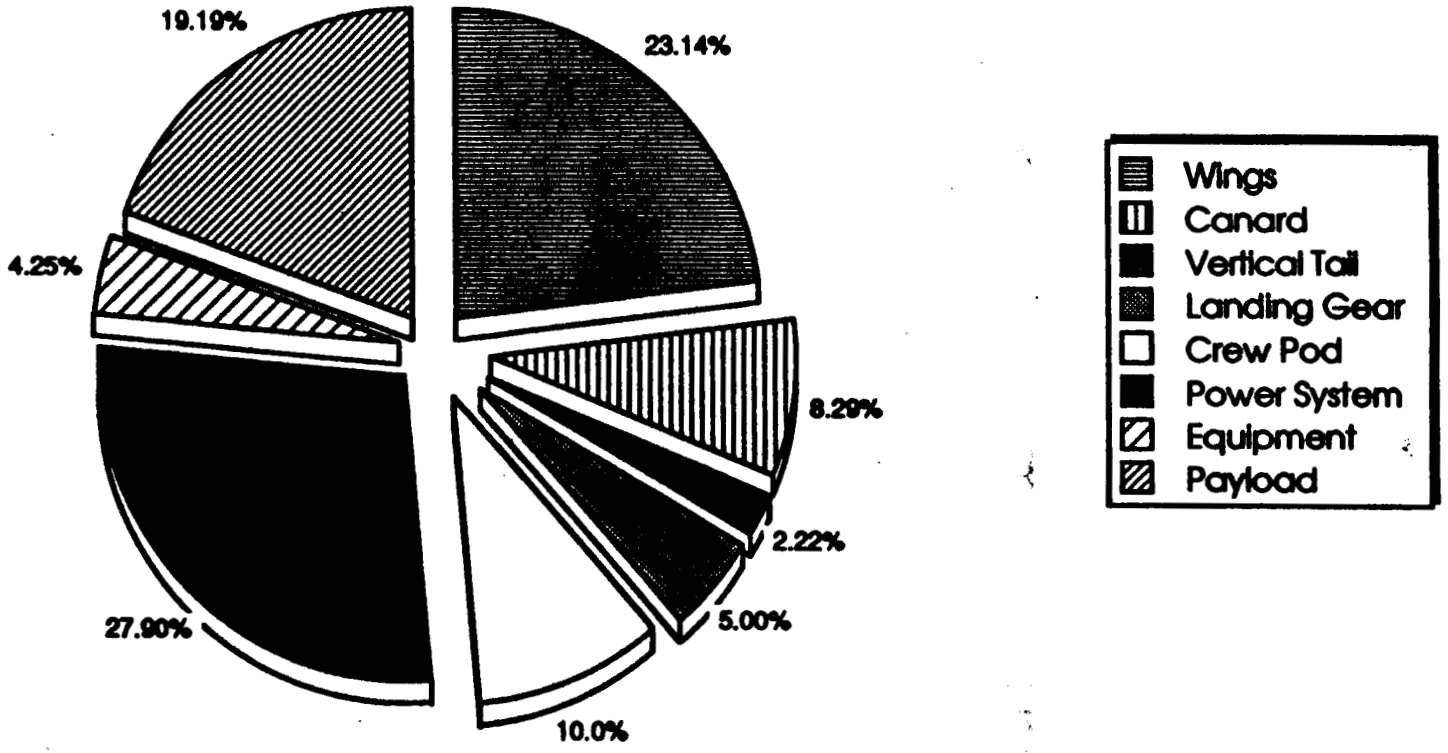

Weight Breakdown by Percentage of Gross Weight

FIGURE 1

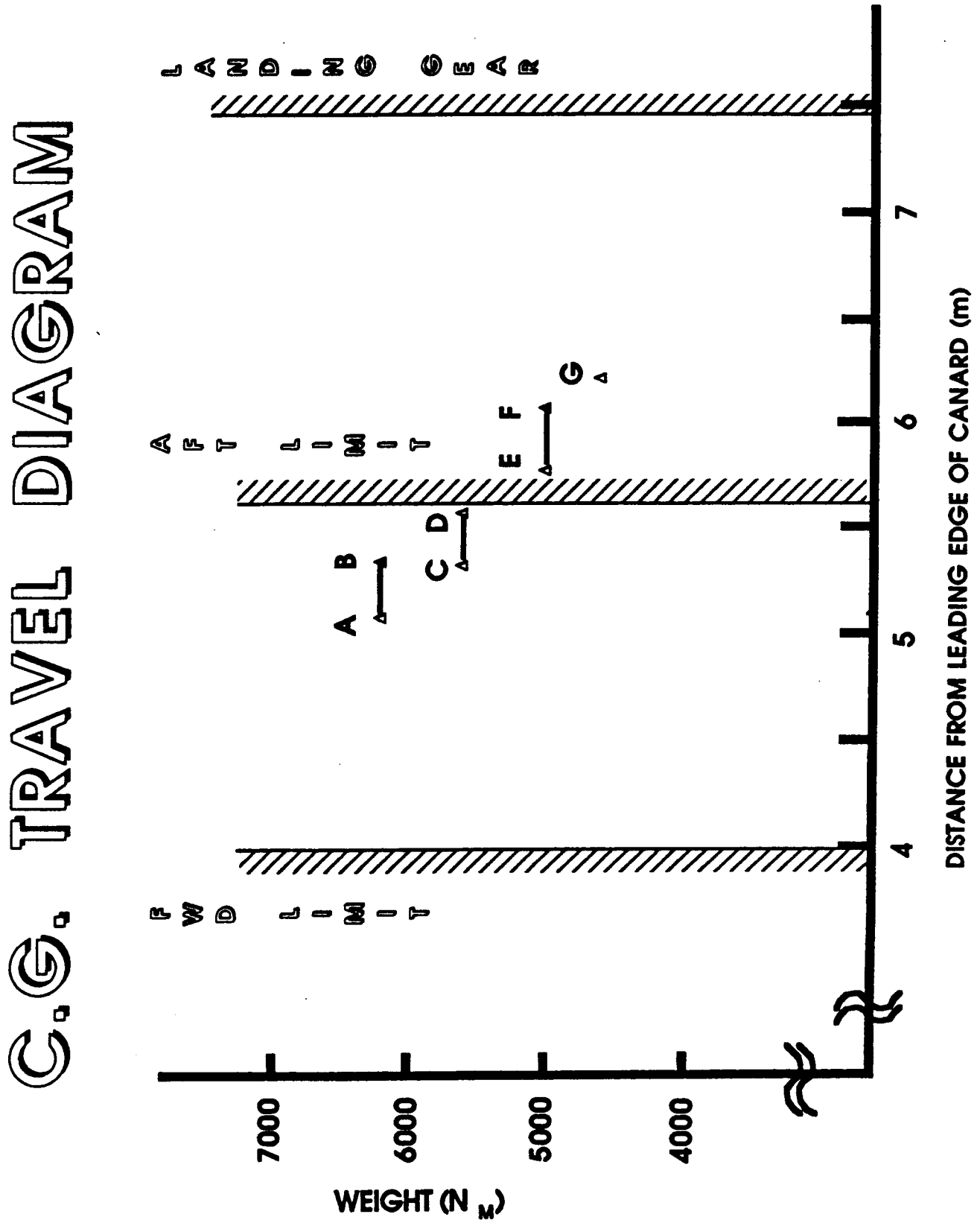
C.G. TRAVEL DIAGRAM
LANDING GEAR
AFT LIMIT
FWD LIMIT
A
B
C
D
E
F
G
7000
6000
5000
4000
WEIGHT (N M)
4
5
6
7
DISTANCE FROM LEADING EDGE OF CANARD (m)

FIGURE 2

ATMOSPHERIC DATA

Kentaro Sugiyama

The atmospheric data used by all group members to do needed calculations is presented in the table below for easy reference and verification. Since temperature and density both vary with increasing altitude, not necessarily one value was used for each of those. For density, the assumption was made that it varied linearly with altitude so the values presented in the table were graphed . Subsequent values needed for calculations at various altitudes were obtained by interpolation or extrapolation of the graph. A similar technique was employed to obtain the temperature used. All other values used for calculations are the standard accepted Mars atmosphere values and are presented in the table. These were assumed to be uniform throughout the Martian atmosphere.

	A	B	C	D	E
1	TABLE OF ATMOSPHERIC DATA USED				
2					
3	description	symbol	value	units	other info
4					
5	density	ρ	0.0156	kg/m^3	at 0 km alt.
6			0.01423	kg/m^3	at 1.5 km alt.
7	gravity	g	0.377*earth	m/s^2	earth is 9.8
8	solar flux intensity	I	0.45	kw/m^2	
9	temperature range	T	200-228	deg K	
10	temperature used	T	214	deg K	
11	kinematic viscosity	ν	5.5227 E-3	m^2/s	

AUXILIARY SYSTEMS

Michael Brody
and
Arlene Zander

The Mars craft has many systems that need control from the cockpit. To keep installation and maintanence of these controls simple, the use of hydraulic devices was discarded. Flaps and control surfaces will be manipulated by wires that run from the control device to the cockpit. For instance, the ailerons will be connect to the control stick and deflected by pushing the stick left or right. The elevators on the canard will be connected to the control stick in the same manner except a deflection of the stick up or down will cause an elevator deflection. The rudder on the vertical tail will controlled by wires that are hooked to floor pedals in the cockpit.

Flaps on the wings will also be controlled with wires. A wire will be looped around a hinge sprocket on each flap. This wire will be brought to the cockpit and hooked up to a turn-wheel. As the wheel is turned, the flaps will be moved. There will be a direct linear relationship between the amount of degrees the wheel turns and the amount of degrees the flaps are deployed.

Spoilers will not have any incremental control. Since spoilers are used only during ground roll, there is no need to be able to trim them. The spoilers will be spring loaded. The spring will be activated by a wire-connected switch in the cockpit. Since deployment of the spoilers during flight would be catastrophic, each spoiler will also have a wire-activated latch thats connected to the flap itself. After landing, the spoiler springs can be reloaded.

The cockpit will contain several miscellaneous pieces of equipment. A radio will be onboard to communicate data and voice to the ground base. This radio will either transmit directly to the base, or it will relay its signal via a communications satellite orbitting the planet. Navigational equipment will also be needed onboard. Some of these instruments will need information about terrain from the satellite, while others, like the artificial horizon, will function independently. Power to operate the radios and other

equipment will be small compared to the available power supplied by the solar cells.

The retracting and deploying of the landing gears will be powered. Electric motors on each gear will control the lengthening and thrinking of the piston control strut. Enough power (up to 8 Kw) will be present at TOL to operate the motors. If for some reason the power is not available or the electric motors fail, an emergency gear latch can be released causing the gears to unfold via gravity. Since the landing gears open up into the wind, the drag force on the gears will lock them into a fully deployed position.

During the rescue scenario, supplies will have to be released from the empty passenger area. The supplies will fall through a trap door controlled by a wire-activated latch. This latch will only be installed during a rescue mission. When the trap door is not in use, it will be bolted shut.

COST ANALYSIS

John Walter

The cost analysis was performed by using a planetary cost model program on Lotus. The program was developed to use for spacecraft cost estimation so several of the inputs required different interpretations. Included in the mass of the structure are the canard, wing, vertical tail, landing gear and propellers. The mass of the thermal portion of the airplane consists of the photovoltaic cells and the space suits. The flight controls are considered to be the attitude control system. The avionics are divided up between the reaction control and communications categories. Also included in the communications category are the accessories which make up a portion of the payload. The following table gives the mass breakdown of the components used in the cost analysis:

Component	Mass(kg)
Structures	846
Thermal Systems	226
Flight Controls	26
Avionics	22
Communications	37
Electrical Power	30
Propulsion	302

TABLE 1

The results of the costs analysis appears in table 2. All values are in millions of dollars using 1985 prices. Communications accounted for the largest cost among the components of the plane. The task of developing a communication system for another planet is much more involved than it is on Earth. Less is known about the power neccessary to communicate long distances on Mars because of the very different atmosphere and terrain. As a result, a great deal of research money is needed to develop such a system. Structures are the second greatest component of cost. Lightweight but strong materials are needed throughout the plane in order to keep the gross weight low and the center of gravity within range. New alloys are required to accomplish this goal and extensive testing must take place. It is because of this that structures make up the greatest portion of the engineering costs. In order to fit comfortably in the crew compartment, the pilots cannot wear bulky spacesuits. Due to the lack of a pressurized cabin the pilots are forced to wear some sort of pressure suit. Such a suit that can handle both of these requirements is not already in existence. Therefore, the development the suits and oxygen supply will be costly. The power system in our design is currently being studied for use in current applications, such as the space shuttle.

With all of these factors in mind it is clear that the project will require major funding. The value of $1.2 billion is not an unreasonable estimate of the final cost considering the amount of high salaried workers required for the program to be successful. In addition, testing and assembly as well as software development are very costly procedures. The program will be successful if costs can be kept to a minimum.

ESTIMATED COST OF MARS AIRCRAFT PROGRAM

(All values are in millions of dollars in 1985)

Component	DDT&E	FHA	Total
Structures	49.0	10.8	59.7
Thermal	11.5	15.6	27.2
Flight Controls	26.2	18.7	44.8
Avionics	8.3	3.2	11.6
Communications	26.5	84.6	111.1
Electrical Power	7.2	27.8	34.9
Propulsion	0.3	0.0	0.3
Subtotal	128.9	160.7	289.6
System Test Hardware	372.5		372.5
System Test Ops	49.2		49.2
GSE	35.0		35.0
SE & I	65.8	23.0	88.8
Prog Mgt	39.9	24.0	63.8
Subtotal	691.3	207.7	899.0
Contingency	138.3	41.5	179.8
FEE	83.0	24.9	107.9
Prog Support	18.3	5.5	23.7
GRAND TOTALS	930.8	279.7	1,210.4

TABLE 2

INTERNAL CONFIGURATION

John Walter

Michael Brody

The task of locating internal structures and components of this aircraft was complex due to the center of gravity limits. Most of the volume of the plane falls behind the C.G. limit. As a result, many of the heavier components had to be located in or near the canard. The fuel tanks, which have considerable mass but small volume were place as far forward in the canard as possible. In order for the plane to be stable about its axis of symmetry, the liquid hydrogen has to be separated into two tanks on either side of one liquid oxygen tank. The fuel cell is too large to fit into the canard or the crew pod so it is located in leading edge of the wing at midspan. Water tanks of equal volume are located on either side of the fuel cells. The exact volume of the tanks is not known but they are expected to be over $7m^3$. The water will be heated be excess heat from the fuel cells so that freezing does not occur. Several pumps and pipes are located throughout the fuel system in order to transport fuel between tanks. The engines are located 10 meters out on the span and 9 meters behind the leading edge of the canard. A long shaft will be used to attach the propellers to the engine

The pilots will be seated back-to-back as shown on the inboard profile. Each pilot will have a small terminal to monitor flight status. Life support systems will be placed under and between the seats. The instrumentation will mainly be of the flat-panel display type in order to give pilots more room. The flight control system will be unpowered and consists of a series of cables and pulleys. For the case of one pilot, the plane can be configured so that a payload storage bay will be located at or in front of the aft center of gravity location. The payload can be as heavy as the weight of the pilot and equipment it is replacing, but if it any heavier the rate of climb and other performance characteristics will be adversely affected. The forward landing gear is located under the crew pod and 1.7 meters behind the leading edge of the canard. The main gear are each 8 meters out on the span and 5.78 meters behind the forward gear.

Inboard Profile

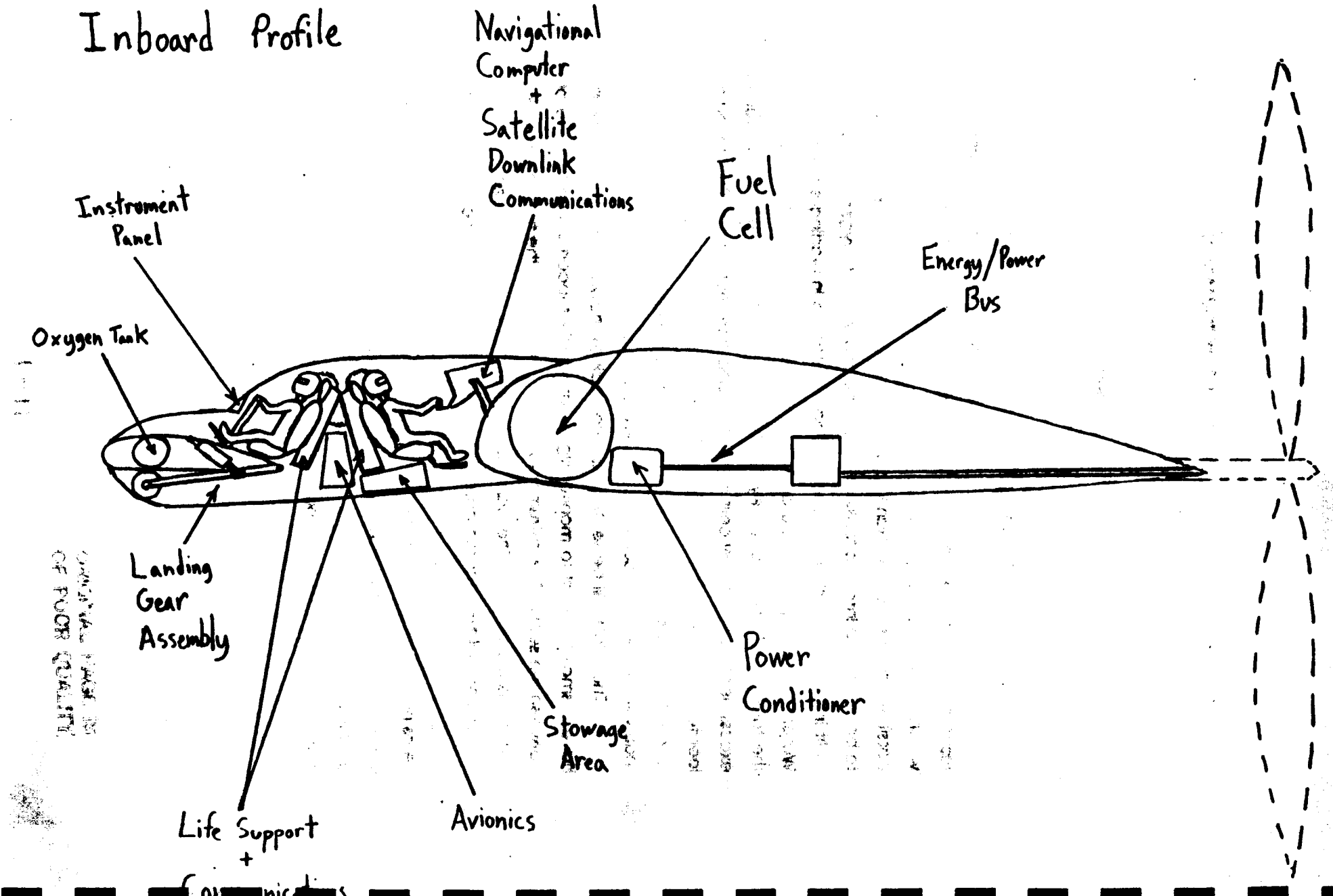

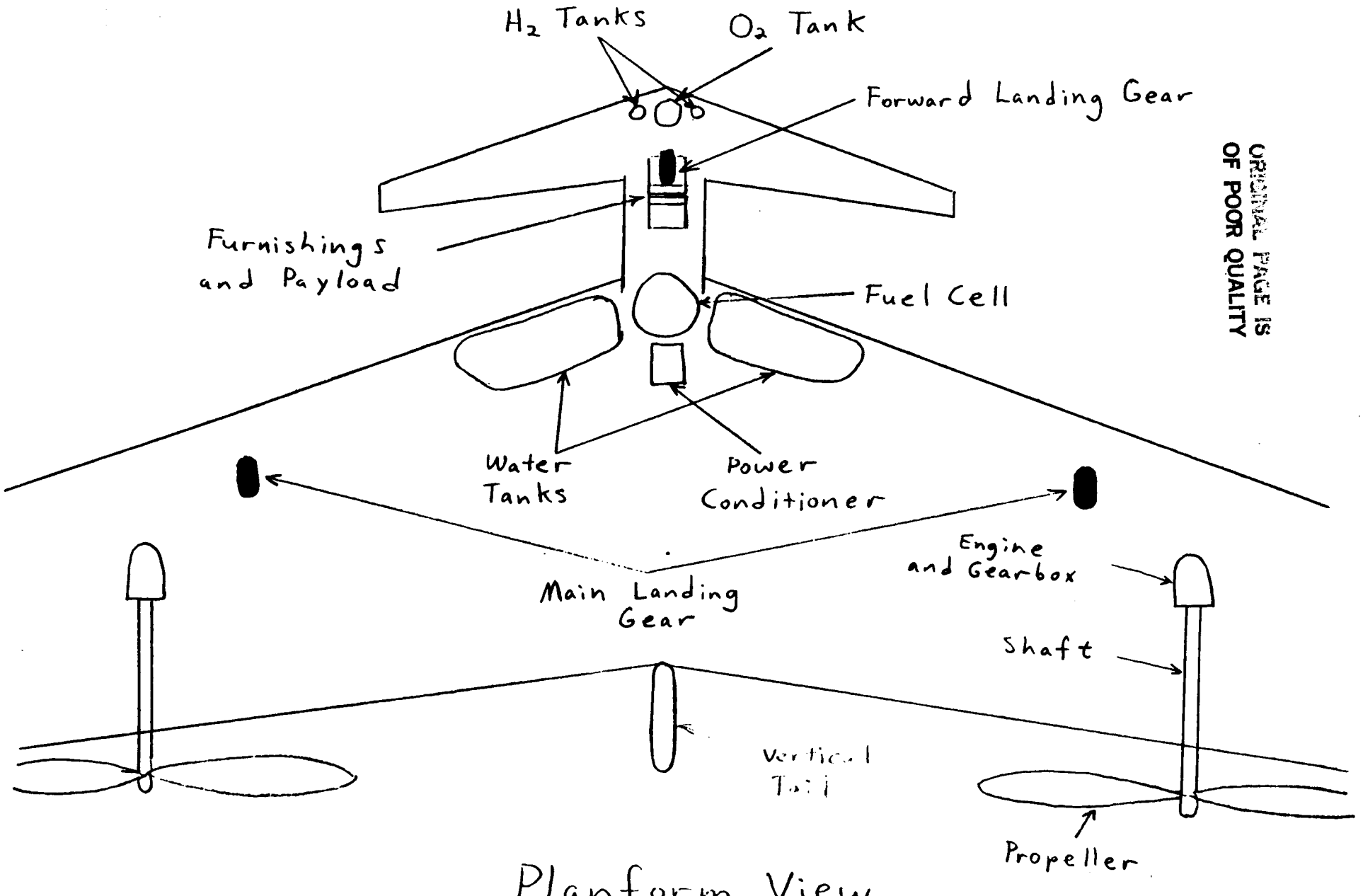

Planform View

Packaging and Assembly

Kurt Heier
Dan Ramshaw

The basic packaging assembly will consist of three cylinders. The first will contain the canard, vertical tail, and the fuselage; the other will stow only the wing parts. Each cylinder has a diameter of 4.5 meters and is 7.5 meters in length. It should be noted that a shuttle can accommodate only one cylinder. Packages of spare parts will be shipped in remaining space in all three cylinders.

The first cylinder will hold three boxes. The canard will be shipped in two halves and placed in a box of dimensions 0.33m x 1.67m x 5.44m. Next to this box will be the vertical tail which will be separated in half and placed in a box of dimensions 0.48m x 3.00m x 5.00m. The fuselage will remain intact and stowed in box of dimensions 1.40m x 1.40m x 1.80m. Any extra space in the cylinder will be utilized by spare parts packages. The remaining two cylinders will contain the wing. It will be totally disassembled into wing spars, ribs, and sheets of skin. Landing gear, engines, and propeller blades will also be shipped in these cylinders.

The assembly of the aircraft on Mars will begin with the construction of the wing. Wing parts will be shipped first in order to allow time for its construction. After the wing is assembled the attachment of the canard, fuselage, and the vertical tail will quickly complete the assembly.

RESCUE SCENARIO

All Groups

At the present time, the aircraft is unable to land anywhere except on a flat runway. The rescue scenario, therefore consists of an airdrop of supplies to the victims and the deployment of a land roving vehicle from a nearby base to bring them to safety. In essence, the aircraft does not have the capability to do actual rescue due to the rough, unpredictable terrain on the surface of Mars. Thus, deployment of life support systems will enable the victims to sustain life until rescue by land is made. It is doubtful whether provisions will be able to be made for the aircraft to land in remote areas because the aircraft requires the magnetic sled in order to take-off. The aircraft will be able to search for victims and relay their position to the land rover. This application will provide greater speed in executing a search and require less manpoweer to do so. All searches of this type must be conducted during the day because of the use of solar powered engines.